A numerical assessment of land reclamation as a strategy for near shore diamond mining

Master Thesis - Joël Anker

Hydraulic Engineering & Resource Engineering
Delft University of Technology
28th February 2016

This work reflects the views and findings of the author and has not been reviewed or formalised with NAMDEB.

Front cover: Selection of photographs of land reclamation activity in the Southern Coastal Diamond Mine in Namibia. Pictures were taken in October 2014 by Joël Anker, Witteveen+Bos, during one of many mine visits.

A numerical assessment of land reclamation as a strategy for near shore diamond mining

by Joël Anker

A final thesis submitted in partial fulfilment of
the requirements for the double degree of

Master of Science

in the field of

Civil Engineering

and

Applied Earth Sciences

at

Delft University of Technology

Delft, The Netherlands

Graduation committee:

Dr. M.W.N. Buxton	Chairman, Delft University of Technology (Resource Engineering Department)
Prof. dr. ir. M.J.F. Stive	Delft University of Technology (Hydraulic Engineering Department)
Ir. H.J. Verhagen	Delft University of Technology (Hydraulic Engineering Department)
Ing. M. van der Wijk	Witteveen+Bos

Abstract

On the south-west coast of Namibia, diamonds were trapped during the Quaternary on bedrock platforms and in bedrock gullies. These were formed by differential erosion due to wave action. The diamonds originated from Kimberlite diamond pipes within the catchment area of the Orange River in South-Africa and Botswana. This river eroded the diamonds from the pipes and transported them over a distance up to 1000 km to the sea. Subsequent deposition resulted in the formation of placer deposits on the south-west coast of Namibia. These diamond deposits form the mineral reserve for the Southern Coastal Mine, operated by NAMDEB, which is the area of interest for this study.

The currently used extraction strategy in the mine is based on the philosophy that the mining method must be selective and land-based. Conventional loading and hauling of overburden and bulk material is applied after which a final cleaning of the bedrock is done with vacuum cleaners. A seawall made out of sand protects the mine along the entire coastline against flooding.

Overburden sand and tailings are constantly transported and dumped onto the beach to achieve land reclamation. This is referred to as the Sand-2-Sea program, developed to expand mining activity in a seaward direction. When enough land is accrued the sandy seawall, protecting the mining operation against flooding, is shifted seawards and new mining area is claimed.

The coastal area is characterized by a highly energetic wave climate. This causes a high erosion rate of the sand nourishment along the coast. The strategic business plan of NAMDEB states that diamond extraction, using the current mining- and land reclamation method, must continue until 2031 reaching a maximum seaward distance of 545 m from the average high water line (Mean Sea Level (MSL) +2m) of 2014. It was hypothesized in this thesis that the feasibility limit of the current mining method is reached before this maximum distance is obtained.

In addition, severe seawall erosion can occur during storm events. A storm in May 2015 was an example of this, causing seawall failure and flooding of an area with ongoing mining activity. This event is used as a case study in this thesis.

The aim of this thesis was to indicate how far seawards the land reclamation strategy for diamond mining can be applied. In addition, research was conducted to define standards for a seawall to effectively protect a mining area against flooding. The main research questions were defined as:

- ***What are the limits of the land reclamation strategy that is applied to expand diamond extraction, with the current mining method, in a seaward direction?***
- ***What is the optimal design for a seawall to protect the nearshore mining operation?***

The geomorphological model XBeach was applied to predict bed profile changes and seawall

erosion. The hydrodynamic boundary conditions were obtained by translating offshore wave-records to nearshore wave conditions with the model SWAN.

Modelling bed profile changes under prevailing wave conditions gave insight into morphological processes in the upper shoreface of the Southern Coastal Mine. Seawall erosion is notable on a weekly basis, which is consistent with the corrective maintenance strategy that is applied by NAMDEB.

The XBeach model also simulated seawall erosion due to storm events. The wave conditions of these storm events were obtained by data analysis of available offshore wave-records. The modelling results showed how the ultimate limit state profile of a seawall cannot be maintained with the currently applied seawall standards for certain storm conditions. No seawall section that was modelled was able to withstand the wave conditions of a storm with a probability of 1/100 per year. For some seawall sections the model simulations showed already failure for storm conditions with a lower probability.

A quantitative sensitivity analysis revealed that the modelling results are most sensitive to variations in wave conditions. Verification of the model set-up was possible through the simulation of the case study of storm induced flooding of a mining cell after seawall failure in May 2015.

Calculated erosion volumes per storm event were used to develop new standards for seawall construction. The seawall standards also include requirements for the beach width and the foreshore steepness, in contrast to the currently applied standards. These requirements have proven to be essential in reducing wave energy effectively. Three alternatives for seawall and foreshore design were proposed, presented in the table below. They are designed to be able to withstand wave conditions of a storm with a probability of 1/100 per year.

Table 1: Values of proposed design standards for a seawall in the Southern Coastal Mine.

	Proposed design standard	**Alternative standard (higher crest)**	**Alternative standard (narrower foreshore)**
Seawall volume $[m^3/m]$ (above MSL +2m)	160	160	250
Crest height $[m]$ (above MSL)	6	7.5	7
Crest width $[m]$ (between windrows)	32	20	43
Beach width $[m]$ (between MSL and MSL +2m)	75	75	60
Foreshore width $[m]$ (between MSL and MSL -9m)	270	270	220

The currently applied land reclamation strategy for the seaward expansion of mining activity was evaluated, using model results and the new seawall standards. Sand volumes required for the construction and maintenance of a stable foreshore were compared to sand volumes available in the mine. It was concluded from this analysis that the limit for land accretion is in the range of 8 to 13 meters water depth on average (measured in 2014) in the area targeted by the Sand-2-Sea program. Sand volumes required to deal with the losses due to longshore sediment transport in particular will become too large.

Due to data gaps in physical parameters, there are uncertainties in the research that was conducted. A thorough investigation into sand properties present, the bathymetry of the upper shoreface and the volumes of sand available for construction purposes will increase the level of confidence in the interpretation of results.

The design of seawall standards were developed for a storm with a probability of 1/100 per year. This is a recommendation, supported with an analysis of how the acceptable risk level can be chosen by a comparison of different costs. NAMDEB can choose a different risk level.

The approach of the seawall design was deterministic, with a conservative choice of the values of parameters involved. A probabilistic design of the seawall will increase the level of confidence and may lead to a different answer. The calculations accompanying such an approach are out of scope for this thesis.

The calculation of longshore sediment transport rates was done by a conservative, but rough, estimation. The resulting answer for the final limit of the applied land accretion strategy is very sensitive to variations in sand losses due to longshore sediment transport.

Preface

In September 2014 I, as an intern, was sent to the Southern Coastal Mine of Namibia by Witteveen+Bos to study the diamond mining operation of NAMDEB. Besides the unforgiving desert on land and the constantly raging sea, I was impressed by the mining operation functioning under the very difficult circumstances. With a closer look it became clear that there is much potential for improvement in the mining strategy. Moreover, the mining method will have to be revised to make it more resilient against forces of nature and to enable expansion of mining activity seawards, since the diamond deposit extends seawards.

In 2015 I continued with this project as a graduate intern for Witteveen+Bos, by working on the master thesis in front of you. This thesis is an assessment of the currently used mining strategy, which is making use of land reclamation by pushing overburden sand and tailings into the sea. When enough land is accrued a sandy seawall is constructed on the beach and diamond extraction can start behind the seawall. First a literature review of relevant geological-, hydrodynamic- and morphological processes was done. From here on a geo-morphological model has been set-up to simulate the evolution of the coast and the erosion to the seawalls. Based on model results and a system analysis, an adjusted standard for seawalls has been proposed. And using these new standards, the limits of the land accretion strategy are indicated.

I want to express my gratitude towards the members my supervising committee. This master project would not have been successful without the input and feedback from Mike Buxton, Henk Jan Verhagen, Marten van der Wijk and Marcel Stive. I am also very grateful for the time, the edifying criticism and the help of Maarten Jansen and Arnold van Rooijen.

I would like to thank Witteveen+Bos for providing me with a challenging subject for my thesis and a nice place to work in their office in Rotterdam. I also would like to thank IMDH Group, Royal IHC and Royal Eijkelkamp Group for giving input for the set-up of my research and for taking part in (organizing) the meetings with the client NAMDEB. And in addition, NAMDEB is thanked for its assistance in gathering data during my internship in Namibia.

Many thanks also to my colleagues and fellow graduate interns at the office of Witteveen+Bos in Rotterdam. I have really appreciated the attentive ears, the willingness to help and the numerous laughs we had.

Witteveen+Bos, Rotterdam J.C. Anker
28th February 2016

Contents

1 Introduction **1**

1.1 Background 1

1.2 Objective of thesis 2

1.3 Hypothesis 3

1.4 Scope of the research 3

1.5 Outline of report 5

2 Local conditions **8**

2.1 Topography 8

2.2 Tides 11

2.3 Winds 12

2.4 Waves 13

2.5 Sand properties 14

3 Mining method and land reclamation strategy used for diamond extraction **15**

3.1 Introduction 15

3.2 Mining target 16

3.3 Exploration 16

3.4 Mining method 17

3.5 Seawalls and crosswalls 19

3.6 Land reclamation to expand mining activity seawards in MA1 19

3.7 Reasoning behind mining strategy 20

4 Current seawalls and crosswalls **22**

4.1 Function 22

4.2 Seawall standards 22

4.3 Construction 23

4.4 Maintenance strategy 24

4.5 Need for a new seawall design standard 25

5 **Linear Beach Terraces: A marine-placer deposit** **26**
5.1 Placer deposits 26
5.2 Deposition of diamonds 27
5.3 Trapping of diamonds on linear (raised) beaches 27
5.4 Orientation of the gullies 28
5.5 Offshore placer deposits / submerged beaches 29

6 **Hydrodynamics and morphological changes in the upper shoreface** **31**
6.1 Coastal profile 31
6.2 Waves affecting dunes 34
6.3 Sediment transport 41
6.4 Dune erosion 46

7 **Methodology** **51**
7.1 Modeling 51
7.2 Deterministic approach for the reliability of a seawall 52

8 **Analyzing SWAN model data** **54**
8.1 Model approach 54
8.2 Model set-up 54
8.3 Model results 59

9 **Modeling seawall erosion and beach profile response with XBeach** **63**
9.1 XBeach: Model approach 63
9.2 XBeach: Model set-up 66
9.3 Application of the developed model 81

10 **Seawall design** **90**
10.1 Deterministic approach of required seawall volume 90
10.2 Alternative seawall design 95

11 **Land reclamation strategy on the long term** **103**
11.1 Shifting of the seawall 103
11.2 Comparison with natural equilibrium profile 106
11.3 Prognosis 109

12 Acceptable risk level **120**
12.1 Investment costs . . . 120
12.2 Risks . . . 121
12.3 Total costs . . . 123

13 Discussion **126**
13.1 Discussion of methodology and interpretation of results . . . 126
13.2 Application of results . . . 128

14 Conclusions and recommendations **131**
14.1 Conclusions . . . 131
14.2 Recommendations . . . 134

Bibliography **136**

Nomenclature **141**

List of Figures **145**

List of Tables **155**

A Map of Southern Coastal Mine **157**

B Current mining method explained **166**
B.1 Mining blocks . . . 166
B.2 Dredging overburden . . . 166
B.3 Conventional stripping of overburden . . . 168
B.4 Dewatering . . . 169
B.5 Mining the terraces . . . 170
B.6 Cleaning the bedrock with Transvacs . . . 170
B.7 After cleaning the bedrock . . . 171
B.8 Difficulties in the current mining process . . . 171

C Land accretion project **173**
C.1 History . . . 173
C.2 Future plan (according to business plan) . . . 173
C.3 Reason for land reclamation . . . 174

C.4 Building groynes . . . 174
C.5 Pumping material to the beach . . . 178
C.6 Major difficulties . . . 178

D Effect of wind to wave-growth **180**

E Input reduction of wave conditions **183**
E.1 Manual grouping of classes . . . 183
E.2 Influence of Tp . . . 186

F Assessment of parameters in XBeach simulations **187**
F.1 Important parameters in the modelling process . . . 187

G Design conditions for the seawall **194**
G.1 Determination of the significant wave height associated with the design storm conditions . . . 194
G.2 Wave peak period (Tp) of design storm conditions . . . 200

H Sensitivity analysis of XBeach input parameters **203**

I Storm conditions (May 2015) of Case Study **209**

J Reliability of a seawall **212**
J.1 Limit state function . . . 212
J.2 Deterministic approach (Level I calculation method) . . . 212
J.3 Probabilistic approach (Level II and Level III calculation methods) . . . 213
J.4 Dune erosion problems . . . 217

K Probabilistic calculation of required seawall volumes **221**
K.1 Probabilistic approach . . . 221
K.2 Design conditions . . . 221
K.3 FORM procedure for the Namibian seawall reliability . . . 221
K.4 Discussion . . . 223

L Additional activities in support of Master Thesis **225**

L.1 Background 225

L.2 Fact-Finding Mission (September – November 2014) 225

L.3 NAMDEB-delegation in the Netherlands (April 2015) 225

L.4 Storm of May 2015 226

L.5 Presentations to NAMDEB 226

Abbreviations

1D	One Dimensional
2DH	Two Dimensional Horizontal
3D	Three Dimensional
ADT	Articulated Dump Truck
BP	Before Present time
CERC	Coastal Engineering Research Center
CoDeS	Coastline Development Tools
COV	Co-variance
CSD	Cutter Suction Dredger
HAT	Highest Astronomical Tide
LAT	Lowest Astronomical Tide
LHS	Left Hand Side
MA1	Mining Area No. 1
MHWN	Mean High Water Neaps
MHWS	Mean High Water Springs
MLWN	Mean Low Water Neaps
MLWS	Mean Low Water Springs
MN-Tool	Mega Nourishment Tool
Morfac	Morphological acceleration factor
MSL	Mean Sea Level
NAMDEB	Namibia De Beers
OR	Orange River
PDP	Prob Drill Platform
PTF	Pre-Treatment Facility (of bulk material)
RFT	Rigid Frame Truck
RHS	Right Hand Side
RoM	Run of Mine
SA	South Africa
SLS	Serviceability Limit State
SSL	Storm Surge Level
SWAN	Simulating Waves Nearshore
ULS	Ultimate Limit State
USD	United States Dollars
WIFS	Wet Infield Screening
XBeach	Extreme Beach Behavior

Chapter 1 – Introduction

1.1 Background

The mining operation of NAMDEB, discussed in this thesis, has been studied during a Fact-Finding Mission carried out by Joel Anker in service of Witteveen+Bos from September to November 2014. NAMDEB extracts diamonds in Namibia's Southern Coastal Mine. Diamonds are hosted in gravels that lie on the bedrock and are covered by a thick package of sand.

The current mining method consists of removing overburden sand until a gravel layer on top of the bedrock, containing diamonds, is reached. While the mining block is constantly being dewatered, the gravel layer is extracted and eventually the bedrock is cleaned with vacuum cleaners. This mining method is unique. However, no alternative has been proven to deliver a similar diamond recovery.

Major difficulties, according to observations and interviews, are first of all in resource estimation. NAMDEB geologists believe that the linear raised beaches, containing diamondiferous gravel deposits, found on land and in the midwater region, can be interpolated to the shallow and ultra-shallow water region. However, this has not been proven. Exploration and survey to back up this theory is very difficult due to the wave climate and steepness of the beaches.

Secondly, the mining operation also experiences difficulties. The dredging operation with Cutter Suction Dredgers is not satisfactory in most cases. Dewatering mining blocks is a major challenge due to the amount of seepage water. The construction and maintenance of seawalls is labour and energy intensive.

The knowledge gaps found during the fact-finding mission at NAMDEB, are, except for the gap in resource estimation in the shallow water regions, mostly in the Sand-2-Sea program. This is the land reclamation activity applied by NAMDEB. By dumping overburden and tailings in the sea, land is reclaimed and mining activity can be expanded seawards. The knowledge of the interaction between sea and sediment nourished can be improved to be able to predict the development of the upper shoreface accurately. It is not yet known to what depth contour line the mining activity can continue, considering seawall stability and water inflow problems. Also the effects and necessary building rate of groynes with loose material are not fully known. For morphological knowledge, NAMDEB has to rely entirely on the output of a one-dimensional coastline model. The results of this did not match the calibrations done by the Survey team in 2014. These calibrations consist of measuring the yearly-averaged high water line (MSL +2m) along the coast.

The most urgent research needed, according to NAMDEB's long-term mine planners and mining engineers, is the determination of the maximum distance offshore for which diamond extraction is economically and technically feasible with the current mining method. In addition, an investigation to define the most important constraints that determine the maximum distance is needed, including parameters such as overburden thickness, hauling distance and seawall stability.

1.1.1 Context of thesis work

The purpose of the fact-finding mission was to develop a better understanding of all the processes involved in land reclamation and mining in Mining Area No. 1, Sperrgebiet, Namibia, also known as the Southern Coastal Mine. The results of the fact-finding mission led to this graduation project, which will support a part of a proposal in which Witteveen+Bos offer their services to NAMDEB. These services will support NAMDEB in their effort to expand diamond mining activity into shallow sea regions in the most optimal way.

1.2 Objective of thesis

The objective of this thesis is to determine the limitations of expanding the mining activity in the Southern Coastal Mine seawards using the current mining method and strategy of land reclamation. Hence, the main research questions are defined as:

- ***What are the limits of the land reclamation strategy that is applied to expand diamond extraction, with the current mining method, in a seaward direction?***
- ***What is the optimal design for a seawall to protect the nearshore mining operation?***

Optimizing the design of the seawall can lead to better cost estimations for its construction. These new design standards can subsequently be used to indicate the maximum distance from the current shoreline until where a seawall and new mining pit can be constructed feasible. At a certain stage costs will become too high to continue mining activity with the current method. This result is necessary to indicate the limitations of the current mining method. A cost-benefit analysis should be done to indicate the economic limits of the mining strategy. The transport costs of sand for land accretion and seawall construction may not outweigh the profits made with the extraction of diamonds.

The main questions can be subdivided into secondary research questions:

1. What is the reasoning behind the current mining method and what are the determining factors/constraints for mining with this specific land reclamation strategy?
2. What is the optimal design standard for a seawall and how does this improve the current seawall construction?
3. What is the final seaward distance from the present-day shoreline where mining is technically feasible with the current mining method?

When the limit is reached for the current mining method, the need for a different, probably water-based, mining method will arise. Designing a different mining method to continue mining seawards into deeper waters is not within the scope of this thesis work. However, indicating the limits of the current method will be the first step towards the derivation of a new method.

1.3 Hypothesis

Two hypotheses have been prepared. The first one concerns the limitations of expanding the mining operation in seaward direction. The second hypothesis refers to the seawall design standards.

The current mining strategy used to extract diamonds from the ultra-shallow water regions in Namibia's Southern Coastal mine is finite. According to the Strategic Business Plan of 2014 the mining operation can continue to be technically and economically feasible until 2031 reaching a maximum seaward distance of 545 m from the average high water line (Mean Sea Level (MSL) +2m) of 2014.

The first hypothesis for this thesis is that the feasibility limit is reached before this maximum distance is obtained, because it becomes technically unfeasible to construct a seawall and economically unfeasible to transport all overburden and bulk material.

The second hypothesis of this thesis is that the design standards for the seawall can be adjusted, particularly considering the shadowing effect of the groynes and the progradation of the coast. In particular, the crest level could be lowered leading to a dramatic reduction in maintenance costs.

1.4 Scope of the research

Figure 1.1 defines what is included in the research scope of this thesis and what is excluded. A few aspects are discussed below, as they need more clarification.

Figure 1.1: Outline of the scope of this Master Thesis

Economic limit of current mining method

Determining the economic limits for the current mining method is out of scope for this thesis. First of all, the diamond production and the price of diamonds are unknown. Secondly, an investigation into bringing material from land to the seawalls and crosswalls could be a thesis work in itself, considering the size of the area, the data gaps and the different transport methods.

Alternative seawall construction methods

This thesis focuses on seawall construction using the method that is currently applied. This involves dumping of sand with dump trucks. Elaboration on the use of different material and construction methods, such as concrete armouring, is out of scope for the research of this thesis.

Seawall failure due to groundwater flow

Risks of seawall failure due to groundwater flow will not be assessed in this thesis. Seepage water and innerslope stability were examined extensively for the currently applied code of practice of NAMDEB for seawalls.

Environmental issues

An environmental impact assessment for the Southern Coastal Mine is not within the scope of this research. The damage to the environment induced by this particular method is considered to be low. Material dumped into the sea is unpolluted and there is no record yet of any substantial disturbance of flora and fauna.

However, as can be derived from Chapter 3 regarding the applied mining method, the fuel consumption in the Southern Coastal Mine is considered to be very high. This results in a large carbon footprint. Reducing the fuel consumption should be an important consideration in the development of an alternative mining method.

Resource/reserve estimation

Since no resource estimation will be carried out for this thesis, it is impossible to determine a reserve.

Alternative mining method

As mentioned, the design and development of a different mining, either water-based or land-based, is not within the scope. This thesis is an assessment of the current mining method, with its land accretion strategy.

1.5 Outline of report

The first chapters of the report explain the situation in the Southern Coastal Mine Namibia, also known as Mining Area No.1, which is the focus of the research of this thesis. Chapter 2 describes the local conditions that are induced by nature. Chapter 3 presents the mining operation used by NAMDEB, and also explains the reasoning behind the mining strategy. Chapter 4 elaborates on the seawalls and crosswalls constructed to serve the mining operation.

The relevant theory, obtained by a literature study, is divided in two parts. The first part (Chapter 5) concerns the formation of the diamond deposit that is mined. Knowledge of the geological setting is important to understand the reasoning behind the mining strategy, which is focused on extracting diamond from bedrock gullies. Chapter 6 describes the hydrodynamic and morphological processes that are relevant to the research undertaken for the Southern Coastal Mine. It describes how wave action leads to dune erosion and changes of the coastal profile. This chapter starts by defining how the coastal profile is built up. It continues with the hydrodynamic processes involved. Then the sediment transport phenomena that lead to morphological changes are described, after which the chapter concludes with how dune erosion develops.

The next chapter elucidates the methodology that will was used to answer the research questions of this thesis. Here the choices and necessity of the different models (SWAN 41.01A and XBeach 1.22.4672) are clarified. The model approach and use of the model SWAN is discussed in the chapter that follows (Chapter 8). The results coming from this model are used in the model simulations of XBeach, described in Chapter 9. First the model approach of XBeach is explained, and thereafter the model set-up used for simulations. Profile changes on the longer term and seawall erosion during storm events have been modeled. The chapter ends with a case study, simulating a storm of May 2015 that caused the breaching of a seawall in the Southern Coastal Mine.

Interpretation of the model results has been done in Chapter 10 and Chapter 11. The first one proposes a new seawall design. The next chapter discusses the used land reclamation strategy on the long run. Both chapters are supported by the understanding of the mining strategy that is currently applied by NAMDEB, and by knowledge of relevant morphological processes.

Chapter 12 explains how the acceptable risk level for the design process can be chosen by NAMDEB.

The obtained results are examined in a discussion chapter (Chapter 13). The main conclusions and recommendations for further research can be found in the final chapter, Chapter 14.

A list of references, a list of figures, a list of tables and a list of used symbols have been added after the final chapter.

Appendices

This report includes multiple appendices as support. Appendix A, B and C are mainly supportive in obtaining a better understanding of the current mining strategy and the land accretion strategy that are applied, since they provide maps and elaborate on the ongoing operations in Mining Area No.1.

Appendix D, E, F, G and H support the modelling involved in the research of this thesis. Appendix D investigates the effect of wind on wavegrowth. Appendix E describes how input reduction techniques should be applied to reduce the number of wave conditions in the modelling process, and thus to reduce the computational effort. Appendix F is a qualitative assessment of the parameters used in the XBeach simulations. Appendix G presents the analysis of time-series of offshore wave conditions, used to define what a storm event is. Appendix H is quantitative assessment, or sensitivity analysis, of input parameters used for XBeach. The results of investigations done in all these appendices are presented in the main report as well.

The wave and weather conditions of the storm that was modeled as a case study, can be found in Appendix I.

The set-up of a probabilistic approach for the design of a seawall can be found in Appendix J and K. The first appendix describes the theory of such an approach. The second one (Appendix K) explains how a probabilistic approach should be applied to the seawalls in the Southern Coastal Mine. These sections have not been adopted in the main report, since necessary computations are out of scope for this thesis.

The last appendix (Appendix L) describes the interaction between the client (NAMDEB) and Witteveen+Bos during the research of this thesis. This section has been added to explain the relevance of activities carried out in support of this thesis.

Chapter 2 – Local conditions

The local natural conditions existing for the Southern Coastal Mine Namibia are introduced in this chapter. The relevant conditions that need to be elaborated are: Topography, Bathymetry, Tides, Winds, Waves and Soil. These local conditions form the nature induced boundary conditions for the research in this thesis. The topographic map of MA1 used by NAMDEB is presented in Appendix A.

2.1 Topography

The research area in this thesis is Mining Area No. 1 (MA1), the green area in Figure 2.1, also known as the Southern Coastal (Diamond) Mine. It is the southern coastal zone of the area known as the Sperrgebiet in Namibia, the restricted area where NAMDEB extracts diamonds from a placer deposit.

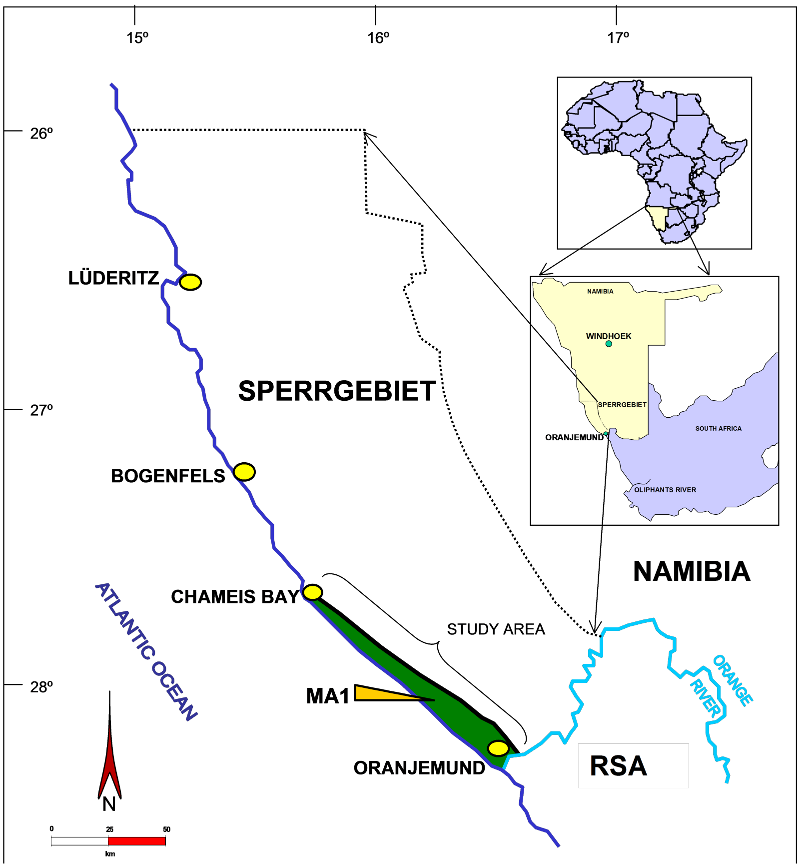

Figure 2.1: Topographic overview of Sperrgebiet, Namibia. The green area is Mining Area No. 1. The yellow dots are old settlements from where diamond mining was started.

The topographic map of MA1 used by NAMDEB is presented in Appendix A. Mining Area No. 1 is long and narrow. The length of the shoreline of MA1 is roughly 50 km. Figure 2.2 presents a schematic drawing of the MA1. The area is built up of three areas: the M-area, the U-area and the G-area. Mining activity in MA1 is ongoing in the U- and the G-area.

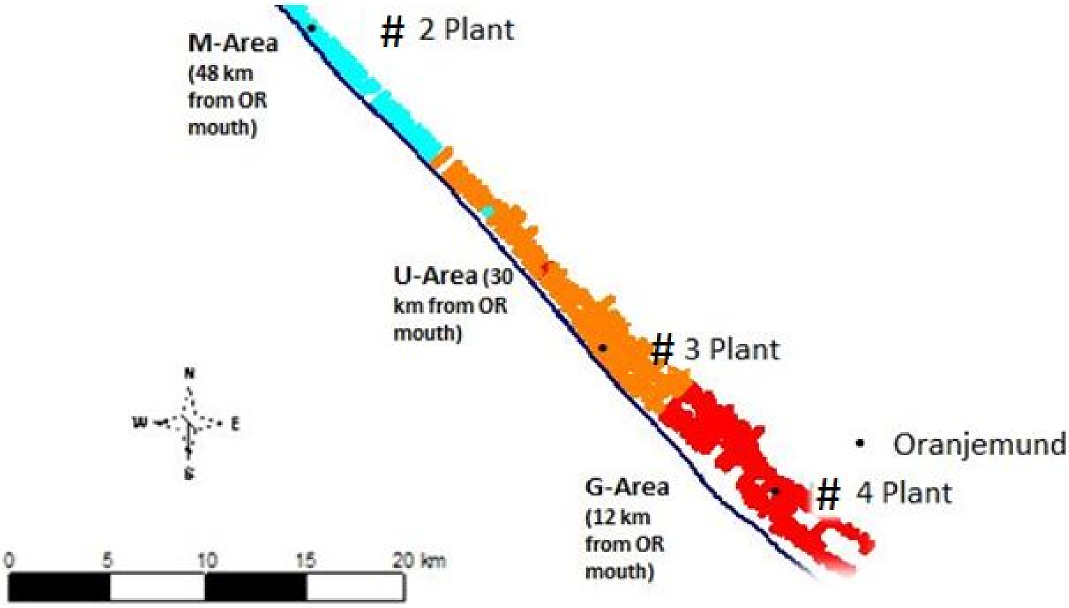

Figure 2.2: Simplified map showing the different areas of mining activity. Mining activity in MA1 is ongoing in the U-area (Orange) and the G-area (Red).

#3-Plant is the plant where bulk material from the mine (Run of Mine) is processed. #2-Plant and #4-Plant are no longer in operation. Tailingsdumps can be found next to each one of these processing plants.

2.1.1 Sand-2-Sea program

NAMDEB introduced in 2013 the Sand-2-Sea program in MA1. This means that on multiple locations along the coastline, material (overburden and tailings) is pushed into the sea to obtain land accretion. The area in the ultra-shallow water region targeted by NAMDEB's land reclamation activity, starts about 2 km from the Orange River (see Figure 2.1) mouth until 26 km from the river mouth (in coastline-parallel direction). This specific area for land accretion is chosen because from historical mining it is known that these areas contain a high concentration of diamonds. NAMDEB needs to expose these areas to get maximum benefit for the money spent on accretion. Section 3.6 elaborates further on this Sand-2-Sea program.

2.1.2 Coastline of MA1

The coastline of Mining Area No. 1 on average faces South-West. The coastline is said to be linear, as it is approximately a straight line, also seen from Figure 2.1.

Figure 2.3: Picture of southern part of the coastline of Mining Area No. 1.

On a smaller scale the coastline is not straight. The picture in Figure 2.3 shows discontinuities along the coastline. These discontinuities are enhanced by the Sand-2-Sea program (see section 3.6), where sand is nourished into the beach from land. Due to the land reclamation works the coastline becomes curved on average. The picture in Figure 2.4 also shows a slight curvature of the coastline. Along (almost) the entire coastline a seawall, made out of sand, is built to protect the mining cells.

Figure 2.4: Aerial image of part of Mining Area No. 1. #3-Plant is visible in the picture. One can see that the coastline has a smooth curvature. This picture shows the northern part of the specific area that is targeted by the Sand-2-Sea program.

2.1.3 Bathymetry / depth contours

Section 5.3 explains how diamonds are trapped on wave-cut terraces. These terraces also occur offshore and are clearly visible when studying the depth contours in front of MA1. The diamond deposit, and with that the terraces, is very wide close to the Orange River Mouth (about 2 km wide) and very narrow up north, close to #2-Plant. This is visualized in Figure 2.5. The formation and definition of terraces (of raised beaches) has been worked out in section 5.3.

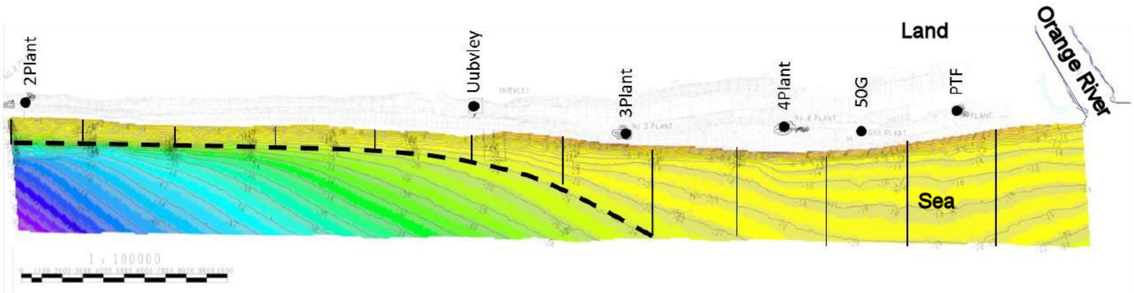

Figure 2.5: Depth contours in front of the coast of MA1, going from orange (shallow) to purple (deep). It can be seen that the terraces are much wider close the Orange River Mouth.

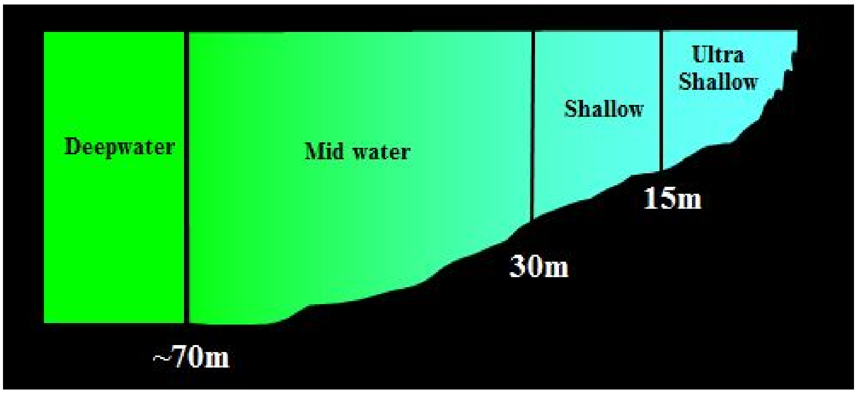

Figure 2.6: Definition of different depth regions in NAMDEB waters

The focus, in expanding the on land mining activity (dry mining) seawards, is on the Ultra Shallow Water and part of the Shallow Water region (Anker, 2014). Figure 2.6 above shows schematically the different water depth regions that are of importance to NAMDEB. The 15m water depth line is 500 to 700 m away from the coastline on average between #4-Plant and PTF (see Figure 2.5).

2.2 Tides

The southern Namibian coastline has a so-called micro-tidal regime (Jacob et al., 2006). The tidal range is less than 2 m normally. Tidal range at neap tide is typically 0.6 m and at spring tide typically 1.6 m. The tides are semi-diurnal (two high and two low tides occur per 24 hours). Table 2.1 presents the tidal ranges for the coast of the Sperrgebiet.

Table 2.1: Tide levels for Port Nolloth (80 km south of Oranjemund) and Luderitz (10 km north of Elizabeth Bay). South African Tide Tables, SA Navy Hydrographic Office, 2011.

	Oranjemund / Port Nolloth	Elizabeth Bay / Luderitz
Highest Astronomical Tide (HAT)	+ 1.325 m	+ 0.935 m
Mean High Water Springs (MHWS)	+ 0.985 m	+ 0.595 m
Mean High Water Neaps (MHWN)	+ 0.475 m	+ 0.165 m
Mean Low Water Neaps (MLWN)	-0.145 m	-0.405 m
Mean Low Water Springs (MLWS)	-0.645 m	-0.825 m
Lowest Astronomical Tide (LAT)	-0.925 m	-1.055 m

2.3 Winds

Southerly winds dominate, and have been dominating, the coastal climate of southern Namibia. It is because of these strong southerly winds (Southerlies) that Aeolian diamond deposits were formed in the northern part of the Sperrgebiet (Schneider, G.I.C. and Miller, 1992). These Southerlies have been constant and long-lasting for millions of years. Wind records for 30 years (1983-2013) are available and have been summarized in a wind-rose, see Figure 2.7. The location is about 100 km offshore of MA1. The wind data (and also the wave data) that are used to study the climate of the Southern Coastal Mine in Namibia are derived from the ECMWF database[1]. It can be seen from the wind-rose that the direction of the prevailing wind is approximately parallel to the coastline.

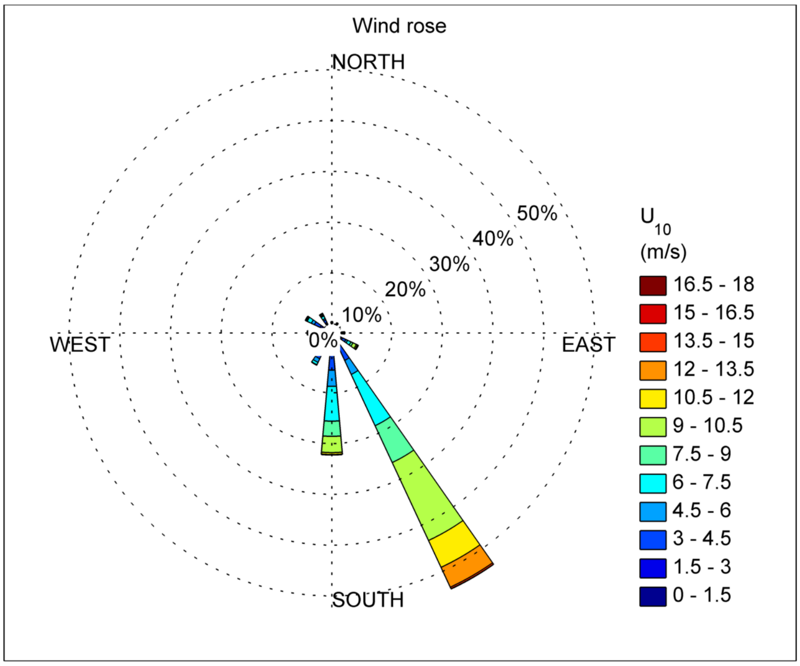

Figure 2.7: Wind rose of wind records at 28.5 degrees South, 15 degrees East.

[1]European Centre for Medium-Range Weather Forecasts (www.ecmwf.int)

Wind speeds are strongest during summer (Dec – Feb). Northerly and easterly winds can occur at times during autumn and winter. Table 2.2 below presents wind measurements from NAMDEB at Oranjemund, which is on land.

Table 2.2: Windspeed measurements, Southern Coastal Mine, Namibia. (NAMDEB 2013).

Percentage exceedance of wind speed				
	50%	10%	5%	1%
Oranjemund	4.6 m/s	8.8 m/s	10.3 m/s	13.2 m/s

Appendix D explains the effect of these winds on the waves approaching the coast. And thus how the winds indirectly influence erosion to the seawalls and change the coast.

2.4 Waves

The wave climate is dominated by long period high swell waves. The swell waves originate mostly from passing frontal systems in the South Atlantic, far south west of Namibia. Wave records, also for 30 years, are available for offshore waves in deep water, in this case a depth of almost 2 km. They are summarized in the wave rose of Figure 2.8. The most frequent wave direction is almost perpendicular to the coastline.

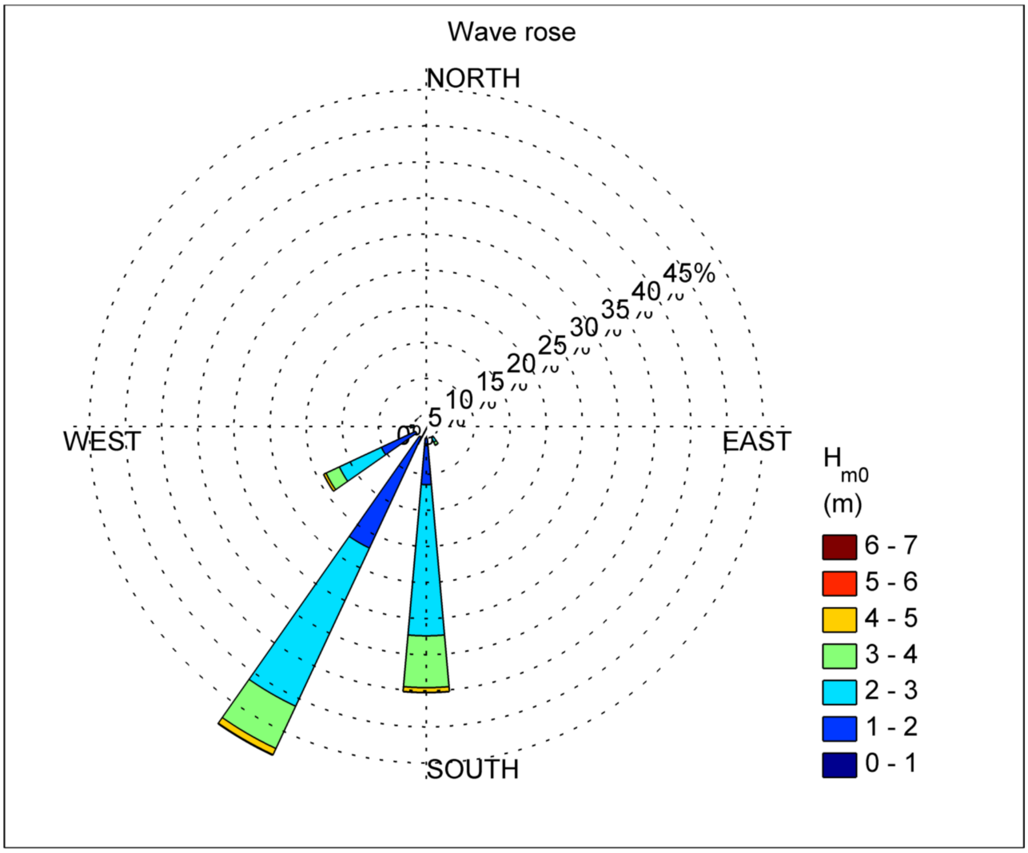

Figure 2.8: Wave rose of wave records at 28.5 degrees South, 13.5 degrees East.

Wave records have been analyzed extensively during the research for thesis. Chapter 8 (Modeling with SWAN) explains how these offshore wave conditions should be translated to near shore wave conditions. Section 9.2.4 and Appendix E discuss how the number of wave conditions can be reduced to find the normative wave conditions acting on the coastline. And lastly, section 9.2.5 and Appendix G elaborate on how storm conditions must be defined in terms of wave conditions.

2.5 Sand properties

The soil of the Southern Coastal Mine is non-cohesive sand. Before mining activity started there was a thick top-layer of fine to medium grained Aeolian sand lying on a thick layer of medium to coarse grained sand. Because of mining activity together with the Sand-2-Sea program the beach sand is relatively coarse. This can also be derived from the picture in Figure 2.4, which is taken on the northern end of mining activity. If we move to the left in this figure we move away from the mining and Sand-2-Sea program and we see the water becoming more turbid. This is because of a difference in grainsizes of the beach sand between the beaches that are part of the Sand-2-Sea program and the beaches that are not.

The particle size distribution of the beach sand has been evaluated for different locations in the Southern Coastal Mine. However, the smallest sieve diameter that was used has a diameter of 1.4 mm. 0 – 1.4 mm is still a considerably large range. And, as can be expected, the largest fraction of the tested sediment lies within this range. For sediment transport the effect of the grain size is very large.

The focus of this research is on the part of the mine where land reclamation is carried out. The beaches in this region are said to be coarse grained (McLachlan, 1996). A median grainsize of 400 μm is chosen to calculate with. However, this must be verified by soil tests.

In addition to sand, there are also tailings present on large tailingsdumps in MA1 (see for example Figure 2.4). This material has a larger median grainsize than sand, but also a wider spreading (grainsizes in the range of 2 to 25 mm). Only sand will be considered as construction material for seawalls.

Chapter 3 – Mining method and land reclamation strategy used for diamond extraction

Data from the Southern Coastal Mine of NAMDEB's diamond mining activities in southwest Namibia were obtained during a fact-finding study carried out by the author, Joel Anker, from September till November 2014. This chapter explains the mining method, with its land reclamation strategy, that is currently used to extract diamonds. It also discusses the reasoning behind the mining method. The diamond deposit and the mining operation to extract these diamonds are complex and unique. Appendix B elaborates further on the mining process used by NAMDEB. Appendix C elaborates on how land reclamation is applied to support the mining process.

3.1 Introduction

A simplified overview of MA1 is presented again in Figure 3.1. Mining activity in MA1 is ongoing in the U- and the G-area.

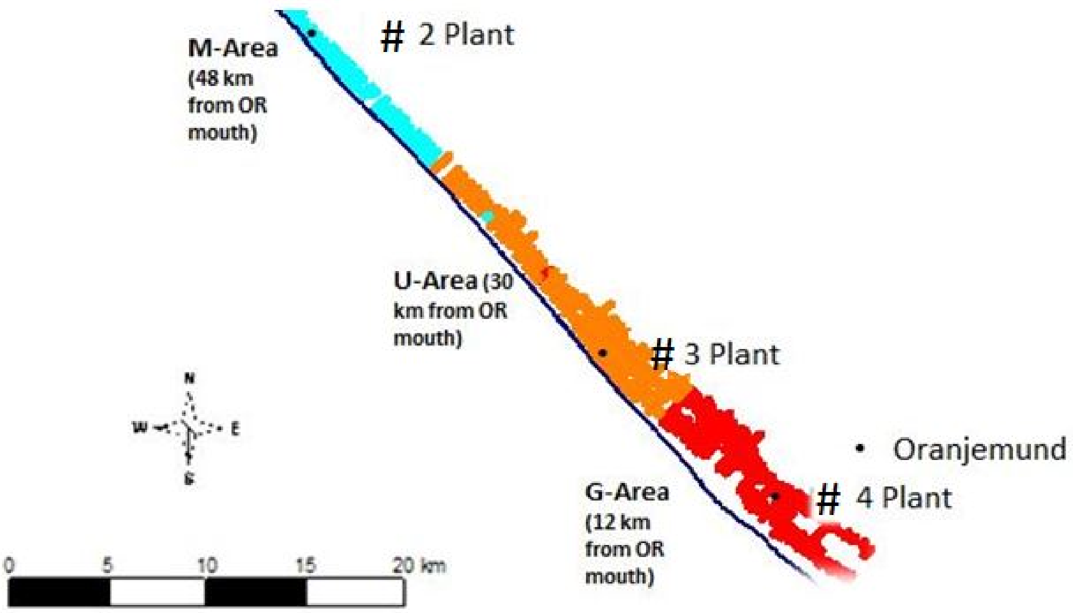

Figure 3.1: Simplified map showing the different areas of mining activity

The most important features of the topography of MA1 are:

- The coastline of MA1 faces on average South-West.
- Along (almost) the entire coastline a seawall, made out of sand, is built to protect the mining cells.

- On multiple locations along the coastline material (overburden and tailings) is pushed into the sea to obtain land accretion.
- #3-Plant is the plant where bulk material from the mine (Run of Mine) is processed.
- The diamond deposit, and with that the terraces, is very wide close to the Orange River Mouth (about 2 km wide) and very narrow up north, close to #2-Plant.

3.2 Mining target

The mining target in the Southern Coastal Mine (MA1) is to reach maximum plant capacity (850 tons/hour) for #3-Plant, with a desirable cash outflow. Everything in the operation has to be in line with this business plan. The life of mine is (determined early 2014) until 2031. Until that year mining is planned and diamond extraction with the current mining method is said to be profitable.

Run of Mine (RoM) is coming from three areas: The U-area (more north in MA1), the G-area (more south in MA1) and from old dumps (for reprocessing). Two completely different areas (G and U) are always mined at the same time. This has to be done to mitigate the risks of having a production break-down. This risk is mainly caused by the probability of seawall failure. Both the G- and U-area are close to the shore and are protected by seawalls and separated by crosswalls.

The choice for mining a specific block is made by looking at the average diamond grade of a certain block. In this way the maximum plant-throughput can be reached while at the same time desired cash outflow can be obtained. When the maximum plant-throughput cannot be delivered by the G- and U-areas, or when the grades of the two blocks that are mined out at the same time are considerably high, old tailings (still containing) diamonds are processed in the plant.

3.3 Exploration

In MA1, for the Linear Beach deposits, exploration is done with a walking platform in the sea, the PDP (Prob Drill Platform). This is done to prove the presence of layers with gravel/pebbles (grainsize $>$ 5 mm), favourable for hosting diamonds. The sampling of soil to determine the diamond grade is done on land in a later stage

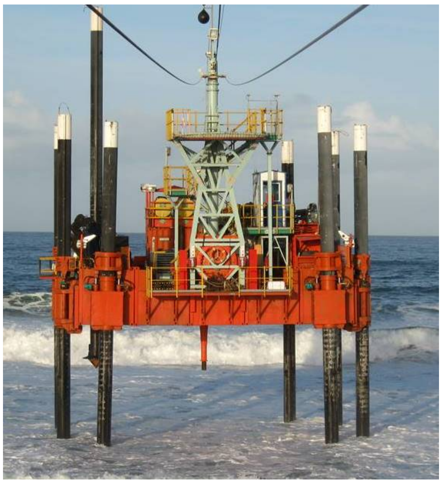

Figure 3.2: PDP (Prob Drill Platform), used by NAMDEB for Exploration in the surf zone

The PDP (Figure 3.2) is a walking platform, drilling in the ultra-shallow water regions. The PDP takes a series of samples every 400 m alongshore. A series of samples is taken perpendicular to the coastline every 12.5 m offshore until a distance of 250 m offshore or until the maximum workable depth is reached. This is defined as 4 m waterdepth + 3 m high swell waves.

3.4 Mining method

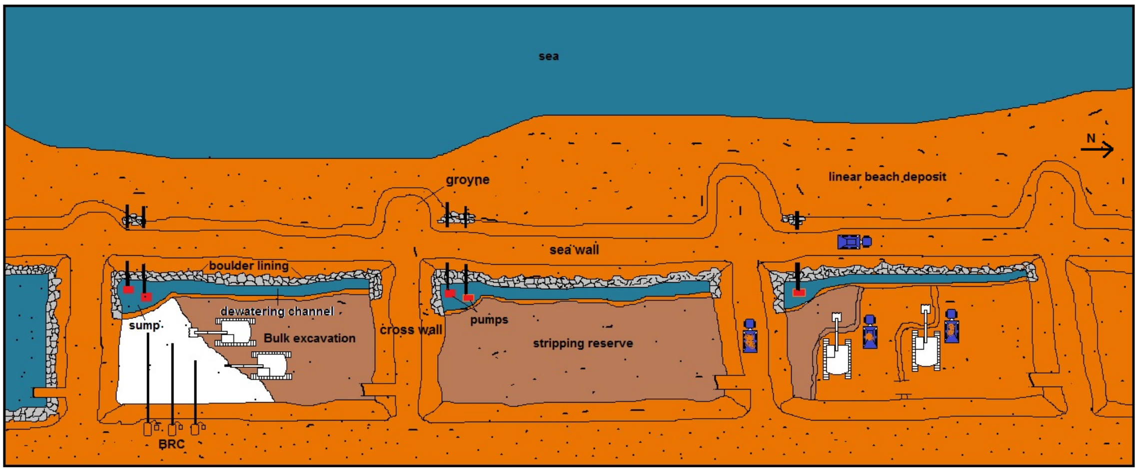

Figure 3.3: Schematic drawing of steps in excavation process

The steps in the mining process are presented in Figure 3.3. The constantly fed extensions of the crosswalls form groynes. One block (the right one) is being stripped until the level of bulk material (block in the middle). The next block (left one) is being mined. A mined out block is no longer dewatered and so it slowly fills up with water. Overburden stripping is done with a CSD (Cutter Suction Dredger) if possible, otherwise by means of conventional excavation (Figure 3.4), using Hydraulic Excavators and Articulated Dump Trucks (ADT).

Bulk excavation (all bulk going to the plant) is done with conventional loading and hauling (Figure 3.5), using Hydraulic Excavators and Rigid Frame Trucks (RFT).

Figure 3.4: Conventional excavation of overburden with Hydraulic Excavators and ADT's

Figure 3.5: Conventional hauling and loading of bulk material.

The final cleaning of bedrock is done with vacuum cleaners (Transvacs), shown in Figure 3.6 and 3.7.

Figure 3.6: Transvacs used in the cleaning the bedrock

Figure 3.7: Cleaning the bedrock. Worker operating a Transvac

All overburden is dumped at the extension of a crosswall. ADTs handle in the order of 10 million m^3 of overburden sand per year (Anker, 2014). When the crosswall is extended enough in seaward direction and the beach has accreted far enough, the seawall is moved seawards and new mining blocks are formed behind the seawall. This land reclamation strategy makes expansion of mining activity in the ultra-shallow water region possible using the same mining method. Between 2013 and 2015 seawall sections in the areas of ongoing mining activity were shifted on average every 18 months with a distance of 80 to 150 meters.

The mining process is described and discussed in more detail in Appendix B.

3.5 Seawalls and crosswalls

Seawalls have been built extensively along the beach of Mining Area No. 1 (MA1). The seawalls are the primary protection for the mining blocks against flooding. The crosswalls separate the large mining blocks from each other. They protect the mining blocks against flooding with water from neighbouring mining blocks. Besides that, they also serve as roads for ADTs. Since the development of the Sand-2-Sea program in 2013 (see section 3.6), the crosswalls are extended seawards to act as groynes.

A seawall is built out of overburden material coming from the mining blocks. With ADTs the material is dumped on the walls. The innertoe of the seawall has a thick layer of gravel and boulders to counteract the outflow of fine material. The seawall also has a channel at the innertoe to collect seepage water, during “dry” operations in the mining pit.

Further description of seawalls and crosswalls follows in the report in Chapter 4. In that chapter also the difficulties in constructing walls and risks of the seawalls are discussed. The standard NAMDEB uses for seawall construction can be seen in the figure below. The standards were developed before the implementation of the Sand-2-Sea program.

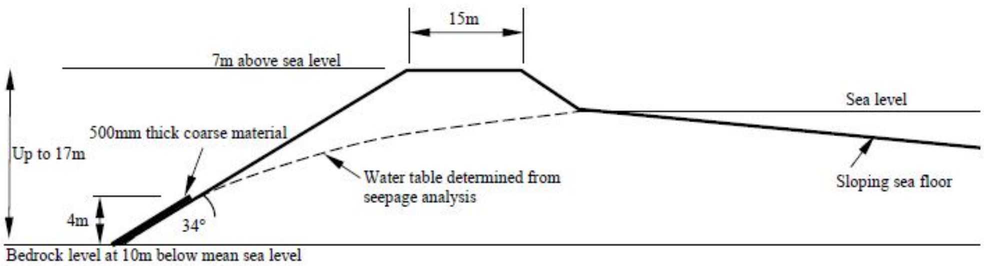

Figure 3.8: Design seawall for mining pit with a depth up to 10m below mean sea level. (NAMDEB)

3.6 Land reclamation to expand mining activity seawards in MA1

As mentioned, all overburden is dumped at the extension of a crosswall. All tailings (plus some old waste dumps) are brought to the end of larger groynes. This is all done with the purpose of reclaiming new land for mining, the so-called Sand-2-Sea program. With the construction of large groynes in combination with smaller groynes (extensions of the crosswalls) land must be reclaimed. Besides groyne-systems, slimes and dredged material are pumped to the beach directly.

There are currently three types of groyne-systems.

1. A large groyne with spreaders near #3-Plant.
2. Conveyor belt systems to bring old waste and tailings to the sea.
3. The extension of crosswalls, carried out by ADT's near the mining operations.

Besides groyne-systems, material is also pumped to the beach at three locations.

1. Dredging vessel Beachcomber is pumping overburden from the stripping operation in the G-area directly to the beach.
2. Dredging vessel Gaeb is pumping material from the tailingsdump next to #4-Plant directly to the beach.
3. Slimes (material with a grainsize smaller than 2 mm) coming from #3-plant are pumped directly to the beach.

The current business plan is until 2031. If possible, mining activity should proceed beyond this year. The reclamation of land should have reached the 12 meter water depth line on average for the targeted areas in 2031. However, for the region close to #3-Plant a depth of 16 meters must be reached. The distance is on average 450 m from the averaged high waterline of 2014. NAMDEB will continue the shifting of the coastline seawards as far as financially and technically feasible. The focus of the Sand-2-Sea program, and so the land reclamation, is solely on the south of MA1. Here the beach terraces are the widest (see section 2.1), meaning that the sea is relatively shallow for a large offshore distance. This is also where relatively the highest diamond grades are expected since it is close to the source, the Orange River mouth (see Chapter 5 for explanation about the diamond deposit). The total pumping rate with this Sand-2-Sea program must increase to be in the order of 20 million m^3 of sand per year.

Appendix C elaborates further on the land reclamation strategy applied by NAMDEB in MA1.

3.7 Reasoning behind mining strategy

The diamond deposits on land in Mining Area No. 1 are nearing depletion. For this reason NAMDEB has expanded its mining activity in a seaward direction. As mentioned before, NAMDEB geologists believe that the linear raised beaches, containing diamondiferous gravel deposits, found on land and in the midwater region, can be interpolated to the shallow and ultra-shallow water region (Anker, 2014).

The most important reason for the application of land reclamation is that "Dry mining" is a must for NAMDEB. With the currently available technology, diamonds in Mining Area 1 (MA1), can only be mined out in dry conditions. Since approximately 60% of the diamonds are found within the gullies, the gullies need to be cleaned properly. Wet mining, by means of dredging, is not selective enough to obtain the same high recovery as dry mining. The roughness of the wave climate in the ultra-shallow water region makes dredging also particularly difficult. For these reasons new land must be reclaimed on the sea first, before mining can be done.

Besides these reasons, the beach accrued even before the Sand-2-Sea program was initiated. This is seen by NAMDEB as a certain guarantee that it will accrue even further with the Sand-2-Sea program.

Chapter 4 – Current seawalls and crosswalls

This chapter describes the necessity, the construction and the maintenance of the current sea- and crosswalls in Mining Area No. 1, also known as the Southern Coastal Mine Namibia. Information was obtained in a fact-finding mission, executed by Joel Anker in 2014

4.1 Function

Seawalls have been built extensively along the beach of MA1. The seawalls are the primary protection of the mining blocks against flooding from the sea. The crosswalls, like the one in Figure 4.1, separate the large mining blocks from each other. They protect the mining blocks against flooding due to water from neighbouring mining blocks. Besides that, they serve as roads for ADT's. Since the development of the Sand-2-Sea program, the crosswalls are extended seawards to act as groynes.

Figure 4.1: Crosswall separating to mining blocks. This wall is also used as a service wall. One can see maintenance of the crosswall being carried out with an ADT and a dozer

4.2 Seawall standards

The standards used by NAMDEB for the construction of seawalls are defined in the code of practice for seawall construction and repair (NAMDEB, 2013). Figure 4.2 below shows the outline of the seawall according to these standards. The crest height of the seawall must be 7 meters above mean sea level. The crest width must be 15 meters.

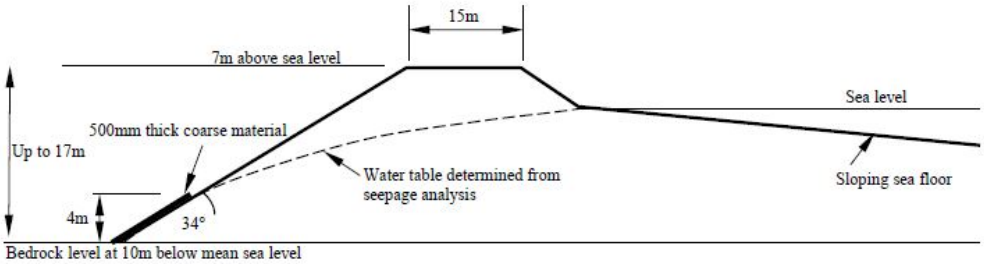

Figure 4.2: Design seawall for mining pit with a depth up to 10m below mean sea level (NAMDEB, 2013).

4.3 Construction

A seawall is built out of overburden material excavated from the mining blocks. With ADT's the material is dumped on the walls. The innertoe of the seawall has a thick layer of gravel and boulders, as shown in Figure 4.3, to counteract the outflow of fine material. The seawall also has a channel at the innertoe, as shown in Figure 4.4 to collect seepage water, during "dry" operations.

Crosswalls are extended into the sea, so they can act as groynes. Once enough land is accrued, the current seawall between two crosswalls is moved 80 to 120 meters in seaward direction. In the direction parallel to the coastline every 300-500 m "normally" a crosswall is constructed.

Figure 4.3: Seawall with clear boulder lining on the innerslope

Figure 4.4: Seepage water channel at the innertoe of the seawall, with waterpumps at the left

Figure 4.5: ADT driving on the seawall to dump material for building a crosswall extension

Figure 4.6: Construction of crosswall extension. Dozer pushing dumped material in the sea.

It can be seen in Figure 4.5 and Figure 4.6 that the extension of the crosswalls is made by dumping material with an ADT and pushing it unto the beach with a dozer.

Figure 4.7 shows a picture of a next crosswall extension taken standing on another crosswall extension (or groyne). Once the crosswall is extended, the seawall close to it experiences less (and decreasing) wave attack.

Figure 4.7: Beachline with crosswalls with a distance of 350 m.

The most abundant material available for seawall construction is overburden sand, which is essentially cohesionless medium to coarse grained marine sand. In some areas the top portion of the overburden consists of Aeolian silty sand. Material with an internal friction angle of less than 34 degrees should not be used for seawall construction, according to the code of practice used by NAMDEB (NAMDEB, 2013).

4.4 Maintenance strategy

Maintenance of the seawalls is difficult. NAMDEB applies a condition-based maintenance strategy. The walls are checked once per day. When the foreman observes that the windrow, (additional dike along the road) is lower because sand is taken away by the sea, additional sand is ordered to be nourished. Seawalls are often over-dimensioned, when compared to their standards.

In the past the maintenance of the seawalls was a very difficult and costly task. Since the start of the Sand-2-Sea program in 2013, the wave attack on the seawalls has become less, as the crosswalls are extended into the sea and beaches have grown.

4.5 Need for a new seawall design standard

In the current situation NAMDEB uses standards for the seawalls according to a code of practice of 2013. This code has been developed before the implementation of the Sand-2-Sea program, so before the land accretion strategy with groyne development. The schematic drawing of this standard was presented in Figure 4.2.

The focus of the current standard is mainly on the stability of the innerslope of the seawall. The width and the crest height of the seawall are determinative for flood protection, but not investigated properly. Standards for the innerslope are still important. Because of the dipping of the bedrock in seaward direction (explained in Chapter 5), more overburden sand needs to be removed when the mining operation expands seawards. As a consequence, the inner slope of the seawall and the hydraulic head in the mining pit become larger, causing more seepage water and larger risks of seawall failure. Measures will have to be taken for the innerslope to prevent dangerous situations. This is included in the currently applied code of practice.

A different standard for the seawall, leading to less maintenance and a lower crest level, could reduce NAMDEBs operation costs with probably millions of USD per year. In 2013 the amount of soil being moved to construct and maintain the seawalls was estimated to be 300,000 m^3 per month.

An important hypothesis of this thesis, as mentioned earlier, is that the design standards for the seawall can be adjusted. In particular, the crest level could be lowered leading to a dramatic reduction in construction and maintenance costs.

Chapter 5 – Linear Beach Terraces: A marine-placer deposit

This chapter describes the deposition of diamonds in Mining Area No. 1 (MA1). Gaps in resource estimation are discussed. Diamonds have been transported and deposited by the Orange River on beach terraces, formed by wave-rock interaction. The terraces with gullies are the trapsites for the diamonds and form a marine-placer deposit suitable for diamond extraction.

5.1 Placer deposits

A placer deposit is an accumulation of economically valuable minerals formed by mechanical processes, such as wind, waves or flow. A placer deposit is characterized by a trapsite where minerals accumulate, and by the mechanical process that brought the minerals to the location of the deposit.

The Southern Coastal Mine Namibia owes its existence to a marine placer deposit. For millions of years the Orange River has eroded Kimberlite pipes, containing diamonds, in the hinterland (South-Africa and Botswana). This caused the transport of diamonds towards the Namibian coast (Moore and Moore, 2004).

Trapsites for diamonds along the coast of Mining Area No. 1 were created by wave-rock interaction. The sections below elaborate on how these processes have led to the formation of a placer deposit along the coast.

5.2 Deposition of diamonds

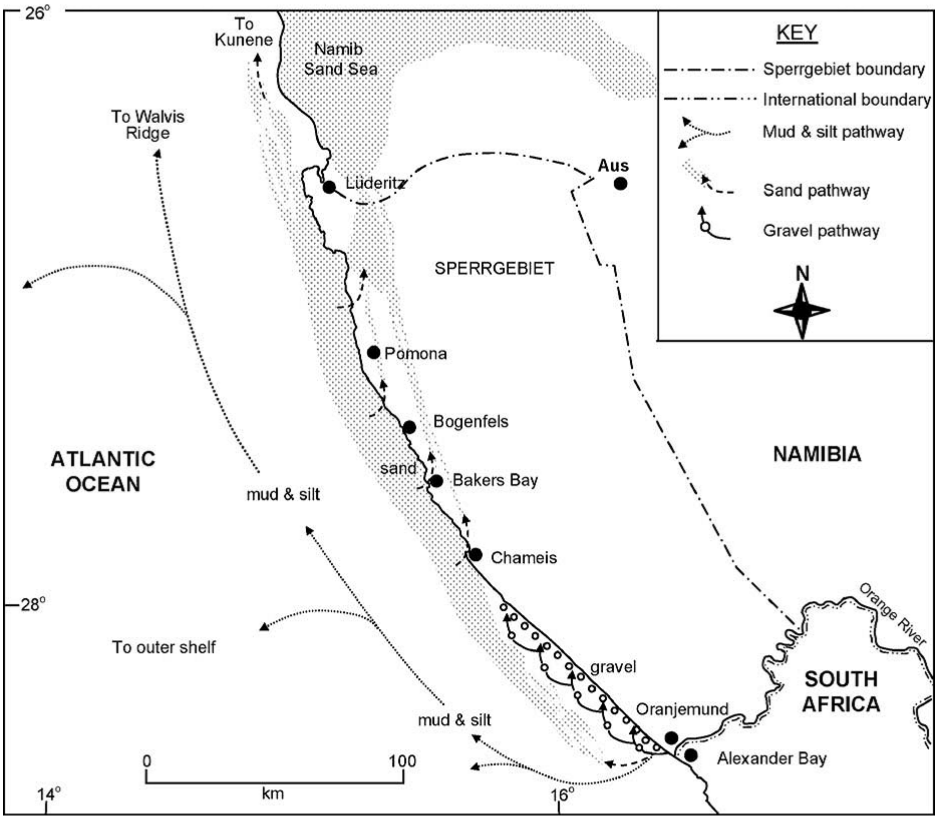

Figure 5.1: Sediment disposal paths for gravel, sand and finer sediment on the continental shelf, offshore Namibia (Spaggiari et al., 2006)

The Southern Coastal Mine (or Mining Area No. 1) is the almost straight (linear) coastline in the most southwestern part of the Sperrgebiet. This diamondiferous Palaeocene-beach deposit is in the form of a very narrow triangle. It is 100 km long and has a width of 3 km at its start at Oranjemund and 200 m at its northern end, Chameis Bay. Diamonds were transported by the Orange River in the south (see Figure 5.1) and transported northwards by the wave-induced longshore current. Diamonds follow the gravel pathway (Figure 5.1). Although diamonds are mainly much smaller in size than the gravel, the specific gravity of diamonds is relatively high (3.52, compared to 1.44 – 2.00 for sand/gravel), causing diamonds to settle together with relatively large grains of gravel / pebbles.

5.3 Trapping of diamonds on linear (raised) beaches

Mining Area No. 1 (MA1) is the part of the Sperrgebiet, where diamonds are trapped in the gullies along the linear beaches. An east-west cross section shows so-called raised-beach deposits. There are six raised-beaches above current sea-level, shown in Figure 5.2.

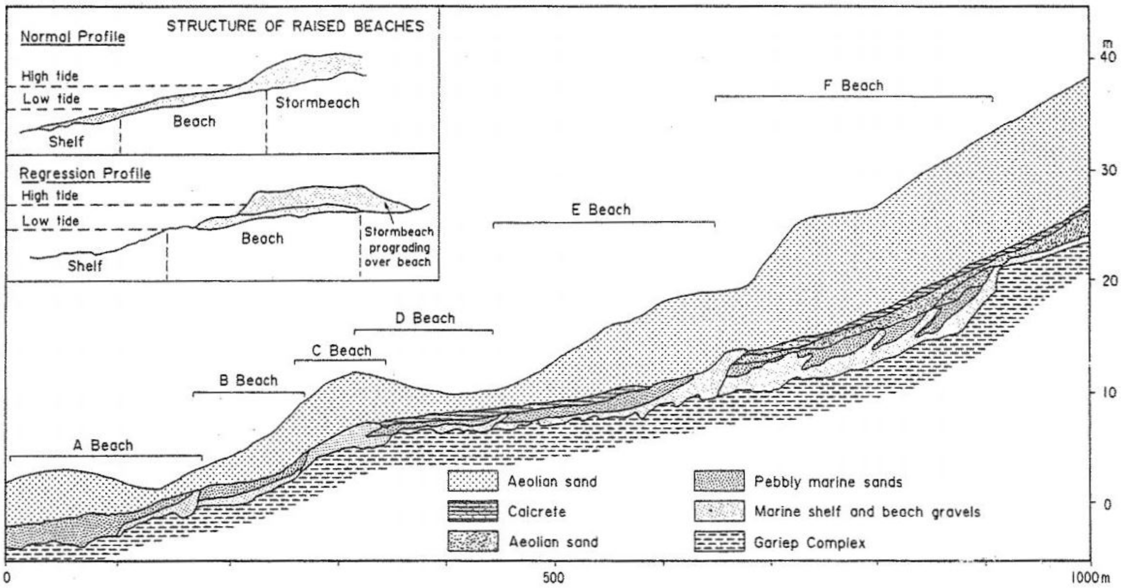

Figure 5.2: Schematic east-west cross section of raised beach deposits of MA1, showing the stratification of sediments deposits on top of the bedrock. (Schneider, G.I.C. and Miller, 1992)

Wave-cut platforms provided trapsites for diamondiferous gravel. The bedrock of these platforms is formed predominantly by siliciclastic rocks of the Late Proterozoic (Jacob et al., 2006). The different wave-cut, or marine-cut, platforms have formed during the Quaternary, and indicate different sea level elevations. The platforms, or raised beaches, slightly dip in a westward direction. The onshore MA1 diamondiferous marine deposits range in age and elevation from the Late Pliocene-Early Pleistocene (D-, E-, F-Beaches, which are +30 to +12 m), through the Mid-Pleistocene (C-Beach, +8 m) to the Late Pleistocene (B-Beach, +4m) and Holocene (A-Beach, +2 m, but its diamond deposit partly below sea level). The bedrock (or footwall) comprises of alternating bands of competent rock (meta-arenites) interbedded with softer, highly weathered rock (chloritic schistose metasediments) (Jacob et al., 2006). Where these alternating layers are between 0.5 m and 3 m thick, differential erosion is promoted and well-developed gullies occur. These gullies form the major trapsite for diamondiferous gravel along the linear coastline of MA1. Decelerating flow in and above the gullies cause heavy particles, like pebbles and diamonds, to settle.

Figure 5.2 also shows the different sediment layers on top of the bedrock (Gariep Complex in Figure 5.2). The top layer in the whole of Mining Area No. 1 is Aeolian sand. Diamonds on the raised-beach deposits are concentrated in the basal 2 m of marine shelf- and beach gravel, which overlies the platforms, but mostly (around 60%) in the gullies.

5.4 Orientation of the gullies

Between the Orange River Mouth and Chameis Bay three different bedrock gully types can be distinguished in the, normally shore-parallel, bedrock platforms. As visualized in figure 5.3, these are the swash-parallel gullies in the south (1), strike-parallel gullies in the central sector

(2) and joint gullies in the north (3). Individual gullies can be up to 100 m long by 4 m wide and 7 m deep.

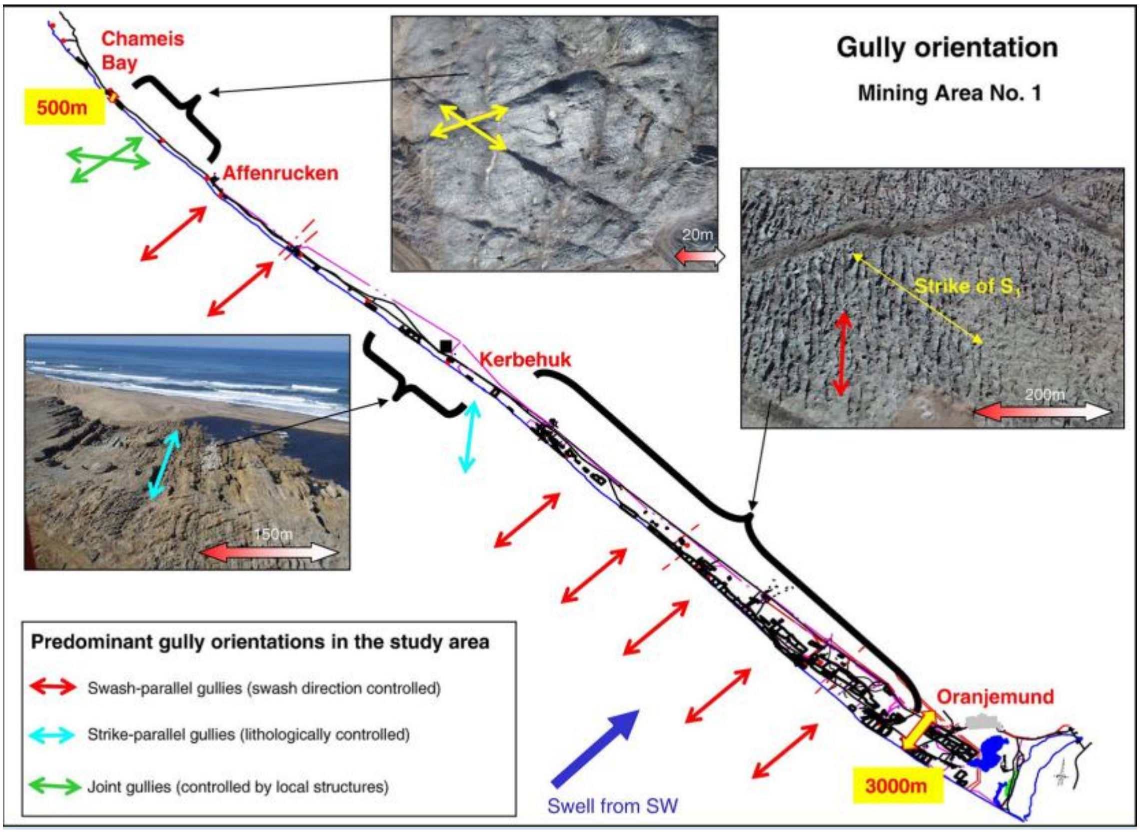

Figure 5.3: Northward gradation in gully type from the Orange River mouth to Chameis Bay, MA1, showing the three different principal gully types. Photographs are oblique aerials and the gullies are ca. 2 m wide (Jacob et al., 2006).

1. Swash-parallel bedrock gullies. These gullies (red arrows in Figure 5.3) occur in the southern part of MA1. The bedrock here dips 45 degrees to the west. Differential erosion has lead here to the formation of swash-parallel gullies.
2. Strike-parallel bedrock gullies. The dip of the bedrock is here nearly vertical. Again differential weathering eroded most of the softer schistose units, forming gullies.
3. Joint gullies. These gullies are structurally controlled. Due to volcanic activity joints were formed. These 'weaknesses' in the bedrock give rise to gully formation.

5.5 Offshore placer deposits / submerged beaches

The diamond placer deposits further offshore are mainly shore-parallel gravel terraces, formed in a similar way as the linear beach deposits. Raised beaches are now called submerged beaches. The platforms/terraces are present at a level of 20, 40 and 120 to 130 m below present mean sea level.

Between 120 to 30 m water depth, the middle continental shelf, the diamondiferous gravel placers rest on cemented Cretaceous sediments acting as footwall (Corbett and Burrell, 2001).

The placer deposits formed again during the Pleistocene, and are found in trap sites like gullies, potholes and cliffs. The largest diamond deposits formed during the last Glacial event of 19,000y BP, when there was a sea-level still stand at 120 m below present sea level.

5.5.1 Shallow water:

In the region between 0 and 30 meters (shallow and ultra-shallow water regions) below present sea level there are many gaps/unknowns in the deposition of diamonds. There is no reason yet to suspect otherwise that there are diamondiferous gravel layers on submerged beaches and in the accompanying gullies. The major assumption, partly confirmed by exploration work with the PDP (see Section 3.3) is that the mining activity can be extended from the existing coastline towards the current 20 meters depth contour line, which is in the shallow water region (see Figure 2.6).

Geologists are currently working on a geological model combining samples with bathymetry and extrapolated data.

Chapter 6 – Hydrodynamics and morphological changes in the upper shoreface

This chapter describes the hydrodynamic and morphological processes that are relevant to the research done for the Southern Coastal Mine. It basically describes how wave action leads to dune erosion and changes of the coastal profile. This chapter starts by defining how the coastal profile is built up. It continues with the hydrodynamic processes involved. Then the sediment transport phenomena that lead to morphological changes are described, after which the chapter concludes with how dune erosion develops.

6.1 Coastal profile

A cross shore coastal profile consists of a lower shoreface and an upper shoreface. The lower face extends from the edge of the continental shelf to the surf zone. A schematic representation of the upper face is found in Figure 6.1. The upper shoreface stretches from the breaker bar up to the first dune row. The breaker bar is where most waves start to break. The surf zone is the region where broken waves propagate through the nearshore until they reach the coast line. The coast line (or shore line) is the intersection between the still water level, at a certain tidal elevation, and land. The swash zone is the area of the beach between maximum wave run-up and run-down.

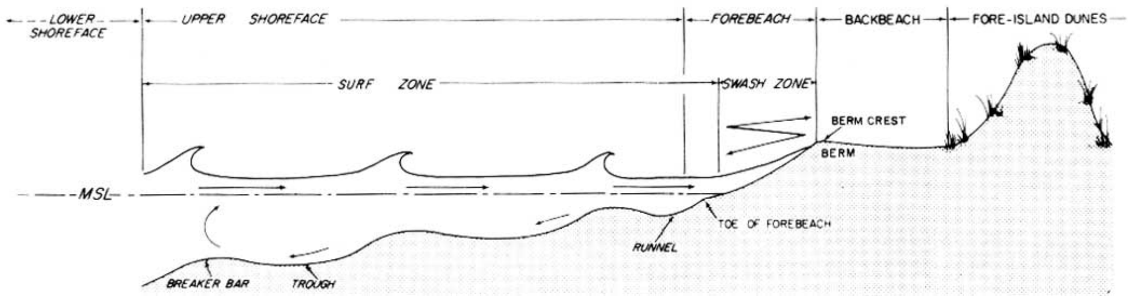

Figure 6.1: Typical upper shoreface profile. After Weise and White (1980)

On the timescale of hours to decades (engineering scales) only the upper shoreface is said to be morpho-dynamically active (Stive and De Vriend, 1995). Therefor, for the investigation of dune erosion only the upper shoreface is relevant.

6.1.1 Beach steepness

The beach state, and with that the beach steepness, can be described with the Iribarren parameter ζ and the dimensionless fall velocity of sediment Ω. The Iribarren parameter states the effect of the bed slope on the breaking process of waves. Equation 6.1, determined by Battjes (1974), shows how this parameter guides the wave breaking process.

$$\zeta = \frac{\tan\alpha}{\sqrt{H_0/L_0}} \tag{6.1}$$

Where $\tan\alpha$ is the beach steepness, H_0 is the significant wave height in deep water and L_0 is the wave length in deep water. Figure 6.2 illustrates the different wave breaker types and how they depend on the Iribarren parameter. For spilling breakers (low Iribarren parameter value) practically all wave energy is dissipated in the wave breaking process. Where surging breakers occur, almost all wave energy is reflected. Collapsing breakers and plunging breakers are intermediate forms.

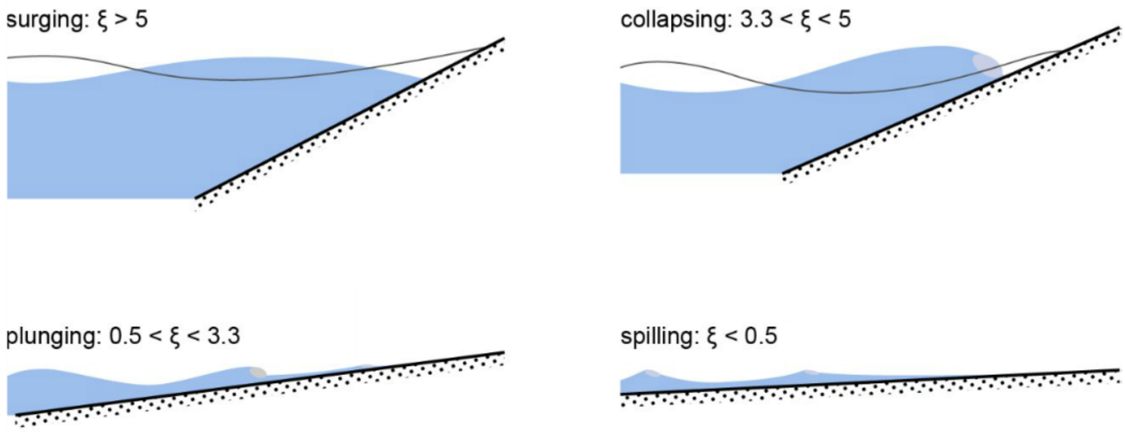

Figure 6.2: Types of wave breaking processes. After Bosboom and Stive (2013).

The beach in front of the Southern Coastal Mine Namibia is known as rather steep. This also follows from bathymetry data as discussed in section 9.2.3. The foreshore goes from MSL -8m to MSL +2m in about 220 m ($\tan\alpha = 0.42$) on average. Both the wave height and the wave period are large. NAMDEB calculates with a significant offshore wave height of 2.5 m and an offshore wave peak period of 14 s. This leads an Iribarren number of about 0.5. Pictures show that plunging breakers are dominant for this beach.

The dimensionless fall velocity Ω is used to state whether a beach state is dissipative, reflective or intermediate in terms of wave energy reduction. This parameter is defined by:

$$\Omega = \frac{H_b}{w_s T} \tag{6.2}$$

Where H_b and T are the wave height and wave period, respectively, at breaking. w_s is the sediment fall velocity (or settling velocity). w_s depends above all on the sediment grainsize D_{50}, and w_s is larger for a larger D_{50}. A reflective beach state is characterized by a beach face that is narrow and steep ($\tan\alpha$ is normally between 0.10 and 0.20). The grainsize of sediment is rather coarse. One speaks of a reflective beach state when $\Omega < 1$.

Dissipative beaches ($\Omega > 6$) on the other hand are mostly wide and flat. The D_{50}-value is rather small (fine sediment).

The beach of the Southern Coastal Mine Namibia is tends toward a reflective beach. Both the wave height and the wave period are large. The median grainsize of sediment is medium to coarse, which would lead to a low value of Ω. plunging breakers are dominant, which is consistent with a more reflective beach state.

Notable features of the Namibian coast are also that the continental shelf is wide. Also land accretion takes place due to mining activity (see section 3.6) at a high rate. Consequently, an equilibrium profile of the upper shoreface can not be reached.

6.1.2 Breaking of waves

When waves become too steep they begin to break. The moment of breaking can best be described by wave-breaking parameter γ.

$$\gamma = \frac{H_b}{h_b} \tag{6.3}$$

This parameter indicates when the wave height of an almost breaking wave H_b, relative to the waterdepth h_b at that location, becomes too high. As a consequence waves break. Battjes and Janssen (1978) investigated the influence of the beach slope on the breaking of waves and found that γ increases for an increasing value of ζ (Iribarren number). They considered γ to be larger than 0.8 for plunging breakers and lower than 0.8 for spilling breakers.

For the Southern Coastal mine ζ is about 0.5. With the application of the Sand-2-Sea program, the beach slope becomes smaller leading to a less reflective beach state. The wave-breaking parameter γ is estimated to be somewhat smaller than 0.8.

6.1.3 Deep and Shallow water

In section 2.1 the designation of different offshore water regions, depending on depth, in front of the Namibian shore was explained. These are the definitions that NAMDEB uses for water depth sections. This is again summarized in Figure 6.3. The region of interest for this thesis is the ultra-shallow water region and part of the shallow water region, namely from 0 to 20 m water depth.

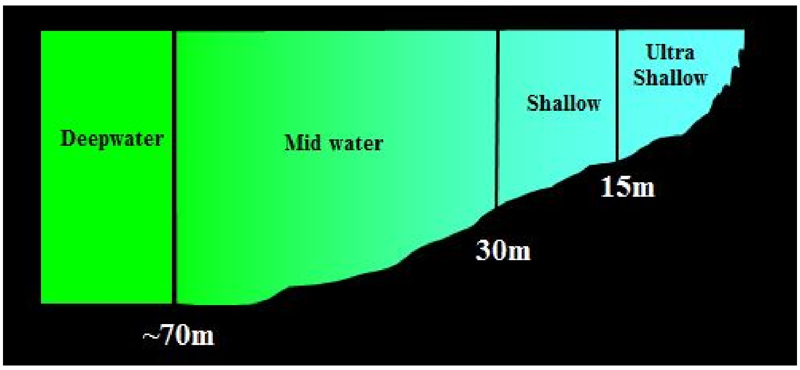

Figure 6.3: Different depth regions in front of the Namibian shore. These definitions are used by NAMDEB.

When discussing offshore hydrodynamics another distinction must be made between deep and shallow water, different from the definitions used by NAMDEB. This is because the characteristics of waves approaching the shore change when they travel from deep to shallow water, as will be explained in the next section (section 6.2). Figure 6.4 shows a wave propagating landwards. When the wave length L is less than half the water depth h ($\frac{h}{L} > 0.5$), literature speaks of deep water (Holthuijsen, 2007). When the depth becomes very little relative to the wave length (wave length is more than twenty times the water depth: $\frac{h}{L} < 0.05$), the depth region is called shallow water.

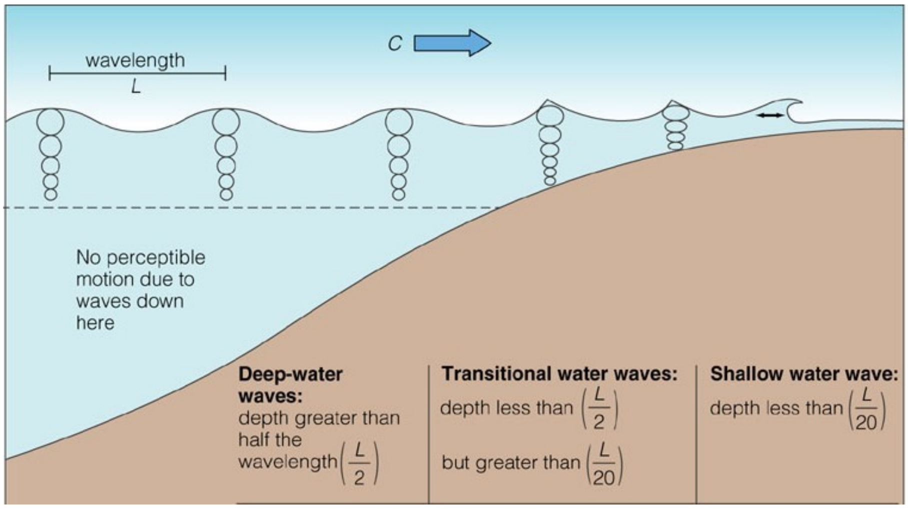

Figure 6.4: Distinction between depth regions when considering waves. After Garrison (2005)

From now on the definitions for shallow and deep water according to literature of hydrodynamics will be used.

6.2 Waves affecting dunes

The hydrodynamics relevant to changes of the upper shore face are explained in the following section. Both long (infragravity) waves, which are most relevant in normal dune erosion studies, and shorter waves, relevant to dune erosion in case of constant human interference, are discussed.

6.2.1 Infragravity waves

Figure 6.5 shows a typical sketch of relative amounts of energy as the function of wave period (1/frequency) in ocean waves. One can easily see that such a deep-water energy spectrum is dominated by gravity waves (wind and swell waves). However, in the ultra-shallow water region and the swash zone the wave energy spectrum shows domination of infragravity waves (also called bound long waves). While short waves start to break at the breaker point, infragravity waves do not, because their wave length is longer and they are less steep. Infragravity waves can reach a dune foot and reflect, and so these waves are most relevant in dune erosion studies.

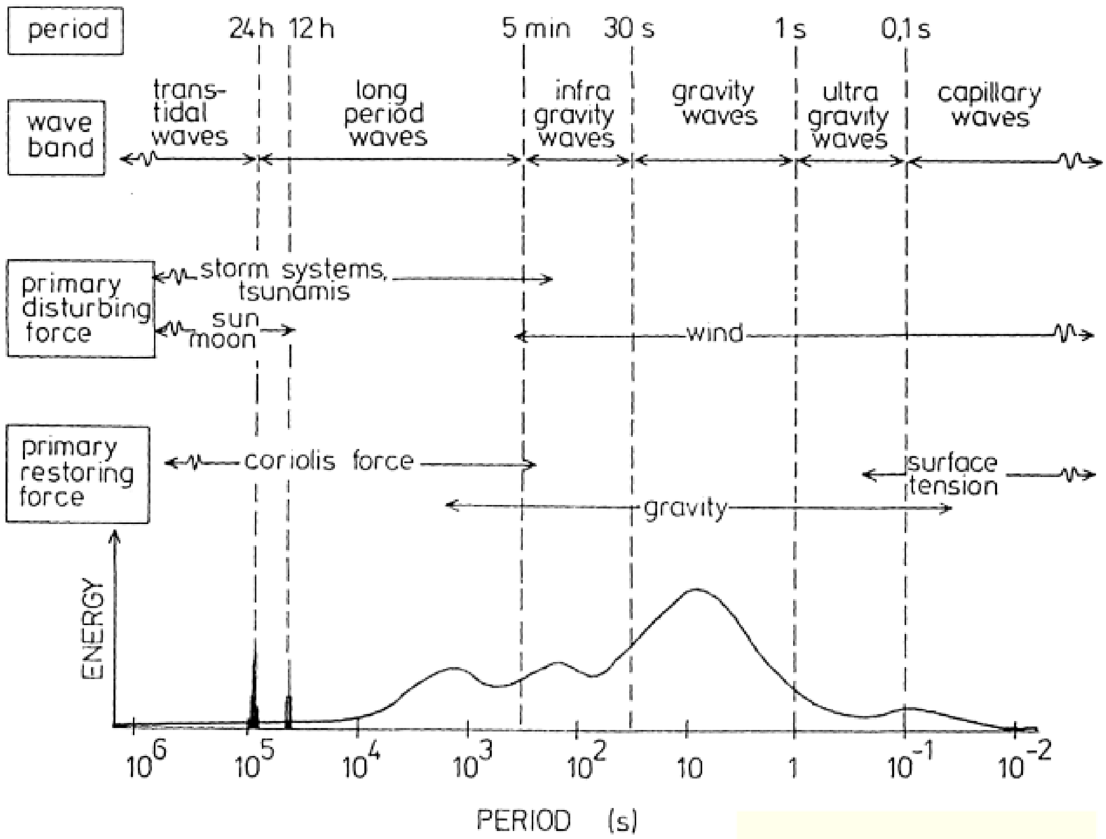

Figure 6.5: Typical wave energy spectrum for oceanic waters. After Kinsman (1965)

Generation of infragravity waves

The generation of infragravity waves can be described by the effect of radiation stresses on groups of waves according to Longuet-Higgins and Stewart (1964). They defined radiation stress as *"the excess flow of momentum due to the presence of waves"*. The transport of wave-induced x-momentum in the x-direction, when x is the direction of wave propagation, can be written as (averaged over time):

$$S_{xx} = \overline{\int_{-d}^{\eta} (\rho u_x \cdot u_x + p_{wave}) dz} = (2n - \frac{1}{2})E \tag{6.4}$$

where u_x is the velocity in the x-direction, p_{wave} is the wave pressure in the x-direction and n is the relation between the velocity of waves in the group and the group velocity. The concept of Longuet-Higgins and Stewart (1964) is discussed here. As waves travel away from their origin in deep water they tend to form groups consisting of waves with approximately the same wave period and length. A wave group is characterized by a wave envelope and a velocity c_g, the group celerity. The energy density has a sinusoidal variation. Surface waves possess momentum directed in the wave propagation direction.

Where the wave group has an antinode (relatively high shorter waves), there is a high energy density region and thus a region with high radiation stresses. A region with low radiation stresses can be found at the node of the wave group. The gradient in the radiation stress is experienced by the water surface as a force travelling with the wave group celerity. Because continuity must be preserved, the water surface is pushed up at regions with low radiation stresses, and pushed down at regions with high radiation stresses. So the stresses are balanced by a pressure force, resulting in variations of the water surface elevation, also travelling with the wave celerity.

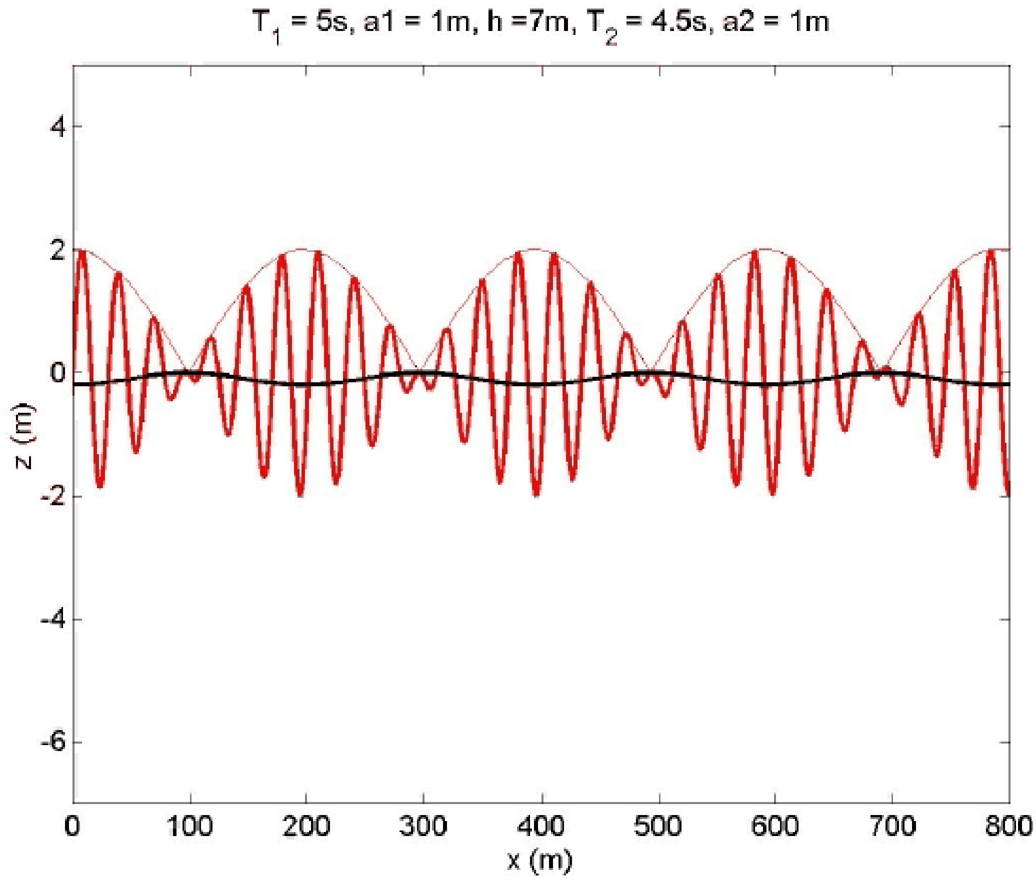

Figure 6.6: Graph schematically showing different types of waves. In red: shorter waves in wavegroup (envelope shown in pink). In black: forced bound long wave (infragravity wave)

Short waves and the bound long wave (infragravity wave) are in antiphase.

By integrating the momentum and mass balances for ideal deep water conditions (stationary uniform situations in longshore direction and normal incident wave trains, with no wave energy dissipation), a formulation was found for the additional water level elevation due to infragravity waves (Longuet-Higgins and Stewart, 1964)(so added up to the surface water level averaged over a wave group):

$$\rho\zeta = -\frac{S_{xx}}{gh - c_g^2} + constant \tag{6.5}$$

Moving towards shallower water, the denominator of equation 6.5 becomes much smaller and this leads to the following expression:

$$\zeta \approx -\frac{S_{xx}}{\rho\sigma_w^2 h^2} = -\frac{3}{2}\cdot\frac{ga^2}{\sigma^2 h^2} \tag{6.6}$$

where σ_w stands for the relative frequency in a moving frame of reference,

$$\sigma_w^2 = gk\tanh(kd) \tag{6.7}$$

Longuet-Higgins and Stewart (1964) suspected that when short waves break in the surf zone, the infragavity waves as bound long waves are released and reflected offshore as free long waves. Herbers et al. (1995) did further research on this topic. Their observations were in line with this theory, but the dynamics are not yet fully understood.

Shoaling of infragravity waves

As waves move into shallower water they start to shoal. The energy flux per unit wave crest width, $U = E \cdot n \cdot c$, is constant according to the energy conservation law. Following the dispersion relationship, the wave propagation speed is affected by the bottom and decreases as waves come into shallower water regions. The wave energy per unit surface area increases. As a result the wave height increases, until the waves become too steep and break.

Infragravity waves behave slightly different when we compare their behavior in the shoaling region with normal long and short waves. This is due to the fact that in the shoaling region the bound long wave travels somewhat slower than the wave groups, which results in a growing phase lag. Van Dongeren and Svendsen (1997) pointed out that this phase shift is crucial, because this allows energy transfer from short waves to the infragravity wave, leading to a stronger amplitude growth than stated in Green's Law. Studies and experiments ((Baldock et al., 2000), (Madsen et al., 1997) and (Van Dongeren and Svendsen, 1997)) led to an expression for the growth rate, defined as β. This β is the normalized bed slope parameter.

$$\beta = \frac{i_x}{\omega}\cdot\sqrt{\frac{g}{h}} \tag{6.8}$$

where i_x is the bedslope, ω the radial frequency of the wave, h the representative depth and g the gravitational acceleration. In wave growth for long waves, the value of β is used as the exponent ($\zeta \propto h^{-\beta}$). For incoming infragravity waves the value of β lies between 0.25 (Green's Law for amplitude grow) and 2.5 (shallow water limit according to Longuet-Higgins and Stewart (1964). The transfer of energy due to the phase lag is described by Battjes et al. (2004) with the formula

$$R \equiv -\langle U\frac{dS_{xx}}{dx}\rangle \cong \frac{1}{2}\cdot k_{lw}\cdot \hat{\mathrm{U}}\cdot \check{\mathrm{S}}\cdot\sin(\Delta\psi) \tag{6.9}$$

in which k_{lw} is the long free wave number, $\hat{\mathrm{U}}$ and $\check{\mathrm{S}}$ the amplitude of U (energy flux) and S_{xx} respectively at the considered frequency.

Reflection and dissipation nearshore

In the surfzone the energy of short waves will be dissipated. Infragravity waves, however, are so long that their wave energy is only partially dissipated. This means that they are also partially reflected at the coast. Still only little is known about the dissipation of bound long waves. Van Dongeren et al. (2007) suggested to consider again a growth parameter (as used for shoaling) β, analogous to the Iribarren number (see section 6.1). Long waves break for a small value of β.

In case of normally incident wave groups, the reflecting infragravity waves reflect away from the coast. They become "leaky waves", escaping the surfzone again. It is also a possibility that the reflecting waves become trapped between the coastline and the breaker line. This type is called "edge waves".

Importance of infragravity waves nearshore

Masselink and Hughes (2003) pointed out that in wave and current spectra behind the breaker point large amounts of energy are associated with frequencies belonging to infragravity waves, so lower frequencies than swell and sea waves. This can be explained as follows. As short incident waves approach the shore they start to break from the breaker point on and their energy is dissipated throughout the surf zone. Infragravity waves however are much longer than short waves and they become less steep while shoaling. Thirdly, energy transfer from short to longer waves takes place in the shallow water region as mentioned in section 6.2.1. These reasons together allow infragravity waves to run up the beach relatively far and reach the toe of a dune during storm conditions. In a wave energy spectrum this phenomena can be recognized by the relative dominance of the infragravity frequency band in the swash zone.

6.2.2 Waves in front of the Southern Coast Namibia

The case treated in this thesis, the Southern Coastal Mine in Namibia, is somewhat different compared to most sandy coastal regions. In most coastal regions elsewhere in the world, for instance the Netherlands, dune erosion takes place when infragravity waves reach the dune toe during a storm surge. Three important features of the coast of the Southern Coastal Mine in Namibia cause the dune/seawall erosion taking place under different conditions.

First of all, the coastal region has a micro-tidal climate. Waves are far more dominant for seawall erosion than the influence of the tide. Secondly, highly energetic and persistent wave conditions of rather long and high swell waves dominate the region. And thirdly, dunes/seawalls are constantly built and maintained close to the high-waterline.

The combination of these three factors ensure that seawall erosion takes place more often than during storm surges only. Strong infragravity waves are generated that can reach the toe of the seawall more easily, since swell waves are high and the seawall toe is relatively close to the water line. Even shorter waves (see gravity waves in Figure 6.5) can reach the dune toe during more heavy weather conditions too. Section 6.4 elaborates on wave impact on dunes, and Appendix G defines what should be called a storm in this specific case.

Gravity waves

Sea waves and, especially, swell waves (i.e. gravity waves in water) must be taken into account when modelling dune erosion and coastal profile change in the case of the Southern Coastal Mine in Namibia. These gravity waves (see Figure 6.5 for explanation) are shorter than infragravity waves and have a higher frequency. Because of the wide ocean, gravity waves in front of the Namibian coast are relatively high and long. During storm events, these gravity waves are considered to be more important than infragravity waves, because of their large wave height and large wave period (see section 2.4). Section 6.4 will explain how these parameters affect dune erosion. For the development of sea and swell waves reference is made to the book of Holthuijsen (2007).

6.2.3 Refraction of waves

When waves approach the shore under an angle, refraction will take place. This is a depth-induced phenomenon in which the wave crest will always turn towards the shallower region. The phase speed is of a wave crest is equal to c in equation 6.10:

$$c = \sqrt{\frac{g}{k}\tanh(kd)} \tag{6.10}$$

Where g is the gravitational acceleration, k the wave number and d the water depth.

This equation tells that a wave crest moves faster in deeper water than in shallower water. In other words, the wave crest moves over a shorter distance in shallower water than it does in deeper water and so it turns. A useful expression was found by Snel van Royen (Holthuijsen, 2007), known as Snel's Law, which states:

$$\frac{d}{dn}\left(\frac{\sin\theta}{c}\right) = 0 \tag{6.11}$$

Where θ is the angle of wave incidence, and n is the relation between the velocity of waves in the group and the group velocity. The formula can be simplified to:

$$\frac{\sin\theta}{c} = constant \tag{6.12}$$

This can be illustrated with the simplified figure below. This figure shows an example of a wave crest (or wave front) travelling towards the shore. When the waves enter shallower water, refraction takes place according to Snel's Law.

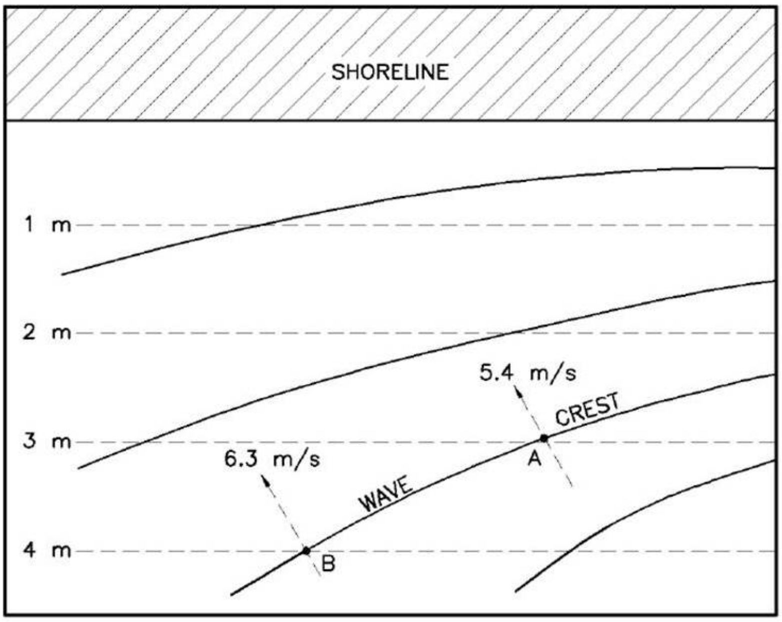

Figure 6.7: Example of wave refraction. As the wave front moves towards the shoreline, it will turn towards shallower water. The dashed lines represent depth contours of the bed.

For the Namibian shore the process of refraction is relevant to investigate, since crosswall extensions are built along the shore. Oblique incident waves are present in front of the Namibian shore. If the front of the waves experience a lot of refraction, the crosswalls will not protect the seawalls against wave attack in a direct matter. If refraction is almost absent, because oblique incident waves do not feel the bottom, the crosswalls can partly block some waves.

6.2.4 Undertow

The mass flux between wave crest and wave trough in the surf zone is considerably larger than outside the surf zone (Bosboom and Stive, 2013). This mass flux consists of a flux due to the progression of waves and a flux due to the surface roller in breaking waves (see equation 6.13 below here).

$$q_{drift} = q_{non-breaking} + q_{roller} = \frac{E}{c} + \frac{\alpha E_r}{c} \tag{6.13}$$

Where E is the wave energy, E_r the roller energy and c the propagation speed. α is an empirical reduction factor, with a value between 0.22 and 2.0 according to various research. At the shoreline, a closed boundary, there should be zero net mass transport in cross-shore direction. This means that the mass flux between wave crest and trough in landward direction must be compensated by a net seaward velocity below the trough level of the wave. This is called the return current. From balancing the seaward and landward directed mass fluxes follows:

$$U_{return} = -\frac{q_{drift,x}}{\rho h} = -\frac{q_{drift} \cdot cos(\phi)}{\rho h} \tag{6.14}$$

With ϕ the angle of wave incidence. The seaward directed velocities below wave trough level are relatively small in case of non-breaking waves. In case of breaking waves the return current is rather large, because the transport of mass between wave crest and wave trough is substantially larger. This large return current under breaking waves is called undertow. The undertow is presumed to be the most important mechanism for transporting eroded sediment from dunes offshore. Sediment is being stirred up by the breaking of waves. Since sediment concentrations are becoming higher closer to the bed, the undertow transports considerably more sediment offshore than the waves mass flux can transport onshore. This explains why the undertow plays an important role in dune erosion and in seawall erosion in the Southern Coastal Mine Namibia.

6.3 Sediment transport

6.3.1 Initiation of motion

Sediment is set into motion when the shear stress due to hydrodynamics exceeds the shear stress under which sediment stays in place. This can be explained by a force balance, in which three different forces (the drag, lift and gravity force) play a role. Figure 6.8 illustrates the different forces on a single particle on the bed.

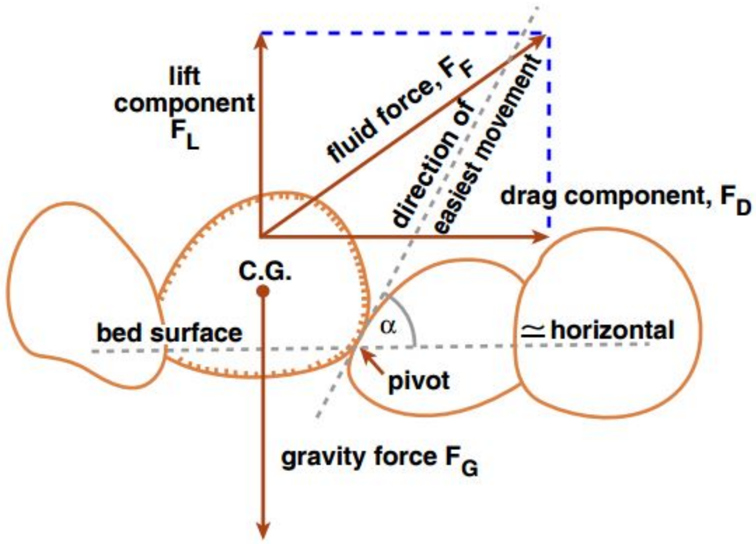

Figure 6.8: Forces acting on a single particle in stationary situation. Drag force (parallel to the flow direction), lift force and gravity force. Figure by MIT OpenCourseWare (accessed July 2015)

The active force (or fluid force in this case) consists of a lift component and a drag component. The gravity force is the passive force. Shields (1936) investigated the proportionality between the forces and found a relation between a dimensionless shear stress and the particle Reynolds-number, presented by equation 6.15. θ_c is known as the Shields parameter.

$$\theta_c = \frac{\tau_c}{(\rho_s - \rho)gD}\theta_c = \frac{u_{*c}^2}{\Delta gd} = f(Re_*) \tag{6.15}$$

$$\tau = \rho_s u_* |u_*| \tag{6.16}$$

τ_c is the critical bottom shear stress induced by water movement, defined as in equation 6.16. Higher values for τ_c lead to particle movement. u_* is the shear stress velocity, an indicator of the shear stress depending on the velocity.

The Re_* (particle Reynolds number) tells whether a particle goes into turbulent motion or stays in the viscous sublayer. Equation 6.17 defines the particle Reynolds number. ν is the kinematic viscosity coefficient.

$$Re_* = \frac{u_* D}{\nu} \tag{6.17}$$

For turbulent flow (high particle Reynolds numbers) the value of the Shields parameter is around 0.05 for sand on a flat bed.

In modelling the upper shoreface of a coast, sediment transport is induced by waves as the hydrodynamic load. When studying dune/seawall erosion, the following considerations must be kept in mind. The bed is not uniform and flat as in the research done by Shields (1936). Oscillatory flow causes ripples in the bed which make the initiation of motion a more complex problem. For a sloping bed in the flow direction (which is the case when one considers an undertow in a dune erosion study), the critical flow velocity will be somewhat lower than for a flat bed. Flow will be turbulent for the breaking waves, leading to a high Reynolds number.

6.3.2 Sediment transport modes

Sediment is set into motion when the shear stress due to hydrodynamic forces exceeds the critical shear stress under which sediment stays in place. Gradients in sediment transport cause changes in coastal morphology. The updating of the bed, due to sediment transport gradients, can be described with Exners' Law:

$$\frac{\delta z_b}{\delta t} + \frac{1}{1-n}\left(\frac{\delta S_x}{\delta x} + \frac{\delta S_y}{\delta y}\right) = V \tag{6.18}$$

Where $\frac{\delta z_b}{\delta t}$ is the change of bed level in time, n is the porosity of the bed and S the sediment transport in x- or y-direction. V represents the sources and sinks for sediment within the computational area (δx x δy). In the discussed case of the Southern Coastal Mine we will see that the construction and maintenance of the seawall will count as a major source of sediment.

Three types of sediment transport are described in literature: bed load transport, suspended load transport and sheet flow (Figure 6.9). The total transported sediment volume is the sum of the three types. Bed load transport is the rolling and sliding of particles close to the bed. Bed load transport responds instantaneous to time varying velocity or shear stress. When particles start to move in multiple layers close to the bed at high shear stresses, we speak of sheet flow. In suspended load transport particles loose contact with the bed. Sediment particles are taken into suspension until they are deposited again when deceleration occurs. This type of transport is supported by turbulent diffusive forces. Suspended sediment transport is current-related and is measured by multiplying the time-averaged velocity and the sediment concentration.

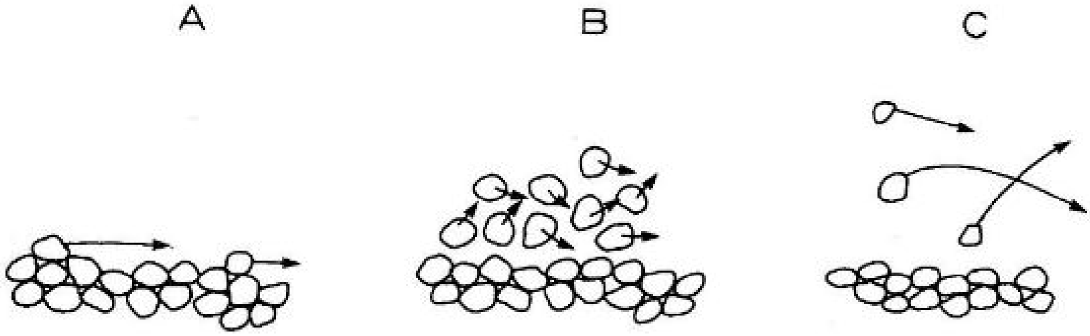

Figure 6.9: Different sediment transport modes. A: bed load transport. B: sheet flow. C: suspended load transport. After Fredsoe and Deigaard (1992)

The grain size of the sediment in the system (often indicated by the median grain diameter D_{50}) plays an important role in the calculation of transported volumes of sediment.

6.3.3 Cross-shore transport

Cross-shore sediment transport has different causes and can be onshore or offshore directed. Onshore directed transport is due to Longuet-Higgins streaming, wave asymmetry and free long waves. Offshore directed sediment transport is caused by bound long waves, undertow and gravity.

Outside the surf zone Longuet-Higgins streaming, first described by Longuet-Higgins (1953), is responsible for onshore transport. In section 6.2.1 the phenomenon of the piling up of wave energy in intermediate water is described. There is mass transport accompanied with this process, leading to boundary layer streaming. This can lead to velocities onshore directed near the bottom. Bound long waves (infragravity waves) on the other hand cause off shore directed sediment transport outside the surf zone. Bound long waves have a trough where short wave energy (and so the stirring up of sediment in shallower water) is highest, leading to nett offshore directed sediment transport.

For the case of the Southern Coastal Mine in Namibia, interest lies in sediment transport within the surf zone. The focus is on the evolution of the beach profile and erosion of the seawall (dune).

In shoaling waves horizontal wave asymmetry occurs. This can be represented by a velocity signal with a high, narrow crest and with a wide trough with a smaller velocity magnitude. These large velocities under the wave crests are stir up sediment more effective than the smaller (offshore directed) velocities accompanying the wave troughs. So wave asymmetry leads to nett onshore directed sediment transport. Free long waves, out of phase with the wave groups in the surf zone as discussed in section 6.2.1, transport mass and thus sediment shoreward.

Undertow (section 6.2.4) is presumed to be the most important mechanism for transporting eroded sediment from dunes offshore. Gravity (sediment rolling downhill) will also lead to a nett offshore directed transport of sediment.

For a more detailed description of cross-shore sediment transport mechanisms reference is made to Bosboom and Stive (2013).

6.3.4 Longshore transport

Longshore sediment transport is defined as the net movement of sediment particles through a fixed vertical cross-section perpendicular to the coastline (Bosboom and Stive, 2013). Oblique incident waves generate a longshore current when they break in the breaker zone. The orbital motion of waves and the breaking of waves, creating an increase of turbulence, stir up sediment that will be transported by the longshore current. The magnitude of the longshore transport depends on the wave conditions (height, period and angle) in the breaker zone and on the availability and gravity force of sediment grains.

The longshore sediment transport can be defined as the longshore current velocity $V(z)$ times the time-mean concentration of sediment $C(z)$ (see equation 6.19). It is assumed that the longshore velocity is relatively time-invariant (Bosboom and Stive, 2013).

$$\langle S_y \rangle = \int_a^h V(z) \cdot C(z) dz \tag{6.19}$$

Where S_y is the net longshore transport, h the water depth and a the thickness of the bed load layer.

Changes in the profile of the coastline are due to gradients in the longshore sediment transport. So erosion and sedimentation/deposition along the shoreline occurs when gradients in sediment transport are present.

Calculating longshore transport

With empirical bulk transport formulas the longshore current velocity and the sediment concentration are quantified. Many different formulas are described in literature for longshore sediment transport. For sediment transport along the Holland coast the Kamphuis formulation (Kamphuis, 1991) has been used widely. Kamphuis included the effect of sand properties into the existing formulation of CERC for longshore sediment transport. For the formulation of CERC and Kamphuis, reference is made to Bosboom and Stive (2013) and Kamphuis (1991). It must be noted that different transport formulas give answers that can differ by a factor 10 or higher. With numerical modelling longshore sediment transport can be modelled more accurately, and also discontinuities of the coastline can be taken into account more easily.

S-ϕ curve

The size of the sediment transport is very much dependent on the obliqueness of breaking waves in front of the beach. According to the sediment transport formula by CERC (explained in Bosboom and Stive (2013)), the transported volume is proportional to the offshore wave angle (ϕ) and the wave height just before breaking (H_b).

$$S \propto H_b^{2.5} \sin 2\phi \tag{6.20}$$

Figure 6.10 presents an "S-ϕ" curve by which the relation between offshore wave angle and longshore transport can be given. For small offshore wave angles the longshore transport varies almost linearly with ϕ. For an angle of about 45 degrees maximum transport occurs, as can be derived from Figure 6.10.

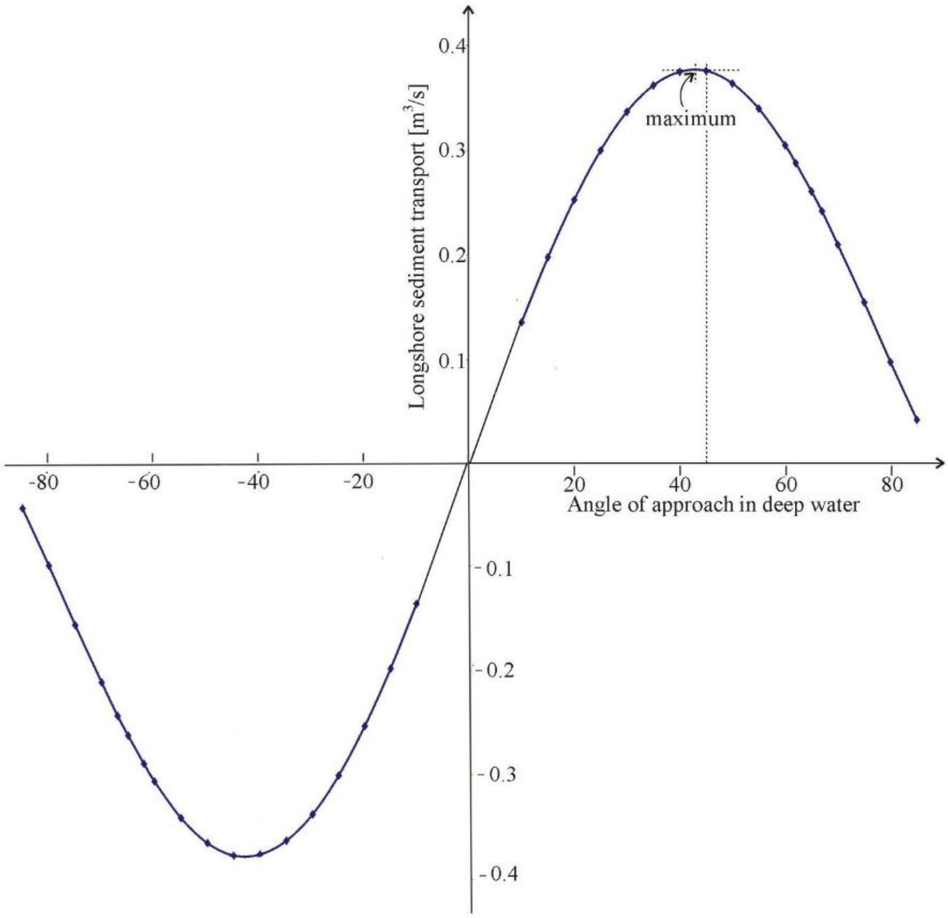

Figure 6.10: Example of an S-ϕ curve, presenting the relation between longshore sediment transport and the angle of wave incidence.

Longshore sediment transport at Southern Coastal Mine Namibia

Oblique incident waves are present along the coast of the Southern Coastal Mine. In section 2.4 a wave rose was shown (Figure 2.8), from which it can be seen that the main angle of incidence is slightly oblique coming from a more southward direction (compared to the orientation of the coastline). This generates a more northward directed current.

The wave climate is characterized as highly energetic, which makes that relatively large amounts of sediments are stirred up in the breaker zone and surf zone. However, sediment is relatively coarse, which has a negative effect on the longshore sediment transport volumes.

Section 3.6 described how sand is nourished unto the beach and crosswalls. These longshore discontinuities cause transport gradients leading to erosion and sedimentation processes. Figure 6.11 shows schematically what happens to a nourishment under oblique incident waves with a wave angle of less than 45 degrees. The angle of wave incidence differs along the coastline, due to different orientations of the coastline itself. According to the S-ϕ curve (see Figure 6.10) this leads to different magnitudes of the longshore transport (represented by the size of the arrows in Figure 6.11), and thus to gradients. The most seaward part of the hump will erode and sedimentation will occur on both sloping sides of the nourishments.

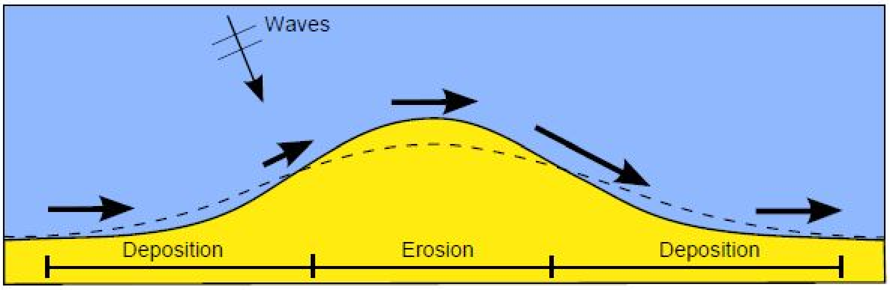

Figure 6.11: Longshore sediment transport gradients along a nourishment. Figure from Steijn (2015).

In section 2.1 a picture of part of the coastline of the Southern Coastal Mine is presented in Figure 2.3. One can see a quite some discontinuities along the coastline on a scale of 100 m. More important is to notice the total curvature of the present coastline. Figure 2.4 also shows some curvature of the coastline with a seawall standing out in seaward direction. Waves will tend to spread out the nourishments and smoothen the coastline by means of longshore sediment transport.

6.4 Dune erosion

As discussed in paragraph 6.1 the focus for dune erosion is on the upper shoreface. The processes of dune erosion will be discussed in the section below.

6.4.1 Sand wash / erosion mechanisms

During severe storm events waves can reach the dune face and impact the dune. Nishi and Kraus (1996) distinguished three erosion mechanisms due to waves impacting the sand dune, visualized in Figure 6.12. Layer separation in case of a nearly vertical slope (1), notching in case of a well-packed, nearly vertical, outer dune slope (2), and sliding and flowing of sand bodies, along a slope approaching the angle of repose (3).

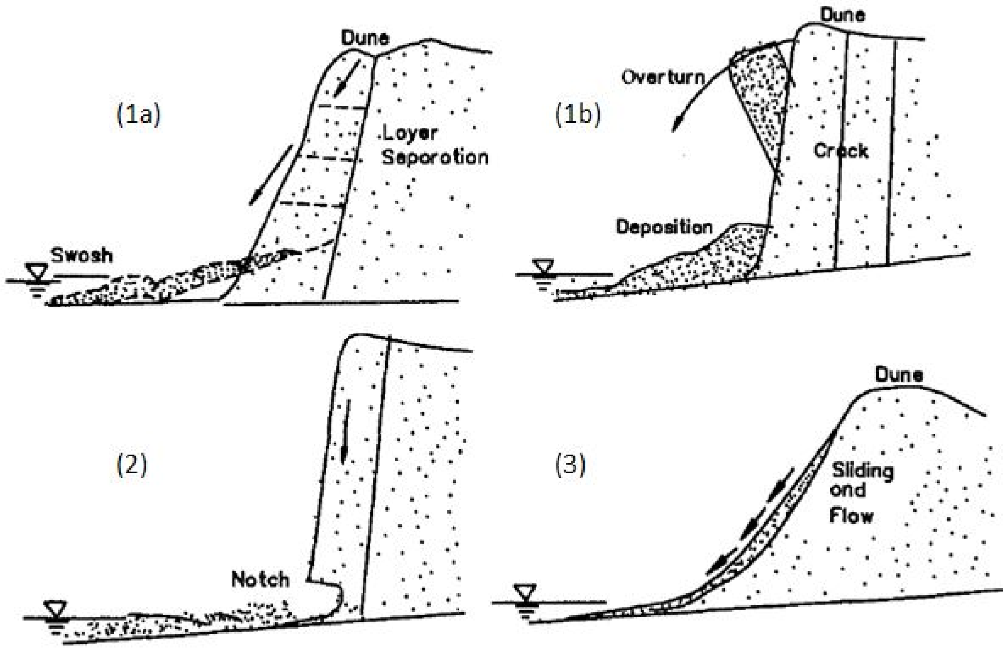

Figure 6.12: Schematic drawings of dune erosion mechanisms. Layer separation (1), notching (2) and sliding/flowing (3). After Nishi and Kraus (1996)

The third erosion mechanism is relevant for a dune where loosely packed sand is dumped, as is the case for the seawall discussed in thesis. For this reason, only this third mechanism is discussed below here. When waves reach the toe of a sand dune primary and secondary dune erosion can occur (Kateman, 2007), schematically presented in Figure 6.13.

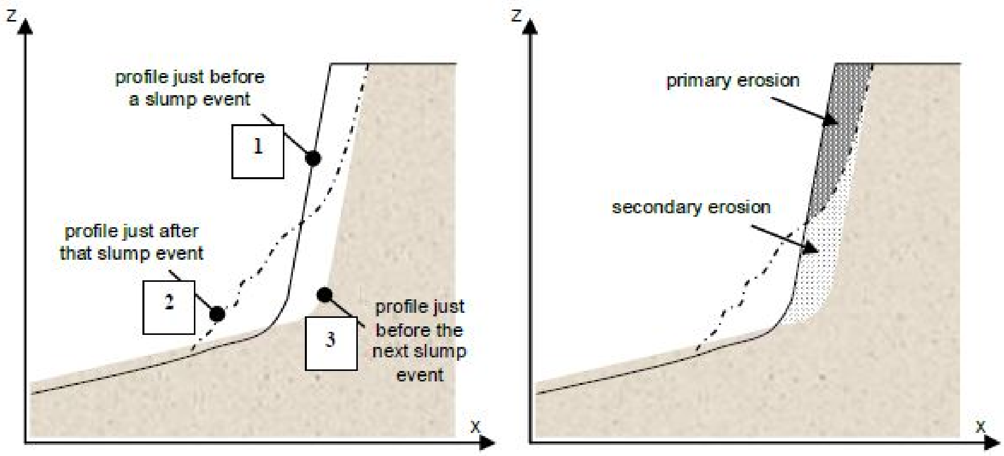

Figure 6.13: Left: different stages in dune erosion process, considering a sand slope around the angle of repose. Right: Volumes of primary and secondary erosion. From Kateman (2007)

Primary erosion of a dune is also known as sliding/slumping of parts of the dune along the outer slope. When the toe of the dune is fluidized the dune slope becomes unstable, considering that the slope angle approaches the angle of repose for unconsolidated grains. Because the wet angle of repose is smaller than the dry angle, modest wave impact at the base of a dune can already cause layers of sand to run/slide down the slope. This process tends to flatten the outer slope of the dune. A steeper dune slope can trigger slumping again under storm conditions. Secondary dune erosion is a sliding and flowing mechanism. Grains of a dune are brought into suspension when the wave runs up the dune and they are carried away with the water. Van Thiel de Vries (2009) concluded that a dune face steepens repeatedly, reaching a critical slope where a new slump can take place. He observed that the width of a slump along a dune is smaller than the width of the impacting wave. Also, the time interval between slumps grows as a storm progresses. This can be explained by the change in the coastal profile, discussed in the section below.

6.4.2 Erosion processes

When dune erosion occurs, sand is transported offshore from the dune by a strong undertow. During storm conditions a strong undertow in combination with high concentrations of suspended sediment close to the base of the dune, results in a large transport capacity directed offshore. This capacity decreases seawards and the sand particles start to settle. Besides this form of settling, accumulation of sand of slumps in front of the dune toe occurs. The resulting upper shoreface is more effective in dissipating the energy associated with incoming waves. Consequently, the dune erosion rate is decreased as the storm continues. Two different models have been developed to examine dune erosion and the change of the upper shoreface profile.

Profile change based on constant equilibrium profile

The first model uses the Bruun Rule (Bruun, 1954) as its basis. This rule states that the profile of the upper shoreface strives to the same profile as it had before the storm. The deposition mechanisms for sand (settling of eroded material and the accumulation of sand after slumping) lead to a coastal profile of the same shape as the equilibrium profile before the storm conditions but now shifted upwards and towards the shore (6.14). This model is basically limited to the long-term and extreme events, so an equilibrium profile can develop entirely.

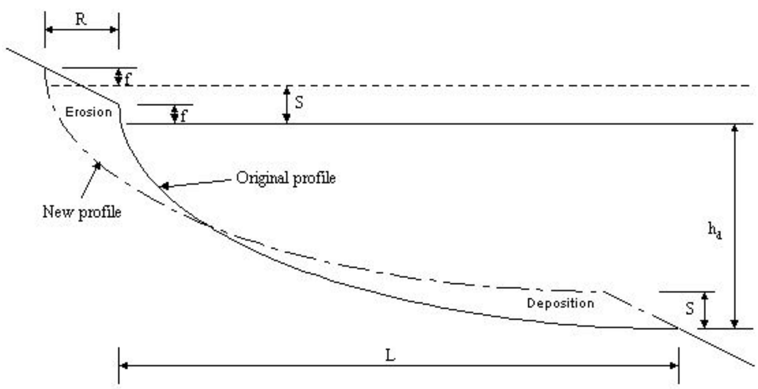

Figure 6.14: Evolution of shoreface according to Bruun Rule. In de figure: S = sea level rise, L = active profile length, R = retreat, f = freeboard.

From the Bruun Rule, it can be derived that the volume of sediment eroded/washed away from the dunes balances the volume of sediment deposited again at deeper water. Stating:

$$DuneRetreat = SSL(L/d) \tag{6.21}$$

SSL is the storm surge level, L the erosion/sedimentation length and d the corresponding height.

For the assessment of Dutch dunes Vellinga (1983) developed a model based on a constant equilibrium profile, derived from the Bruun Rule. Figure 6.15 visualizes schematically how the equilibrium profile looks like. The model states that erosion occurs, because the upper shoreface strives towards a post-storm equilibrium profile. This 1D dune erosion model, DUROS, was used to determine the retreat distance of a dune per storm event. In Appendix J is further explained how the assessment of Dutch dunes is carried out by means of a guideline, based on the model of Vellinga (1983).

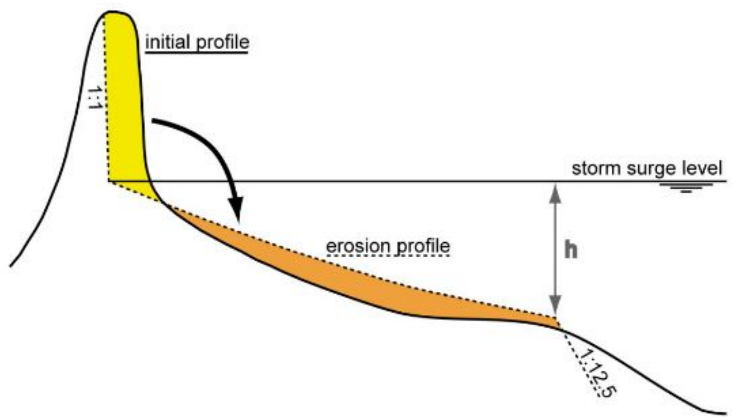

Figure 6.15: Visualization of balance between pre-storm and post-storm profile. After Vellinga (1982)

Profile change based on wave impact and volume calculations

The second model was proposed by Fisher and Overton (1984) and further developed by Fisher and Overton (1986). This model is based on a relation between the wave impact force and the volume of eroded dune material (as schematically drawn in Figure 6.15). Here, individual swash uprush is used to determine the dune erosion. The total erosion during a storm is determined by the summation of effects of individual uprushes impacting the dune. This method does not require the development of a post-storm equilibrium profile for the upper shoreface, this makes it also applicable to cases with more frequent swash uprush. The approach of dune profile change based on wave impact and volume calculations is implemented in the software model XBeach (Roelvink et al., 2009). Chapter 9 (Model approach of XBeach) elaborates further on this.

Applicability to case of Southern Coastal Mine Namibia.

Under current conditions in Mining Area No. 1 dune erosion of the seawall is complex. The toe of the dune is close to the high water line and an equilibrium profile for the upper shoreface cannot develop due to constant human interference in the natural processes. After slumping events new sand is nourished on the outerslope of a seawall by trucks. The consequence of this action is that there is a sediment transport gradient in the alongshore direction. Besides this, the focus is on the short-term. We are interested in what happens directly after a slumping event. Therefore, calculations under the assumption of a constant equilibrium profile are not consistent. The concept of dune erosion based on wave impact is applicable.

6.4.3 Wave impact

The eroded sediment volumes (ΔV) are related to the individual wave momentum flux, which is a force (F). Fisher and Overton (1986) found that this relation is approximately linear.

$$\Delta W = C_e \cdot F \tag{6.22}$$

With C_e being an empirical coefficient obtained from model tests. ΔW is the weight of the volume of eroded sediment.

$$\Delta W = \Delta V \cdot \rho_s \cdot (1 - p)g \tag{6.23}$$

ρ_s is the density of sediment, p the porosity and g the acceleration of gravity. Van Thiel de Vries (2009) conducted tests to examine equation 6.22. He found a decrease in wave impact in time. The relation between wave impact and dune erosion changes when the beach profile changes, which is logical since the new upper shoreface is more effective in dissipating the energy associated with incoming waves.

Chapter 7 – Methodology

This chapter describes the methodology applied for the research in this thesis.

7.1 Modeling

Chapter 1 (Problem statement) stated that the objective of this thesis is to find the optimal seawall design standard for the Southern Coastal Mine Namibia. In addition, the mining method, using a land reclamation strategy, is assessed. A numerical model that is able to simulate hydrodynamic processes and morphological changes is most useful for this thesis. The erosion to seawalls and the bed level changes on the short-term (up to 100 days) need to be simulated with such a coastal model.

7.1.1 Applicability of modelling software XBeach

For the simulation of changes to the upper shoreface, including seawall erosion, a coastline model modelling the coastline as a whole, is not applicable.

The XBeach Model (eXtreme Beach behaviour) has been selected to perform simulations of the behaviour of the Namibian coast and seawall erosion. To determine whether XBeach is applicable for modelling in the Southern Coastal Mine of Namibia, the capability of representing relevant processes is questioned. These processes are the following:

- Dissipation of wave energy due to wave breaking and bottom friction.
- Wave run-up on the beach for both short and long (infragravity) waves.
- Bed level updating.
- Dune/seawall erosion.

The description of the model approach of XBeach (see section 9) indicates that this model can represent these four processes. XBeach has been employed for various projects where the model performance for each of these processes has been assessed. Research, such as in Razak et al. (2013) and Van Thiel de Vries (2009), has demonstrated the applicability of XBeach with each of the four processes that are most relevant to the case of the Southern Coastal Mine.

As an alternative to XBeach, DUROS (Vellinga and Van Banning, 1984) could be used, since this model was used for the development of a guideline for the Dutch dunes (see also section J.4). The most important difference between the XBeach and DUROS is that XBeach is a process based model and DUROS a behaviour based model. Process based means that the equilibrium follows from the balances of forces and transport contributions from which the model is derived. In behaviour based models the equilibrium is forced. For DUROS this is explained in section J.4, where the forced equilibrium is the post-storm profile.

For a complex coastline DUROS has a lower performance, as it was designed for a uniform coastline. XBeach is more generic, and has a high performance for complex coasts such as the Southern Coastal Mine Namibia, where a lot of discontinuities exist (crosswalls, dredging pipelines, etc.). XBeach has been selected, because the effect of alongshore discontinuities should also be possible to assess.

According to Brandenburg (2010) XBeach is, compared to the DUROS model, less sensitive to storm surge height, but more sensitive to variations in wave period. This is relevant to the Namibian coast where large swell waves occur, but where the tidal range is relatively small.

Another option would be to choose a coastline model, such as UNIBEST (Deltares, 2010). A coastline model simulates how the whole coast as a single line develops. However, coastline models are not designed to model dune/seawall erosion on the short-term. Coastline models are also known to be less accurate on a scale smaller than in the order of 1 km.

7.1.2 Need for modeling software SWAN

The SWAN Model (Simulating WAves Nearshore) (Holthuijsen, 2007) creates the hydrodynamic boundary conditions that serve as input for the XBeach model. Since the wave climate in front of the Namibian Coast is only known relatively far offshore (ca. 200 km) and XBeach is relatively a computationally intensive model, an additional model has been selected to model the wave conditions nearshore, where the computational grid of the XBeach model starts. Translating off shore waves to near shore waves has been carried out with SWAN. XBeach has a built in feature which can read the output from the SWAN model.

7.1.3 Difference between 1D-model and 2DH-model

In numerical hydrodynamic models a distinction is made between one-dimensional (1D), two-dimensional horizontal (2DH) and three-dimensional (3D) models is made. The computational effort and the complexity of the models increases generally from 1D to 3D models.

A 1D numerical model is used to model changes in a particular cross-section (only 1 horizontal direction). The momentum balance and continuity equation for water are spatially averaged over cross-section segments and time-averaged over the turbulent fluctuations.

A 2DH model is used to model changes in both horizontal directions. The momentum balance and continuity equation for water are spatially averaged over the water depth. Time-averaging is again done over all the turbulent fluctuations, but can also be done over only smaller turbulent fluctuations. This is used when large eddies need to be accounted for in the model.

3D-models (same as 2DH, but not spatially averaged) will not be used for the modelling of the coastal profile in the Southern Coastal Mine of Namibia. XBeach can not run in a 3D mode. Besides, turbulent fluctuations are not of interest for this thesis, based on the large length scales used.

7.2 Deterministic approach for the reliability of a seawall

For the calculation of the seawall erosion volumes a deterministic approach has been used. This means that the chance of exceeding the result is 50% (see Appendix J for explanation).

In the model set-up of XBeach (see section 9.2) the values for the input parameters have been chosen conservatively. This must decrease the failure probability the seawall design, leading to a more safe design. A probabilistic approach with these (conservative) values would thus lead to a rather small failure probability, because the mean values of different parameters are more conservative. However, a level II probabilistic approach can lead to a better insight in the influence of parameters and a more accurate statement of the reliability of a seawall.

Appendix J (Reliability of a seawall) elaborates on a probabilistic approach for the assessment of seawalls. This Appendix also explains how a probabilistic approach for the safety assessment of Dutch dunes has led to a guideline for Dutch Coastal Managers. The application of such a strategy for the Southern Coastal Mine Namibia is discussed in Appendix K (Probabilistic calculation of required seawall volumes). This appendix gives a set-up, but the simulations needed are not within the scope of this thesis.

The recommended seawall standard and design, following in Chapter 10 (Seawall Design), are tested by the model, which has already proven its applicability in a case study (see section 9.3.1).

Chapter 8 – Analyzing SWAN model data

With the numerical model SWAN (Simulating WAves Nearshore) offshore waves from the ocean are translated to waves nearshore. The output of the model are wave spectra, containing information about the wave period, wave height and direction of the waves entering the domain (nearshore) which will be modelled with XBeach. A brief description of the modeling process with SWAN is given below. Important assumptions in the model set-up are explained in more detail.

8.1 Model approach

SWAN is a third-generation wave model that can be used to calculate waves near shore. The model is driven by local wind and offshore wave conditions that serve as boundary conditions for the model set-up. Running in the third-generation mode, SWAN accounts for the processes of wind generation, quadruplet wave-wave interaction, bottom friction and whitecapping. Different to traditional third-generation wave models, SWAN also computes triad wave-wave interaction and depth induced breaking of waves. SWAN uses an implicit numerical scheme to calculate the propagation of waves and other relevant physics. This makes the model rather economic in terms of computational effort. For a full explanation of the model approach and the physics involved, the reader is referred to Booij et al. (1999), Ris et al. (1999), Holthuijsen (2007) and to the SWAN manual.

8.2 Model set-up

8.2.1 Computational grid and bathymetry

The first actions in the model set-up are creating a grid and assigning a water depth for every grid cell, by loading in the bathymetry of the area of interest. A coarse grid is chosen, as visualized in Figure 8.1, to compute wave conditions for a large region. With the option of nesting, a finer grid close to the Southern Coastal Mine (also presented in Figure 8.1) can be computed. By doing this the outcome of the model is considered to be accurate close to the shore, while at the same time the computational effort is reduced when modelling the entire region. The coordinates of the offshore edges of the coarse grid match with offshore locations for which wave conditions are known. The wave data that are used to model nearshore waves for the Southern Coastal Mine in Namibia are derived from the ECMWF database[1]. This database is used by Witteveen+Bos Consultancy for projects where waves conditions are needed to be known in deep water. A waverecord of 30 years has been used in this research.

[1] European Centre for Medium-Range Weather Forecasts (www.ecmwf.int)

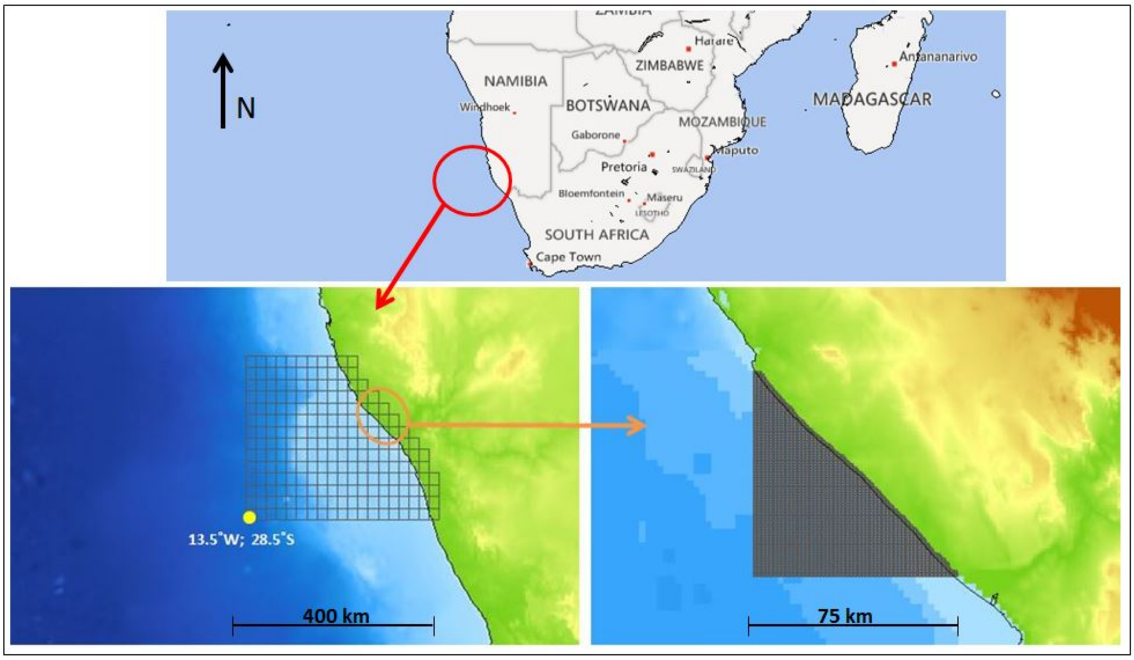

Figure 8.1: Map showing the location and computational grid that are used for computations by SWAN. The left image shows the coarse grid, the right image a fine grid that is nested into the coarse grid. The yellow dot shows the coordinates for which wave data are available.

The bathymetry associated with the coarse and the fine computational grids were obtained from the GEBCO database[2]. This database is being used by Witteveen+Bos Consultancy in projects where bathymetry data are needed in deep and intermediate water. The bathymetry data from the GEBCO database are considered to be accurate enough for the deep and intermediate water regions. The shallow water regions of the Southern Namibian Coast are highly energetic and as a consequence the bed level is changing constantly. SWAN output data, to be used in the XBeach model set-up, should therefore not be generated in shallow water regions but in intermediate water regions to guarantee more reliability.

8.2.2 Boundary conditions

The hydrodynamic boundary conditions for the SWAN model come from wave roses and scatter plots, representing the wave conditions for off shore locations in deep water. Figure 8.1 shows a map of the coastline of interest (Southern Coastal Mine, Namibia) and the location where the wave conditions are known. The wave rose for this location, with a longitude of 13.5 degrees West and a latitude of 28.5 degrees South, is presented in Figure 8.2.

[2]General Bathymetry Chart of the Oceans (www.gebco.net)

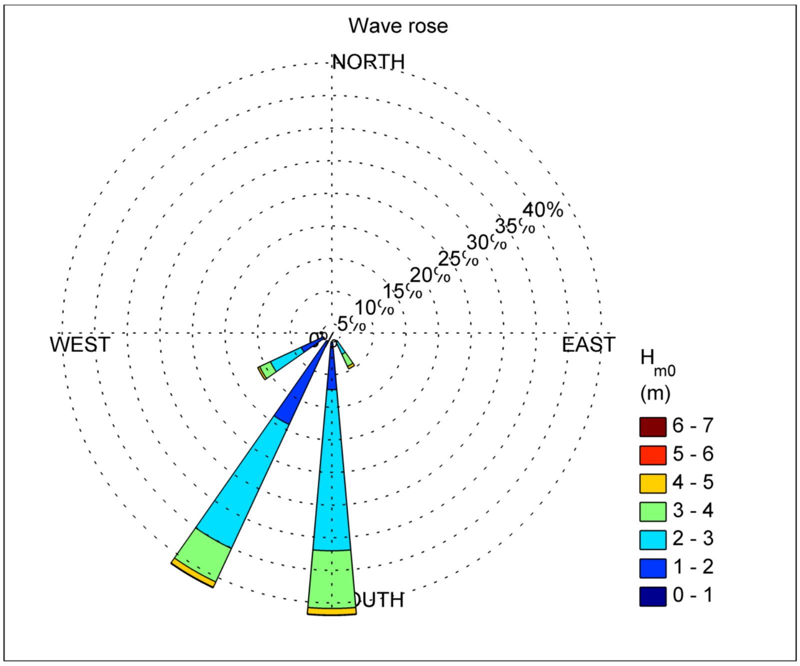

Figure 8.2: Wave rose for offshore waves, used as input for SWAN model. Location: 13.5° W , -28.5° N

The wave scatterplot is dominated by waves entering the domain from the south and southwest. The coastline of NAMDEBs Southern Coastal Mine is on average 50 degrees North (in clockwise direction). So it's approximately facing southwest.

The offshore wave conditions can be derived from the timeseries of wave measurements. The scatterplots belonging to the wave rose (Figure 8.3 and Figure 8.4) show 484 wave conditions (combinations of significant wave height, wave peak period and mean wave direction) that can occur during a year.

Wave height H_{s} (m)		Wave period T_{p} (s)													
		4.00	5.00	6.00	7.00	8.00	9.00	10.00	11.00	12.00	13.00	14.00	15.00		
lower	upper	5.00	6.00	7.00	8.00	9.00	10.00	11.00	12.00	13.00	14.00	15.00	16.00	sum	cum sum
0	0.5	-	-	-	-	-	-	-	-	-	-	-	-	-	-
0.5	1	-	-	0.00	0.01	0.01	0.00	0.00	-	-	-	-	-	0.03	0.03
1	1.5	-	-	0.21	0.82	1.49	1.30	0.45	0.09	0.01	-	-	-	4.35	4.39
1.5	2	-	0.01	0.95	3.51	5.48	6.05	3.66	1.22	0.19	0.02	-	-	21.09	25.48
2	2.5	-	-	0.80	5.76	7.67	6.91	5.25	2.65	0.86	0.13	0.01	-	30.05	55.52
2.5	3	-	-	0.10	3.95	6.73	4.87	3.58	2.49	1.04	0.27	0.04	-	23.08	78.61
3	3.5	-	-	-	0.92	3.85	2.93	2.16	1.49	1.05	0.31	0.04	0.00	12.75	91.35
3.5	4	-	-	-	0.07	1.44	1.30	1.03	0.98	0.60	0.27	0.06	0.01	5.76	97.12
4	4.5	-	-	-	-	0.30	0.49	0.36	0.34	0.29	0.21	0.05	0.01	2.06	99.17
4.5	5	-	-	-	-	0.02	0.11	0.12	0.14	0.09	0.08	0.03	0.00	0.60	99.77
5	5.5	-	-	-	-	-	0.01	0.04	0.06	0.02	0.03	0.02	0.00	0.17	99.95
5.5	6	-	-	-	-	-	-	0.01	0.01	0.00	0.01	0.01	0.00	0.05	99.99
6	6.5	-	-	-	-	-	-	0.00	-	0.00	-	-	0.00	0.01	100.00
6.5	7	-	-	-	-	-	-	-	-	-	-	-	-	-	100.00
	sum	-	0.01	2.06	15.05	26.97	23.97	16.68	9.46	4.17	1.35	0.25	0.03	100.00	

Figure 8.3: Scatterplot of significant wave heights (vertical axis) and wave peak periods (horizontal axis) with their relative frequency of occurrence on a yearly basis.

Wave height H_{s} (m)		Wave direction (\circ N)													
		15.00-	15.00	45.00	75.00	105.00	135.00	165.00	195.00	225.00	255.00	285.00	315.00		
lower	upper	15.00	45.00	75.00	105.00	135.00	165.00	195.00	225.00	255.00	285.00	315.00	345.00	sum	cum sum
0	0.5	-	-	-	-	-	-	-	-	-	-	-	-	-	-
0.5	1	-	-	-	-	-	-	0.01	0.02	0.01	-	-	-	0.03	0.03
1	1.5	-	-	-	-	-	0.02	0.82	2.70	0.78	0.03	-	-	4.35	4.39
1.5	2	-	-	-	-	0.00	0.15	6.48	11.39	3.00	0.07	0.00	-	21.09	25.48
2	2.5	-	-	-	-	0.00	0.76	12.97	13.01	3.18	0.11	0.01	-	30.05	55.52
2.5	3	-	-	-	-	-	1.28	11.73	7.96	2.02	0.08	0.01	-	23.08	78.61
3	3.5	-	-	-	-	-	1.25	6.38	3.82	1.23	0.07	0.01	-	12.75	91.35
3.5	4	-	-	-	-	-	0.80	2.48	1.84	0.59	0.05	0.01	-	5.76	97.12
4	4.5	-	-	-	-	-	0.35	0.79	0.66	0.26	0.01	-	-	2.06	99.17
4.5	5	-	-	-	-	-	0.08	0.20	0.24	0.07	0.01	0.00	-	0.60	99.77
5	5.5	-	-	-	-	-	0.01	0.06	0.09	0.01	-	-	-	0.17	99.95
5.5	6	-	-	-	-	-	0.00	0.01	0.03	0.00	-	-	-	0.05	99.99
6	6.5	-	-	-	-	-	-	0.00	0.00	-	-	-	-	0.01	100.00
6.5	7	-	-	-	-	-	-	-	-	-	-	-	-	-	100.00
	sum	-	-	-	-	0.01	4.70	41.94	41.75	11.16	0.41	0.04	-	100.00	

Figure 8.4: Scatterplot of significant wave heights (vertical axis) and main wave directions (horizontal axis) with their relative frequency of occurrence on a yearly basis.

8.2.3 Effect of wind to wave-growth

Wind speed and wind direction are important parameters when modelling waves with a SWAN model. The determination of these parameters for different wave conditions occurring offshore the Namibian Coast are discussed in Appendix D. Analyzing the correlations between waves and wind was done in Appendix D and has led to the following conclusions:

- In order not to underestimate the effect of wind the wind direction is chosen to be 225 degrees: Wind blowing perpendicular to the coast.
- Wind is accounted for only in case of short waves (Tp $<$ 10sec). From plotting all conditions (see Appendix D) it followed that there is hardly any positive effect of wind to long waves notable.
- The maximum wind speed is 10 m/s. Stronger winds blow only perpendicular or in opposite direction to the main wave direction according to the analyzed time-series.
- For short waves with a wave height of more than 4 m, wind is also not accounted for. Again because in that case winds blow only perpendicular or in opposite direction to the main wave direction according to the analyzed time-series.
- For short waves a linear relation is derived by means of a best-fit curve through the data: $Windspeed = 2.60 \cdot H_s + 0.55$. The plotted, used in the analysis of Appendix D, are presented again in Figure 8.5. It can be seen from the spreading of point in this figure that the linear relation is weak and that there is a large bias, which introduces uncertainties into the modelling process.

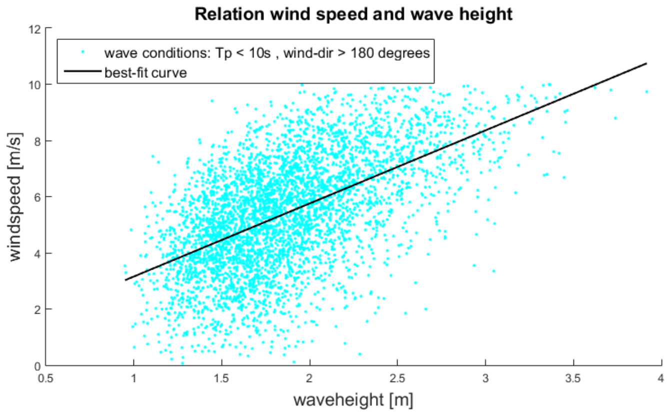

Figure 8.5: Best-fit curve to relate between wind speed and wave growth.

8.2.4 Model settings

The SWAN (version 41.01A) model runs in its third generation mode. This means that nonlinear wave-wave interactions are included by the model. With the settings of Westhuysen (see SWAN manual), wind and nonlinear saturation-based whitecapping are accounted for. Waves entering the computational domain are described by a JONSWAP spectrum with a significant wave height, wave peak period and mean wave direction specified by the user. An overview of the model settings is given in Figure 8.6.

```
PROJECT 'NAMDEB' '<FNUM>'

$ ********---- Heading ----**********
$ Witteveen+Bos, March 2015
$ Project NAMDEB
$ Wave modelling Sperrgebiet --- COARSE GRID
$ ANKJ2

$ *******---- start-up ----**********
SET NAUTical
MODE STAT TWOD
COORD SPHErical CCM

$ *******---- grid as set-up in delftdashboard ----*******
CGRID REGular 13.5 -30.0 0. 3.64 2.1 182 105 CIRcle 36 0.02 1.00

$ ******---- read bathymetry (from GEBCO) and wind ----*****
INPGRID BOT REGular 13.5 -30.0 0. 182 105 0.02 0.02
READINP BOTtom 1.0 'SWgrid7.bot'
WIND <WINDSP> 225

$ *****---- boundary conditions and initial conditions ----*****
BOU SHAP JONswap 3.3 PEAK DSPR DEGR
BOUNDSPEC SIDE South CONstant PAR hs=<WAVEH> per=<WAVEPER> dir=<WAVEDIR> dd=30
BOUNDSPEC SIDE West CONstant PAR hs=<WAVEH> per=<WAVEPER> dir=<WAVEDIR> dd=30
BOUNDSPEC SIDE North CONstant PAR hs=<WAVEH> per=<WAVEPER> dir=<WAVEDIR> dd=30
INITial DEFault

$ *****----- physics ----*****
GEN3 WESTH
BREAKING CONSTANT
FRICTION

$ *****--- numerics ----*****
PROP BSBT
NUMerics STOPC dabs=0.005 drel=0.01 curvat=0.005 npnts=99.5 STAT mxitst=30
```

Figure 8.6: Model set-up of SWAN (version 41.01A) model on a relatively coarse grid to simulate the wave regime in front of the Southern Coastal Mine Namibia.

```
PROJECT 'NAMDEB' '<FNUM>'

$ ********---- Heading ----**********
$ Witteveen+Bos, March 2015
$ Project NAMDEB
$ Wave modelling Sperrgebiet  --- FINE GRID

$ *******---- start-up ----**********
SET NAUTical
MODE STAT TWOD
COORD SPHErical CCM

$ *******---- grid as set-up in delftdashboard ----*******
CGRID REGular 15.68 -28.56 0. 0.68 0.6 170 150 CIRcle 36 0.02 1.00

$ ******---- read bathymetry and wind ----*****
INPGRID BOT REGular 15.68 -28.56 0. 170 150 0.004 0.004
READINP BOTtom 1 'SWnear7.bot'
WIND <WINDSP> 225

$ ---- boundary conditions and initial conditions ----
BOUNDNEST1 NEST 'NESTRUN25' CLOSED

$ ----- physics ----
GEN3 WESTH
BREAKING CONSTANT
FRICTION
$ TURBULENCE

$ --- numerics ----
PROP BSBT
NUMerics STOPC dabs=0.005 drel=0.01 curvat=0.005 npnts=99.5 STAT mxitst=30

$ ---- output ----
POINT 'pnt01' xp=16.172 yp=-28.444
SPECOUT 'pnt01' SPEC2D ABS 'SPEC_<FNUM>.sp2'
```

Figure 8.7: Model set-up of SWAN (version 41.01A) model on a fine grid close to the shore to simulate the wave regime in front of the Southern Coastal Mine Namibia.

8.3 Model results

The output of SWAN is in the form of a wave energy spectrum at a desired location near shore. The wave spectrum can be used as input (wave boundary condition) for the XBeach model, which models the near shore region. As mentioned before, 484 different wave conditions can occur. To present the model results of SWAN, three cases of wave conditions are discussed here and their results are presented.

The first combination of wave conditions is the most abundant case, exceeded in 50% of all cases. This case has been modelled to get a proper insight into the wave forces working on the shoreface. The second case is a combination of wave height, period and direction which is exceeded only 1% of all cases per year. The motivation is that the upper shoreface will most likely strive to form an equilibrium profile consistent with these conditions. The third case occurs under the most extreme wave conditions that have been recorded in the timeseries of 10 years, which were analyzed. The derivation of these conditions comes directly from adding up frequency values in the scatterplot of wave heights and wave periods in Figure 8.3, under the assumption that higher and longer waves have a bigger impact on changes to the upper shoreface and in particular to the seawalls.

	Most abundant condition	1%-condition	Most extreme condition (return period of 10 years)
Probability of exceedance	+/- 50 %	1 %	0.0041 %
Duration of exceedance per year	4380 hour	87.6 hour	0.36 hour
Significant wave height (Hs)	2.25 m	4.25 m	6.25 m
Wave peak period (Tp)	8.5 s	11.5 s	15.5 s
Wave direction (North = 0 degrees)	210 degrees	230 degrees	210 degrees

Table 8.1: Input of combinations of conditions for offshore waves in SWAN

The model results are visualized in Figure 8.9 to 8.11. Figure 8.8 repeats the frame of reference again.

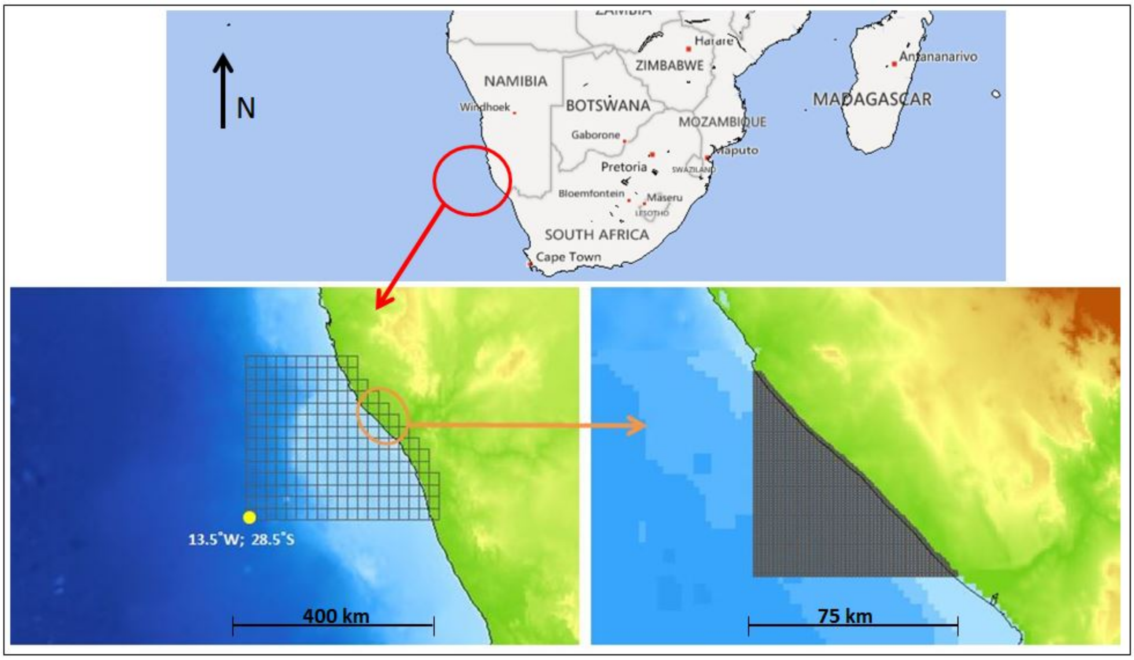

Figure 8.8: Repetition of Figure 8.1: Map showing the location and computational grid that are used for computations by SWAN.

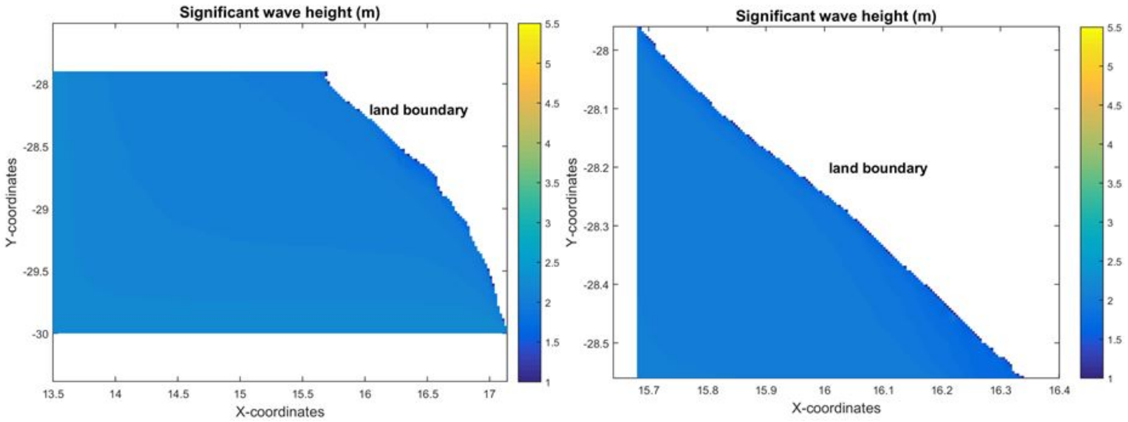

Figure 8.9: Graphical visualization of the significant wave height (Hs) for the Southern Namibian shore under the most abundant offshore wave conditions (see table 8.1). Left: calculation for a coarse grid. Right: calculation for a finer grid nested in the coarse grid on the left.

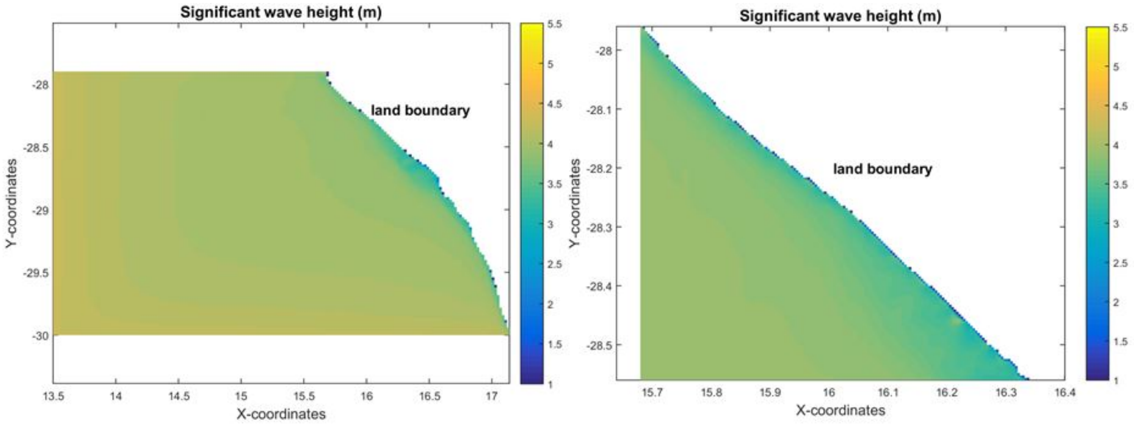

Figure 8.10: Graphical visualization of the significant wave height (Hs) for the Southern Namibian shore under the offshore wave conditions occurring 1% of the time (see table 8.1). Left: calculation for a coarse grid. Right: calculation for a finer grid nested in the coarse grid on the left.

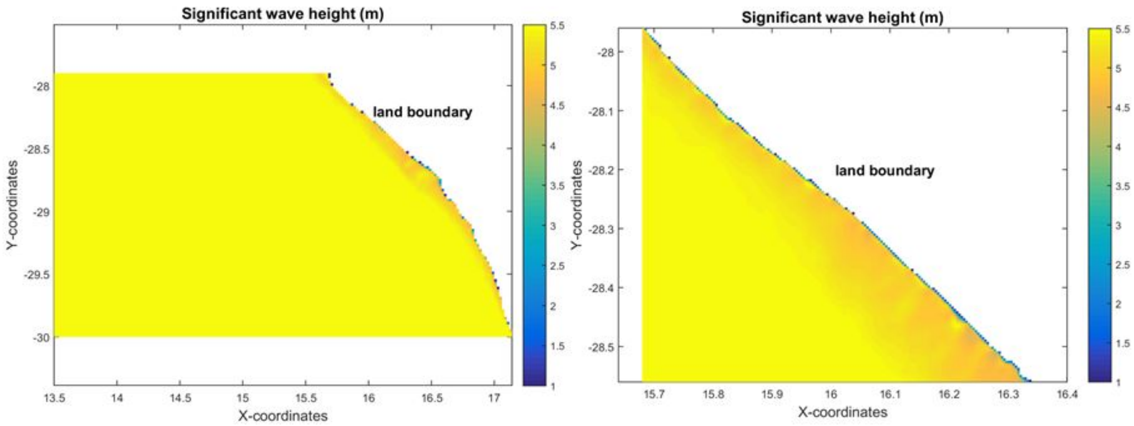

Figure 8.11: Graphical visualization of the significant wave height (Hs) for the Southern Namibian shore under the most extreme offshore wave conditions (see table 8.1). Left: calculation for a coarse grid. Right: calculation for a finer grid nested in the coarse grid on the left.

These three cases count as examples. The modelling process with SWAN is a necessary step for setting up a coastal model with XBeach (section 9.2). The focus of this research will logically be on the results of the XBeach model.

Chapter 9 – Modeling seawall erosion and beach profile response with XBeach

The Model XBeach (eXtreme Beach behaviour) (Roelvink et al., 2009) has been developed to model the response of beach profiles during a storm. The necessity of a model like XBeach became clear after several hurricanes hit the sandy shores of the south-east of the USA between 2000 and 2005. XBeach is a process-based nearshore model used to calculate coastal response during time-varying storm and hurricane conditions (so on the short-term), including dune-erosion and overwash. The software program is therefore definitely useful and relevant for modelling the coastline of the Southern Coastal Mine, because it can well simulate the seawall and beach profile in front of it, as is the purpose for this thesis.

9.1 XBeach: Model approach

XBeach uses a two-dimensional horizontal (2DH) approach to solve swash dynamics and avalanching processes. A brief discussion of the model approach is given below, focusing on the features relevant to the case of dune erosion in NAMDEB's Southern Coastal mine. For a more detailed description of XBeach and its features, one is referred to the manual (Roelvink et al., 2010) or the article by Roelvink et al. (2009).

9.1.1 Coupling wave-action to flow

XBeach is a 2DH numerical model solving wave propagation, flow, sediment transport and change of the upper shoreface for different boundary conditions. The calculations are wave-group averaged, thereby considering the changes in short wave energy to obtain long wave motions. This phenomenon has been discussed in section 6.2.1.

Wave action balance

A 2DH description of wave-groups entering the domain, with infragravity waves accompanying them, is employed to resolve swash dynamics. Wave forcing in the shallow water region is obtained by using the wave action balance developed by Holthuijsen et al. (1989) for the HISWA model[1]. This balance (see equation 9.1 below) takes the directional distribution of the incoming waves into account, but represents the frequency spectrum by the spectral parameter $f_{m-1,0}$. The use of this single representative peak period assumes a narrow banded frequency spectrum. The wave action balance is:

$$\frac{\delta A}{\delta t} + \frac{\delta c_x A}{\delta x} + \frac{\delta c_y A}{\delta y} + \frac{\delta c_\theta A}{\delta \theta} = -\frac{D_w}{\sigma} \tag{9.1}$$

[1] Hindcasting of waves in shallow-water (HISWA)

Here A represents the wave action by:

$$A(x,y,t,\theta) = \frac{S_w(x,y,t,\theta)}{\sigma(x,y,t,\theta)} \tag{9.2}$$

With S_w being the wave energy and σ the radian wave frequency. The wave celerity is represented by c, c_x for the cross-shore celerity and c_y for the alongshore celerity. In equation 9.1 the first LHS (left hand side) term accounts for the change of wave action in time, the second and third LHS term are spatial advection terms for the wave energy. The fourth term represents directional advection, meaning that it accounts for refraction.

The dissipation of wave energy due to breaking (D_w in equation 9.1) is modelled by XBeach by default with (Roelvink, 1993):

$$\bar{D_w} = 2\frac{\alpha}{T_{rep}} Q_b E_w \frac{H_{rms}}{h} \tag{9.3}$$

In where Q_b is a probability function that describes the fraction of breaking waves. α is a first order calibration factor, T_{rep} is the representative wave period (the peak period in the energy density spectrum) and E is the wave energy. The last term ($\frac{H_{rms}}{h}$) is a modification by Van Thiel de Vries (2009).

Wave energy dissipation due to bottom friction can be included in the calculations by applying an additional dissipation term, D_f:

$$D_f = \frac{2}{3}\rho\pi f_w \left(\frac{\pi H}{T_{rep} \cdot sinh(kh)}\right)^3 \tag{9.4}$$

With f_w being the friction factor depending on the type of bottom.

In case of modelling the Southern Coastal Mine Namibia, both dissipation due to wave breaking and due to bottom friction are relevant. The total dissipation is the sum of both $D = (D_w + D_f)$.

Roller energy balance

To calculate the wave force, the wave action balance is coupled to the roller energy balance. Roelvink et al. (2009) elaborates on this process. The result is that the wave force can be calculated using the radiation stresses (see equation 9.5 and 9.6 below).

$$F_x(x,y,t,\theta) = -\left(\frac{\delta S_{xx,w} + \delta S_{xx,r}}{\delta x} + \frac{\delta S_{xy,w} + \delta S_{xy,r}}{\delta y}\right) \tag{9.5}$$

$$F_y(x,y,t,\theta) = -\left(\frac{\delta S_{xy,w} + \delta S_{xy,r}}{\delta x} + \frac{\delta S_{yy,w} + \delta S_{yy,r}}{\delta y}\right) \tag{9.6}$$

Nonlinear Shallow Water Equations

Wave action is coupled to flow in the shallow water regions by means of implementing the wave force in the Nonlinear Shallow Water (NLSW) equations. A depth-averaged Generalized Lagrangian Mean (GLM) formulation is used to find an expression for wave induced mass flux and the subsequent flow. The LHS of equation 9.7 and 9.8 is the response of the water to the force described by the RHS of the transport equations.

$$\frac{\delta u}{\delta t} + u\frac{\delta u}{\delta x} + v\frac{\delta u}{\delta y} - fv - \nu_h(\frac{\delta^2 u}{\delta x^2} + \frac{\delta^2 u}{\delta y^2}) = \frac{\tau_{sx}}{\rho h} - \frac{\tau_{bx}}{\rho h} - g\frac{\delta \eta}{\delta x} + \frac{F_x}{\rho h} \tag{9.7}$$

$$\frac{\delta v}{\delta t} + u\frac{\delta v}{\delta x} + v\frac{\delta v}{\delta y} + fu - \nu_h(\frac{\delta^2 v}{\delta x^2} + \frac{\delta^2 v}{\delta y^2}) = \frac{\tau_{sy}}{\rho h} - \frac{\tau_{by}}{\rho h} - g\frac{\delta \eta}{\delta y} + \frac{F_y}{\rho h} \tag{9.8}$$

$$\frac{\delta \eta}{\delta t} + \frac{\delta hu}{\delta x} + v\frac{\delta hv}{\delta y} = 0 \tag{9.9}$$

η is the water level, h the water depth. On the left hand side (LHS) the second and third term account for the advection. The fourth for the Coriolis effect. The fifth LHS term represents the Reynold stresses, using the turbulent viscosity ν. On the right hand side (RHS), the first term represents the surface shear stress, the second term the bed shear stress, for which reference is made to the approach of Ruessink et al. (2001). The third RHS term accounts for the pressure force due to water level gradients. The fourth term is the wave induced force on the water body.

The velocity u (in x-direction) and v (in y-direction) are the sum of the Eulerian velocity (u^E), the short-wave-averaged velocity observed from a fixed point, and the Stokes drift (u^S) according to Philips (1977).

9.1.2 Sediment Transport

A depth-averaged advection-diffusion equation was developed by Galappatti and Vreugdenhil (1985) and is used by XBeach to model sediment transport (equation 9.10):

$$\frac{\delta hC}{\delta t} + \frac{\delta hCu}{\delta x} + v\frac{\delta hCv}{\delta y} + \frac{\delta}{\delta x}(D_h h\frac{\delta C}{\delta x}) + \frac{\delta}{\delta y}(D_h h\frac{\delta C}{\delta y}) = \frac{hC_{eq} - hC}{T_s} \tag{9.10}$$

Where C is the depth-averaged sediment concentration, varying on the timescale of wave groups, and C_{eq} the equilibrium concentration. D_h is the sediment diffusion coefficient and T_s represents the adaptation time scale for the entrainment of sediment, depending on the local water depth and the sediment fall velocity. XBeach calculates the entrainment or deposition of sediment by determining the mismatch between the actual sediment concentration (C) and the equilibrium sediment concentration (C_{eq}). This can be seen on the RHS of equation 9.10 (the source term).

$$C_{eq} = \frac{A_{sb} + A_{ss}}{h}\left(\left(\left|u^E\right|^2 + 0.018\frac{u_{rms}^2}{C_d}\right)^{0.5} - u_{cr}\right)^{2.4}(1 - \alpha_b m) \tag{9.11}$$

Here A_{sb} and A_{ss} are coefficients accounting for bed-load sediment transport and suspended sediment transport respectively. u^E is the Eulerian flow velocity as mentioned earlier. The factor 0.018 accounts for irregular waves and not for regular waves Van Thiel de Vries (2009).

9.1.3 Morphological evolution

Bed level change

Morphological change can firstly be seen by bed level changes. XBeach updates the bed according by calculating gradients in sediment transport. This is done with the formula that has already been discussed in section 6.3. The important (and only) difference is the application of the morphological acceleration factor f_{mor}.

$$\frac{\delta z_b}{\delta t} = -\frac{1}{1-p}\left(\frac{\delta q_x}{\delta x} + \frac{\delta q_y}{\delta y}\right) \cdot f_{mor} \tag{9.12}$$

z_b is the bed level elevation. q_x and q_y in equation 9.12 are transported sediment quantities in the x- and y-direction respectively. The morphological acceleration factor (in short: Morfac) provides the possibility to speed up morphological evolution, (on morphological timescales) relative to hydrodynamic timescales. The purpose of applying a Morfac is to decrease the required computation time. For example, a simulation of one hour with a Morfac of 12 will effectively simulate morphological changes over 12 hours.

Avalanching

The avalanching mechanism can be modelled with XBeach to account for the slumping of sandy slopes during wave attack on a dune. XBeach updates the bed after a slumping event, which happens when the critical bed-slope is exceeded (equation 9.13).

$$\left|\frac{\delta z_b}{\delta x}\right| > m_{cr} \tag{9.13}$$

When a wave reaches the dune toe and (partly) inundates it, the critical wet bed-slope ($m_{cr,wet}$=0.3 according to standard model settings) is exceeded and XBeach adjusts the two grid cells at the dune toe during the first timestep of this event. In the following timesteps a chain reaction is set into motion in landward direction to update the profile of the slope. Also the critical dry bed-slope ($m_{cr,dry}$=1.0 according to standard model settings) is now exceeded. Sand from the dry dune profile enters the wet profile and can be transported in seaward direction by an undertow or the backwash of waves.

9.2 XBeach: Model set-up

9.2.1 Introduction

An XBeach (version 1.22.4672) model is set up to determine wave run-up and dune erosion associated with the seawalls. These results can subsequently be used to determine the required crest height and thickness (or volume) of a seawall.

XBeach is applied in its 1D-mode to model the changes of a cross-shore profile in the Southern Coastal Mine, but also dune/seawall erosion volumes in specific. First the long-term evolution (100 days) of the upper shoreface under actual wave conditions is modelled. This is done to gain inside in the physical processes occurring. From here on the erosion of the seawalls will be modelled under 'storm' conditions / extreme events (i.e. short-term). The adopted definition of a storm is also explained (see section 9.2.5).

9.2.2 Location

One cross shore profile (the highlighted cross-section of Figure 9.2) was chosen to be modelled in first instance. Later similar model set-ups can be used at different locations along the coast of the Southern Coastal Mine.

The main focus of the Sand-2-Sea program is on a particular part of the G-area and the U-area of the linear beaches. This is where the largest diamond deposits are most likely to be found according to NAMDEB. As a consequence the major activity in terms of seawall construction is concentrated here. The most severe wave attack on the seawalls is also expected to be in these regions, since the seawall will be located relatively close to the high-waterline on the beach.

Bathymetrical data are available in single lines perpendicular to the coast. Every 250 m along the coast of MA1 a single-beam survey is done by measuring the bed level in a single line. An overview of survey data is given in Figure 9.1, where Figure 9.2 zooms in on the target region. The red lines in the figures are the survey lines, and each line is perpendicular to the coast. The numbers of the survey lines correspond to the distance in meters from the Orange River mouth.

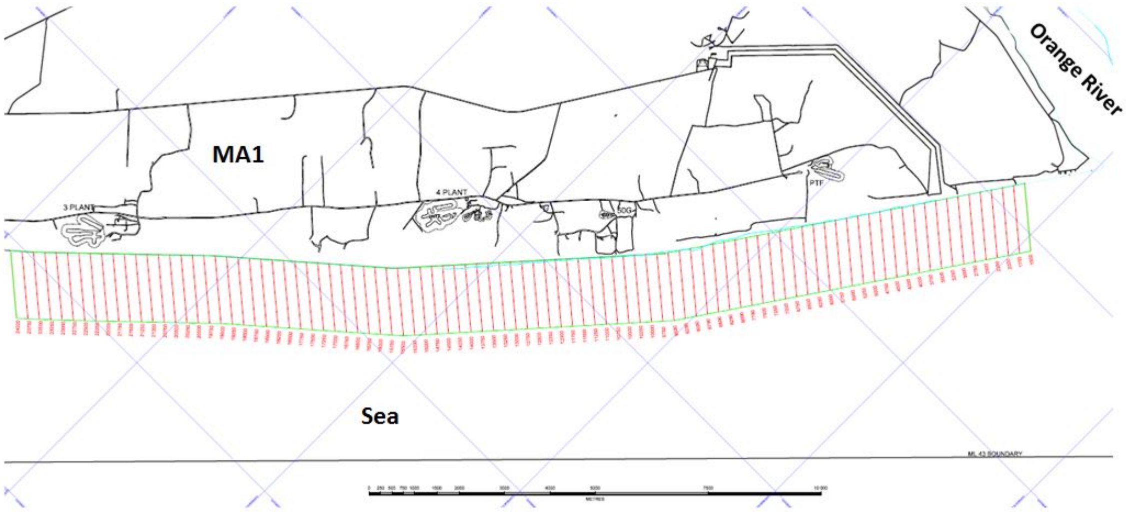

Figure 9.1: Overview of survey to obtain bathymetry nearshore the Southern Coastal Mine Namibia. The red lines represent the single-beam survey done in the shallow and intermediate water (midwater) regions.

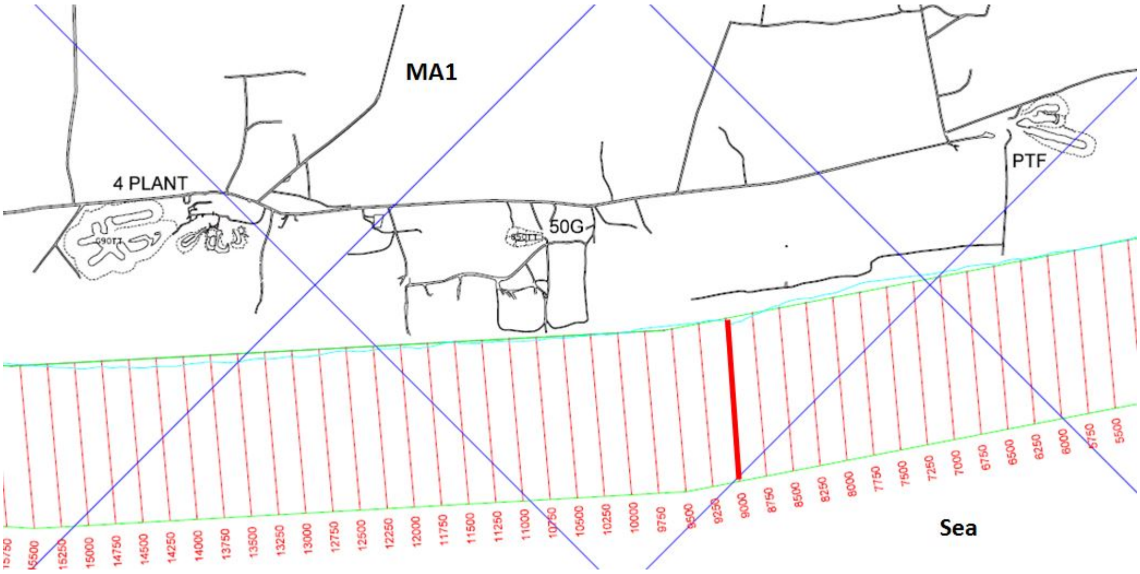

Figure 9.2: Zoomed in on the mining activity in the G-area. Survey Line 9000 is high-lighted in red.

Pictures taken during the fact-finding mission (see Chapter 3), such as Figure 9.3, together with the plans for expanding the mining activity seawards, show that Line 9000 (see Figure 9.2) and Line 9500 (see Figure 9.4) will probably experience the heaviest wave attack in the G-area.

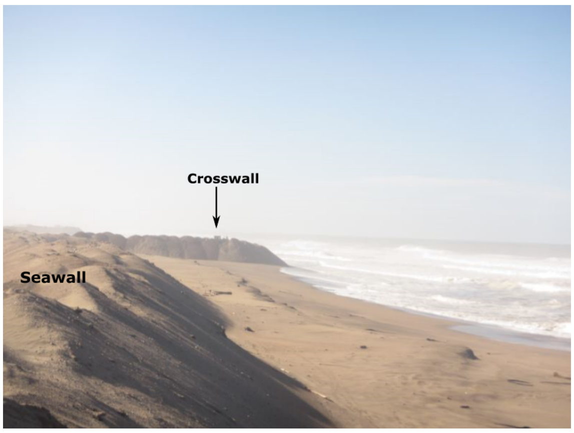

Figure 9.3: Picture of seawall on the beach in the G-area (close to Survey Line 9000). In the distance a groyne / crosswall extension in visible

Figure 9.4: Picture of seawall on the beach in the G-area (close to Survey Line 9500).

At first, Line 9000 will be modelled as a single line. As a case study (section 9.3.1) a seawall breach during a storm in May 2015 was simulated. This was on the location of survey lines 22250, 22500 and 22750 in the U-area, not in the G-area. Apparently wave attack is heavier in that area. The case study will elaborate on that and also show how the same model set-up can be used at a different location along the coast of the Southern Coastal Mine.

9.2.3 Model input

Bathymetry

The bathymetry that was used to set-up the model was derived from measurements done by the Survey team of NAMDEB in October 2014. In the representation of the bed level (Figure 9.5 and Figure 9.6) a breaker bar is visible (high-lighted in purple). Wave records show that the survey was done during very mild wave conditions.

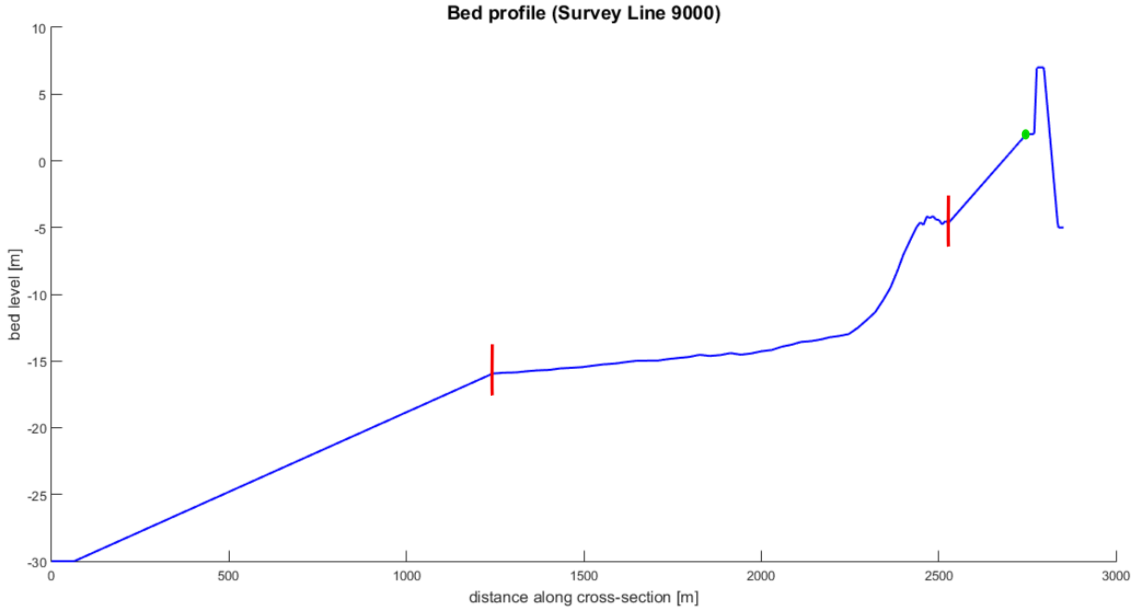

Figure 9.5: 1D cross-shore bed profile of Survey Line 9000 of the Southern Coastal Mine Namibia. The curved line between the two red lines is the bathymetry data received from NAMDEB. The green dot represents the MSL +2m location on the beach.

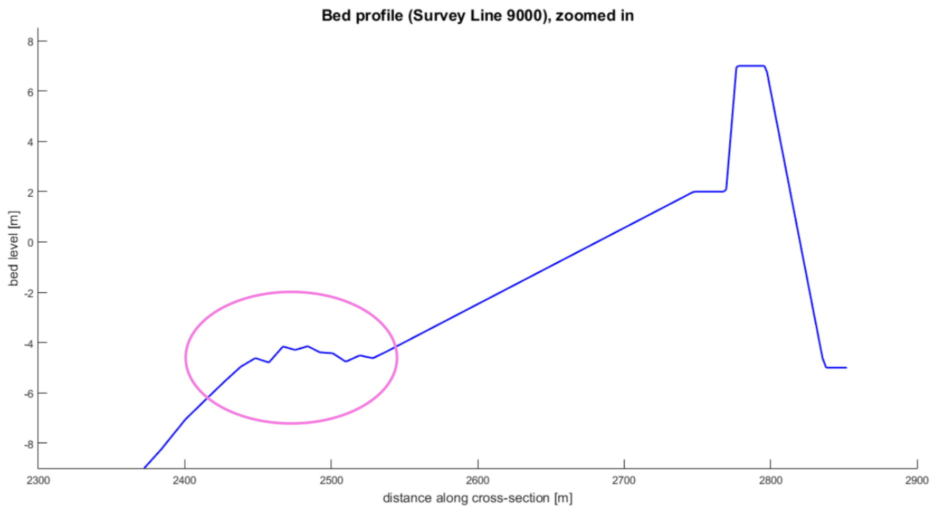

Figure 9.6: 1D cross-shore bed profile of Survey Line 9000, zoomed in on the upper shoreface. The purple circle high-lights the breaker bar present under the wave conditions in which the Survey was executed.

The bathymetry data used as input for XBeach are under discussion. First of all the survey line is perpendicular to the coast but not entirely straight. Curves are smoothened out, but this can impact the reliability of the final answer. Secondly, the survey line stops at a water depth of about MSL -4 m. This is just outside the breaker zone. The surfzone and swash zone are not part of the measured profile. So there is a data gap until a height of +2m, because this (high water) contourline is measured along the beach also. Thirdly, the outerslope (1/3) and height (7m) of the seawall are known, but the position of the seawall in cross shore direction is unknown. The toe of the seawall is chosen at the MSL +2m contourline of the shore, based on analyzing pictures, like the one in Figure 9.3 and Figure 9.4, where it looks like the toe of the seawall is very close to the high-waterline.

Figure 9.5 is constructed as follows: The area between the red lines represents the provided bathymetry data. These are manually extended on the left to deeper water (with a bed slope of 1/50), so the domain where waves enter starts with deep water. The green dot in the figure is the provided location of the high-waterline (MSL +2 m). The data gap between this point and the red line is filled up by a linear interpolation of the bed profile. On the right side of the green dot the seawall is manually added to the data according to the seawall standards presented in Figure 3.8 of section 3.5.

Waves

The modelling results from SWAN in the form of nearshore wave-spectra (see Chapter 8) form the hydrodynamic boundary conditions for the model. The selection of wave conditions depends on the purpose of the modelling process. This will be explained in further sections.

Grain sizes

The particle size distribution of the beach sand has been evaluated for different locations in the Southern Coastal Mine (Anker, 2014). However, the smallest sieve diameter that was used has a diameter of 1.4 mm. 0 – 1.4 mm is still a considerably large range. And, as can be expected, the largest fraction of the tested sediment lies within this range. For sediment transport the effect of the grain size is very large.

The choice of grainsize distribution has significant impact on the cross-shore sediment transport and thus the erosion volume. The two parameters that represent the distribution (in XBeach) are D_{50} and D_{90}, with D_{50}/D_{90} the ratio of grading. For an average Dutch beach D_{50} is about 300 μm and D_{90} is 450 μm (ratio D_{50}/D_{90} is 0.667). The Namibian Southern Coast is now known for its coarse-grained beaches, mainly because of mining activity in the Southern Coastal Mine. However, it is still a sandy beach and not a gravel beach (see Figure 9.16).

The assumption is made that the grading of sediment is the same as for a Dutch beach (D_{50}/D_{90}), although this has to be verified. If the D_{50} for Dutch beachsand represents the lower 20% fraction (D_{20}) of the Namibian beach-sand distribution, then D_{50} and D_{90} for the Namibian Southern Coast are 400 μm and 600 μm respectively.

9.2.4 Long-term simulations

Long-term simulations give insight in the behaviour of coastal evolution, and can also be used to test the influence of different parameters that are not known a priori. The long-term simulations calculate 14 days (spring/neap tide cycle) with a morphological acceleration factor (Morfac) of 5, representing a total of 70 days.

Application of input reduction on the wave conditions

The hydrodynamic boundary conditions for the XBeach model are the wave conditions that were translated to nearshore conditions by the SWAN model (see Chapter 8). In Figure 8.3 a scatterplot of wave conditions was presented. About 484 different wave conditions (combination of wave height, period and direction) occur on a yearly basis. To limit the computational effort a set of wave conditions needs to be found to represent the entire wave climate. To find this set different input reduction techniques have been developed. The different steps of the method that is applied for this case are worked out in full in Appendix E. In the method applied here wave conditions have first been grouped manually according to their frequency of occurrence and their wave height and wave period. Then the impact of each group on the total annual sediment transport is determined. This is done in a rather rough way by multiplying the frequencies of occurrence with $H_s^{2.5}$, because sediment transport is almost proportional with this factor[2]. From here on the relative influence of different wave conditions to sediment transport can be determined. Within the formed groups representative wave conditions for each group/block are chosen and their probability of occurrence is scaled up, depending on their impact, so they can be applied in the XBeach model.

The list of offshore wave conditions, translated to nearshore conditions by the SWAN model, that is used is presented in table 9.1. The number of wave conditions has been brought back from 484 to 17 different conditions. Freq is the frequency of occurrence of the group of wave conditions of which the representative wave peak period and significant wave height have been chosen. Freq(original) is the original frequency of occurrence of that specific wave condition. F_{up} is the upscaling factor with which the impact of a wave conditions is scaled up.

[2]According to the simple CERC method (Bosboom and Stive, 2013) also a factor $\sin 2\phi$ must be incorporated to account for the wave angle relative to the coastline. Judging on the narrowness of the wave rose (Figure 8.2) and the fact that all waves refract towards an almost normal incident, this factor is not required in the calculations here.

Table 9.1: Upscaling per wave condition after application of input reduction

$H_{s,rep}$	$T_{p,rep}$	Freq	Freq(original)	F_{up}
2.25	7.5	9.18%	5.76%	1.59
2.75	7.5	5.61%	3.95%	1.42
1.75	9.5	18.06%	6.05%	2.99
2.25	8.5	7.67%	7.67%	1.00
2.75	8.5	6.73%	6.73%	1.00
3.25	8.5	3.85%	3.85%	1.00
4.25	9.5	1.59%	0.49%	3.26
2.25	9.5	6.91%	6.91%	1.00
2.75	9.5	4.87%	4.87%	1.00
3.25	9.5	2.93%	2.93%	1.00
3.75	9.5	2.74%	1.30%	2.10
2.25	10.5	7.90%	5.25%	1.50
2.75	10.5	6.07%	3.58%	1.69
3.25	10.5	3.65%	2.16%	1.69
3.75	12.5	2.95%	0.60%	4.88
4.25	12.5	1.67%	0.29%	5.67
2.75	12.5	4.10%	1.04%	3.92

With these conditions the cross shore profile is modelled. The results are shown in Figure 9.7.

Long term simulation results

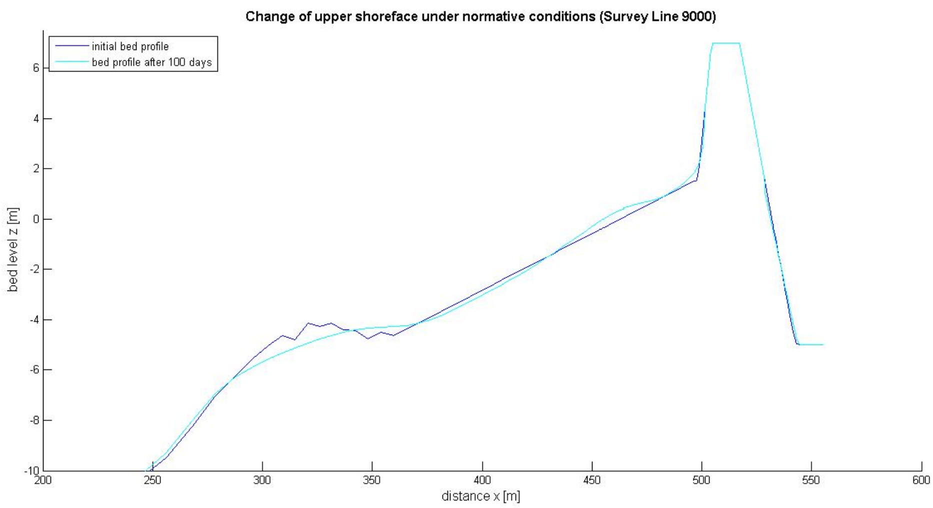

Figure 9.7: Long-term simulation (100 days) of 1D cross-shore bedprofile of Survey Line 9000 of the Southern Coastal Mine Namibia. Table 9.1 counts as input for the hydrodynamic boundary conditions.

It can be seen that the profile of the beach changes. This is predictable since the straight line, that was added manually because of a data gap, is not to be expected in a natural situation.

The beach becomes flatter around mean sea level and steeper close to the breaker bar. The breaker bar itself disappears or shifts in seaward direction. Due to the highly energetic wave climate, no stable breaker bar is to be expected. Besides, the breaker bar was measured during very mild wave conditions. On the outerslope of the seawall some erosion is visible. The seawall toe is quite close to the high waterline so during heavier wave conditions some erosion seems logical. NAMDEB corrects this by dumping extra sand on the seawall when needed (discussed in section 4.4).

In the following section model input parameters are assessed. This is done to get a better understanding of how the model performs, and also to increase the reliability of the model.

Assessment of model input parameters

Multiple long-term simulations have been carried out to study the behaviour of the upper shoreface. Appendix F discusses the influence of input parameters on the updating of the bed profile. The following cases/parameters are assessed:

- Different significant wave heights (Hs)
- Influence of different wave peak periods (Tp)
- Influence of different wave directions
- Different grainsize distributions
- Additional onshore sediment transport (Facua-coefficient)
- Different positions of the seawall on the beach

The assessment of parameters (Appendix F) is qualitative, not quantitative. The purpose is to study the evolution of the bed. For the analysis of seawall erosion a quantitative assessment can be done. This will be discussed in section 9.2.5. The qualitative assessment is carried out by simulating long-term bed profile change of the 1D cross-shore model of Survey Line 9000, like in the previous sections. Each time a certain parameter is changed to see its influence on the change of the upper shoreface.

From the analysis done in Appendix F it can be concluded that an equilibrium bed profile is never reached due to the constantly varying wave conditions. The bed profile can change very quickly because of the highly energetic wave climate. It can also be concluded that for the median grainsize (D_{50}) and the position of the toe of the seawall measured data are needed for accurate results, since their impact on bed profile change is significant. The calibration factors Facua Sk and Facua As (implemented together in XBeach as the Facua-coefficient) account for extra onshore transport due to wave skewness and wave asymmetry. Implementation was done because XBeach doesn't simulate the wave shape. The Facua-coefficient is unknown for the Southern Coastal Mine, but most likely higher than zero.

Deltares (2015) investigated and calibrated different input parameters/settings for XBeach. Where a model parameter is unknown, the settings found by Deltares (2015) will be used. An overview of these settings is given in table 9.2. Notable maybe the rather low value of the wave breaking parameter γ (gamma). Section 6.1.2 proposes a larger value of gamma, because plunging breakers seem to be present in front of the Southern Coastal Mine.

Table 9.2: XBeach optimization results (WTI-settings) found by Deltares (2015).

Parameter	Default	WTI settings
fw	0	0
cf	0.003	0.001
gammax	2	2.364
beta	0.1	0.138
wetslp	0.3	0.26
alpha	1	1.262
facSk	0.1	0.375
facAs	0.1	0.123
gamma	0.55	0.541

Figure 9.8 presents the results of the same computation that was done before (results presented in Figure 9.7), but now with the model settings according to Deltares (2015) instead of the default settings. The difference is clearly visible. The new settings result in a less steep beach profile, but also in more erosion to the seawall. In the case of the Namibian Coast, the new settings by Deltares (2015) can be considered as more conservative.

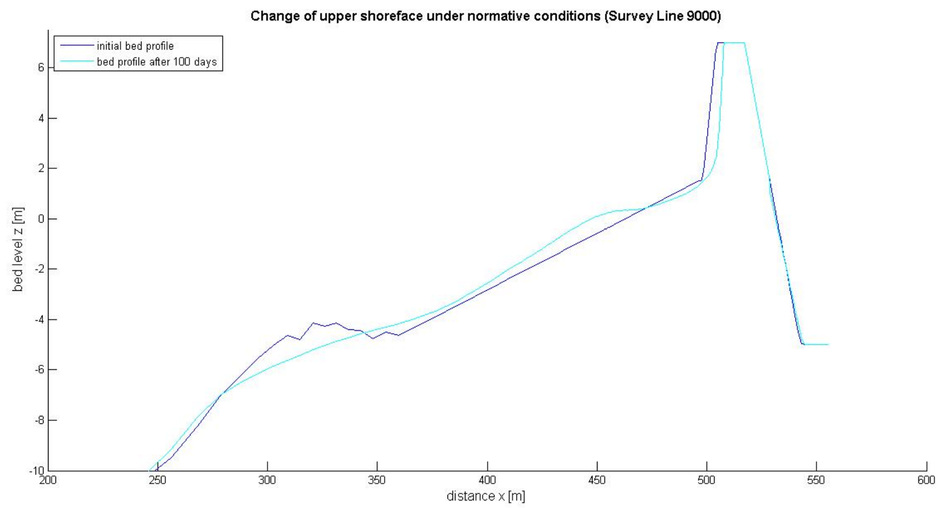

Figure 9.8: Long-term simulation (100 days) of 1D cross-shore bedprofile of Survey Line 9000 of the Southern Coastal Mine Namibia. Table 9.1 counts as input for the hydrodynamic boundary conditions.

Conclusions from long term model simulations

From the long term simulations of a cross shore profile of Southern Coastal Mine the following conclusions can be drawn:

Firstly, no equilibrium profile seems to develop in time. The wave climate is highly energetic and so significant profile changes happen when wave conditions vary. Chapter 10 explains how one must deal with a varying bed profile when designing a seawall. That chapter will also discuss the difficulties that NAMDEB experiences when the wrong equilibrium profile is chosen.

Secondly, erosion to the seawalls occurs on the timescale of weeks. This is consistent with the maintenance activities that NAMDEB carries out (Anker, 2014). On a weekly basis corrective maintenance is done by sand dumping on the outer slope of the seawall.

From the assessment of model parameters (Appendix F) it could be seen that a lot of variables influence the model results. For the short-term simulations a quantitative assessment will be carried out. The settings found by Deltares (2015), presented in 9.2, will be used in further simulations.

9.2.5 Short-term simulations

To model single storm conditions and extreme events acting on the shore of the Southern Coastal Mine, short-term simulations were carried out in the same XBeach model set up as used for long term simulations. The purpose is to determine the erosion volumes of sand from the seawalls during a storm. With this information one can design a seawall based on specific design conditions.

Storm conditions

The seawall must be designed to withstand certain storm conditions. A storm condition is defined in this case as the combination of wave height and wave period with a duration of 24 hours. Due to refraction, the wave direction will not play a significant role (see also Appendix F). It is important to note that the tide and the wind set-up are of minor influence on a storm, as explained earlier in section 6.2.2. Appendix G shows how waverecords were used to define different design storms. Calculating the probability of certain storm conditions or extreme events resulted in the wave conditions shown in table 9.3. For the analysis of storm conditions timeseries of 30 years of wave data were available. Only wave data above a certain threshold for the significant wave height were chosen to be able to investigate the extreme events. Next, an extreme value distribution must be chosen to approximate the distribution of extreme wave data as accurate as possible. From Appendix G can be concluded that a Gumbel distribution is the most appropriate approximation. The Gumbel extreme value distribution can be written as:

$$P(H \leq H_{ss}) = Q = \exp\left[-exp\left(-\frac{H_{ss}-\gamma}{\beta}\right)\right] \tag{9.14}$$

This can be translated to a significant wave height, belonging to a storm with a certain exceedance probability per year:

$$H_{ss} = \gamma - \beta \cdot ln(ln(\frac{N_s}{N_s - Q_s})) \tag{9.15}$$

Plotting the wave data on logarithmic scale results in Figure 9.9, summarized in table 9.3

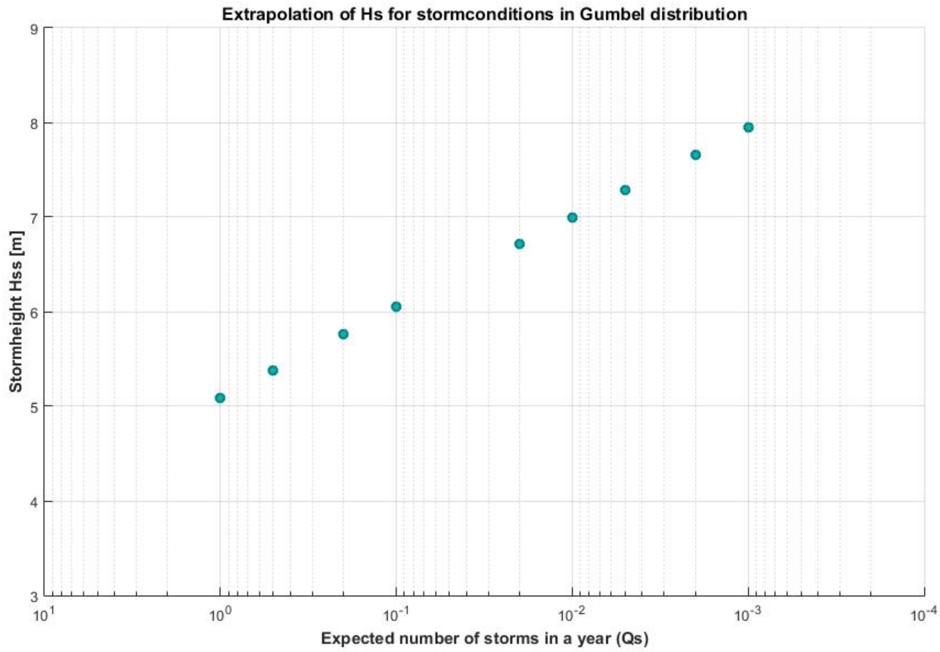

Figure 9.9: Wave heights, according to the Gumbel distribution, belonging to certain probabilities of occurrence.

Table 9.3: Offshore H_{ss}- and T_p-values associated with design storms (yearly probability). Values of H_{ss} are approached with a Gumbel extreme values distribution. The analysis done for finding values of T_p is explained below in detail.

Design storm [prob. per year]	1/1	1/2	1/5	1/10	1/50	1/100
H_{ss} [m]	5.09	5.38	5.76	6.05	6.71	7.00
T_p [s]	12.34	12.69	13.15	13.49	14.27	14.61

Note that results shown in table 9.3 present the significant wave height occurring off shore (Longitude: 13.5 degrees, Latitude: -28.5 degrees). They are to be translated to near shore data with the SWAN model (section 8.2).

The relation between wave peak period Tp and significant wave height Hs for storm events has also been investigated (see Appendix G). This has been done by plotting wave conditions above a certain threshold for both Hs and Tp. By curve-fitting the relation was found. This is in the form of equation 9.16, which followed from the plot presented in Figure 9.10. This linear relation only applies to this specific set of data points above the chosen threshold for Hs and Tp.

$$T_p = 0.973 \cdot H_s + 8.127 \tag{9.16}$$

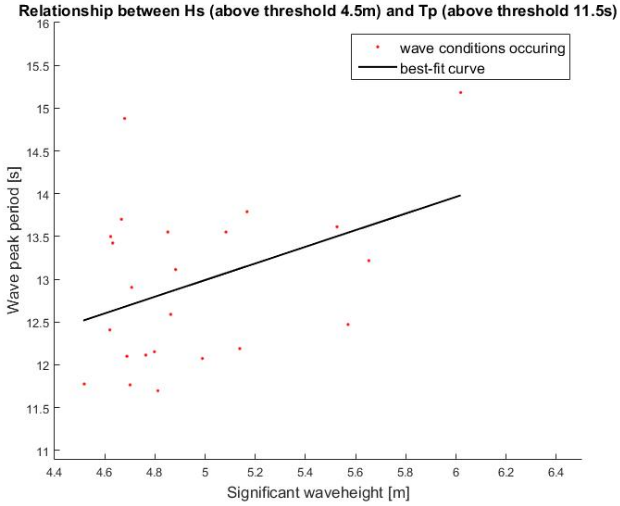

Figure 9.10: Relationship between significant wave height H_s and wave peak period T_p for data above the threshold of Hs = 4.5m and Tp = 11.5s.

From this analysis it can be concluded that the relationship between Hs and Tp is very weak. A large standard deviation of 2s for Tp should be chosen to cope with the large uncertainties of the relationship.

Simulating storm events

The impact of storm events on the seawall can now be modelled. This is explained in the section below.

Appendix G (Storm Conditions) states that a storm condition is a condition that lasts 24 hours. Studying the timeseries of wavebouy data, one can see that extreme events have a duration of approximately 3 days. Within this 3 days the most extreme condition lasts less than 24 hours. For this reason the model simulates 3 days; starting with the 1/1 per year storm, then the design storm, and then the 1/1 per year storm again. This is to reduce the chance of an underestimation of seawall erosion. The water levels at the offshore boundaries represent the spring-tidal signal (plus the day before and after), according to table 2.1 in section 2.2.

The profile of the seawall (black line in Figure 9.11) is according to the design standards of NAMDEB. On both sides of the crest of the seawall is a windrow (see also Figure 4.5 in section 4). The results of the simulations of design storm conditions are presented in Figure 9.11. Each coloured line represents the resulting profile of the seawall after a storm.

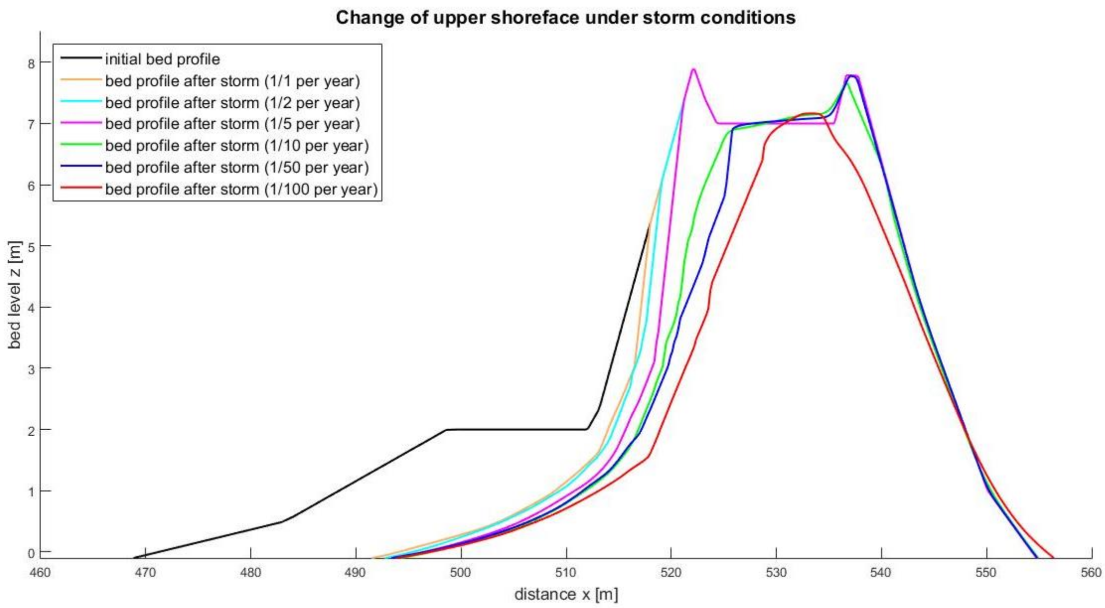

Figure 9.11: Plot of the seawall on Survey Line 9000. The coloured lines represent the resulting bed profile after specific storm conditions.

The beach in front of the seawall experiences erosion due to any storm event. Sand is transported further offshore. The more severe the storm condition are, the more sand is eroded from the seawall. Figure 9.11 shows that the serviceroad on top of the wall is no longer usable when a storm with a probability of 1/10 per year has occurred. The storm with a probability of 1/100 per year does not lead to seawall failure, but does lead to dangerous situations. Also important to notice is that only in the 1/100 per year storm overtopping is seen. Table 9.4 shows the calculated erosion volumes per storm condition. The erosion volumes are calculated between the toe of the seawall (at a level of $+2$ m) and the crest of the seawall. The total volume of the seawall is 135.4 m^3/m per cross-section.

Table 9.4: Resulting seawall erosion volumes per storm condition.

Design storm [prob. per year]	1/1	1/2	1/5	1/10	1/50	1/100
Eroded volume $[m^3/m]$	2.9	6.0	15.9	38.1	56.5	80.2

According to the model the seawall does not fail entirely during a storm with a probability of 1/100 per year. However, the model has uncertainties. These are discussed by means of a sensitivity analysis (next section). Appendix K describes how one should deal with model uncertainties by means of probabilistic approach for a seawall design.

9.2.6 Sensitivity Analysis

A sensitivity analysis was carried out to study the influence of certain model parameters. This analysis has been made quantitative by calculating the volume of sand in m^3/m taken away from the seawall at the end of the simulation time. A summary is presented here. Appendix H presents the full sensitivity analysis.

Table 9.5 presents the parameters that were tested.

Table 9.5: Parameters to be tested in sensitivity analysis. For each parameter the mean, maximum and minimum value are given.

Parameter	Unit	Mean	Max variation to be tested (%)	Max variation to be tested	Left bound	Right bound
Critical angle wet slope	tan(α)	0.26	15%	0.039	0.221	0.299
Critical angle dry slope	tan(α)	1	10%	0.1	0.9	1.1
Median grainsize	μm	400	25%	100	300	500
Facua As	-	0.123	33%	0.0406	0.0824	0.1636
Facua Sk	-	0.375	33%	0.1238	0.2513	0.4988
Vertical Position Toe Seawall	m (above normal sealevel)	1.5	33%	0.5	1	2
Orientation Coastline	degrees	50.654	5%	2.533	48.121	53.187
Significant wave height	m	6	15%	0.9	5.1	6.9
Wave peak period	s	13.5	15%	2.025	11.475	15.525
Mean wave direction	degrees	210	15%	31.5	178.5	241.5

Each time a simulation is done with the mean values of each parameter, except for one parameter each time. This parameter is varied to study the influence of that parameter on the eroded sand volume. The results of the simulations are summarized in the graph of Figure H.6.

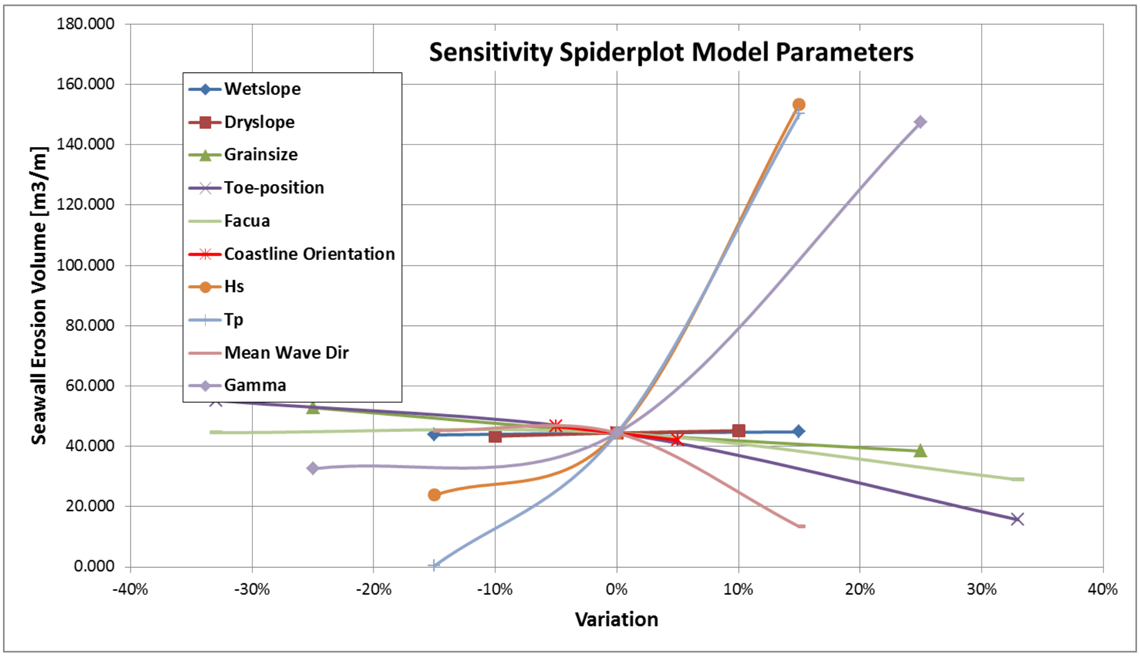

Figure 9.12: Spiderplot presenting the influence of all relevant parameters for eroded sand volumes in the 1D XBeach Model.

Of all model settings the gamma, or wave breaking, parameter has the largest influence. A higher value of gamma means that more higher waves are present in shallow water, since they break in a later stage (explained in section 6.1). As a consequence of a higher value for gamma, more waves reach the toe of the seawall and more seawall erosion is present. In section 9.2.4 was explained that a value of 0.541 for gamma would be chosen, according to calibration work done by Deltares (2015) on Dutch beaches. To give a conservative answer, a slightly higher value of gamma is recommended to apply on the Southern Coastal Mine, under the consideration that the foreshore is rather steep.

The model setting Facua (accounting for onshore sediment transport) has the second largest influence of the model settings. Changes in the wave peak period (Tp) and the significant wave height (Hs) have the largest impact on the result amongst the wave conditions. One can see the difference between variations in wave conditions and variations in settings of model parameters. A thorough investigation of wave conditions and an accurate transformation with SWAN are of vital importance for the reliability of the final result, the eroded sand volume. The effect of grainsize variations is limited. In modeling erosion of Dutch dunes, the impact of variations in grainsize is much larger. For the model used here (Southern Coastal Mine Namibia) one single, rather large, median grainsize was chosen to describe the entire upper shoreface. This decision reduces the effect of variations.

9.3 Application of the developed model

In the previous sections a model was developed to study the updating of the bed profile of the upper shoreface, and to determine quantitatively the erosion of the seawalls in the Southern Coastal Mine in Namibia. This model can be applied along the whole coastline of the mine.

In the section below the application of the model is presented. At first a case study is presented, namely a storm that occurred at the end of May 2015 causing a seawall to fail. By using the same model set-up, the applicability of the XBeach model can be assessed.

Later in Chapter 10 the XBeach model will be used to test a different seawall design.

9.3.1 Case study: Storm of May 2015

Due to a storm that lasted from the 30th of May to the 1st of June 2015 almost 700 meters of seawall length was washed away. The storm and its effects are discussed and modelled as a case study within this master thesis.

Location

The seawall that failed was protecting the ongoing mining activity in the U30 area. Figure 9.13 shows the location of the breach on a map. The location is just north of the tailingsdump belonging to #3-Plant (see also Figure 2.2). As indicated on the map in Figure 9.13 a stretch of 667.8 m of seawall failed. Pictures taken on the day of the failure show that a gap developed after which breaching of the sand took place (see Figure 9.14).

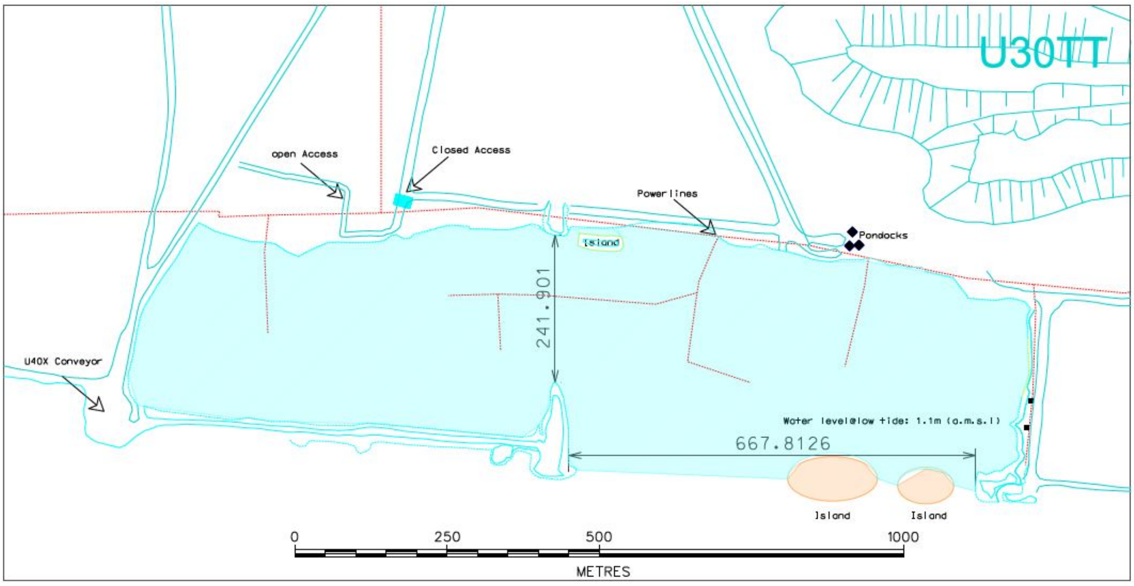

Figure 9.13: Map of Southern Coastal Mine where the seawall (and crosswall) failures are indicated.

Figure 9.14: Picture showing the breach (in the middle of the picture) of the seawall on June 1st 2015

As a consequence of the penetration of seawater into the mine, a crosswall also failed over a length of 242 m.

Figure 9.15: Aerial image of area of interest for case study. The seawall of interest is high-lighted by the red circle. Picture taken on May 25th 2015.

In Figure 9.15 an aerial image of the area is presented. One can see in the photo that the part of the seawall that collapsed stood out in seaward direction. This was already noticeable in October 2014 (see Figure 9.16). Compared to seawalls at other locations, this seawall had a rather narrow and steep beach lying in front of it. A situation like this created a kind of 'hotspot' for wave attack.

Also, because of ongoing mining activity, the hydraulic head (difference between ocean water level and water level in the mining block) is much larger than the hydraulic head present in other mining blocks.

Section 2.1 (Coastline orientation) pointed out that the coastline of the Southern Coastal Mine is curved. The seawall that breached was on the peak (outer edge) of the curve. Section 6.3.4

about longshore sediment transport explained how such a situation leads to erosion of the beach, which is again unfavourable for wave energy reduction.

Figure 9.16: Picture of seawall next to mining activity in U-area of Southern Coastal Mine Namibia. Picture taken during Fact-Finding Mission in October 2014.

Conditions

The seawall collapsed on the 1st of June after multiple days of heavy wave conditions. In Appendix I the weather forecast of that specific week is shown. Figure I.2 and I.3 of Appendix I indicate that a storm passed Antarctica, generating large swell waves that travelled in all directions (including the direction of the Namibian coast).

The most severe waves at the Southern Namibian Coast were present on May 30th and May 31st 2015. Reaching a maximum significant wave height (Hs) of 5.4 m and a peak period (Tp) of almost 17 s offshore. According to the data analysis of Appendix G (Storm conditions) this combination of wave height and wave period had a probability of occurrence of about 1/75 per year. Also according to these data a storm often lasts multiple days (ca. 3 days), only the storm peak has a maximum duration of 24 hours. This was also the case for the storm of May 2015.

Model set-up

The 1D model is set up with XBeach in the same way as was done in section 9.2. The bathymetry of the cross shore profile (Survey Line 22500) is quite different from Line 9000 (section 9.2.3). The 1D-profile of Line 22500 is shown in Figure 9.17 and Figure 9.18. In Figure 9.18 is zoomed in on the upper shoreface. Important differences between this cross-shore profile and Line 9000 are that the beach in this case is narrower and no breaker bar has formed. The seawall is so to speak standing out in seaward direction.

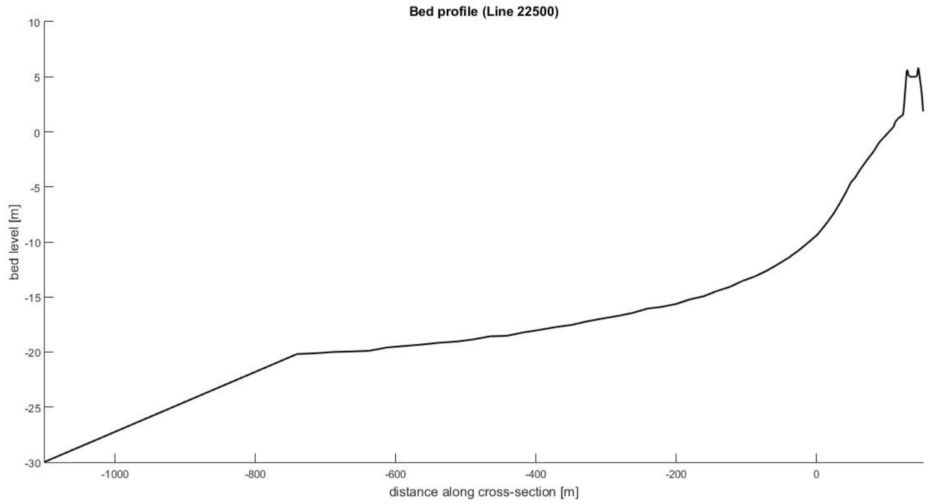

Figure 9.17: 1D cross-shore bedprofile of Survey Line 22500 of the Southern Coastal Mine Namibia.

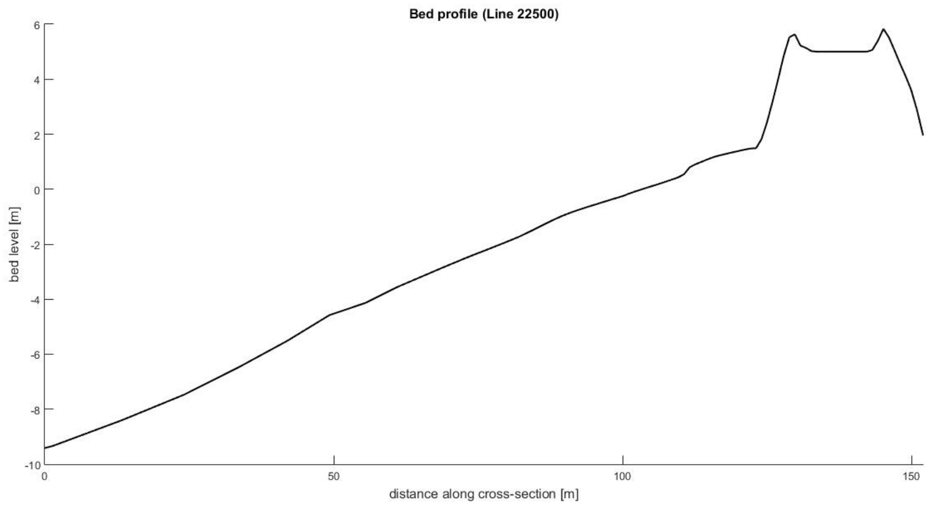

Figure 9.18: 1D cross-shore bedprofile of Survey Line 22500 of the Southern Coastal Mine Namibia, zoomed in on the beach and seawall.

Also a 2DH model was set up by expanding the 1D model in alongshore direction. For the 2DH model three Survey Lines have been used, namely Line 22250, Line 22500 and Line 22750. Line 22250 and Line 22750 represent the cross shore profiles of the seawall sections on both sides of the breached seawall. Line 22500, also used for the set up of the 1D model, is part of the seawall that breached. Between the three seawall sections two crosswalls are inserted, according to pictures. In Figure 9.19 the model set-up of the 2D model is visualized. In the lower part of the figure is zoomed in on the seawall of the Transect.

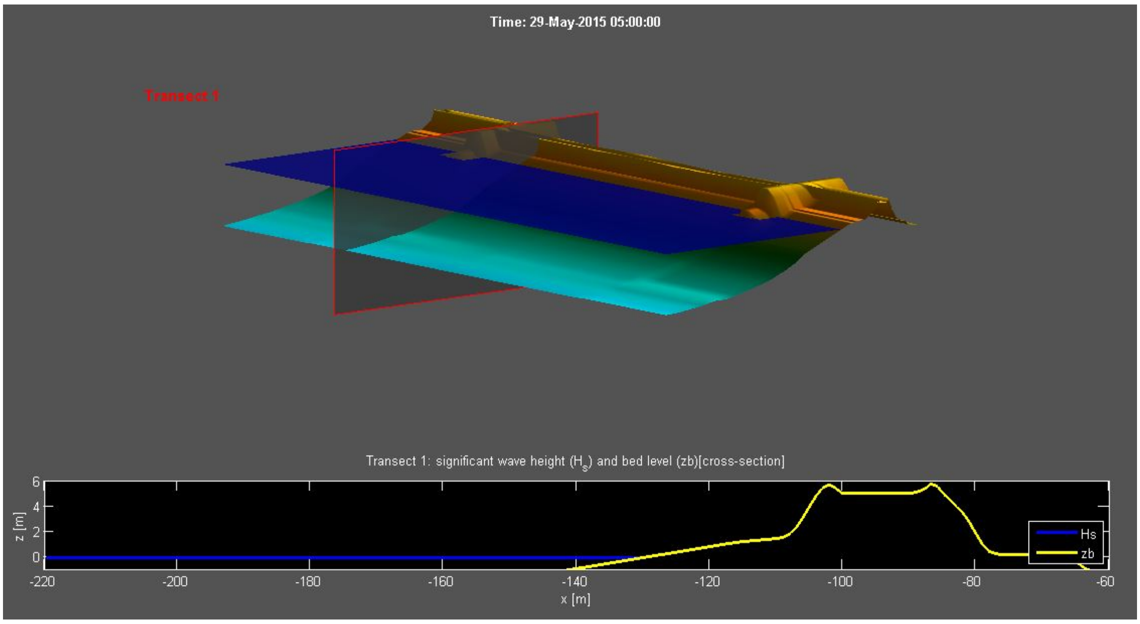

Figure 9.19: Bed profile according to model set-up. In the upper picture a 3D visualization of the seawall with its crosswalls. In the lower figure a cross-section of the seawall.

Hydrodynamic boundary conditions are again obtained with the existing SWAN model. The significant offshore wave height of the peak of the storm is 5.4 m (see Appendix I) and the wave peak period 17 seconds. SWAN translates this to nearshore wave energy spectra, where the significant wave height is 4.9m and the wave peak period 13.3 seconds.

Model results

The results of the storm simulation are presented in the figures of this section. Figure 9.20 shows the 1D model results. By studying the different lines of the graph, all representing a different point in time,it can be seen that erosion immediately takes place above a depth of about -1 m. In section 9.2.4 was explained how the XBeach model uses a wave breaking parameter γ.

$$\gamma = \frac{H_b}{h_b} \simeq 0.541 \tag{9.17}$$

A rough estimation can be made with this formula for the development of the foreshore. With a significant wave height of about 4.9 m, waves will break at a depth of about 9 m. This means that a foreshore should develop during the storm until a depth of 9 m to reduce wave energy. One can see Figure 9.20 that a wider beach foreshore develops until a depth of 9 m. The sand needed for the foreshore comes mainly from the eroding seawall. However, the foreshore does not become wide enough for the seawall to withstand the storm.

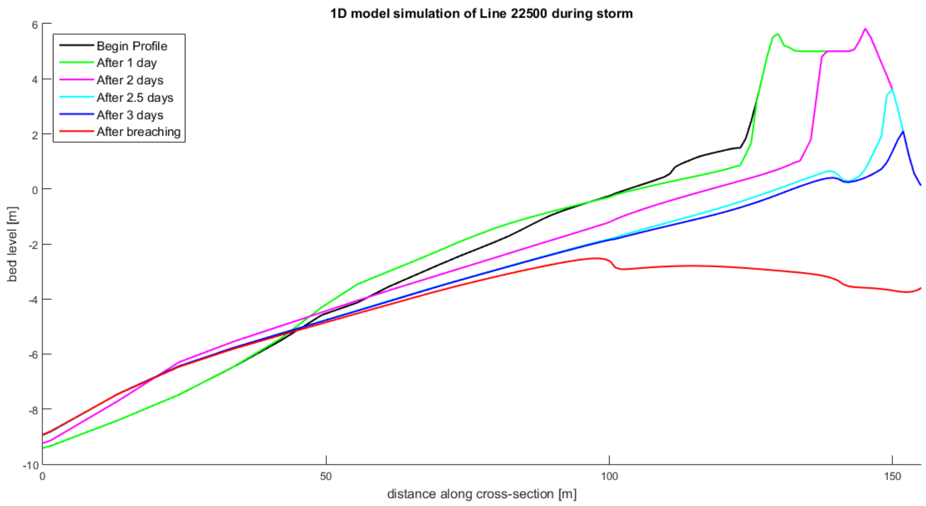

Figure 9.20: Graph showing the development of the bed profile during the simulated storm for the 1D model of XBeach.

The seawall in Figure 9.20 shows an avalanching profile even until it has a height of only 2.5 meters. This means that no overtopping of waves and water takes place for the seawall.

2DH model results

For the 2DH model Figure 9.21 shows result of the storm for which the seawall failed. In the figure one can see a 3D representation of the 2DH model and a cross shore profile of the seawall in question. In both sub-figures we zoom in on the ultra-shallow water region (the beach and the seawall).

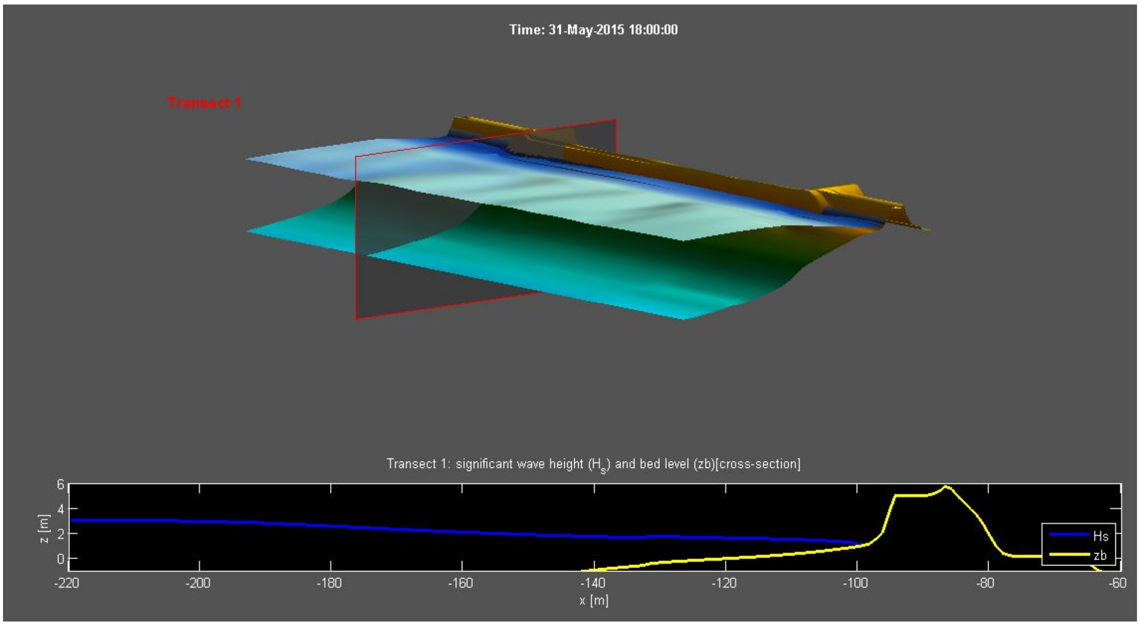

Figure 9.21: State of the seawall after the storm. The upper figure is somewhat zoomed out compared to Figure 9.19.

According to these 2DH model results the seawall does not fail, although a lot of erosion is visible. This is not according to the real-life situation, where the seawall failed after 50 hours of storm. Apparently the model makes an underestimation of the seawall erosion.

It is peculiar that the 1D model led to failure and the 2DH model did not. The most logical explanation is that the crosswalls have a certain effect. The crosswalls stand out much further in seaward direction than the seawalls. Material is taken away from the crosswalls and redeposited along the shore to form a foreshore a little more favourable for wave breaking.

In the sensitivity analysis of Appendix H the uncertainties of the model were assessed. In particular, a small change in wave peak period or significant wave height has a large impact on the model results. The values of Hs and Tp for the model input were chosen conservative (so rather high), but still by a deterministic approach. The possibility of the wave conditions being slightly different is still present. Appendix J explains how one should deal with uncertainties in the model results.

When the significant wave height of the storm conditions is raised by 5%, the seawall does fail entirely. The end result of this simulation is shown in Figure 9.22 below.

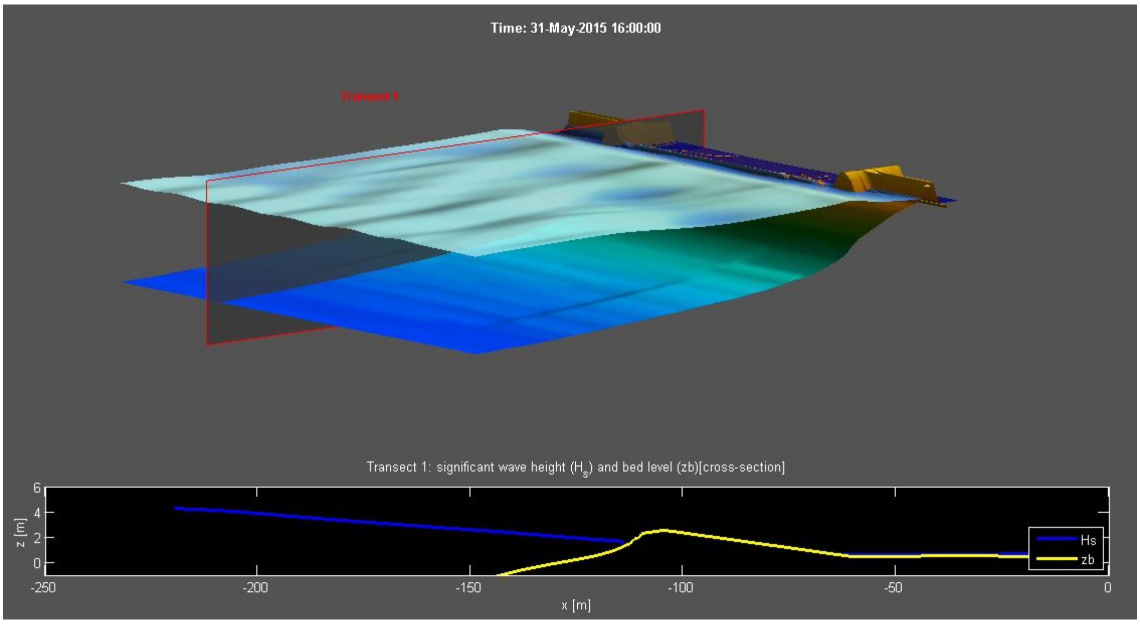

Figure 9.22: Situation after almost 3 days of storm. A part of the seawall has failed.

Once a first gap develops in the seawall, water will flow through the seawall into the mining pit behind it. When this happens, breaching of the sandy seawall is initiated and soon the gap will grow. The breaching of sand-dikes is described by Visser (1998). The speed of sand breaching is useful to know when a large low-lying area is at risk and one should know how much time is available for evacuation. In the case of the Southern Coastal Mine, the breaching speed is less interesting since the mining pit will have a fill-up time in the order of an hour. This is because of the relatively small mining pit behind the seawall with a large hydraulic head, because the mining pit is deeper than MSL.

Discussion of Storm Case

The seawall in the U30-area was the only seawall that failed. The model showed that seawall section 9000 experienced erosion, but did not fail. This is consistent with the real-life situation. It is notable that the seawall section in question stood out in seaward direction and clearly had a narrower beach in front of it (see Figure 9.15). As a consequence the beach was steeper and wave energy was reduced less than in front of other seawall sections.

The effect of crosswalls during storm conditions is limited. Waves are coming in under an almost normal incident (90 degrees), due to refraction. This is mainly because of a relatively wide region of shallow water in front of the Southern Coastal Mine. The effect of refraction is especially large for high waves, as they feel the bottom earlier and start to refract further offshore as a consequence. By studying the simulation results of the storm, it can be seen that there is some wave mitigation in front of the beach, because sand taken away from the crosswalls settles in front of the beach. This is however not uniform, so some parts of the beach experience no wave energy reduction at all due to this effect.

9.3.2 Conclusions drawn from short term simulations

When studying the short-term simulations, including the case study, some important conclusions can be drawn.

From the sensitivity analysis it could be seen that the coastline is most sensitive to variations in wave conditions. Variations in tide, grainsizes and wave directions have limited impact on seawall erosion.

Another important conclusion is that the width of the beach (or foreshore) is very important to wave energy reduction. In the case of the seawall that breached, the foreshore was relatively narrow. This effect was enhanced by longshore transport, since the location of the seawall is the peak of the Sand-2-Sea (land accretion) program. During the storm the foreshore is fed by sand that eroded from the seawall. So the larger the volume of the seawall, the more effective the foreshore can become in reducing wave energy.

By studying the 1D model and 2DH model simulations in the case study, it could be seen that an avalanching profile of the seawall developed when erosion started to take place. Another important conclusion is that no overtopping of the seawall occurred, except for when a 1/100 per year storm was modelled. From this it can be concluded that the crest height of the seawall is probably larger than needed.

The effect of crosswalls on wave attack is limited when one considers the blockage of waves. Due to refraction, waves have an almost normal incident to the coastline. However, sand taken away from the crosswalls helps in wave energy reduction as it fills up part of the sand shortage that the foreshore has to reduce wave energy effectively.

Chapter 10 – Seawall design

This chapter evaluates the currently used seawall standard and proposes adjustments to this standard. It also discusses the possibility of an alternative design, making use of the current construction method for seawalls, which is explained in Chapter 4.

10.1 Deterministic approach of required seawall volume

The modelling results of XBeach state an eroded sand volume for storms with a certain probability of occurrence per year. The storm conditions are a certain combination of significant wave height and wave peak period with a certain return period. These return periods are presented (again) in table 10.1 below, together with the sand volumes that erode from the seawall during the storm. The calculations are based on the cross-section of Survey Line 9000 of MA1.

Table 10.1: Resulting seawall erosion volumes for cross-section of Survey Line 9000 per storm condition.

Design storm [prob. per year]	1/1	1/2	1/5	1/10	1/50	1/100
Eroded volume [m^3/m]	2.9	6.0	15.9	38.1	56.5	80.2

According to the Dune Erosion Guideline (Van de Graaff, 1984*a*) the eroded volume must be multiplied by a factor of 1.25, because of model uncertainties and uncertainties in the duration of the storm (further explained in Appendix J). This leads to the volumes presented in table 10.2 below.

Table 10.2: Resulting seawall erosion volumes per storm condition, according to calculation guidelines.

Design storm [prob. per year]	1/1	1/2	1/5	1/10	1/50	1/100
Eroded volume [m^3/m]	3.6	7.5	19.9	47.6	70.6	100.3

By plotting the results (see Figure 10.1), a trendline through the results can be drawn. The trendline roughly presents the relation between probability and eroded sand volume. The plot can be used to gain insight into how erosion volumes increase for different return periods of storm conditions. The trendline approaches an exponential function, as can be derived from the plot. In particular, the position of the 1/100 per year storm can be different. When overtopping becomes more important, the eroded sand volume is larger. When no overtopping occurs, the sand volume is smaller.

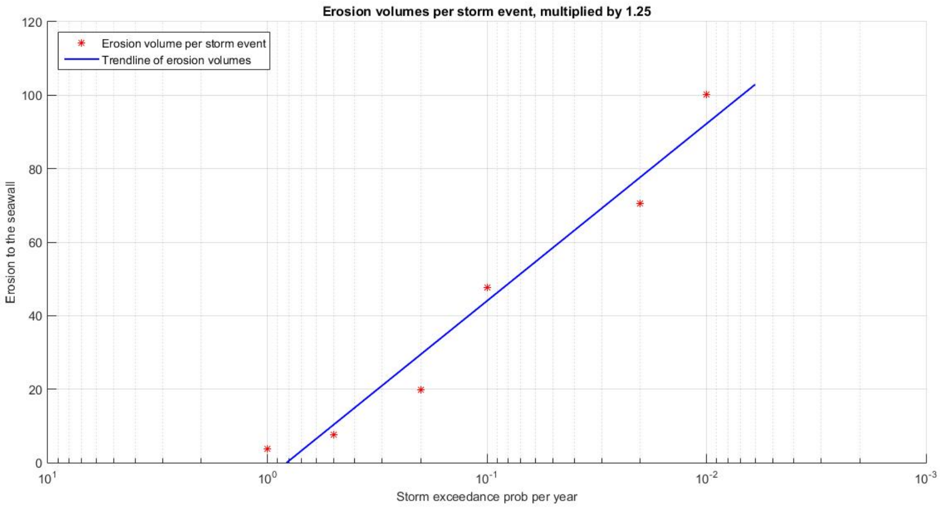

Figure 10.1: Plot of eroded sand volumes per storm event with a certain yearly probability. Volumes are calculated for Survey Line 9000.

The required volume of sand for a seawall can now be calculated. This volume depends on the design conditions chosen. NAMDEB will have to determine what the acceptable failure risk is for a seawall or mining block behind a seawall. This is a cost-benefit analysis that is out of scope for this thesis. As a recommendation protection against a storm with a yearly probability of 1/100 is proposed, corresponding to a probability of occurrence of 2.96% during a 3-years lifetime of a seawall (see Appendix G for explanation).

The seawall discussed in the case study (section 9.3.1) was not designed to withstand a storm with a yearly probability of 1/75, let alone a storm with a probability of 1/100 per year. If the storm conditions corresponding to a 1/100 per year storm were the design conditions for the construction of this seawall section, the seawall would not have failed. Appendix K explains how a standard could be chosen in a probabilistic calculation. The proposed design in this chapter will have a deterministic approach.

Definition of limit state

Both the Serviceability Limit State (SLS) and the Ultimate Limit State (ULS) must be defined. The exceedance of the Serviceability Limit State means that the service road on top of the seawall is no longer usable. When the outerslope is eroded, such that the windrows on the edge of the service roads are gone, the serviceroad may no longer be used. Consequences of exceeding the SLS are mainly costly maintenance and delays in the mining operation, since trucks are needed for maintenance and serviceroads are unavailable. Exceedance of the SLS makes maintenance to the seawalls difficult, because the places where maintenance is needed may become inaccessible for trucks. For this reason, corrective maintenance cannot be accounted for in calculations with the Ultimate Limit State.

Exceedance of the Ultimate Limit State means that the seawall can no longer act as a flood defense for the mine behind it. When the seawall is eroded away by wave action or when piping occurs on a large scale, the seawall fails as a flood defense. Consequences of exceedance of the ULS can vary a lot. Downtime for the mining operation is very likely and extensive maintenance will be needed to restore the seawall and restart the mining activity. If evacuation can't be done in time, material may be lost and even loss of life is, although very unlikely, possible. Mining activity in the block behind the former seawall must be started up again.

The SLS is of less interest to the research done in this thesis. With the corrective maintenance strategy applied and with the option of redirecting vehicles in the mine, exceedance of the SLS is not unacceptable. Exceedance of the ULS, like in the discussed case study of this report, is immediately problematic. To ensure a conservative approach, no corrective maintenance will be accounted for in calculations with the ULS. In this thesis only the Ultimate State Limit will be assessed. When talking about the limit state or limit state profile in this chapter, the ULS is meant and not the SLS.

Limit state profile

In Appendix J (section J.4) the limit state of Dutch dunes was discussed. This limit state is again visualized in Figure 10.2 below.

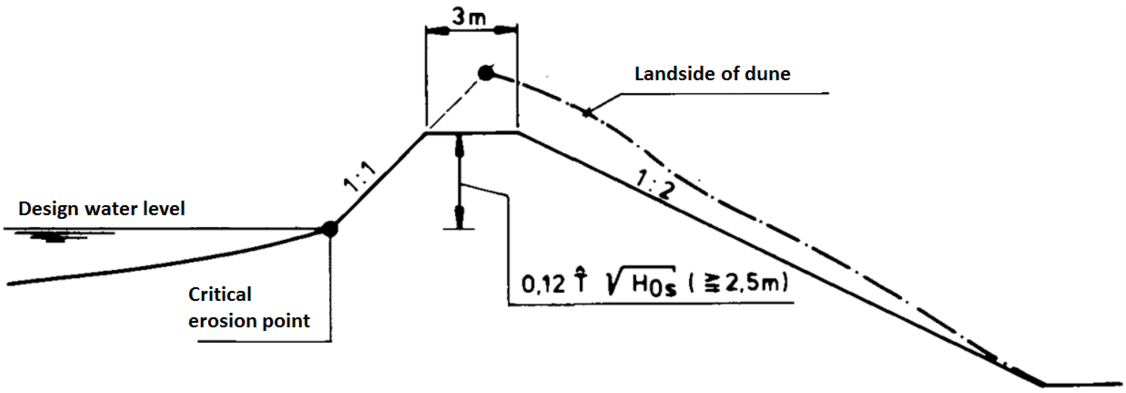

Figure 10.2: Limit state profile (ULS) of a Dutch dune.

For the Southern Coastal Mine a similar profile can be proposed. The proposed crest width is 5 m, which is larger than the 3 m crest width for the limit state profile of Dutch dunes. This is because the innerslope of a seawall is steeper (1:3) leading to a smaller limit state volume in general. A crest width of 5 m will also enable maintenance with ADT's after a storm. The outerslope of both the dune and the seawall is 1:1, due to avalanching of sand. A seawall height of 5 meters above MSL is proposed. Figure 10.3 shows schematically the proposed limit state of a seawall. Note that the figure is not to scale, since the scale of the x-axis and the y-axis are different. The black line represents the outline of the seawall according to the design standards of NAMDEB. The red line represents the proposed limit state of the seawall.

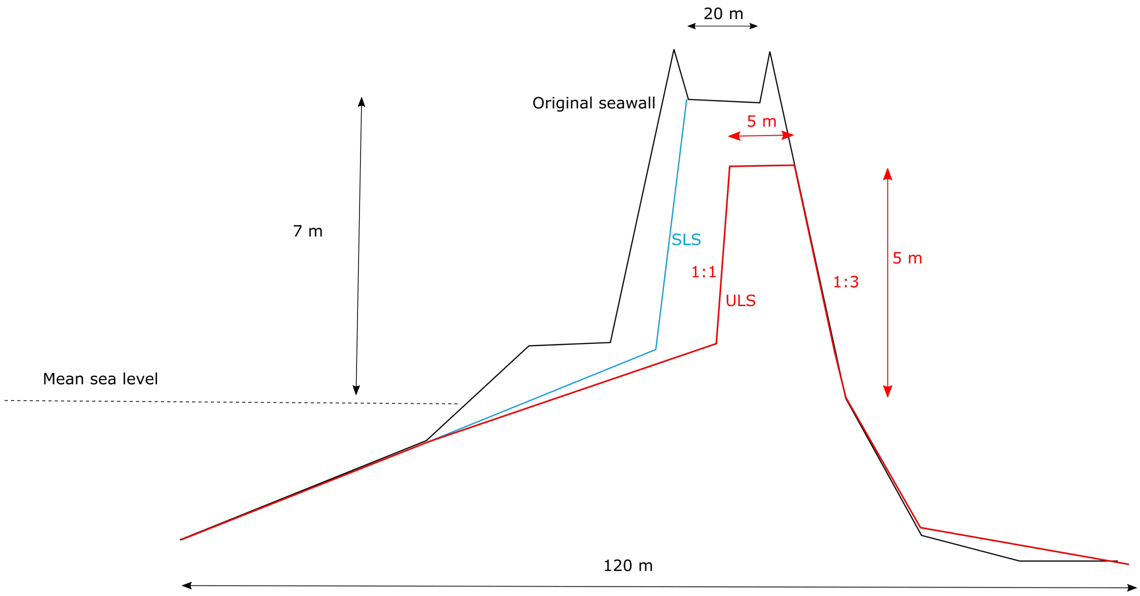

Figure 10.3: Limit state profile of a NAMDEB seawall, represented by the red line. The blue line represents the SLS.

The seawall volume of the original seawall (black line in Figure 10.3) is 135.4 m^3, starting from the seawall toe at MSL +2 m. The sand volume of the limit state profile is 45 m^3 above MSL +2m, corresponding to 75 m^3 above MSL. The volume of the total seawall must be at least the volume of the limit state profile (45 m^3) plus the volume that eroded during a 1/100 per year storm. This comes down to a volume of 145 m^3/m (rounded of to 150 m^3/m) for the seawall that was tested in Chapter 9, which is Survey Line 9000. The new cross-section is presented in Figure 10.4. The crest height will remain according to the original standards. By widening the crest with 3 m, a volume of 15 m^3 is added to the seawall cross-section.

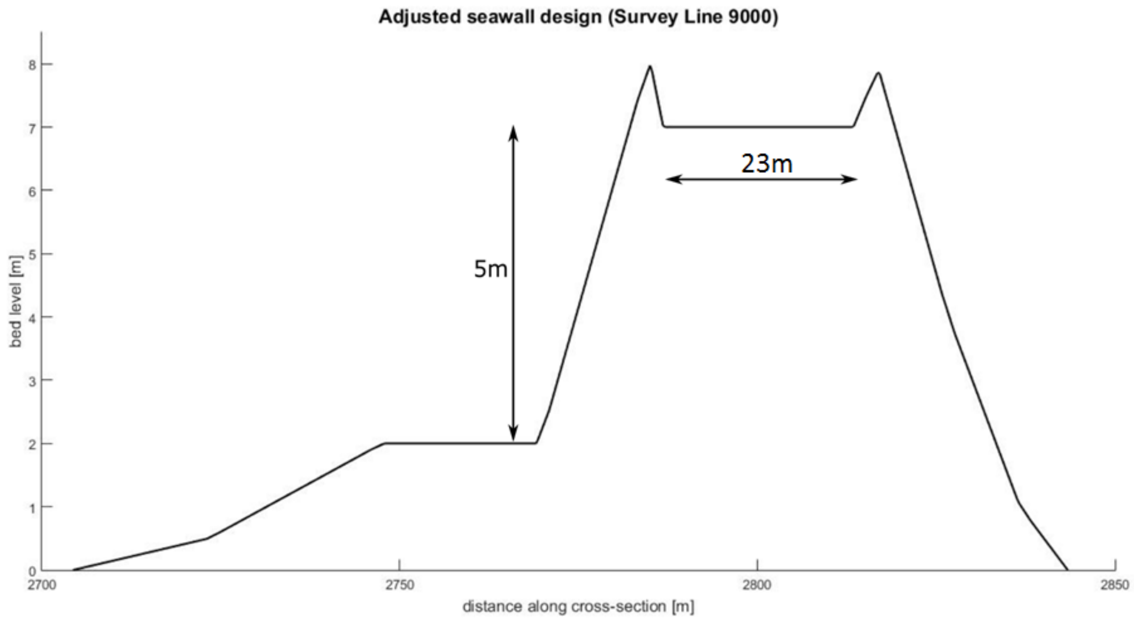

Figure 10.4: Seawall with adjusted standard after a storm with a probability of occurrence of 1/100 per year.

Survey Line 22500

The storm of May 2015 pointed out that seawall sections with a steep and narrow foreshore are most vulnerable to storm conditions. The adjusted standard for the seawall of Survey Line 9000 will not be sufficient for the seawall section at Survey Line 22500, which breached (see case study 9.3.1). For this seawall section a seawall volume of 225 m^3 above MSL $+2$ m is needed to withstand an 1/100 per year storm. This volume was found iteratively by modelling. Modeling results are shown in Figure 10.5. The design of this seawall is again according to the current seawall standards, but with an increased width. The crest width is increased with 18 m to obtain an additional volume of 90 m^3 of sand. When the amount of seawall erosion is multiplied with a factor 1.25, the limit state profile is still maintained.

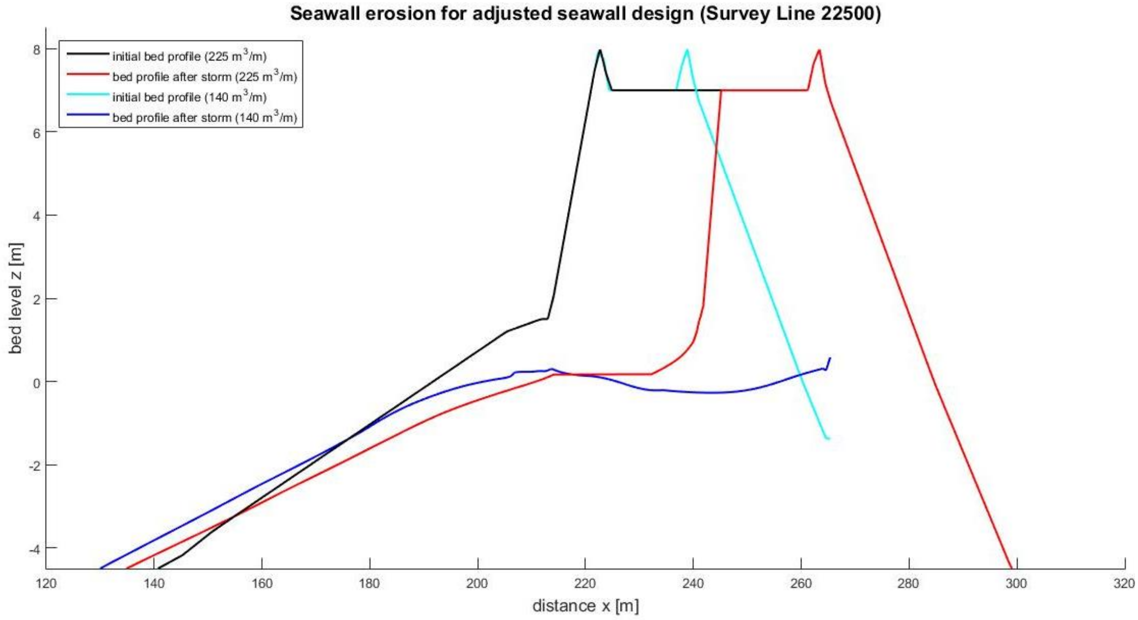

Figure 10.5: Seawall with adjusted standard after a storm with a probability of occurrence of 1/100 per year. The red line presents the bed profile after the simulation of the storm with the adjusted seawall volume (225 m^3). The blue line presents the resulting bed profile of the seawall with the old standards.

For the purpose of minimizing the flood risks, this volume of 225 m^3 for a seawall cross-section could be used as a standard for all seawalls of the Southern Coastal Mine. In this way extra safety is obtained in case of a steep foreshore. In the next sections an alternative design method will be discussed.

10.2 Alternative seawall design

This section gives a consideration of different aspects of a seawall design. It discusses every relevant aspect for an improved seawall design. As a conclusion of this section the proposed seawall design is presented and explained.

From the case study, where the storm of May 2015 on the Namibian Coast was modelled, it became clear that parts of the seawall of the Southern Coastal Mine are insufficient to withstand a storm with a probability of occurrence of 1/75 per year, let alone a 1/100 per year storm.

From the XBeach model simulations it can be concluded that a seawall requires more than just a standard for width and height. The width of the beach and location of the toe of the seawall play an important role when it comes to the safety of a seawall.

Width of the beach and upper shoreface

The beach in front of a seawall requires sufficient width to prevent waves from reaching the toe of the seawall. But to reduce wave energy by wave breaking, the surf zone and swash zone (see section 6.1 for explanation) must be wide enough. With the current Sand-2-Sea program the beach is growing (becoming wider) in time, because sand is nourished unto the beach and crosswalls are extended and eroded. With the nourishment of sand, nature can strive towards a profile that can reduce wave energy most effectively.

The model results of the case study (Storm of May 2015) showed that not only the seawall eroded away, but also a large volume of sand from the beach was taken away during the storm. This happens also for other sections of the seawall, as the storm simulations of Survey Line 9000 pointed out. For this last-mentioned the foreshore could reduce the wave energy sufficiently to prevent the seawall from failing. The width of the beach, so between MSL and the toe of the seawall is about 80 m for Line 9000 at the time of the survey. The steepness of the foreshore between 9 m waterdepth (where waves with a height of 4 m start to break) and MSL is 1:36 for Line 9000. The width of the beach in front of the seawall that breached (Survey Line 22500) was 40 m at the time of the survey, and the steepness of the foreshore was 1:17.

For seawall construction it is important that land accretion has developed far enough for the beach to reduce wave energy efficiently. For the current seawall construction method this means that a seawall can only be constructed on a beach that has developed to be wide enough. Standards for the width of the beach are presented with the proposed seawall at the end of this section.

Chapter 11 will elaborate on how the beach can expected to be developing at different locations along the shore.

Minimum height of the seawall

The risk of overtopping should always be minimized because it will lead to dangerous situations in the mining pit. Model results (again presented in Figure 10.6) have shown that overtopping does not occur for a storm with a probability of occurrence of even 1/50 per year. But for a 1/100 per year storm overtopping can be distinguished (see section 9.2.5), although it does not lead directly to seawall failure. If a 1/50 per year is chosen as the design storm, then the seawall can be lower than MSL +7 m. Simulations with a seawall height of MSL +6 m also show no overtopping. But, if a 1/100 per year is chosen as the design storm for the seawall, the crest should remain at a height of MSL +7 m. If lowering of the seawall is desired, the foreshore and beach must first become more efficient in reducing wave energy by breaking.

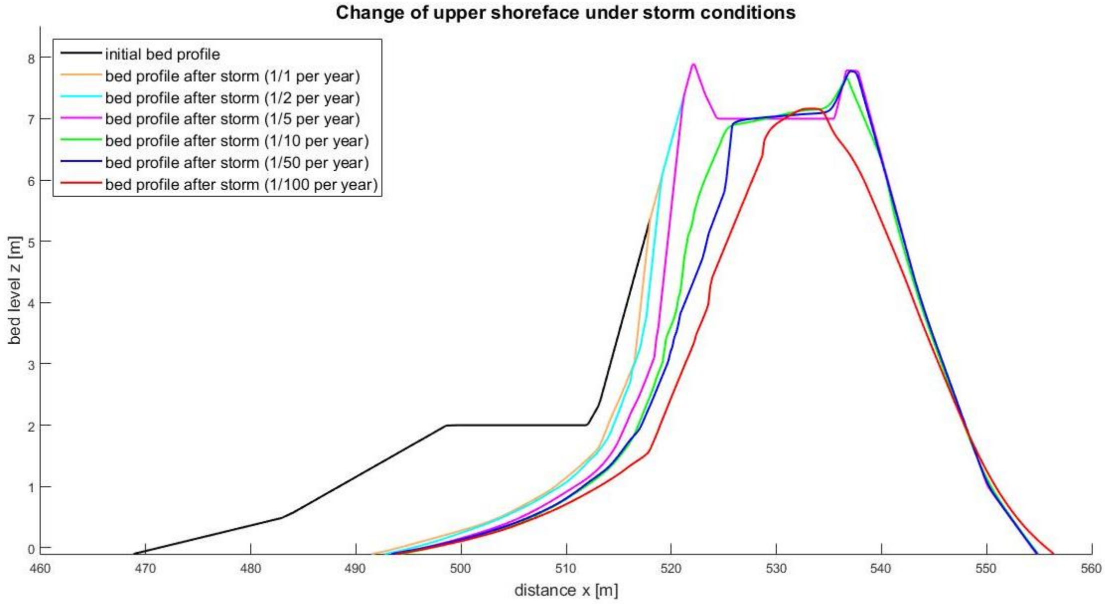

Figure 10.6: Plot of the seawall on Survey Line 9000. The colored lines represent the resulting bed profile after specific storm conditions.

Width of the seawall

The width of the seawall is determined by the volume of the seawall and the height. The width of the crest should have a minimum of 20 m to meet the requirements of a service road (i.e. the SLS). A volume of 225 m^3/m was determined to withstand a storm with a probability of 1/100 per year. However, this is for the case where the width of the foreshore is minimal. With requirements for the foreshore in mind, the volume of the seawall can be lower. The new standards (section 10.2.2 below) show that the volume can even be lowered to 160 m^3. This will lead to a reduction of construction costs.

From model results it could be concluded that the more sand erodes from the seawall, the more wave energy reduction is possible. This is because sand taken away from the seawall during a storm is redeposited in the foreshore again. A larger width, and thus a larger volume, of the seawall will be more effective as a flood defense.

Less steep outer slope

An outer slope with a lower steepness will lead to less avalanching of material when the slope is flatter than the critical wet-slope angle ($m_{cr,wet}$). However, the seawall requires more volume in this case, because the crest width needs to be the same as in the old standards for the purpose of a serviceroad. Construction of a seawall with a less steep outer slope is also more difficult, because in the current construction method only sand-dumping from the top of the seawall is applied.

10.2.1 Alternative measures in seawall design

This section will touch upon two measures that can lead to a different seawall design by still using the current construction method.

Compacting of material

Compacting of material can decrease the porosity of the seawall. An advantage of this is that the slopes of the seawall will become more stable. As the water of waves can less easily penetrate the seawall toe, the volume of sand in an avalanche is smaller. However, compacting techniques are expensive and, because the seawalls also serve as service roads, the seawall will deform constantly. Also the level of compaction is difficult to test, introducing large uncertainties in seawall designs.

Use of different material: Tailings

This thesis focuses in particular on the current construction method for seawalls, thus using sand. In addition to sand, there is an abundance of tailings from the tailings dumps available in the Southern Coastal Mine for the construction of a seawall. The dumps consist of crushed rock with a grainsize of 2 mm to 25 mm. The use of tailings can be considered as favourable for seawall construction purposes. The larger grainsizes lead to a lower mobility of sediment (see section 6.3), and thus to less erosion. After an avalanching event, much less material will be taken away by the sea when the seawall is made up out of coarser grains instead of sand. The critical wetslope and critical dryslope of the seawall will be more favourable (steeper) with the use of tailings, compared to a seawall made out of sand. However, the grading of grainsizes is very wide, which makes the determination of critical slopes uncertain. And thus no steeper slope can be presumed.

Seawall erosion can again be modelled with the geomorphological model XBeach. However, XBeach has not been calibrated yet for a case with a very wide grading of relatively coarse grains, such as the use of these tailings. Before accurate predictions of seawall erosion can be made, physical tests must be carried out. These tests, although they are out of scope for this thesis, can be conducted in a laboratory, where wave-soil interaction can be simulated on a large scale. An example of such a laboratory are the facilities of Deltares, the Netherlands (van der Werf et al., 2009).

Another disadvantage of the use of tailings for seawall construction is that transport costs will increase, because tailings have to come from further away. Figure 10.7 illustrates how this differs at least a factor three.

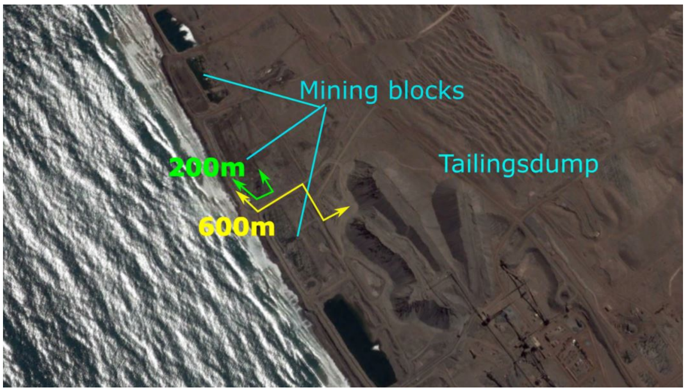

Figure 10.7: Map showing the tailingsdump of #3-Plant in MA1 and the mining blocks of ongoing mining activity. The arrows show the hauling distance for material to the seawalls.

10.2.2 Proposed seawall design standard

With the current mining strategy a seawall is required. The newly proposed seawall design standard is presented here. This is a standard that can be applied along the entire coastline of Mining Area No. 1. It is iteratively found by studying the tested 1D models (Survey Line 9000 and 22500) and simulations with the storm conditions that have a yearly probability of occurrence of 1/100, which is chosen as the design storm. When lower design conditions are chosen, for instance the 1/50 per year storm, based on a cost-benefit analysis, the seawall standards can be lowered as well. This thesis will focus solely on the 1/100 per year storm as design storm. In particular to mitigate the risks of overtopping of the seawalls. A schematic drawing of the proposed design standard is presented in Figure 10.8.

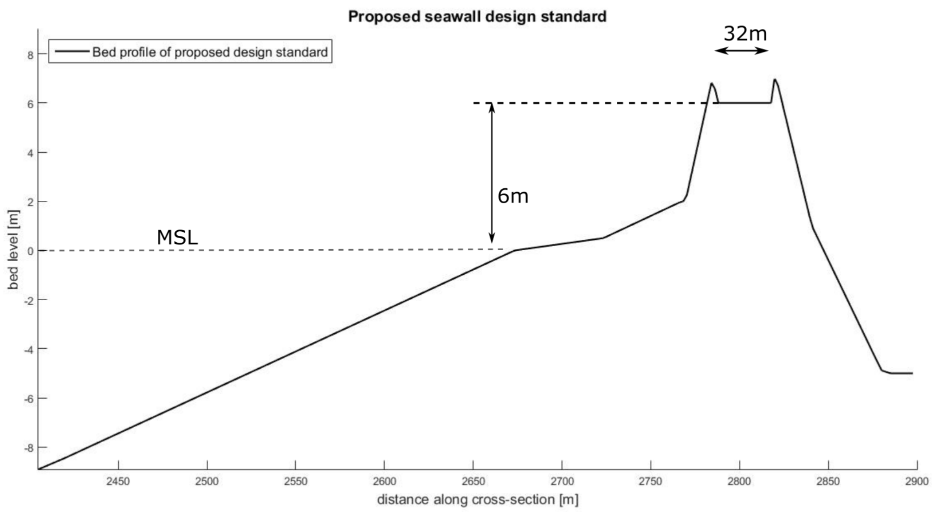

Figure 10.8: Proposed standard for the seawall and its foreshore.

The proposed crest height is MSL +6 m, which is a meter lower than the standard that was used until now. The recommended seawall volume is 160 m^3/m above MSL +2 m. The innerslope (1:3) is the same as in the old standards, because the standards for the innerslope (section 4.5) are considered to be sufficient. The outerslope is also left unchanged in the new standard, because of construction consideration as discussed above. The windrows on both sides of the crest are also still maintained. This means that the crest width must be 32 m between the windrows.

This seawall design is not very different from the seawall standards that NAMDEB is currently using (see section 4.5). The most important difference is that the foreshore now has requirements as well. A width of the beach of about 75 m, measured during winter, is recommended together with a steepness of the foreshore of 1:30 maximum. This is equal to a width of 270 m between the 9 m depth contour and MSL. Results of model simulations are presented in Figure 10.9 below. It can be seen that the limit state profile (crest height of 5 m above MSL and crest width of 5 m) is still maintained after the storm.

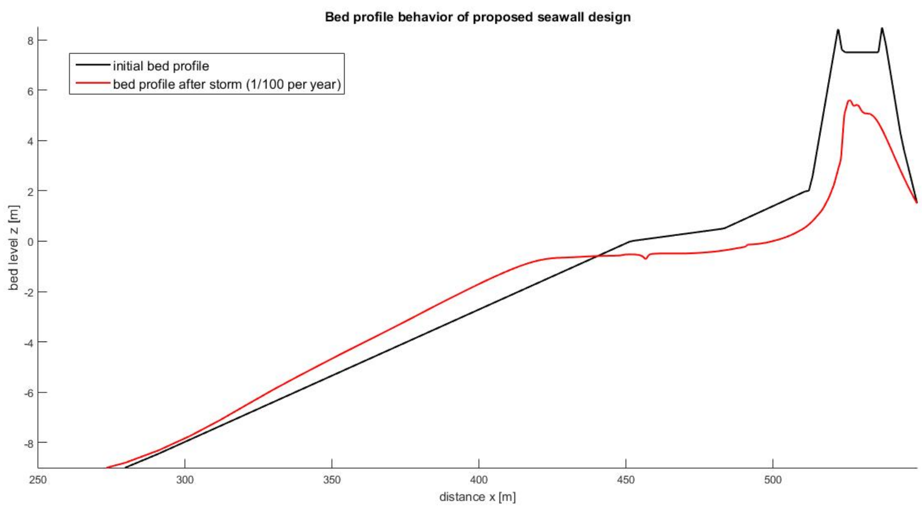

Figure 10.9: Bed profile of proposed standard after a simulation with wave conditions of a storm with a probability of 1/100 per year.

Alternatives

Two alternatives to the proposed design standard are touched upon here. The crest height of MSL +6 m is considered to be the minimum height in maintaining an adequate flood defense. The crest width is based on the required volume of 160 m^3/m above MSL +2 m. Maintenance is considered to be easier for a seawall with a lower crest. However, when a the crest width must be smaller for operational reasons, a higher crest can be proposed to maintain the required seawall volume. Increasing the crest height with 1.5 m (to 7.5 m above MSL), can narrow the crest width down from 32 m to 20 m between the windrows.

The second alternative can be chosen when the requirements for the foreshore cannot be met. In that case it is possible to increase the volume of the seawall. In previous sections was explained how seawall erosion during storm events leads to the reduction of wave energy by changing the foreshore profile. When the beach and the foreshore (between MSL and MSL -9 m) become narrower, the seawall volume must be increased to maintain sufficient safety against seawall failure. When the both become narrower with 20%, the required seawall volume is estimated to demand 250 m^3/m. This is equal to a crest height of MSL +7 m and a crest width of 35 m. The corresponding values for the beach width (60 m) and foreshore width (220 m, steepness of 1:24.5) are considered to be minimum values.

Table 10.3 below presents the values of the three design standard that were proposed. Figure 10.10 shows the designs in one drawing. It can be seen that for the third alternative (red line) indeed a much larger seawall volume is required to feed the foreshore effectively during storms, because the bed profile below MSL is lying significantly lower than for the other two designs standards.

Table 10.3: Values of proposed design standards for a seawall in Mining Area No. 1.

	Proposed design standard	**Alternative standard (higher crest)**	**Alternative standard (narrower foreshore)**
Seawall volume $[m^3/m]$ (above MSL +2m)	160	160	250
Crest height $[m]$ (above MSL)	6	7.5	7
Crest width $[m]$ (between windrows)	32	20	43
Beach width $[m]$ (between MSL and MSL +2m)	75	75	60
Foreshore width $[m]$ (between MSL and MSL -9m)	270	270	220

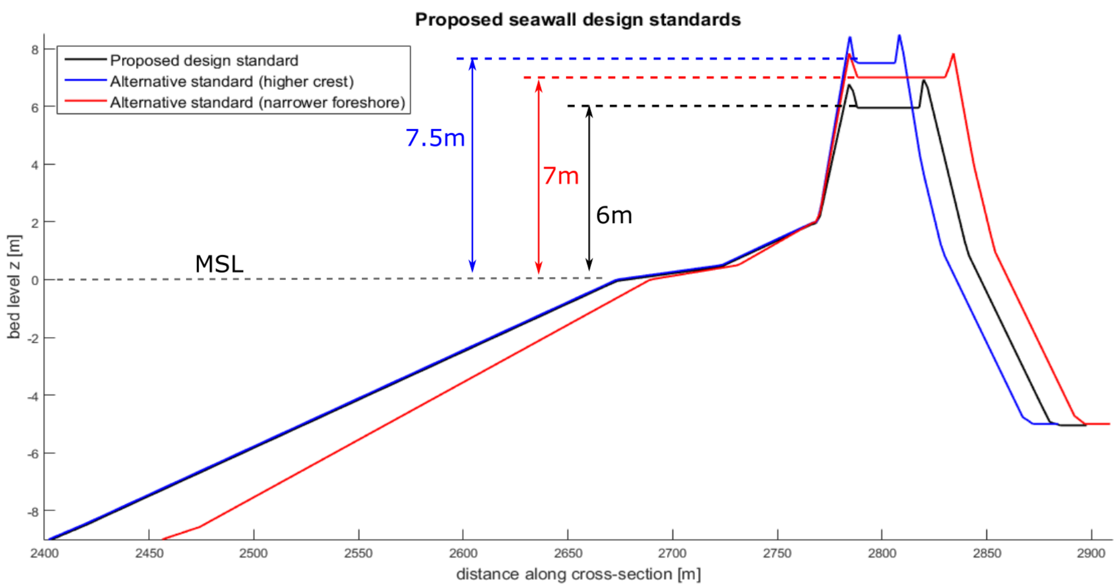

Figure 10.10: Bed profiles of the three alternatives for the standards of the seawall and its foreshore.

When the storm conditions of the 1/100 per year storm are simulated, for each of the proposed designs the limit state profile (as defined in section 10.1) is maintained, also when the eroded sand volumes are multiplied with a factor of 1.25.

Compared to the proposed adjustments for the seawall of Survey Line 9000 (see section 10.1), the requirements for beach width and steepness of the foreshore are less strict, while the volume of the seawall is larger. On the other hand, for the seawall of Survey Line 22500 this is right-about. The effect of the location along the sand nourishment is very important to keep in mind when designing the seawall standards. This is because waves tend to spread out a sand nourishment along the shoreline. The next chapter (Chapter 11) will elaborate further on this phenomenon.

10.2.3 Application of maintenance

Corrective maintenance must be applied when erosion to the seawalls becomes visible from the side of the service road on the seawall crest. This is the case when parts of the windrows are avalanching down the outer slope of the seawall, due to erosion at the toe of the seawall. The best indication of this is when a windrow section is visibly lower than its neighbouring windrow sections. This maintenance strategy requires monitoring of the seawalls on approximately a daily basis, which is also the case in the currently applied maintenance strategy.

In addition to the maintenance of the seawalls, monitoring of the foreshore is required on a regular basis. Sand losses are due to longshore sediment transport, as will be elaborated on in Chapter 11. Considering the nett longshore sediment transport rates, monitoring of the foreshore is recommended on a seasonal basis (four times per year). When the foreshore does not meet the stated requirements, extra sand needs to be fed with the Sand-2-Sea program, or the volume of the seawall must be increased to be able to withstand the design storm.

However, it is strongly recommended to switch from a corrective maintenance strategy to a more predictive maintenance strategy. The advantage of this is that the frequency of inspections can be lowered and maintenance can probably be applied more efficient, leading to a reduction in costs. A predictive maintenance strategy would consist of using numerical models, such as the applied XBeach model, to predict beach- and seawall erosion along the coast of MA1.

Chapter 11 – Land reclamation strategy on the long term

This chapter assesses the currently used land reclamation strategy. It uses knowledge from the literature review and model results to show that mining with this land reclamation strategy is finite in the Southern Coastal Mine. As a conclusion a prognosis of the limit for land accretion is given.

11.1 Shifting of the seawall

The beach is being fed by sand, eroded from the groynes, which is redeposited on the beach by waves and currents. Once the beach has grown enough the seawall is shifted seaward so mining activity can be expanded. The shifting of seawalls is explained for the cases of the seawall cross-sections of Survey Line 9000 and 22500. The locations of these cross-sections are shown again in Figure 11.1 and Figure 11.2.

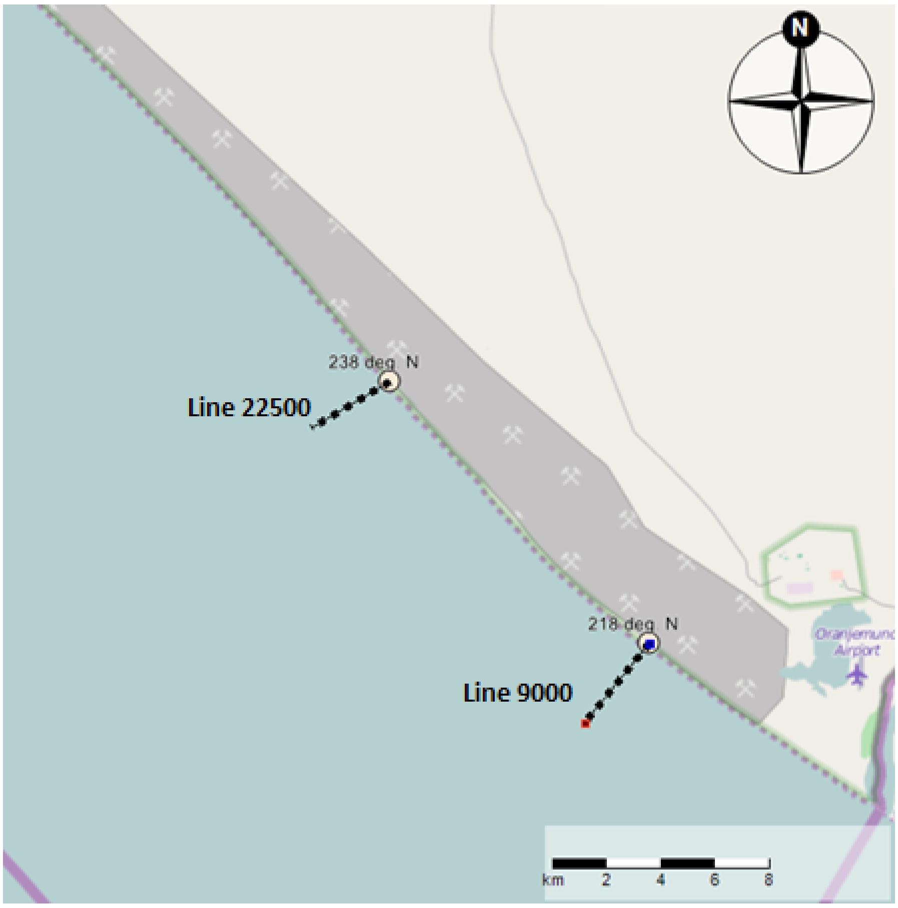

Figure 11.1: Simplified map of MA1, showing the location of Survey Line 9000 and 22500.

Figure 11.2: Aerial image of MA1. The orange straight line presents the average coastline orientation of MA1. The green lines present the average coastline orientation on a smaller scale.

Survey Line 9000

For the seawall at Survey Line 9000 (just south of the ongoing mining activity in the G-area) the steps of the shifting seawall are visualized.

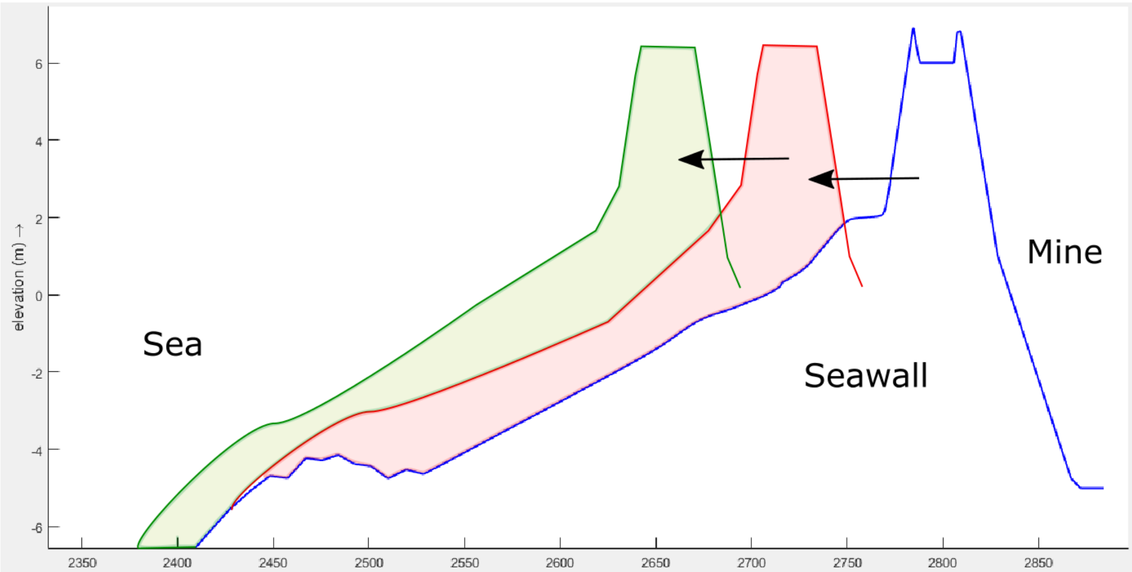

Figure 11.3: Impression of the seaward shifting of a seawall close to Survey Line 9000 (NAMDEB).

The blue line represents the seawall in its current state. After one or two years the beach should have accrued far enough so the seawall can be moved. The moved seawall is represented by the red line in Figure 11.3. The pink volume is the volume of sand needed for the new situation. The volume of the seawall itself is still the same, but there is also a lot of sand needed for land accretion. This is more than the volume of the seawall. After a while the seawall will be shifted again. Now represented by the green line in Figure 11.3. Even more sand on the foreshore is needed. This volume of sand comes from the Sand-2-Sea program. Line 9000 is in a favourable position along the coast for beach accretion. This is consistent with the theory of longshore transport (section 6.3, summarized again in Figure 11.4). Line 9000 is on the edge of where sand nourishment takes place and so deposition due to longshore sediment transport can be expected. This can also be derived from Figure 11.1 and Figure 11.2, showing how

Line 9000 is on the oblique side of the nourishing activity.

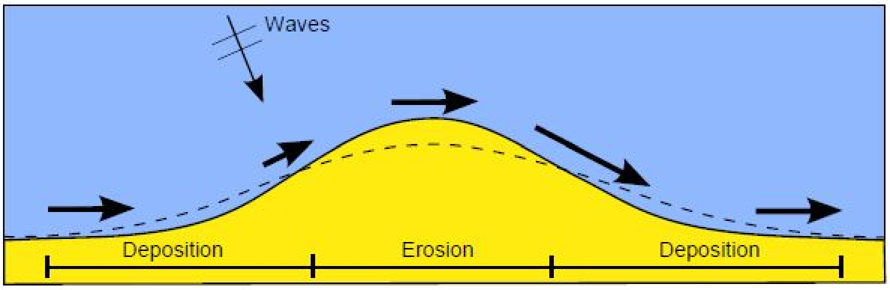

Figure 11.4: Longshore sediment transport gradients along a nourishment. Figure from Steijn (2015).

Survey Line 22500

Figure 11.5: Aerial view of MA1, zoomed in on the area where the seawall breach of May 2015 took place (circled in red). The yellow line highlights the curvature of the coast and how some seawall sections stood out.

The situation of Line 22500 is different. This line was also modelled in the case study of section 9.3.1 (Storm of May 2015). When looking at the simplified figure of longshore transport (Figure 11.4), beach erosion can be expected at this location due to longshore sediment transport, because Survey Line 22500 is on the frontline of the Sand-2-Sea program. In Figure 11.2 the location of Survey Line 22500 was shown. Figure 11.5 above zooms on the area of Line 22500 and shows how the coastline is curved here. The seawall that breached in May 2015 is high-lighted in red, and it can be seen that this seawall stood out in seaward direction.

A similar figure of a shifting seawall, as was drawn for Line 9000, can be drawn for Line 22500. This is done in the figure (Figure 11.6) below.

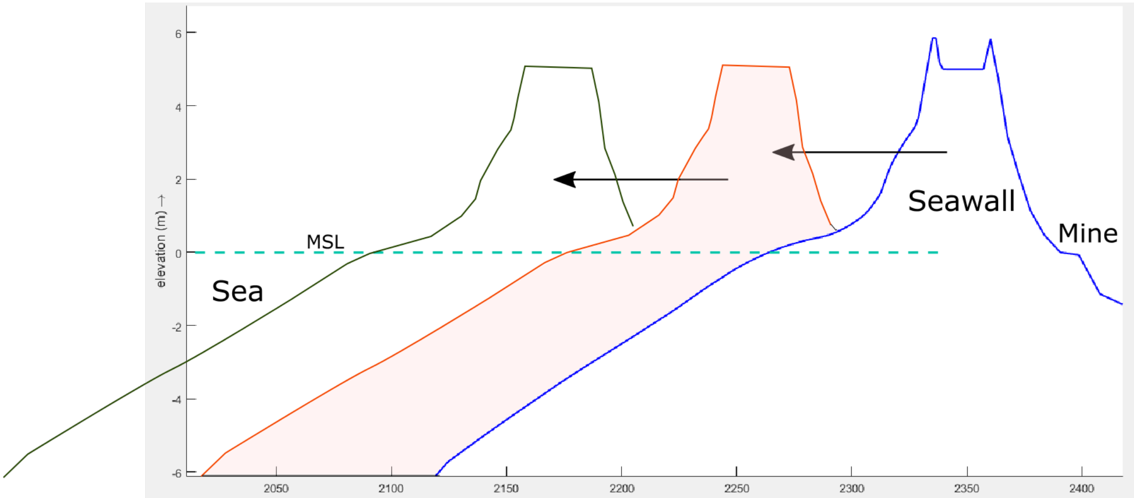

Figure 11.6: Impression of the seaward shifting of a seawall close to Survey Line 22500 (NAMDEB).

The first thing that is notable is that the foreshore is significantly steeper for this region than for the region where Line 9000 is in. This means that much more sand will be needed to create a beach width where a seawall can be shifted seawards. This because for the new seawall standards a foreshore profile has to develop that is less steep. Also in this case even more sand is needed when moving to the next shift. Another issue is that the steepness and narrowness of the beach lead to relatively little wave energy dissipation. Meaning that waves can reach the toe of the seawall relatively often. This was also seen when this area was modelled as a case study. Seawall erosion will take place on a weekly basis with a high probability.

11.2 Comparison with natural equilibrium profile

From the modelling results it could be derived that no equilibrium profile of the upper shoreface will develop. However the state of the seawalls can be compared with the equilibrium profile nature strives for with the once-per-year storm. This can be considered as a conservative approach since it is most unfavourable for the state of the seawall and very likely to happen on a yearly basis. The comparison is explained stepwise with Figure 11.7 to Figure 11.11.

Equilibrium profile

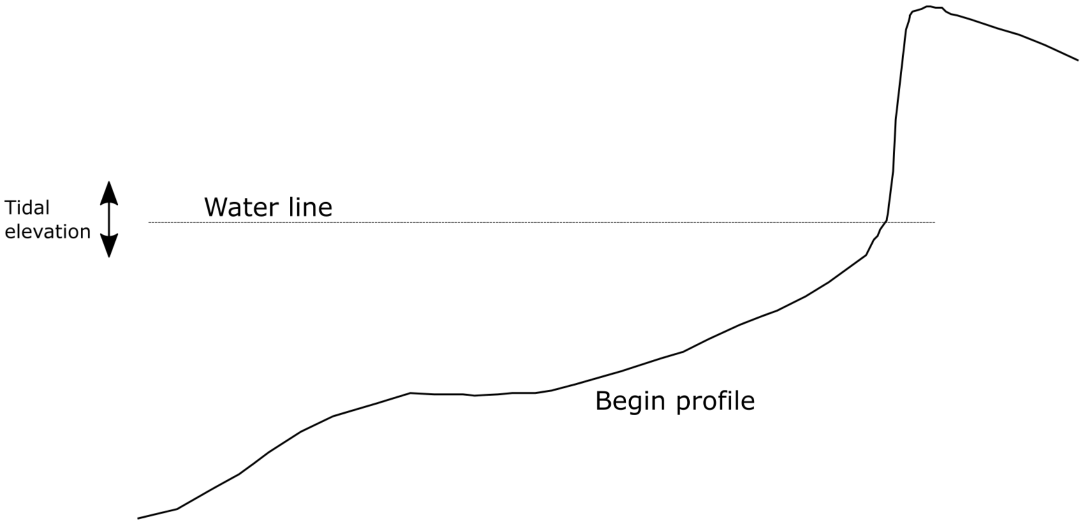

Figure 11.7: Example of a cross-section of sandy coast.

As explained in Chapter 6 a coastal profile is dynamic and it changes with changing hydrodynamic conditions. An example of a coastal profile is given in Figure 11.7 above. In storm conditions a post-storm equilibrium profile forms, depending on the forces working on the coast. The formation of an equilibrium profile was explained in section 6.4 and is according to Vellinga (1983). A sketch of the once-per-year profile for the Southern Coastal Mine is presented in Figure 11.8 below. The gray area in the figure represents the volume of sand taken away from the seawall and redeposited beneath the water level.

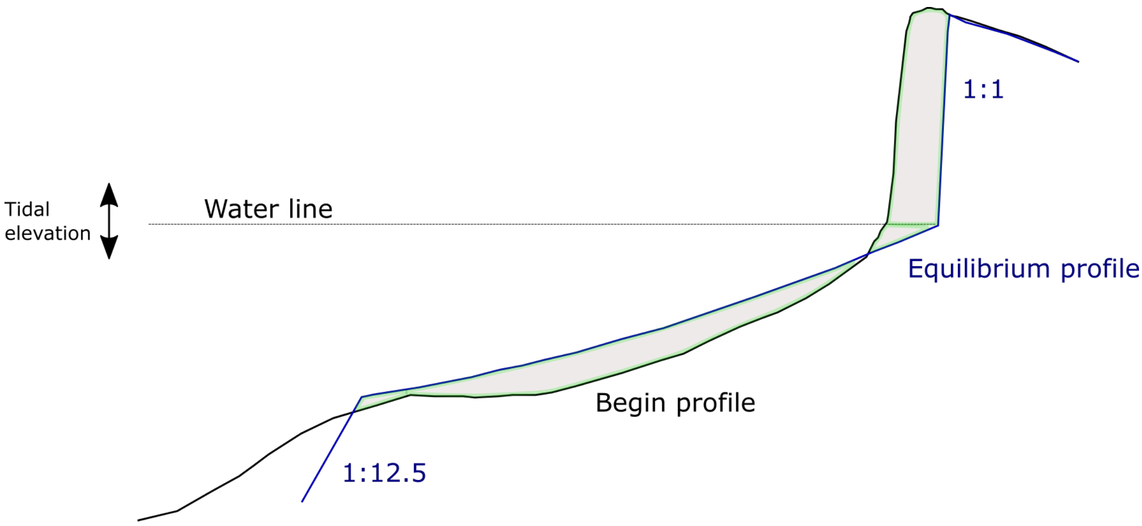

Figure 11.8: Outline of an equilibrium cross-shore profile according to hydrodynamic conditions of a storm with a probability of occurrence of 1/1 per year.

Construction of seawalls

The seawalls constructed on the beach in the Southern Coastal Mine are closer to the high water line than the toe should be according to the outline of the equilibrium profile. In Chapter 9 was shown how a storm with a return period of 1 year already leads to erosion on the seawall. Figure 11.9 shows also that the lower part of the upper shoreface (below the water line) is lying lower than the lower part of the equilibrium profile. There is a lack of sediment (gray area) that needs to be fed. So extra sand is required, for instance from the Sand-2-Sea program, to create profile that can reduce wave energy effectively.

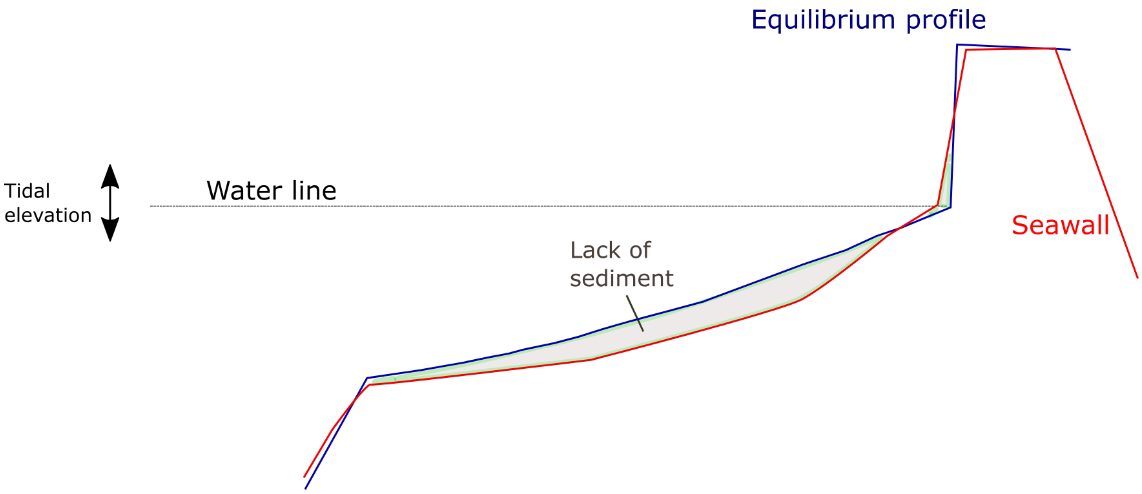

Figure 11.9: Schematic comparison of the cross-shore profile with a seawall (red) and of the equilibrium profile (blue) according to the storm conditions with a return period of 1 year.

Seaward shift of the seawall

When enough land is accrued, the seawall will be shifted in seaward direction. The figure below (Figure 11.10) shows that there is much more sediment needed to make this shift possible than just the volume of the seawall.

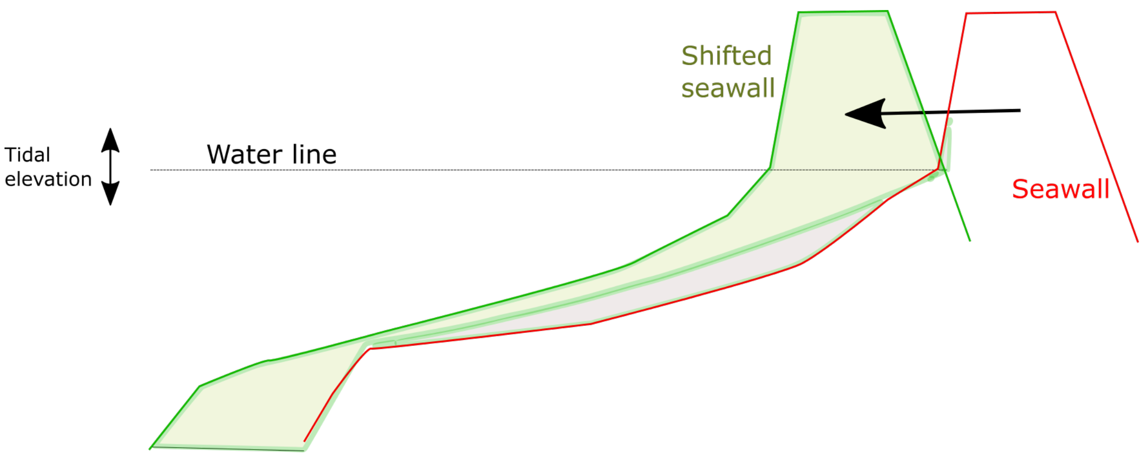

Figure 11.10: Schematic drawing of a seaward seawall shift (in green).

Due to longshore sediment transport and due to the dipping of the bedrock, there is an increasing volume of sand needed for a seawall shift. The new shifted seawall and foreshore are most likely in the same form as the earlier seawall. So also this shifted profile differs from the equilibrium profile. Figure 11.11 below illustrates this. With progressing land accretion the losses of sand due to longshore sediment will increase, making it even more difficult to establish an effective equilibrium profile.

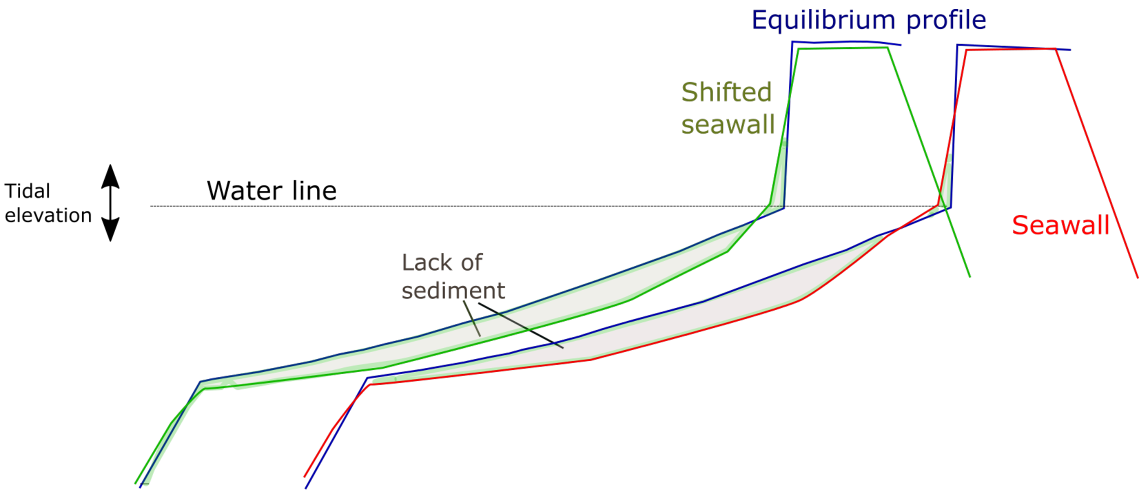

Figure 11.11: Schematic comparison of the cross-shore profile with a shifted seawall (green) and of the shifted equilibrium profile (blue) according to the storm conditions with a return period of 1 year.

This problem with longshore sediment transport will become larger for Survey Line 22500 and other seawall sections on the seaward peak of the nourishment. With a retreating beach at these locations, an effective equilibrium profile will need significantly more extra sand volume than other location.

11.3 Prognosis

This section gives an estimation of the progression of shifting seawalls. The new standards for seawall volume and foreshore (see Chapter 10) are used for this prognosis.

11.3.1 Timescale of Business Plan

Based on the analysis of model results and theory, the conclusion can be drawn that the currently applied land reclamation strategy is a short-term method. The sand nourishment, focused on the area between G30 and U50 (see the maps in Appendix A), is spreading out along the entire coastline. And besides this, the formation of an equilibrium cross-shore profile takes more time and sediment than it is given before the seawall is shifted seaward. Considering the size and lack of sediment volume, the positioning of the seawall and the wave climate, the timescale of forming an equilibrium is considered to be in the order of years.

The strategic business plan of NAMDEB presumes the continuation of this mining and land accretion strategy until 2031, and beyond this year if possible. Appendix C elaborates on the business plan. This is a long-term strategy, that does not comply with the methods that are currently used. A large volume of extra sand will be needed to feed the coastline for this plan.

If the rate of sand nourishment and the rate of the spreading out of the nourishment along the coast are known, one can predict how the coastline will behave in a shore-parallel direction. The rate of sand nourishment should be known from the administration of NAMDEBs mining activity. The rate of spreading out can be investigated with, amongst others, the Mega Nourishment Tool (MN-Tool), described by Steijn (2015). This tool involves the use of a numerical coastline model and it assesses the life time of large sand nourishments along the coast. Such an assessment is out of scope for the research of this thesis. But based on insight gained from XBeach model results and from theory described in this thesis, an estimate has been made for the continuation of the land accretion strategy.

11.3.2 Determination of sand volumes

The methodology of establishing a prognosis of the limit for land accretion is explained here. In Figure 11.12 again the shift of a seawall is presented schematically. Now also the bedrock is drawn beneath the sand body. The bedrock slightly dips in seaward direction as described in Chapter 5. The seawall is constructed according to the standards determined in Chapter 10, represented by the pink fill in Figure 11.12. The cyan line and the blue line represent the erosion profiles, based on the model results of long-term simulations with the XBeach model.

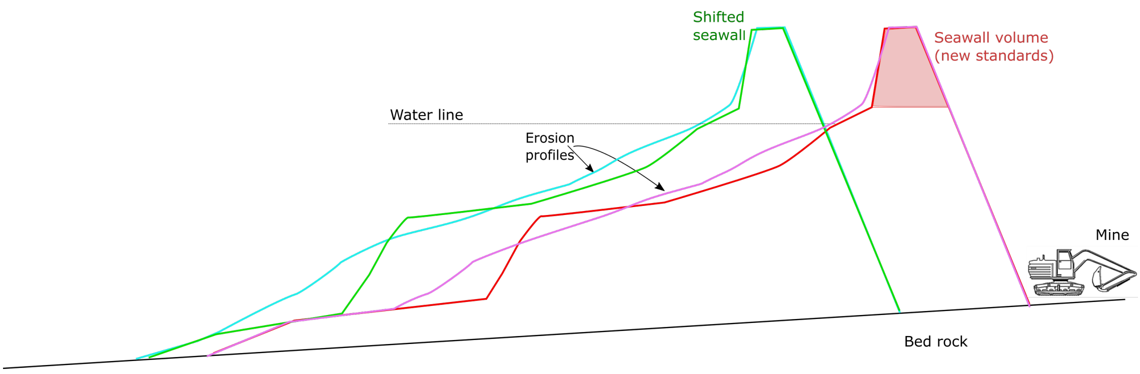

Figure 11.12: Schematic drawing of a seaward seawall shift. The sand body of the entire foreshore is given for the original seawall (red line) and the shifted seawall (green line). The erosion profiles are given in purple and and cyan.

With every shift the seawall is moved over a distance x, once the beach is accrued far enough. A yearly accretion rate of 40 m on average is assumed, which will be explained in the next section. Material for the new seawall and for the lack of sediment in the foreshore has to come from the stripping of overburden and from stripping the old seawall. Figure 11.13 shows in brown the body of sand that is excavated in the stripping operation once the seawall is shifted. The green area is the volume of sand needed for a relatively stable seawall and foreshore.

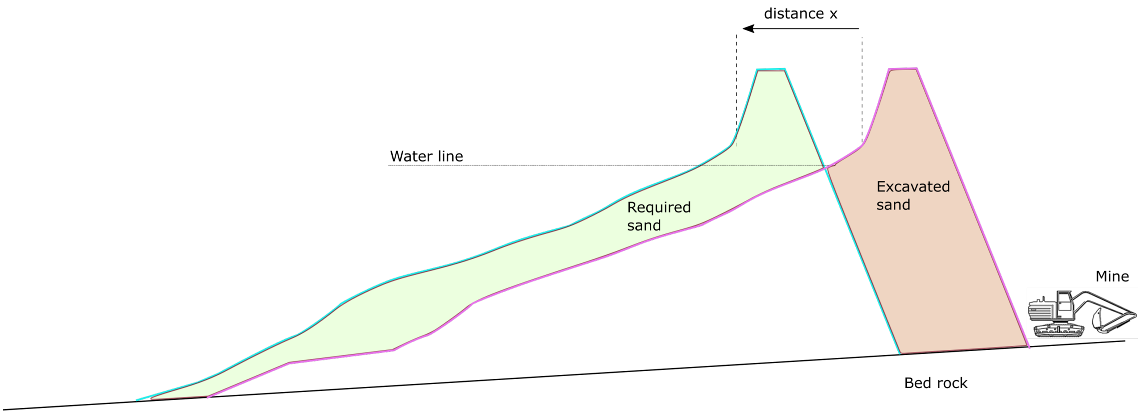

Figure 11.13: Schematic drawing of the sand volume needed for a seaward seawall shift. The outlines of the two different seawalls match the erosion profiles (cyan and purple lines) of Figure 11.12. The brown area is the volume of sand that needs be excavated for the mining operation. The green area is the volume of sand needed for a relatively stable seawall and foreshore.

In the currently applied mining method sand for the foreshore comes from the Sand-2-Sea program (see section 3.6) and from feeding the seawalls with overburden material. The amount of material needed for the foreshore depends on the distance x and on the workable depth. The depth value is the depth of the toe of the seawall on the location of a depth contour line measured in 2014. The relation between the volume of sand (V_{shift}) needed and the depth ($d_{seawall}$) can be sketched in a graph. This has been done in Figure 11.14.

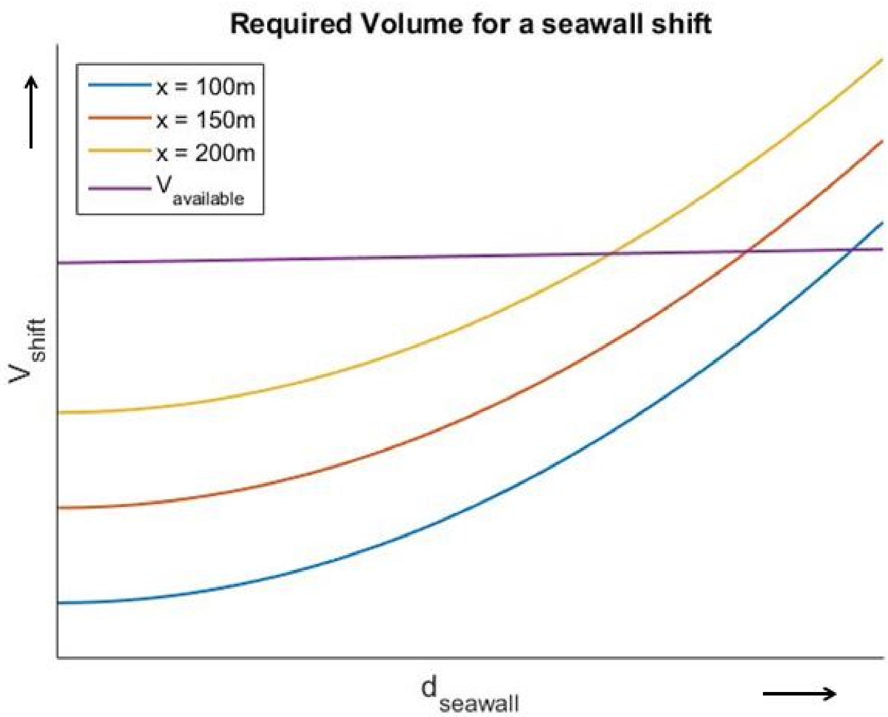

Figure 11.14: Graph representing the relation between the required volume of sand for a seaward seawall shift and the depth. The different lines stand for different stepsizes x. $V_{available}$ is the volume of sand that is directly available through the mining process.

The different lines represent different values of x over which the seawall is shifted per time. These lines are approximately quadratic. Because of the seaward dip of the bedrock, there is a larger volume of sand needed for each seawall shift. While the bedrock dips approximately linear, the sand demand is expected to grow quadratic. But more important, the volume of sand needed for maintenance will increase dramatically when land accretion progresses. This will be explained below. The required volumes can also be presented in a table, as is done in Table 11.1.

Table 11.1: Volumes required per year for the shifting of seawalls.

$d_{seawall}$ $[m]$	x $[m]$	V_{shift} $[m^3/m]$	$V_{construction}$ million $[m^3/year]$	$V_{maintenance}$ million $[m^3/year]$	$V_{required}$ million $[m^3/year]$
4	100	1140	8.55	12.72	21.27
	150	1653	8.27	12.72	20.98
	200	2166	8.12	12.72	20.84
8	100	1197	9.58	15.50	25.08
	150	1736	9.26	15.50	24.76
	200	2274	9.10	15.50	24.60
12	100	1317	11.19	19.27	30.46
	150	1909	10.82	19.27	30.09
	200	2502	10.63	19.27	29.90
16	100	1514	13.63	24.09	37.72
	150	2196	13.17	24.09	37.26
	200	2877	12.95	24.09	37.03
20	100	1817	17.26	30.27	47.53
	150	2635	16.69	30.27	46.95
	200	3452	16.40	30.27	46.67

The table describes the sand volumes required for forward steps in terms of depth in meters. It repeats V_{shift}, but also includes $V_{maintenance}$, which is the volume of sand required for maintenance. All volumes of sand are given in million $m^3/year$. $V_{construction}$ represents the yearly needed demand of sand for seawall construction, based on the accretion rate, total seawall length along the coast and V_{shift} for specific values of x and $d_{seawall}$. The following estimates are required to construct table 11.1:

- V_{shift} is equal to the green area in Figure 11.13 and increases when land accretion progresses, as is discussed in the sections before (section 11.1 and section 11.2). A seaward shift of 100 m requires a volume of about 7 times the seawall volume, which is 1140 m^3/m. A value of 160 m^3/m is held for the seawall.
- Shifting the seawall further than 100 m will require more sand for land accretion, but less sand is expected to be lost in the construction of the seawall itself. Therefore, the amount of sand required for a seawall shift of 200 m is not twice the amount of a shift of 100 m. A factor of 1.9 between V_{shift} for a distance of 200 m and a distance of 100

m is estimated. For $x = 150$ m this is a factor of 1.45. And so the yearly sand demand for seawall construction ($V_{construction}$) is lower for a larger x.

- On average land accretion is about 40 m per year in the area of MA1 that is targeted by the Sand-2-Sea program. This is based on the knowledge that between 2013 and 2015 seawall sections in the areas of ongoing mining activity were shifted on average every 18 months with a distance of 80 to 150 meters (see section 3.4). For a more conservative approach a lower average accretion rate is assumed. Also the demands for the width of the beach and the steepness of the foreshore are higher with the newly developed standards. An accretion rate of 40 m per year is held for the first years. The accretion rate is expected to decrease in later stages of land accretion when longshore sediment transport start to play a larger role.
- The total alongshore length of the seawall is in the order of 15 km. It is expected to grow when the sand nourishment grows. From this the yearly sand volumes needed to construct the total length of seawalls, $V_{construction}$, can be calculated.
- The volumes of sand required for maintenance of the seawall and of the foreshore, $V_{maintenance}$, are equal to the volume of sand that leaves the system due to longshore transport. This will be explained below with Figure 11.15.
- $V_{maintenance}$ will increase when land accretion proceeds. The section below explains how much this increase is due to a changing coastline orientation.

The range of these estimates is discussed in section 11.3.3 below.

Required sand volume for maintenance ($V_{maintenance}$)

$V_{maintenance}$ is equal to the volume of sand needed for seawall maintenance due to erosion plus the volume of sand lost in the system. Figure 11.15 explains the losses of sand in the system. It is known that sand nourishments on a beach tend to spread out along the coast (see Figure 11.4). Spreading out becomes undesired when sand leaves the area targeted for land accretion. In Figure 11.15 two cross-shore transects are drawn, representing the edges of the target area of the Sand-2-Sea program, and thus the target area of land accretion.

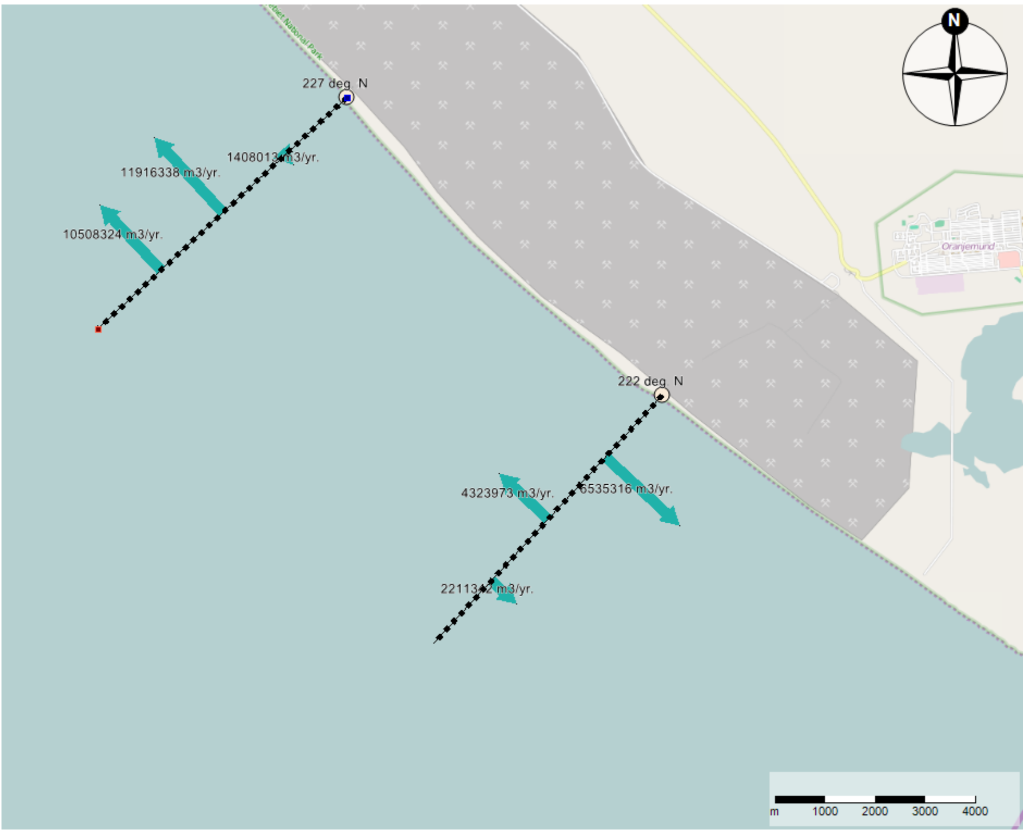

Figure 11.15: Map of Southern Coastal Mine Namibia, zoomed in on the area targeted by the Sand-2-Sea program. Two cross-sections are visible, where the longshore sediment transport volumes are computed with CoDeS. From coast to sea: the first two arrows represent the gross sediment transports. The last arrow represents the nett sediment transport.

The figure is obtained with the software program CoDeS (version 1.0) (Coastline Development Tools), to give an indication of the orders of magnitude of longshore sediment transport. The model input for CoDeS is the location of interest and the wave conditions occurring. With the longshore transport formulas of either Kamphuis (1991) or CERC (Bosboom and Stive, 2013), the gross transport volumes of sand along the coast can be determined. This has been done for the Southern Coastal Mine, as shown in Figure 11.15. The wave conditions used are the 17 conditions that were obtained by input reduction techniques, described in section 9.2.4. Since the simple CERC formula was used in the process of wave input reduction (see Appendix E) and because the CERC formula is relatively conservative in its outcome (Bosboom and Stive, 2013), the approach of CERC will also be used here.

The two cross-shore transects in Figure 11.15 are perpendicular to the coastline. The arrows represent the longshore sediment transport rates through the transects. The arrow standing out the most in seaward direction represents the nett sediment transport. This arrow describes how much sand leaves the system, and thus how large $V_{maintenance}$ is. From the figure can be seen that about 10.5 million m^3 sand per year leaves in northward direction and about 2.2 million m^3 sand per year leaves in southward direction. $V_{maintenance}$ is therefore considered to have an order of magnitude of 12.7 million m^3 sand per year.

The further the land accrues, the more dominant longshore sediment transport becomes with respect to cross-shore sediment transport. The calculated losses for the area of beaches that are targeted by the Sand-2-Sea program will increase with progressing land accretion. Fuhrboter (1991) estimated an additional loss of about 40% of sand, which can thus not be used effectively, for nourishments on Dutch beaches. It is out of scope to accurately determine these losses for the Southern Coastal Mine, but again an estimation can be given with the use of CoDeS. This is explained with Figure 11.16.

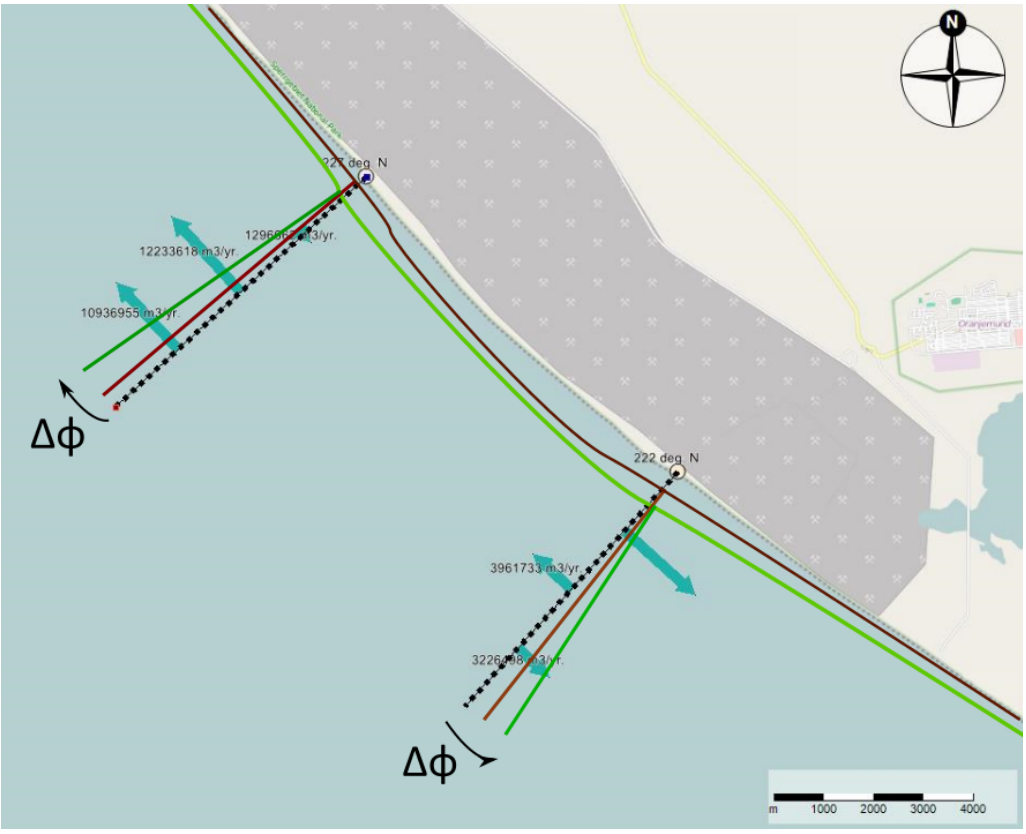

Figure 11.16: Map of Southern Coastal Mine with the same cross-sections as in Figure 11.15. The brown line represents a step in the land accretion process and the green line an even further step. For both land acrretion steps the cross-sections are drawn again at the same location perpendicular to the coast. $\Delta\phi$ represents the changing coastline orientation. Figure is not to scale.

The figure presents again the cross-sections on the edges of the target area. When land accretion proceeds, the orientation of the coastline will change. This is illustrated with the brown and green lines of the figure above. The cross-sections are again drawn perpendicular to the coast at the same location. From the changing angle of the orientation of the cross-sections ($\Delta\phi$) it can be derived that the coastline orientation (ϕ) relative to the angle of wave incidence changes as well. The figure is not to scale, since land reclamation is drawn exaggerated with the purpose of illustrating changes in coastline orientation. In section 6.3.4 it was explained, with the aid of an S-ϕ curve, how longshore sediment transport rates changes when either the orientation of the coastline or the angle of incidence of wave changes. Figure 11.17 shows the expected coastline orientation for the situation where land has accrued until the 20 m depth contour line.

The steps of land accretion are presented in table 11.2 below, together with the values of sand losses (or $V_{maintenance}$. The depth values and distances from the average high water line of 2014 are an estimation for the average coastline of the area targeted by the Sand-2-Sea program. Nett longshore transport volumes are obtained with CoDeS, using the approach of CERC.

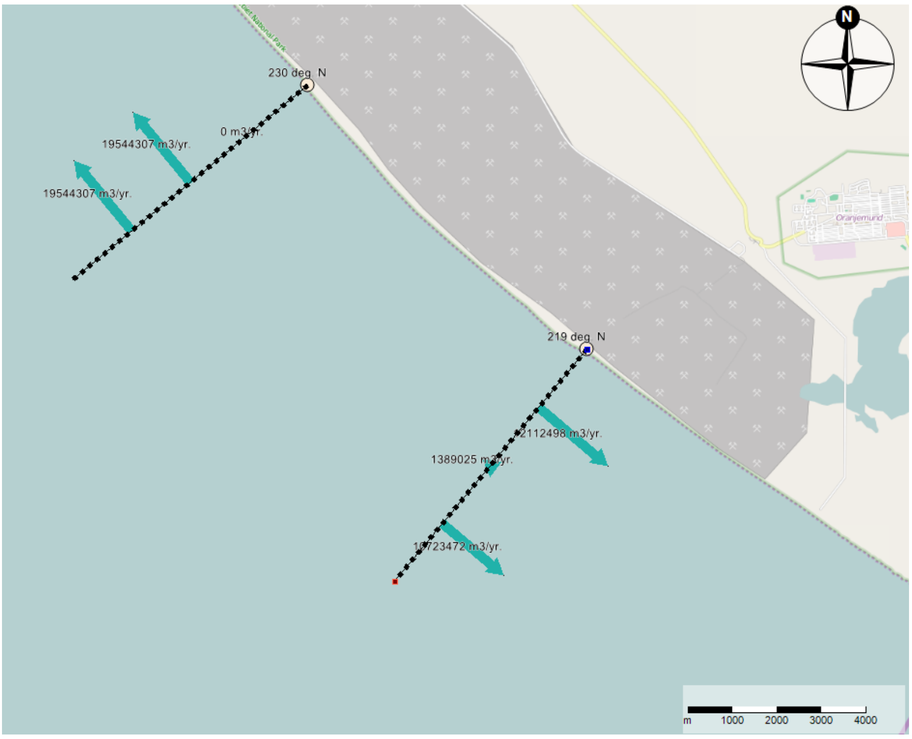

Figure 11.17: Two cross-sections imitating the situation of land accretion until the 20 m depth contour line. Longshore sediment transport volumes are computed with CoDeS. From coast to sea: the first two arrows represent the gross sediment transports. The last arrow represents the nett sediment transport.

Table 11.2: Volumes required for the maintenance of cross-shore profiles per step in changing coastline orientation due to land accretion.

$d_{seawall}$ $[m]$	Average distance from high water line 2014 $[m]$	$\Delta\phi$ [degrees]	Nett longshore transport volume at southern cross-section [million $m^3/year$]	Nett longshore transport volume at northern cross-section [million $m^3/year$]	$V_{maintenance}$ million $[m^3/year]$
4	120	0.5	2.21	10.51	12.72
8	280	1.2	4.08	11.42	15.50
12	420	1.75	5.89	13.38	19.27
16	600	2.5	7.36	16.72	24.09
20	900	3.5	10.72	19.54	30.27

From this table it can be concluded that $V_{maintenance}$ will increase dramatically when land accretion proceeds.

Sand volumes available ($V_{available}$)

Figure 11.13 presents in brown the material that is available for a seawall shift. This volume is about the same size of the volume needed for a seawall shift (V_{shift}). This overburden material is excavated for the extraction of diamonds and dumped on the beach. The total volume of material that comes available because of the mining operation is estimated to be in the order of 10 million m^3 per year (see section 3.4).

The material coming from the mining operation will not be sufficient to feed the foreshore. For this reason the Sand-2-Sea program was implemented. The total pumping rate with this Sand-2-Sea program is in the order of 20 million m^3 per year (see section 3.6). The total amount of material available per year ($V_{available}$) is thus about 30 million m^3. However, due to technical difficulties in the Sand-2-Sea operation, as described in Appendix C, this maximum capacity of 20 million m^3 per year is generally not reached. $V_{available}$ is revised downwards to 25 million m^3 of sand per year.

11.3.3 Prognosis of final distance

Proposed shifting distance

The most optimal distance of x over which the seawall should be shifted is probably about 150 m. When a distance of 100 m is chosen the seawall has to be shifted rather often and more material and effort has to be put in seawall construction. A value for x of 200 m is probably too large. The mining block behind the seawall becomes very large, leading to more pumping of water from the mine. But also the consequences of flooding of a mining block become larger, since more area will be flooded. A distance of 150 m also has the advantage that the yearly required sand volumes are lower than the volumes required for $x = 100$ m and $x = 200$ m (see table 11.1).

Determination of the depth contour line

When the available sand volumes are smaller than the required volumes ($V_{available} < V_{required}$), then the costs of land accretion and seawall maintenance will rise dramatically because material has to come from elsewhere. With $V_{available}$ being about 25 million m^3 per year, this limit is reached after accretion to the 10 m depth contour on average, as can be derived from table 11.1. With the overload of available material in the Sand-2-Sea program in the early stages of land accretion, it can be expected that a relatively stable cross shore profile can even establish at the 12 m depth contour.

Reaching the depth contour of 10 m corresponds to a distance of 360 meters on average, measured from the average high water line of 2014. With an average accretion rate of 40m (decreasing in time), this distance is reached after 10 years.

Range of final answer

The determination of the final depth contour line for land accretion contains uncertainties, which can make a significant difference. For this reason the margin of errors has been estimated for different relevant aspects. Subsequently the range of the final answer can be given.

- The uncertainty of $V_{construction}$ is presumed to be in the order of one seawall volume for a seaward seawall shift of 100 m. Therefore, 1/6 (a little larger than 1/7) of the total volume (16.7%) is held.
- From calculating $V_{maintenance}$ it could be concluded that the answer is very sensitive to changes in coastline orientation, judging from the large differences in volumes for small values of $\Delta\phi$. Also the prevailing wave conditions and the chosen calculation approach (CERC) have uncertainties. It is recommended to do a proper investigation into longshore sediment transport rates before proposing a final answer. For now a margin of 20% is proposed, which is presumed to be a conservative approach.
- For $V_{available}$ a value of 25 million m^3 per year was proposed. Research into the current mining operation showed that the value of 30 million m^3 per year approaches maximum capacity. In addition, it was found that the maximum capacity can hardly be reached due to technical, social and regulation difficulties (Anker, 2014). A margin of 20% is chosen, which means that the maximum capacity of 30 million m^3 per year is met in the most favourable scenario.

The values of table 11.1 for $x = 150$ m have been recalculated with the aforementioned uncertainty margins. The results are presented with the graph in Figure 11.18. For each value of $d_seawall$ the $V_{required}$ (sum of $V_{construction}$ and $V_{maintenance}$) for $x = 150$ m is plotted, together with the most favourable scenario (green line) and the most unfavourable scenario (red line) for the required sand volumes. The most unfavourable scenario for the required sand volume is when both $V_{maintenance}$ and $V_{construction}$ turn out to be larger, with 20% and 16.7% respectively, than their estimated values. On the other hand, the most favourable scenario occurs when both $V_{maintenance}$ and $V_{construction}$ turn out to be 20% and 16.7% lower than their estimated values, respectively.

The most unfavourable scenario for the sand volume available (red dashed line) is when $V_{available}$ turns out to be 20% lower than the assumed 25 million m^3 per year. On the other hand, the most favourable scenario (green dashed line), in terms of $V_{available}$, occurs when the value is 20% higher.

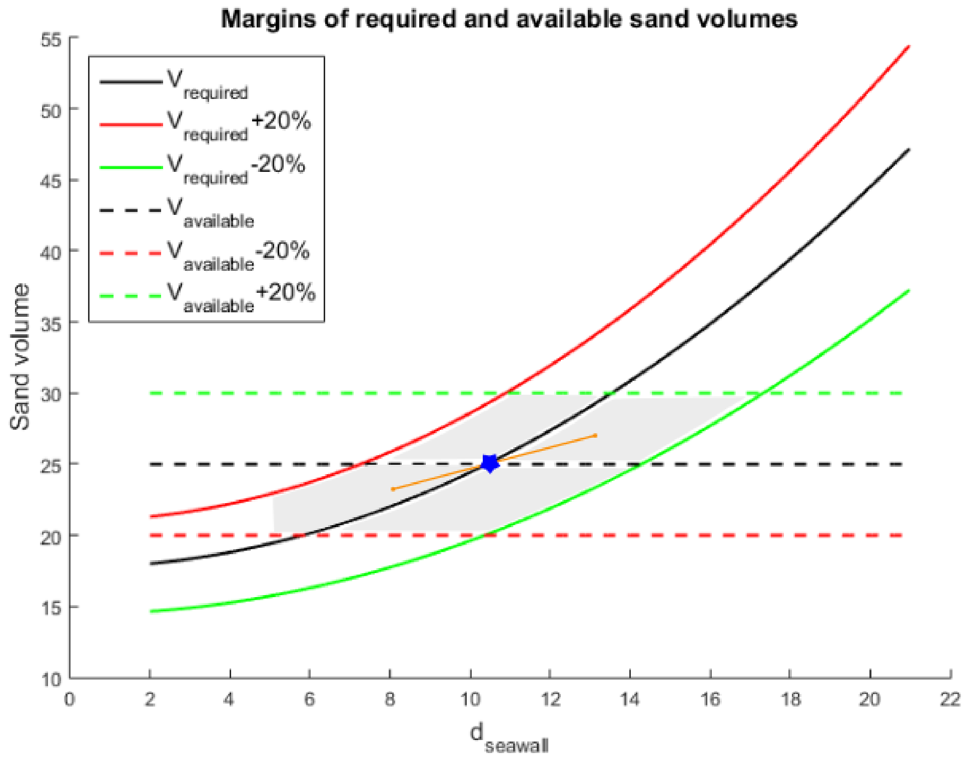

Figure 11.18: Graph showing the required sand volumes and available sand volumes for land accretion, plotted against the depth at which the seawall must be constructed. The grey area indicates the range where limit for land accretion is in.

The area in the graph that is marked grey is the range where the limit for land accretion is most likely to be in. The point with the highest likelihood (under current knowledge) is where the black lines intersect, marked by the blue dot. This is at $d_{seawall} = 10.5$ m. Under very favourable circumstances land accretion is expected to be feasible until the 17 m water depth contour line on average. Under very unfavourable circumstances land accretion is expected to be feasible no further than the 5 m water depth contour line on average, which is considered to be the lower boundary since the red lines in Figure 11.18 do not intersect.

From studying the margins of available and required sand volumes it can be concluded that the limit for land accretion is in the range of 8 to 13 meters water depth on average in the area targeted by the Sand-2-Sea program. This range is indicated with the orange line in the graph of Figure 11.18.

Chapter 12 – Acceptable risk level

Design standards were proposed in this report for a seawall to withstand storm conditions with a probability of occurrence of 1/100 per year. As mentioned before, NAMDEB will have to determine what the acceptable risk level is for a seawall of mining block behind a seawall. This section explains how the acceptable risk level can be chosen. The risk level is related to the probability of occurrence of certain storm conditions. The common way to choose the acceptable risk level is by studying the minimum of the total costs of the mining operation in a mining block behind a seawall. The total costs are defined as the sum of the investment costs and the risks.

12.1 Investment costs

The investment costs are defined as the unit costs of sand (in USD/m^3) for constructing a seawall and a relatively stable foreshore profile. The costs of loading, hauling and dumping of overburden sand are unknown (to be determined by NAMDEB), but assumed to be 5 USD/m^3. This is considered to be a low price in comparison to other land reclamation and dune construction projects. However, the hauling distances in the Southern Coastal Mine are relatively small and overburden sand is freely available to NAMDEB for construction purposes.

Table 11.1 in Chapter 11 presented the sand volumes that are required per year for the continuation of the mining operation. The required volumes for $V_{construction}$ will differ per design storm condition (1/100 per year, 1/50 per year, etc.), because the impact on a seawall and on the foreshore is different for different storm conditions, as can be illustrated by Figure 9.11 showing erosion to the seawall. Determining design standards for different storm conditions is out of scope for this research, but the design method that was described in Chapter 10 for the 1/100 per year storm conditions can also be applied to other storm conditions (or risk levels). A rough estimation of required seawall- and foreshore volumes is given in table 12.2 below. The seawall volumes are estimated on the basis of table 10.2 in Chapter 10, which is repeated in here (see table 12.1). The build-up of the presented values of table 12.2 is explained hereafter.

Table 12.1: Resulting seawall erosion volumes per storm condition. Repeated from Chapter 10.

Design storm [prob. per year]	1/1	1/2	1/5	1/10	1/50	1/100
Eroded volume [m^3/m]	3.6	7.5	19.9	47.6	70.6	100.3

Table 12.2: Build-up of investment costs for different risk levels.

Storm condition $[prob/year]$	Seawall volume above MSL +2m $[m^3/m]$	V_{shift} $[m^3/m]$	$V_{construction}$ [million $m^3/year]$	$V_{maintenance}$ [million $m^3/year]$	$V_{required}$ [million $m^3/year]$	Investment costs per mining block in million [USD$/year$]
1/1	90	914	0.15	0.41	0.56	2.81
1/2	100	1015	0.17	0.41	0.58	2.89
1/5	110	1117	0.19	0.41	0.60	2.98
1/10	120	1218	0.20	0.41	0.61	3.06
1/50	140	1421	0.24	0.41	0.65	3.23
1/100	160	1653	0.28	0.41	0.68	3.42

The table is constructed in the same way as table 11.1 in Chapter 11 was constructed for the 1/100 per year storm only. A shifting distance x of 150 m is used in these calculations. A seaward shift of 100 m requires a volume of about 7 times the seawall volume (above MSL +2m). For a shift over 150 m, this value must subsequently be multiplied by a factor of 1.45 (see section 11.3) to find the value of V_{shift}.

Only a single mining block is considered in this risk analysis, meaning that a (shore-parallel) length of 500 m (instead of 15 km) for the seawall is held. The sand volumes required for maintenance are kept the same, but now also downscaled to account for the alongshore distance of 500 m. $V_{required}$ differs very little between different design conditions, because the share of $V_{maintenance}$ is relatively high.

12.2 Risks

The risks are defined as the costs of the consequences of seawall failure multiplied by the probability of occurrence of the storm conditions that lead to failure.

The costs of the consequences, i.e. costs of flooding of a mining block, depend on the stage of the mining activity. The costs are determined by loss of equipment, the loss of diamonds and costs of starting up the mining activity again. Three stages are distinguished: the early stripping stage, the middle stage and the final cleaning stage. For each stage a cost estimate is made to show how eventually an acceptable risk level can be determined. The costs of the consequences of a flooding must be re-defined by NAMDEB.

12.2.1 Early stripping stage

The early stripping stage exists when there is only stripping of overburden and pumping of seepage water present in a mining block, illustrated with Figure 12.1. The costs of a flooding are low compared to the other two stages, and starting up the operation again is relatively easy. The costs of consequences are estimated to be in the order of 10 million USD.

Figure 12.1: Early stripping stage in mining operation. Repeated from Chapter 3.

12.2.2 Middle stage

The mining operation is in the middle stage when the transition is made from overburden stripping to stripping of bulk material, illustrated with Figure 12.2. When a mining block floods, the morphology of the bulk material is likely to be changed by the water. The loss of equipment increases slightly because heavier water pumps and more trucks are present in this stage. Compared to the early stage, the start-up of mining activity after flooding is also likely to be more expensive, because the pit was already deeper. The costs of consequences are estimated to be in the order of 30 million USD.

Figure 12.2: Middle stage of mining operation: stripping of bulk material. Repeated from Chapter 3.

12.2.3 Final cleaning stage

Flooding when mining activity is in the final cleaning stage is considered to be the most costly. This stage is present when the transition is made from the stripping of bulk material to the cleaning of the bed rock, presented in Figure 12.3 and 12.4. More equipment is used in this stage (also Transvacs), so the costs of loss of equipment are expected to be higher. The mining pit is now at its deepest level, so the costs of a start-up are considered to be the highest. Flooding of the block can wash away diamonds in this stage and mix it with sediment, which can also be considered as extra costs/losses. The costs of a flooding in this stage are estimated to be in the order of 50 million USD.

Figure 12.3: Final cleaning stage: Transvacs. Repeated from Chapter 3.

Figure 12.4: Final cleaning stage: Worker operating a Transvac. Repeated from Chapter 3.

12.2.4 Combination of stages

A combination of different mining stages in a single mining block is also possible when a flood occurs. As a conservative approach, the cost of consequences of the most expensive mining stage are proposed to calculate with.

An important consideration is that the costs of a flooding are the same for all levels of the probability of failure. In other words, when a flood occurs due to storm conditions of an 1/10 per year storm, the costs of the consequences are the same as for a flood induced by an 1/100 per year storm. These are independent variables.

12.3 Total costs

By plotting the total costs as a function of the accepted probability of storm conditions, the acceptable risk level can be chosen. This has been done in Figure 12.5 to 12.7 below. The different figures correspond to the different stages where mining activity in a mining block is in. The red lines represent risks in million USD/year. In other words, the costs of consequences multiplied by the probability of occurrence of storm conditions that lead to failure. The blue lines represent the investment costs, again in million USD/year. The black line is the sum of the two lines, thus presenting the total yearly costs. At the minimum of the total costs, a green dot is plotted. All the graphs are extrapolated to the probability of occurrence of 1/1000, visualized with the dotted lines. This has been done to illustrate that when the risks approach 0 USD, the total costs increase with the investment costs.

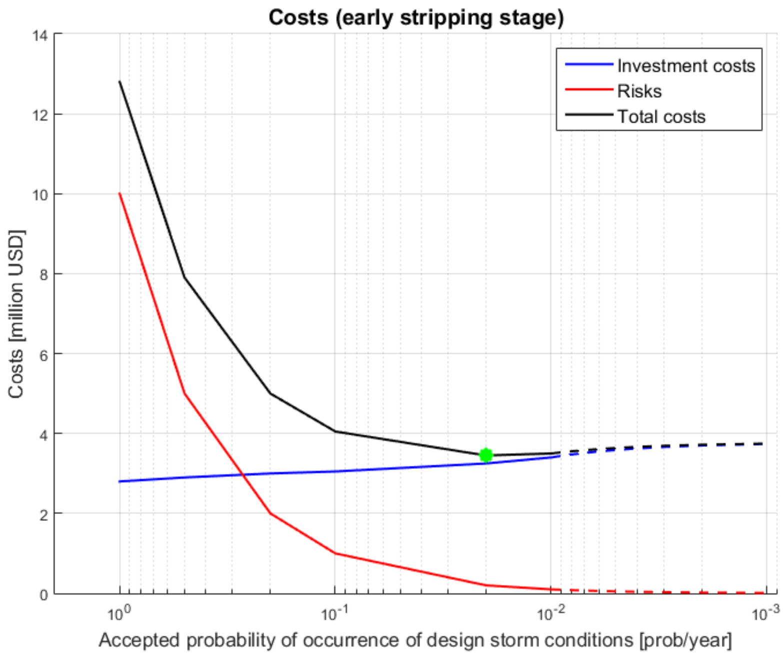

Figure 12.5: Graph showing the costs as a function of the accepted probability of storm occurrences. This is for the early stripping stage, where failure costs are assumed to be in the order of 10 million USD.

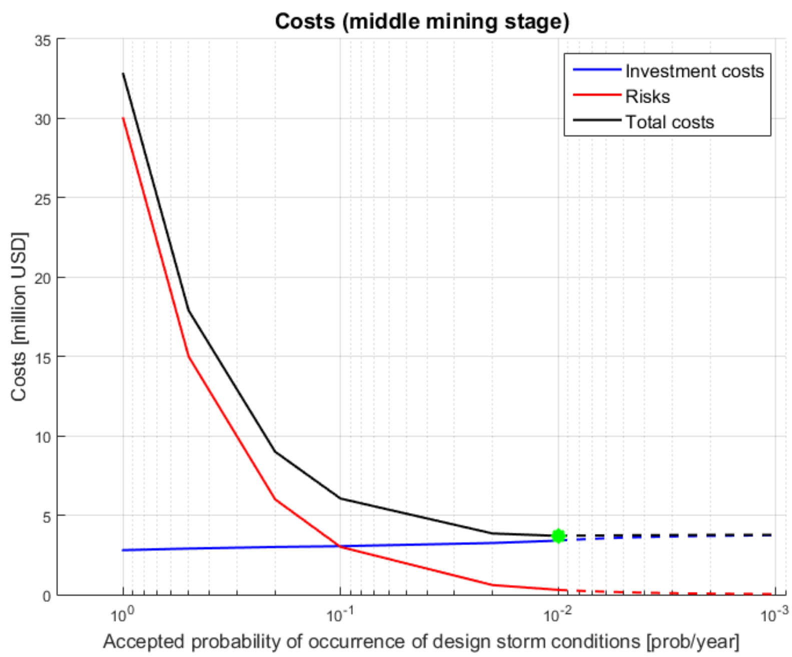

Figure 12.6: Graph showing the costs as a function of the accepted probability of storm occurrences. This is for the middle mining stage, where failure costs are assumed to be in the order of 30 million USD.

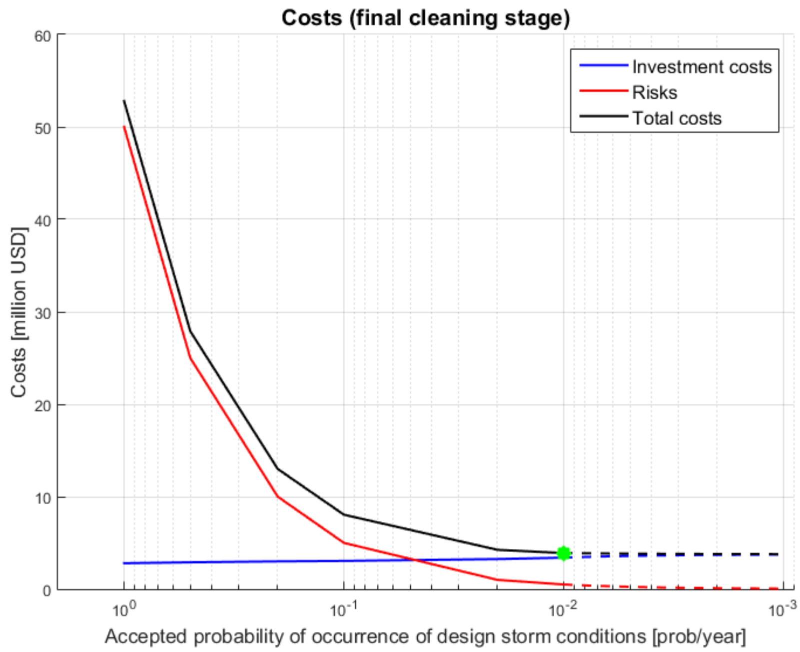

Figure 12.7: Graph showing the costs as a function of the accepted probability of storm occurrences. This is for the final cleaning stage, where failure costs are assumed to be in the order of 50 million USD.

12.3.1 Interpretation of figures

The economical optimum is found where the sum of the costs is minimal. In the early stage (Figure 12.5) this minimum is found at 1/50 per year, indicated by the green dot. In the middle stage (Figure 12.6) this minimum goes to 1/100 per year. In the final cleaning stage (Figure 12.7) the minimum is found at 1/100 per year.

The gradient of the investment costs is small. It can be seen that the increase in investment costs, needed to reduce the probability of failure, is low compared to the reduction of the risks. From the comparison of the different figures (of different mining stages), it can be derived that the investment costs become relatively higher, when the costs of consequences of a flooding become lower.

Although no data of cost (neither the unit costs of sand, nor the costs of seawall failure) are available, a recommendation is made to choose the 1/100 per year storm as design conditions for the seawall and the foreshore. The investment costs do not differ much from the investment costs for the 1/10 or 1/50 per year storm, but the reduction of the risk is significant. Moreover, when mining activity progresses, the economical optimum is found at an accepted probability of occurrence of 1/100 per year as the design storm conditions (represented by the green dots in Figure 12.6 and 12.7).

Chapter 13 – Discussion

This chapter discusses how major assumptions used in the research of this thesis are justified. It also discusses the reliability of results and how the results of the applied numerical models are verified. In all foregoing chapters the obtained results were discussed after their presentation. This chapter summarizes the most important parts of these discussions. The correctness of the methodology is also touched upon here.

13.1 Discussion of methodology and interpretation of results

To answer the research questions of this thesis (stated in Chapter 1) a literature review, a system analysis, the application of software models and data analysis were performed. All were presented in this report. The system analysis was mainly done by means of a fact-finding mission in MA1.

Two software models were used to quantify morphological changes due to wave action. The first model is the SWAN model (version 41.01A), used to translate offshore wave data to nearshore wave spectra. XBeach (version 1.22.4672) is the second model. A third model, CoDeS (version 1.0), was used to estimate longshore sediment transport rates.

13.1.1 System analysis

The system analysis was executed to gain insight in the mining strategy, but also to obtain the required data for the modelling process and the application of model results. The most important gaps in the system analysis are the properties of sand, the incomplete bathymetry and the position of the seawall on the beach. The discussion of the XBeach model below explains these data gaps were dealt with. The aforementioned fact-finding mission (reported in Anker (2014)) was also a tool to verify the model results of the XBeach model.

13.1.2 SWAN

Wave timeseries were obtained from ECMWF, which could not be calibrated for this research. The assumption that the wave timeseries are useful is supported by calibrations of the ECMWF data in different projects at different locations. It is out of scope to investigate the reliability of these data. SWAN has proven itself to be useful and reliable in various other projects.

Nesting a fine grid into a coarser grid resulted in an increase in the accuracy of wave-bottom interaction near the shore, while at the same time the computational effort was still manageable. The output location of SWAN was chosen at relatively deep water (30 m water depth). The advantage of this is that inaccuracies in the bathymetry, present close to the shore, are of minor influence. Also less nonlinear processes are involved, because the influence of bottom friction on waves is still limited. The SWAN model could in the case of the Southern Coastal Mine be applied, using mainly default settings and a recti-linear grid. For this reason the results from SWAN are considered to be accurate enough to be used in further modelling processes.

13.1.3 XBeach

The second model applied is the XBeach model. Inaccuracies mainly enter the model due to a lack of data of the seawall position, the bathymetry of the surf zone and the grainsize distributions of the sand. Appendix F describes how different variables influence the development of the foreshore. Appendix H quantifies the influence of variations in model parameters on seawall erosion volumes. It is notable that variations in the wave conditions, counting as hydrodynamic boundary conditions, have the largest impact on seawall erosion.

Verification of the XBeach model has been done in different ways. First of all the development of the foreshore in the long term was simulated. Some, but no severe, erosion to the seawalls was visible in the results. This is consistent with the corrective maintenance strategy for seawalls applied by NAMDEB.

Secondly, a case study was modelled. The resulting seawall breach after the simulated storm showed that the XBeach model is applicable for the Southern Coastal Mine. However, in the first model set-up no seawall breaching was present. But increasing the significant wave height only very slightly (5%) lead to seawall failure. The 2DH model makes in first instance an underestimation of the situation. Another conclusion that can be drawn from this is that knowledge of the impact of different parameters, i.e. knowledge of the sensitivity of the model, is very important. Most parameters were chosen conservatively, except for the wave-breaking parameter γ, to which the model is quite sensitive. Increasing the value of γ, which can be justified for rather steep beaches, leads also to more waves reaching the seawall, and thus to seawall failure.

The third verification of the model was done by observations and studying pictures from the fact-finding mission carried out in the Southern Coastal Mine in September 2014 by the author, Joël Anker. This gave insight in the construction and maintenance. However, it is unclear during what kind of (weather- and tidal) conditions these pictures were taken, making it more difficult to describe the beach and seawall position.

As described in Chapter 9 the XBeach modelling software originally was developed to model extreme beach behaviour on the south eastern coast of the USA where hurricanes occur. The model has been further developed, calibrated and applied to the Dutch coast. The Namibian coastal environment is very different from both situations. No hurricanes are present here. And compared to the Dutch coast there is a very small tidal range, but a highly energetic wave climate with large swell waves. No reference projects are known yet where XBeach was used in a climate similar to the Namibian climate. Based on the previously mentioned verifications and on the purpose of the XBeach model (see Chapter 7 Methodology) XBeach is still applicable to the Southern Coastal Mine Namibia.

13.1.4 Coupling of SWAN and XBeach models

The coupling of different models can introduce new inaccuracies to model results. In the XBeach model a built-in entry for SWAN output (in the form of wave spectra) is present. This has been calibrated in the modelling of, amongst others, the Dutch Coast. In this thesis it is assumed that the coupling is correct and that no significant mistakes enter the process, because the results are reliable. The output location of the SWAN model, as for the input location of the XBeach model, was chosen at deep water (30 m water depth), to ensure as little nonlinear processes as possible are involved.

13.1.5 CoDeS

The third model applied in the research of this thesis is CoDeS (Coastal Development Tools). The correctness of the model outcome is discussed together with the interpretation of result in evaluating the land accretion strategy in the section hereafter.

13.2 Application of results

Results of the system analysis, the literature review and the simulations with numerical models have led to design recommendations for the mining operation of NAMDEB, by the application of the obtained results. The first design recommendation is a revised design standard for the seawalls used as flood defense for the mining block. The second recommendation is for the final limit of land accretion. The certainty of both design recommendations is assessed.

13.2.1 Seawall design standard

The revised seawall standard is presented as the conclusion of Chapter 10. The reliability of this design is considered to be proportional to the reliability of the XBeach model set-up, which was discussed in section 13.1 above. Rationality has been drawn from observations, literature research and model simulations. The proposed adjustments to design standards were assessed with the same model set-up that was used previously. The design standards are deterministic. A probabilistic design of the seawall will increase the level of confidence and may lead to a different answer. The calculations accompanying such an approach are out of scope for this thesis.

Only failure of the seawalls due to erosion of the outerslope and overtopping were assessed. Groundwater flow was not examined. Failure due to instability of the innerslope and seepage water are already included in the currently used code of practice of NAMDEB for seawall construction (see section 4.5). However, the hydraulic head between mining pit and sea level will increase when mining activity expands seawards. This will also lead to an increase in amounts of seepage water through the seawall.

The distance between crosswalls, and thus the length of seawall sections, has not been discussed. A smaller distance would lead to a larger number of crosswalls and to smaller mining cells. The advantage is that a smaller seawall section is easier to maintain, reducing the risk of failure. Another advantage is that the rate of pumping seepage water away can be lowered, since the active mining cell is smaller. A disadvantage of having more crosswalls is that a larger area is required, which consequently cannot be used for mining. Having less crosswalls leads to longer seawall sections and more water that need to be pumped away for a dry mining operation in the larger mining cells.

Chapter 14 (Conclusions and recommendations) elaborates on recommended further research to minimize the uncertainties of the model outcome.

13.2.2 Land accretion limit

The uncertainties in the design recommendations for the land accretion strategy are significantly higher than in the seawall design standards. Chapter 11 concluded with a prognosis of the limit for the current land accretion strategy. The required volumes for the shifting of the seawall, the losses of sand due to longshore sediment transport and the available sand volumes are all estimations.

The required volumes were estimated based on knowledge from long-term simulations with XBeach. For the amount of sand available a conservative estimate was made. Sand pumping rates of the Sand-2-Sea program, together with volumes of moved overburden sand, were listed by NAMDEB. A 20% lower volume of sand available per year was chosen. This is based on a study into the difficulties with the Sand-2-Sea program (Anker, 2014), which is elaborated on in Appendices B and C.

The losses of sand were estimated with the model software CoDeS, making use of the relatively conservative CERC formulation for longshore sediment transport. Changing the coastline orientation by two to four degrees leads to changes in sediment volumes of 25 to 40%, which is considered to be large. Also, this software does not include the ongoing land reclamation. It is strongly recommended to conduct a proper investigation into the volumes of nett longshore sediment transport to calculate the losses of sand in the Sand-2-Sea program.

Altogether, the approach of evaluating the land accretion strategy is considered to be conservative. The result is a range for the depth limit of 8 to 13 m water depth, as mentioned in section 11.3.

The overburden thickness as a limit to the mining method has not been assessed. Because the bedrock dips in a seaward direction, the overburden that needs to be removed for the extraction of diamonds becomes thicker seawards. The costs of mining will consequently increase. When these costs outweigh the profit made on diamonds, the limit for mining is also reached. This, however, is a cost-benefit analysis that is out of scope for this thesis. NAMDEB will have to carry out this analysis, which is strongly dependent on the commodity price of diamonds. When the overburden becomes thicker, also the hydraulic head between mean sea level and mining pit becomes larger. This will enlarge the risk of instability of the innerslope and the risks associated with groundwater flow, as was discussed in Chapter 4. These risks were not assessed in this thesis, because they are included in the currently applied code of practice for the construction of seawalls.

13.2.3 Acceptable risk level

For the design standards and the evaluation of the land accretion strategy, storm conditions with a probability of occurrence of 1/100 per year were used. Designing with a lower standard will reduce the investment costs, but higher the risk of flooding of a mining block. Chapter 12 explained how the acceptable risk level can be chosen. A recommendation (the use of the 1/100 per year storm conditions) is given, but data of investment costs and costs of consequences of a flooding are needed to support this recommendation. These data are assumed to be known by NAMDEB. NAMDEB can use these data do the cost analysis proposed in Chapter 12.

Chapter 14 – Conclusions and recommendations

The conclusions drawn from the research performed for this thesis are summarized in this chapter. In addition, recommendations for further research and for decreasing the level of uncertainty of the results are listed. The main research questions for this thesis, as stated in Chapter 1, are repeated first. Research was done by means of a literature review, a system analysis, the application of software models and data analysis. The following paragraphs explain how this has enabled answering the research questions.

14.1 Conclusions

> ***What are the limits of the land reclamation strategy that is applied to expand diamond extraction, with the current mining method, in a seaward direction?***
> ***What is the optimal design for a seawall to protect the nearshore mining operation?***

The thesis started with a clarification of the current situation of the Southern Coastal Mine Namibia. From the analysis of the natural conditions it can be concluded that the wave climate is highly energetic, with long and high swell waves refracting towards the coast. The tide has only a minor influence on the dynamics of the coast.

From the investigation into the mining operation it can be derived that the reasoning behind the applied mining strategy is that, according to NAMDEB, "Dry mining" is a must and it has proven itself in the past. Land accretion, by means of the Sand-2-Sea program is applied to extend the land-based mining operation seaward. Bedrock gullies are the most important trapsites for diamonds, and for that reason a very selective mining method is applied. The roughness of the wave climate is said to make a water-based mining method impossible. The seawalls, made out of overburden sand, act as flood defense for the mine. Their standard is mainly focused on the innerslope of the seawall and corrective maintenance is regularly needed. In May 2015 a large stretch of seawall washed away after a storm, causing major problems to the mining operation. From the system analysis it can be concluded that the flood defense of the mine must be adjusted for the current mining method.

A coastal morphological model has been set up to simulate the upper shore of the Southern Coastal Mine. Its applicability has been verified by means of observations, a case study and a sensitivity analysis. From long term simulations it can be concluded that the upper shoreface responds quickly to changes in wave conditions, and that no equilibrium profile seems to develop. This results in a lack of sediment in the foreshore, making the construction of a seaward shifted seawall even more complicated.

Short term model results, of simulations performed on a seawall section on the southern edge of ongoing mining activity showed that the current seawall cannot cope with storm conditions that can occur with a probability of 1/100 per year. The foreshore in this area is relatively favourable for the reduction of wave energy, compared to seawall sections that are closer to the peak of the area targeted by the Sand-2-Sea program. These sections are more vulnerable to wave attack, and some of the seawalls will fail at an earlier stage. The sensitivity analysis of short-term XBeach simulations illustrated how sensitive the results are to changes in the wave conditions. Small enlargements in the wave height or wave period of a wave spectrum can lead to a dramatic increase of erosion to the seawalls. Variations in tide, grainsizes and wave directions have limited impact on seawall erosion.

Also the case study, simulating the seawall breach of May 2015, clearly showed that the width and flatness of the foreshore are very important to wave energy reduction. In the case of the seawall that breached, the foreshore was relatively narrow. This effect was enhanced by longshore transport, since the location of the seawall is the peak of the nourishment in the Sand-2-Sea (land accretion) program. During the storm the foreshore is fed by sand that eroded from the seawall. So the larger the volume of the seawall, the more effective the foreshore can become in reducing wave energy.

An important aspect to consider is that after each shift the seawall becomes more vulnerable to wave attack. The probability of seawall failure becomes higher, and thus the risks of flooding as well.

14.1.1 Seawall design standard

It was hypothesized that the design standards of the seawall can be adjusted. The groynes would have such a favorable shadowing effect on the seawalls that wave attack would be reduced significantly. Besides, it was presumed that the crest height of the seawalls could be lowered.

Simulations of the 2DH model pointed out that the effect of crosswalls on wave attack is limited when one considers the blockage of waves. Due to refraction, waves have an almost normal incidence towards the coastline. However, sand taken away from the crosswalls helps in wave energy reduction as it fills up part of the sand shortage that the foreshore has to reduce wave energy effectively. Nevertheless, the coastline between two crosswalls will always have irregularities and therefore weak spots.

By studying the seawall crest in the 1D model and 2DH model simulations of the case study, it could be seen that an avalanching profile of the seawall developed when erosion started to take place. No overtopping took place. Also in the short-term simulations of design storm conditions (section 9.2.5) it was seen that overtopping did not occur for any storm condition, except for the storm with a probability of occurrence of 1/100 per year. From this it can be concluded that the crest height of the seawall is probably larger than needed. However, when a 1/100 per year storm is said to be the design condition, then the crest height cannot simply be lowered.

Chapter 10 explained how it is recommended to adjust the design standards for seawalls, as was hypothesized. From the analysis done a seawall of 160 m^3/m was proposed, together with standards for the beach- and foreshore width. The three alternatives are repeated in table 14.1

Table 14.1: Values of proposed design standards for a seawall in the Southern Coastal Mine.

	Proposed design standard	**Alternative standard (higher crest)**	**Alternative standard (narrower foreshore)**
Seawall volume $[m^3/m]$ (above MSL +2m)	160	160	250
Crest height $[m]$ (above MSL)	6	7.5	7
Crest width $[m]$ (between windrows)	32	20	43
Beach width $[m]$ (between MSL and MSL +2m)	75	75	60
Foreshore width $[m]$ (between MSL and MSL -9m)	270	270	220

Most important in these new standards is that the beach and foreshore have requirements as well. This is in contrast to the current seawall standards used by NAMDEB. With the use of a numerical model, such as the applied XBeach model, a switch can be made from a corrective maintenance strategy to a predictive maintenance strategy.

14.1.2 Land accretion limit

The other hypothesis was that the feasibility limit, for the mining operation with the use of land reclamation, will be reached before the maximum distance proposed by NAMDEB is obtained, because it becomes technically unfeasible to construct a seawall and economically unfeasible to transport all overburden and bulk material. According to the Strategic Business Plan of 2014 the mining operation can continue to be technically and economically feasible until 2031 reaching a maximum seaward distance of 545 m from the average high water line (MSL +2m) of 2014.

The first conclusion, with respect to the land accretion strategy, is that this is a short term strategy. Both the literature review and the model results point this out by showing that no equilibrium cross shore profile is formed and by showing that longshore sediment transport causes significant losses of sand in the system. At the same time the Business Plan of NAMDEB is based on land accretion until at least 2031. This is a long term plan and thus in contradiction with the strategy applied. The further the land accrues, the more dominant longshore sediment transport becomes with respect to cross-shore sediment transport. This leads to large sand losses to the area of beaches that are targeted by the Sand-2-Sea program.

The dipping of the bedrock has two disadvantages that are relevant to the progressing land accretion. The first one is that more sand is needed to for land reclamation, when progressing seawards. The second disadvantage is that more overburden sand needs to be removed when the mining operation expands seawards. As a consequence, the inner slope of the seawall and the hydraulic head in the mining pit become larger, causing more seepage water and larger risks of seawall failure.

Chapter 11 estimated the final limit for land accretion by comparing available volumes of sand with volumes needed for the construction of seawalls and maintenance of a relatively stable foreshore. The recommended distance to shift a seawall per time is 150 m. The prognosis is that at least the 10 m depth contour line, measured in 2014, can be reached. This corresponds to a distance of about 360 meters on average measured from the average high water line of 2014. From studying the margins of available and required sand volumes it can be concluded that the limit for land accretion is in the range of 8 to 13 meters water depth on average in the area targeted by the Sand-2-Sea program.

14.2 Recommendations

The discussions of the applied methodology and of the results found (Chapter 13) revealed that the level of uncertainty for the final results can be lowered. This paragraph makes recommendations how to lower the level of uncertainty by additional investigations that were out of scope for the research of this thesis.

Simulation of bed profile changes and seawall erosion

Investigations were done to see how sensitive model results are to changes in certain input parameters. It can be concluded that a proper investigation needs to be done into the breaker parameter γ, which has large influence in the 1D model.

In terms of physical parameters, it is recommended to do a more thorough investigation into the sand properties of MA1 to obtain a more accurate grainsize distribution dataset. It is also advisable to investigate the location of the seawall toe on the beach and how the beach profile can be interpolated between a breaker bar and the high water line, i.e. more complete bathymetry dataset.

In addition, a higher level of confidence in the model set-up can be achieved by simulating more known events, such as the storm of the modelled case study, and by simulating more seawall sections along the coast. With these investigations the model can be verified further.

Designs

A probabilistic approach for the design of a seawall standard can lead to significantly higher reliability. The theory of such an approach and the set-up of a probabilistic approach for dunes and seawalls are given in Appendix J and K, respectively. Also, it is advised to do carry out a cost-benefit analysis to determine the acceptable failure risk for seawalls in MA1. This may lead to choosing different design storm conditions and, consequently, a different seawall sand volume.

Groundwater flow was not examined in the research of this thesis. Although the risks of seawall failure due to seepage water and instability of the innerslope of the seawall are included in the currently applied code of practice of NAMDEB (section 4.5), an assessment of these risks is recommended for further research. This will become more relevant when land accretion proceeds and the hydraulic head between mining pit and sea level increases.

An investigation into the use of different construction material for the seawall was out of scope for this thesis. Section 10.2 proposed the use of tailings as an alternative to sand. Further investigation into the use of tailings is suggested.

The optimization of the number of crosswalls along the coast, and thus the length of seawall sections, is suggested for further research. The risk of flooding is partly dependent on the length of a seawall section.

For the evaluation of the land accretion method it is strongly recommended to investigate longshore sediment transport rates, which lead to sand losses in the area of interest. Section 11.3 described how the spreading of nourishments can be assessed. Such an investigation was out of scope for this thesis.

The final recommendation is to investigate the feasibility of an alternative mining strategy. There is already a high level of confidence that a diamond reserve can be established beyond the 13 m depth contour line (which was proposed as the limit for land accretion in the given range of Chapter 11). The current "Dry mining" strategy is, however, not applicable to that region.

Bibliography

Anker, J. C. (2014), Fact-finding mission in Mining Area No.1, Sperrgebiet, Namibia, Technical report, Unpublished report, 78 pp, Delft University of Technology.

Baldock, T. E., Huntley, D. A., Bird, P. A. D., O'Hare, T. and Bullock, G. N. (2000), 'Break-point generated surf beat induced by bichromatic wave groups', *Coastal Eng* **39**, 213–242.

Battjes, J. A. (1974), 'Surf Similarity', *Proceedings of 14th international conference of coastal engineering* (1), 467–479.

Battjes, J. A., Bakkenes, H. J., Janssen, T. T. and van Dongeren, A. R. (2004), 'Shoaling of subharmonic gravity waves', *Journal of Geophysical Research: Oceans* **109**, 1–15.

Battjes, J. and Janssen, J. P. F. M. (1978), 'Energy loss and set-up due to breaking of random waves', *Proceedings of the 16th international conference on coastal engineering* **1**(16), 569–587.

Booij, N., Ris, R. C. and Holthuijsen, L. H. (1999), 'A third-generation wave model for coastal regions 1 . Model description and validation', *Journal of Geophysical Research* **104**, 7649–7666.

Bosboom, J. and Stive, M. J. (2013), *Coastal Dynamics I , Lecture Notes CIE4305*, 53rd edn, Delft Academic Press / VSSD, Delft.

Brandenburg, P. (2010), Scale dependency of dune erosion models, 133 pages, Delft University of Technology, Netherlands.

Bruun (1954), 'Coast Erosion and the Development of Beach Profiles', *U.S. Army Corps of Engineers, Technical Memo* **44**, 79 pp.

Corbett, I. and Burrell, B. (2001), 'The earliest Pleistocene(?) Orange River fan-delta: An example of successful exploration delivery aided by applied Quaternary research in diamond placer sedimentology and palaeontology', *Quaternary International* **82**, 63–73.

CUR (1997), *Probabillities in civil engineering, Part 1: Probabilistic design in theory*, 1st edn, Stichting CUR, Gouda, Netherlands.

Deltares (2010), 'Unibest-cl+ 7 manual, user and theoretical manual'.

Deltares (2015), XBeach 1D - Probabilistic model: ADIS, settings, Model uncertainty and Graphical User Interface, Technical report, 65 pp, Deltares, Delft.

Den Heijer, C. (2013), The role of bathymetry, wave obliquity and coastal curvature in dune erosion prediction, PhD thesis, Delft University of Technology.

Fisher, J. and Overton, M. (1984), 'Numerical Model for Dune Erosion due to Wave Uprush', *Coastal Engineering Proceedings* **1**(19), 1488–1506.

Fisher, J. and Overton, M. (1986), 'Field measurements of dune erosion', *Coastal Engineering* pp. 1107–1115.

Fredsoe, J. and Deigaard, R. (1992), *Mechanics of coastal sediment transport*, 2nd edn, Singapore.

Fuhrboter, A. (1991), 'Eine theoretische Betrachtung iiber Sandvorspulungen mit Wiederholungsintervallen', *Die Kuste* **52**, 241–254.

Galappatti, G. and Vreugdenhil, C. (1985), 'A depth-integrated model for suspended sediment transport', *Journal of Hydraulic Research* **23**(4), 359–377.

Garrison, T. S. (2005), *Essentials of Oceanography*, 4th edn, Cengage Learning, Belmont, USA.

Grooteman, F. (2011), 'An adaptive directional importance sampling method for structural reliability', *Probabilistic Engineering Mechanics* **26**(2), 134–141.

Hasofer, A. and Lind, N. (1974), 'Exact and invariant second-moment code format', *Journal of the Engineering Mechanics division* **100**(1), 111–121.

Herbers, T., Elgar, S., Guza, R. and O'Reilly, W. (1995), 'Infragravity-Frequency (0.005-0.05 Hz) Motions on the Shelf. Part II: Free Waves', *American Meteorological Society* **25**(6), 1063–1079.

Holthuijsen, L. H. (2007), *Waves in Oceanic and Coastal Waters*, 2nd edn, Cambridge University Press, Cambridge.

Holthuijsen, L. H., Booij, N. and Herbers (1989), 'A prediction model for stationary, short-crested waves in shallow water with ambient currents', *Coastal Engineering* **13**(1), 23–54.

Jacob, J., Ward, J. D., Bluck, B. J., Scholz, R. A. and Frimmel, H. E. (2006), 'Some observations on diamondiferous bedrock gully trapsites on Late Cainozoic , marine-cut platforms of the Sperrgebiet , Namibia', *Ore Geology Reviews* **28**(4), 493–506.

Kamphuis, J. W. (1991), 'Alongshore Sediment Transport Rate', *Journal of Waterway, Port, Coastal, and Ocean Engineering* **117**(6), 624–640.

Kateman, I. (2007), Wave-impact driven dune face erosion processes, Technical report, 83 pp, Delft University of Technology.

Kinsman, B. (1965), *Wind Waves. Their generation and propagation on the ocean surface*, 1st edn, Courier Corporation, North Chelmsford, Massachusetts.

Longuet-Higgins, M. (1953), 'Mass transport in water waves', *Philosophical Transactions of the Royal Society of London A: Mathematical, Physical and Engineering Sciences* (245), 535–581.

Longuet-Higgins, M. and Stewart, R. (1964), 'Radiation stresses in water waves; a physical discussion, with applications', *Deep Sea Research and Oceanographic Abstracts* **11**, 529–562.

Madsen, P. A., Sorensen, O. R. and Schaffer, H. A. (1997), 'Surf zone dynamics simulated by a Boussinesq type model. part II: Surf beat and swash oscillation for wave groups and irregular waves', *Coastal Engineering* **32**(4), 289–319.

Masselink, G. and Hughes, M. (2003), *Introduction to Coastal Processes and Geomorphology*, 1st edn, Hodder Arnold, London.

McLachlan, A. (1996), 'Physical factors in benthic ecology: Effects of changing sand particle size on beach fauna', *Marine Ecology Progress Series* **131**(1), 205–217.

Moore, J. M. and Moore, A. E. (2004), 'The roles of primary kimberlitic and secondary Dwyka glacial sources in the development of alluvial and marine diamond deposits in Southern Africa', *Journal of African Earth Sciences* **38**(2), 115–134.

NAMDEB (2013), Code of Practice - The Design, Monitoring, Maintenanace and Repair of Seawalls and Cross walls, Technical report, NAMDEB Diamond Corporation PTY Ltd, Unpublished report, Luderitz, Namibia.

Nishi, R. and Kraus, N. C. (1996), 'Mechanism and calculation of sand dune erosion by storms', *Proceedings of the 25th Coastal Engineering Conference* pp. 3034–3047.

Philips, O. (1977), *The Dynamics of the Upper Ocean*, 2nd edn, Cambridge University Press, Cambridge.

Razak, M., Dastgheib, A. and Roelvink, D. (2013), 'Sand bypassing and shoreline evolution near coastal structure , comparing analytical solution and XBeach numerical modelling', *Journal of Coastal Research* (65), 2083–2088.

Ris, R. C., Holthuijsen, L. H. and Booij, N. (1999), 'A third-generation wave model for coastal regions 2. Verification', *Journal of Geophysical Research* **104**, 7667–7681.

Roelvink, D., Reniers, A., van Dongeren, A., van Thiel de Vries, J., Lescinski, J. and McCall, R. (2009), 'Modelling storm impacts on beaches, dunes and barrier islands', *Coastal Engineering* **56**(11-12), 1133–1152.

Roelvink, D., Reniers, A., van Dongeren, A., van Thiel de Vries, J., Lescinski, J. and McCall, R. (2010), XBeach model description and manual, Technical report, Deltares, Delft.

Roelvink, J. (1993), 'Dissipation in random wave groups incident on a beach', *Coastal Engineering* **19**, 127–150.

Ruessink, B. G., Miles, J. R., Guza, R. T., Feddersen, F. and Elgar, S. (2001), 'Modeling the alongshore current on barred beaches', *Journal of Geophysical Research* **106**, 22451 – 22463.

Schneider, G.I.C. and Miller, R. (1992), 'The Mineral Resources of Namibia - Diamonds', *Mineral Resource Series* **50**, 5.1.1 – 5.1.32.

Shields, A. (1936), 'Anwendung der Aehnlichkeitsmechanik und der Turbulenzforschung auf die Geschiebebewegung', *Preussischen Versuchsanstalt für Wasserbau* pp. 5–26.

Spaggiari, R. I., Bluck, B. J. and Ward, J. D. (2006), 'Characteristics of diamondiferous Plio-Pleistocene littoral deposits within the palaeo-Orange River mouth, Namibia', *Ore Geology*

Reviews **28**, 475–492.

Steetzel, H., Coeveld, E. M., Van de Graaff, J. and Van Gent, M. (2007), Dune erosion; Product 3: Probabilistic dune erosion prediction method, Technical report, 195 pp, Deltares (WL), Delft.

Steijn, P. W. V. (2015), Global Assessment on the Lifetime of Mega Nourishments, Technical report, 120 pp, Delft University of Technology.

Van de Graaff, J. (1984*a*), Leidraad voor de beoordeling van de veiligheid van duinen als waterkering, Technical report, 37 pp, Gravenhage, Netherlands.

Van de Graaff, J. (1984*b*), Probabilistische methoden bij het duinontwerp, Delft University of Technology, Delft, pp. 1–115.

Van de Graaff, J. (1986), 'Probabilistic design of dunes; an example from the Netherlands', *Coastal Engineering* **9**(5), 479–500.

van der Werf, J. J., Schretlen, J. J., Ribberink, J. S. and O'Donoghue, T. (2009), 'Database of full-scale laboratory experiments on wave-driven sand transport processes', *Coastal Engineering* **56**(7), 726–732.
URL: *http://linkinghub.elsevier.com/retrieve/pii/S0378383909000131*

Van Dongeren, A., Battjes, J., Janssen, T., van Noorloos, J., Steenhauer, K., Steenbergen, G. and Reniers, A. (2007), 'Shoaling and shoreline dissipation of low-frequency waves', *Journal of Geophysical Research: Oceans* **112**(August 2006), 1–15.

Van Dongeren, A. and Svendsen, A. (1997), Quasi 3-D Modeling of Nearshore Hydrodynamics, Technical report, 262 pp, University of Delaware, Delaware.

Van Thiel de Vries, J. (2009), Dune erosion during storm surges, PhD thesis, 220 pp, Delft University of Technology.

Vellinga, P. (1982), 'Beach and dune erosion during storm surges', *Coastal Engineering* **6**(4), 361–387.

Vellinga, P. (1983), 'Predictive computational model for beach and dune erosion during storm surges', *Proceedings Coastal Structures '83* pp. 806–819.

Vellinga, P. and Van Banning, G. K. F. M. (1984), Duinafslag ten gevolge van de stormvloed op 1 en 2 februari 1983: toetsing van het rekenmodel DUROS voor de verwachting van duinafslag tijdens stormvloed, Technical report, 148 pp, Deltares (WL), Delft.

Verhagen, H. J., D'Angremond, K. and Van Roode, F. (2009), *Breakwaters and closure dams*, 2nd edn, VSSD, Delft.

Visser, P. (1998), 'Breach erosion in sand-dikes', *Coastal Engineering Proceedings* **1**(26), 3516–3528.

Vrijling, J. and Bruinsma, J. (1980), 'Hydraulic Boundary Conditions', *Hydraulic Aspects of Coastal Structures* **1**, 109–133.

Weise, B. and White, W. (1980), Padre Island National Seashore: A guide to geology, natural environments, and history of a Texas Barrier Island., *in* 'Guidebook', 2nd edn, University of Texas, Austin, Texas, chapter 17, p. 94.

– Nomenclature

WAVES AND WATER

α	Empirical reduction factor	[-]
β	Normalized bed slope parameter	[degrees]
ζ	Iribarren number	[-]
ϕ	Angle of wave incidence	[degrees]
ρ_s	Density of sediment	$[kg/m^3]$
ρ_w	Density of water	$[kg/m^3]$
σ_w	Relative frequency in a moving frame of reference	[1/s]
Ω	Dimensionless fall velocity of sediment	[-]
ω	Radial frequency of the wave	[rad/s]
c	Wave propagation speed	[m/s]
c_g	Wave group celerity	[m/s]
D_{20}	Grainsize diameter. 20% of particles of the total sample has a smaller diameter.	[m]
D_{50}	Median grain size	[m]
D_{90}	Grainsize diameter. 90% of particles of the total sample has a smaller diameter.	[m]
E	Wave energy	[J]
E_r	Roller energy	[J]
g	Gravitational acceleration	$[m/s^2]$
h	Water depth	[m]
H_0	Significant wave height in deep water	[m]
H_s	Significant wave height	[m]
H_{ss}	Significant storm wave height	[m]
i_x	Bedslope	[-]
k	Wave number	[1/m]
k_{lw}	Long free wave number	[1/m]
L	Wave length	[m]
L_0	Wave length in deep water	[m]
n	Relation between the velocity of waves in the group and the group velocity	[-]
p_{wave}	Wave pressure	$[N/m^2]$
q	Sediment flux between wave crest and wave trough	$[m^3/s/m^2]$
S_{xx}	Transport of wave-induced x-momentum in the x-direction (Radiation stress)	[N/m]
T_p	Wave peak period	[s]
T_{ps}	Storm wave peak period	[s]
U	Energy flux per unit wave crest width	$[J/m^2]$
U_{10}	Average windspeed at height of 10 m	[m/s]
u_x	Velocity in the x-direction	[m/s]
w_s	fall velocity	[m/s]

SEDIMENT PROPERTIES AND SEDIMENT TRANSPORT

$\Delta\phi$	Change of coastline orientation	[degrees]
ΔW	Weight of the volume of eroded sediment	[kg]
ΔV	Eroded sand volume	$[m^3]$
θ_c	Shields parameter	[-]
ν	Kinematic viscosity coefficient	$[m^2/s]$
τ_c	Critical bottom shear stress induced by water movement	$[N/m^2]$
ϕ	Coastline orientation	[degrees]
C_e	Empirical erosion coefficient	[-]
F_D	Drag force on grains	$[N/m^2]$
F_G	Gravity force on grains	$[N/m^2]$
F_L	Lift force on grains	$[N/m^2]$
n	Porosity of sediment	[-]
Re_*	Particle Reynolds number	[-]
S	Sediment transport	$[m^3/s/m^2]$
u_*	Shear stress velocity	[m/s]
V	Sources and sinks for sediment	$[m^3]$
z_b	Bed level	[m]

WAVE STATISTICS

β	Calculation factor in Weibull or Gumbel distribution	[-]
γ	Coefficient in Weibull or Gumbel distribution (theoretically representing the threshold)	[-]
$H_{s,Threshold}$	Threshold of significant wave height	[m]
N_s	Number of storms	[-]
$P(H \leq H_{ss})$	Probability of wave height H being smaller than or equal to H_{ss}	[-]
Q_s	Probability of occurrence of certain storm condition. (Expected value per year)	[-]

SAND VOLUME CALCULATION

$d_{seawall}$	Depth of the toe of the seawall on the location of a depth contour line measured in 2014	[m]
$V_{available}$	Sand volume available for land accretion and seawall construction	$[m^3/year]$
$V_{construction}$	Sand volume needed to construct a foreshore and seawall	$[m^3/year]$
$V_{maintenance}$	Sand volume needed to maintain a foreshore and seawall	$[m^3/year]$
$V_{required}$	Total required volume for constructing and maintaining a foreshore and seawall	$[m^3/m]$
V_{shift}	Sand volume needed to construct a foreshore and seawall	$[m^3/year]$
x	Distance over which a seawall is shifted seawards	[m]

NUMERICAL MODELING

α	First order calibration factor for wave energy dissipation	[-]
η	Water level	[m]
ν	Turbulent viscosity	$[m^2/s]$
σ	Radian wave frequency	[rad/s]
A	Wave action	$[Nm/m^2$
A_{sb}	Coefficient accounting for bed-load sediment transport	[-]
A_{ss}	Coefficient accounting for suspended sediment transport	[-]
C_{eq}	Equilibrium sediment concentration	$[m^3/m^3]$
c_x	Cross-shore celerity	[m/s]
c_y	Alongshore celerity	[m/s]
D_f	Wave energy dissipation due to bottom friction	$[W/m^2]$
D_h	Sediment diffusion coefficient	$[W/m^2]$
D_w	Dissipation of wave energy due to wave breaking	$[W/m^2]$
$f_{m-1,0}$	Spectral frequency	[1/s]
f_{mor}	Morphological acceleration factor	[-]
F_{up}	Upscaling factor	[-]
f_w	Friction factor depending on the type of bottom	$[N/m^2]$
F_x	Wave force in x-direction	[N/m]
F_y	Wave force in y-direction	[N/m]
$m_{cr,dry}$	Critical dry bed-slope	[-]
$m_{cr,wet}$	Critical wet bed-slope	[-]
Q_b	Probability function describing the fraction of breaking waves	[-]
q_x	Transported sediment quantities in the x-direction	$[m^3/s/m^2]$
q_y	Transported sediment quantities in the y-direction	$[m^3/s/m^2]$
S_w	Wave energy	[J/m]
T_{rep}	Representative wave period	[s]
T_s	Adaptation time scale for the entrainment of sediment	[s]
u^E	Eulerian velocity	[m/s]
u^S	Stokes drift	[m/s]
z_b	Bed level elevation	[m]
alpha	Wave dissipation in Roelvink formulation	$[W/m^2]$
beta	Dissipation parameter long wave breaking turbulence	$[W/m^2]$
cf	Friction coefficient flow	[-]
facAs	Calibration factor time averaged flwos due to wave skewness	[-]
facSk	Calibration factor time averaged flwos due to wave assymetry	[-]
Facua	Coefficient accounting for extra onshore transport	[-]
Freq	Frequency of occurrence of the group of wave conditions	[1/s]
Freq(original)	Original frequency of occurrence of specific wave condition	[1/s]
fw	Bed friction factor	[-]
gamma	Breaker parameter in Roelvink formulation	[-]
gammax	Maximum ratio wave height to water depth	[-]
wetslp	Critical avalanching slope under water	[-]

List of Figures

1.1 Outline of the scope of this Master Thesis 4

2.1 Topographic overview of Sperrgebiet, Namibia. The green area is Mining Area No. 1. The yellow dots are old settlements from where diamond mining was started. 8

2.2 Simplified map showing the different areas of mining activity. Mining activity in MA1 is ongoing in the U-area (Orange) and the G-area (Red). 9

2.3 Picture of southern part of the coastline of Mining Area No. 1. 10

2.4 Aerial image of part of Mining Area No. 1. #3-Plant is visible in the picture. One can see that the coastline has a smooth curvature. This picture shows the northern part of the specific area that is targeted by the Sand-2-Sea program. . 10

2.5 Depth contours in front of the coast of MA1, going from orange (shallow) to purple (deep). It can be seen that the terraces are much wider close the Orange River Mouth. 11

2.6 Definition of different depth regions in NAMDEB waters 11

2.7 Wind rose of wind records at 28.5 degrees South, 15 degrees East. 12

2.8 Wave rose of wave records at 28.5 degrees South, 13.5 degrees East. 13

3.1 Simplified map showing the different areas of mining activity 15

3.2 PDP (Prob Drill Platform), used by NAMDEB for Exploration in the surf zone 17

3.3 Schematic drawing of steps in excavation process 17

3.4 Conventional excavation of overburden with Hydraulic Excavators and ADT's . 18

3.5 Conventional hauling and loading of bulk material. 18

3.6 Transvacs used in the cleaning the bedrock 18

3.7 Cleaning the bedrock. Worker operating a Transvac 18

3.8 Design seawall for mining pit with a depth up to 10m below mean sea level. (NAMDEB) 19

4.1 Crosswall separating to mining blocks. This wall is also used as a service wall. One can see maintenance of the crosswall being carried out with an ADT and a dozer 22

4.2 Design seawall for mining pit with a depth up to 10m below mean sea level (NAMDEB, 2013). 23

4.3 Seawall with clear boulder lining on the innerslope 23

4.4 Seepage water channel at the innertoe of the seawall, with waterpumps at the left 23

4.5 ADT driving on the seawall to dump material for building a crosswall extension 23

4.6 Construction of crosswall extension. Dozer pushing dumped material in the sea. 23

4.7 Beachline with crosswalls with a distance of 350 m. 24

5.1 Sediment disposal paths for gravel, sand and finer sediment on the continental shelf, offshore Namibia (Spaggiari et al., 2006) 27

5.2 Schematic east-west cross section of raised beach deposits of MA1, showing the stratification of sediments deposits on top of the bedrock. (Schneider, G.I.C. and Miller, 1992) 28

5.3 Northward gradation in gully type from the Orange River mouth to Chameis Bay, MA1, showing the three different principal gully types. Photographs are oblique aerials and the gullies are ca. 2 m wide (Jacob et al., 2006). 29

6.1 Typical upper shoreface profile. After Weise and White (1980) 31

6.2 Types of wave breaking processes. After Bosboom and Stive (2013). 32

6.3 Different depth regions in front of the Namibian shore. These definitions are used by NAMDEB. 33

6.4 Distinction between depth regions when considering waves. After Garrison (2005) 34

6.5 Typical wave energy spectrum for oceanic waters. After Kinsman (1965) 35

6.6 Graph schematically showing different types of waves. In red: shorter waves in wavegroup (envelope shown in pink). In black: forced bound long wave (infragravity wave) 36

6.7 Example of wave refraction. As the wave front moves towards the shoreline, it will turn towards shallower water. The dashed lines represent depth contours of the bed. 40

6.8 Forces acting on a single particle in stationary situation. Drag force (parallel to the flow direction), lift force and gravity force. Figure by MIT OpenCourseWare (accessed July 2015) 41

6.9 Different sediment transport modes. A: bed load transport. B: sheet flow. C: suspended load transport. After Fredsoe and Deigaard (1992) 43

6.10 Example of an S-ϕ curve, presenting the relation between longshore sediment transport and the angle of wave incidence. 45

6.11 Longshore sediment transport gradients along a nourishment. Figure from Steijn (2015). 46

6.12 Schematic drawings of dune erosion mechanisms. Layer separation (1), notching (2) and sliding/flowing (3). After Nishi and Kraus (1996) 47

6.13 Left: different stages in dune erosion process, considering a sand slope around the angle of repose. Right: Volumes of primary and secondary erosion. From Kateman (2007) 47

6.14 Evolution of shoreface according to Bruun Rule. In de figure: S = sea level rise, L = active profile length, R = retreat, f = freeboard. 48

6.15 Visualization of balance between pre-storm and post-storm profile. After Vellinga (1982) . . . 49

8.1 Map showing the location and computational grid that are used for computations by SWAN. The left image shows the coarse grid, the right image a fine grid that is nested into the coarse grid. The yellow dot shows the coordinates for which wave data are available. . . . 55

8.2 Wave rose for offshore waves, used as input for SWAN model. Location: 13.5° W , -28.5° N . . . 56

8.3 Scatterplot of significant wave heights (vertical axis) and wave peak periods (horizontal axis) with their relative frequency of occurrence on a yearly basis. . 56

8.4 Scatterplot of significant wave heights (vertical axis) and main wave directions (horizontal axis) with their relative frequency of occurrence on a yearly basis. . 57

8.5 Best-fit curve to relate between wind speed and wave growth. . . . 58

8.6 Model set-up of SWAN (version 41.01A) model on a relatively coarse grid to simulate the wave regime in front of the Southern Coastal Mine Namibia. . . . 58

8.7 Model set-up of SWAN (version 41.01A) model on a fine grid close to the shore to simulate the wave regime in front of the Southern Coastal Mine Namibia. . 59

8.8 Repetition of Figure 8.1: Map showing the location and computational grid that are used for computations by SWAN. . . . 60

8.9 Graphical visualization of the significant wave height (Hs) for the Southern Namibian shore under the most abundant offshore wave conditions (see table 8.1). Left: calculation for a coarse grid. Right: calculation for a finer grid nested in the coarse grid on the left. . . . 61

8.10 Graphical visualization of the significant wave height (Hs) for the Southern Namibian shore under the offshore wave conditions occurring 1% of the time (see table 8.1). Left: calculation for a coarse grid. Right: calculation for a finer grid nested in the coarse grid on the left. . . . 61

8.11 Graphical visualization of the significant wave height (Hs) for the Southern Namibian shore under the most extreme offshore wave conditions (see table 8.1). Left: calculation for a coarse grid. Right: calculation for a finer grid nested in the coarse grid on the left. . . . 61

9.1 Overview of survey to obtain bathymetry nearshore the Southern Coastal Mine Namibia. The red lines represent the single-beam survey done in the shallow and intermediate water (midwater) regions. . . . 67

9.2 Zoomed in on the mining activity in the G-area. Survey Line 9000 is high-lighted in red. . . . 68

9.3 Picture of seawall on the beach in the G-area (close to Survey Line 9000). In the distance a groyne / crosswall extension in visible . . . 68

9.4 Picture of seawall on the beach in the G-area (close to Survey Line 9500). . . . 69

9.5 1D cross-shore bed profile of Survey Line 9000 of the Southern Coastal Mine Namibia. The curved line between the two red lines is the bathymetry data received from NAMDEB. The green dot represents the MSL +2m location on the beach. 70

9.6 1D cross-shore bed profile of Survey Line 9000, zoomed in on the upper shoreface. The purple circle high-lights the breaker bar present under the wave conditions in which the Survey was executed. 70

9.7 Long-term simulation (100 days) of 1D cross-shore bedprofile of Survey Line 9000 of the Southern Coastal Mine Namibia. Table 9.1 counts as input for the hydrodynamic boundary conditions. 73

9.8 Long-term simulation (100 days) of 1D cross-shore bedprofile of Survey Line 9000 of the Southern Coastal Mine Namibia. Table 9.1 counts as input for the hydrodynamic boundary conditions. 75

9.9 Wave heights, according to the Gumbel distribution, belonging to certain probabilities of occurrence. 77

9.10 Relationship between significant wave height H_s and wave peak period T_p for data above the threshold of Hs = 4.5m and Tp = 11.5s. 78

9.11 Plot of the seawall on Survey Line 9000. The coloured lines represent the resulting bed profile after specific storm conditions. 79

9.12 Spiderplot presenting the influence of all relevant parameters for eroded sand volumes in the 1D XBeach Model. 81

9.13 Map of Southern Coastal Mine where the seawall (and crosswall) failures are indicated. 82

9.14 Picture showing the breach (in the middle of the picture) of the seawall on June 1st 2015 83

9.15 Aerial image of area of interest for case study. The seawall of interest is highlighted by the red circle. Picture taken on May 25th 2015. 83

9.16 Picture of seawall next to mining activity in U-area of Southern Coastal Mine Namibia. Picture taken during Fact-Finding Mission in October 2014. 84

9.17 1D cross-shore bedprofile of Survey Line 22500 of the Southern Coastal Mine Namibia. 85

9.18 1D cross-shore bedprofile of Survey Line 22500 of the Southern Coastal Mine Namibia, zoomed in on the beach and seawall. 85

9.19 Bed profile according to model set-up. In the upper picture a 3D visualization of the seawall with its crosswalls. In the lower figure a cross-section of the seawall. 86

9.20 Graph showing the development of the bed profile during the simulated storm for the 1D model of XBeach. 87

9.21 State of the seawall after the storm. The upper figure is somewhat zoomed out compared to Figure 9.19. 87

9.22 Situation after almost 3 days of storm. A part of the seawall has failed. 88

10.1 Plot of eroded sand volumes per storm event with a certain yearly probability. Volumes are calculated for Survey Line 9000. 91

10.2 Limit state profile (ULS) of a Dutch dune. 92

10.3 Limit state profile of a NAMDEB seawall, represented by the red line. The blue line represents the SLS. 93

10.4 Seawall with adjusted standard after a storm with a probability of occurrence of 1/100 per year. 94

10.5 Seawall with adjusted standard after a storm with a probability of occurrence of 1/100 per year. The red line presents the bed profile after the simulation of the storm with the adjusted seawall volume (225 m^3). The blue line presents the resulting bed profile of the seawall with the old standards. 95

10.6 Plot of the seawall on Survey Line 9000. The colored lines represent the resulting bed profile after specific storm conditions. 97

10.7 Map showing the tailingsdump of #3-Plant in MA1 and the mining blocks of ongoing mining activity. The arrows show the hauling distance for material to the seawalls. 99

10.8 Proposed standard for the seawall and its foreshore. 99

10.9 Bed profile of proposed standard after a simulation with wave conditions of a storm with a probability of 1/100 per year. 100

10.10 Bed profiles of the three alternatives for the standards of the seawall and its foreshore. 101

11.1 Simplified map of MA1, showing the location of Survey Line 9000 and 22500. . 103

11.2 Aerial image of MA1. The orange straight line presents the average coastline orientation of MA1. The green lines present the average coastline orientation on a smaller scale. 104

11.3 Impression of the seaward shifting of a seawall close to Survey Line 9000 (NAMDEB). 104

11.4 Longshore sediment transport gradients along a nourishment. Figure from Steijn (2015). 105

11.5 Aerial view of MA1, zoomed in on the area where the seawall breach of May 2015 took place (circled in red). The yellow line highlights the curvature of the coast and how some seawall sections stood out. 105

11.6 Impression of the seaward shifting of a seawall close to Survey Line 22500 (NAMDEB). 106

11.7 Example of a cross-section of sandy coast. 107

11.8 Outline of an equilibrium cross-shore profile according to hydrodynamic conditions of a storm with a probability of occurrence of 1/1 per year. 107

11.9 Schematic comparison of the cross-shore profile with a seawall (red) and of the equilibrium profile (blue) according to the storm conditions with a return period of 1 year. 108

11.10 Schematic drawing of a seaward seawall shift (in green). 108

11.11 Schematic comparison of the cross-shore profile with a shifted seawall (green) and of the shifted equilibrium profile (blue) according to the storm conditions with a return period of 1 year. 109

11.12 Schematic drawing of a seaward seawall shift. The sand body of the entire foreshore is given for the original seawall (red line) and the shifted seawall (green line). The erosion profiles are given in purple and and cyan. 110

11.13 Schematic drawing of the sand volume needed for a seaward seawall shift. The outlines of the two different seawalls match the erosion profiles (cyan and purple lines) of Figure 11.12. The brown area is the volume of sand that needs be excavated for the mining operation. The green area is the volume of sand needed for a relatively stable seawall and foreshore. 111

11.14 Graph representing the relation between the required volume of sand for a seaward seawall shift and the depth. The different lines stand for different stepsizes x. $V_{available}$ is the volume of sand that is directly available through the mining process. 111

11.15 Map of Southern Coastal Mine Namibia, zoomed in on the area targeted by the Sand-2-Sea program. Two cross-sections are visible, where the longshore sediment transport volumes are computed with CoDeS. From coast to sea: the first two arrows represent the gross sediment transports. The last arrow represents the nett sediment transport. 114

11.16 Map of Southern Coastal Mine with the same cross-sections as in Figure 11.15. The brown line represents a step in the land accretion process and the green line an even further step. For both land acrretion steps the cross-sections are drawn again at the same location perpendicular to the coast. $\Delta\phi$ represents the changing coastline orientation. Figure is not to scale. 115

11.17 Two cross-sections imitating the situation of land accretion until the 20 m depth contour line. Longshore sediment transport volumes are computed with CoDeS. From coast to sea: the first two arrows represent the gross sediment transports. The last arrow represents the nett sediment transport. 116

11.18 Graph showing the required sand volumes and available sand volumes for land accretion, plotted against the depth at which the seawall must be constructed. The grey area indicates the range where limit for land accretion is in. 119

12.1 Early stripping stage in mining operation. Repeated from Chapter 3. 122

12.2 Middle stage of mining operation: stripping of bulk material. Repeated from Chapter 3. 122

12.3 Final cleaning stage: Transvacs. Repeated from Chapter 3. 123

12.4 Final cleaning stage: Worker operating a Transvac. Repeated from Chapter 3. . 123

12.5 Graph showing the costs as a function of the accepted probability of storm occurrences. This is for the early stripping stage, where failure costs are assumed to be in the order of 10 million USD. 124

12.6 Graph showing the costs as a function of the accepted probability of storm occurrences. This is for the middle mining stage, where failure costs are assumed to be in the order of 30 million USD. 124

12.7 Graph showing the costs as a function of the accepted probability of storm occurrences. This is for the final cleaning stage, where failure costs are assumed to be in the order of 50 million USD. 125

A.1 Satellite image of MA1. The numbered blocks show where the maps of Figure A.3 to Figure A.9 are in the Topography of the coastal stretch. 157

A.2 Topographic legend belonging to the map of MA1, presented in Figure A.3 to Figure A.9 158

A.3 Part of the map. No.1 (outline is drawn in Figure A.1) 159

A.4 Part of the map. No.2 (outline is drawn in Figure A.1) 160

A.5 Part of the map. No.3 (outline is drawn in Figure A.1) 161

A.6 Part of the map. No.4 (outline is drawn in Figure A.1) 162

A.7 Part of the map. No.5 (outline is drawn in Figure A.1) 163

A.8 Part of the map. No.6 (outline is drawn in Figure A.1) 164

A.9 Part of the map. No.7 (outline is drawn in Figure A.1) 165

B.1 Schematic drawing of steps in excavation process 166

B.2 Snip from a topographic map of MA1. In green the areas that will be stripped with a dredging operation. 167

B.3 Overburden stripping in G-area by Cutter Suction Dredger (Beachcomber) . . . 167

B.4 Dewatering mining block after dredging operation 168

B.5 Conventional overburden stripping with excavators and ADT's 168

B.6 Dewatering mining block during mining operation 169

B.7 Mining of terraces in the U-area. 170

B.8 Transvacs used in the cleaning of bedrock 170

B.9 Cleaning the bedrock. Worker operating a Transvac 171

B.10 Mining block after bedrock cleaning 171

B.11 Dewatering mining block during mining operation. Water is constantly flowing in from the sides at a high rate. 172

C.1 Picture taken from the top of the tailingsdump. Conveyor belt feeding groyne system at #3-Plant. Just behind the conveyor belt is a jetty with pipelines, through which slimes are pumped. 175

C.2 Picture taken from the end of the groyne. Image shows the conveyor belt coming from #3-Plant 175

C.3 Spreaders dumping tailings from #3-Plant at the end of the groyne 175
C.4 Spreaders at #3-Plant at maximum distance 175
C.5 Groyne built out of tailings coming from #4-Plant 176
C.6 Via spreaders material is dumped into the sea to extent the groyne at #4-Plant 176
C.7 Spreaders at the end of the groyne disposing old tailings from #4-Plant 176
C.8 Loading old tailings from the dump on to a conveyor belt next to the old #4-Plant 176
C.9 Under construction: new conveyor belt system for sending old waste dumps to the sea (1) 177
C.10 Under construction: new conveyor belt system for sending old waste dumps to the sea (2) 177
C.11 Under construction: camelback for extention of the new conveyor belt system when needed (3) 177
C.12 Under construction: new conveyor belt system (4). End of conveyor belt between dunes / old waste dumps. 177
C.13 ADT driving on the seawall to dump material for building a crosswall extension 178
C.14 Construction of crosswall extension. Dozer pushing dumped material in the sea. 178

D.1 windspeed (m/s) and waveheight (m) for part of a time record. Latitude: -28.5 , longitude: 13.5 180
D.2 wind and wave direction for the same time record. Latitude: -28.5 , longitude: 13.5 181
D.3 Scatterplot (wave height and wind speed) for entire time record (one year) . Latitude: -28.5 , longitude: 13.5 181
D.4 Best-fit curve to relate between wind speed and wave growth. 182

E.1 Scatterplot of waverecords of Southern Coastal Mine Namibia. Conditions have been sorted for wave height bins and wave period bins 183
E.2 Scatterplot presenting sediment transport per wave condition. Calculations done with the simple CERC approach. 184
E.3 Scatterplot presenting relative sediment transport per wave condition. 184
E.4 Wave conditions grouped manually based on equal contribution to sediment transport. 185

F.1 1D cross-shore bedprofile of Survey Line 9000 of the Southern Coastal Mine Namibia 187
F.2 Coloured lines (representing different mild wave conditions) showing the changes in bed level after 100 days. The red line shows the least mild conditions, the green line the mildest wave conditions. 188

F.3 Coloured lines (representing different grainsize distributions) showing the changes in bed level after 100 days. From coarse to fine sand: Cyan - Red - Green - Orange . . . 189

F.4 Colored lines (representing different values of Facua) showing the changes in bed level after 100 days. Cyan line: Facua = 0. Red line: Facua = 0.5. Green line: Facua = 1.0. . . . 190

F.5 Colored lines (representing different positions of the seawall on the beach) showing the changes in bed level after 100 days. Blue line: Tp = 12.5 s. Red line: Tp = 7.5 s. . . . 191

F.6 Colored lines (representing different peak periods for the wave conditions) showing the changes in bed level after 100 days. Blue line: Tp = 12.5 s. Red line: Tp = 7.5 s. . . . 191

F.7 Colored lines (representing different peak periods for the wave conditions) showing the changes in bed level after 100 days. Blue line: Tp = 12.5 s. Red line: Tp = 7.5 s. . . . 192

F.8 Colored lines (representing different main directions for the wave conditions) showing the changes in bed level after 100 days. Blue line: Dir = 180 degrees North. Red line: Dir = 210 degrees North. Green line: Dir = 240 degrees North. Orange line: Dir = 270 degrees North. . . . 193

G.1 Comparison of wave height data (Hs) for averaging over 1 day . . . 195

G.2 Comparison of wave period data (Tp) for averaging over 1 day . . . 195

G.3 Wave height data (Hs) averaged over 1 day, zoomed in on a period of 40 days. 196

G.4 Wave conditions with a duration of 24 hours exceeding a significant wave height of 4m . . . 196

G.5 Exponential distribution of wave conditions . . . 198

G.6 Wave heights, according to the Gumbel distribution, belonging to certain probabilities of occurrence. . . . 200

G.7 Graph showing a 10 year wave record, with a trend-line through the data points. (Significant wave height H_s and wave peak period T_p) . . . 201

G.8 Relationship between significant wave height H_s and wave peak period T_p for data above the threshold of Hs = 4.5m and Tp = 11.5s. . . . 202

H.1 Example of a simulation to determine the influence of model settings for the 1D XBeach model. . . . 205

H.2 Same simulation result as in figure H.1. Zoomed in on the seawall to determine the eroded sand volume. . . . 205

H.3 Erosion volumes (m^3/m) for varying settings of the 1D XBeach Model. . . . 205

H.4 Spiderplot presenting the result of the sensitivity analysis done for the 1D XBeach Model. . . . 206

H.5 Spiderplot presenting the impact to the 1D XBeach Model, due to variations in wave conditions. 207

H.6 Spiderplot presenting the influence of all relevant parameters for eroded sand volumes in the 1D XBeach Model. 207

I.1 Weather forecast for May 26th to June 5th 2015 for Oranjemund, Namibia. . . 209

I.2 Wave conditions offshore of the Orange River Mouth, Namibia, on May 29th 2015. 210

I.3 Wave conditions offshore of the Orange River Mouth, Namibia, on May 30th 2015. 211

J.1 Schematic representation of FORM procedure. Probability density functions of R and S are combined in the graph. The curved line represents the nonlinear limit state function. 216

J.2 Follow up of Figure J.1. New design point is found by iterative process of FORM. 216

J.3 Schematic drawing of a dune cross-section. Under the influence of a storm surge, the profile strives towards a post-storm equilibrium profile, as prescribed by Vellinga (1983). Labels are in Dutch. afslag = erosion, afslagprofiel = erosionprofile, stormvloedpeil = storm surge level, aanzanding = sedimentation, beginprofiel = beginprofile. 218

J.4 Cross-section of dune profile showing the post-equilibrium profile. The eroded volume is A. An additional volume T must be taken into account, because of model uncertainties. (rekenpeil = design water level) 220

J.5 Limit state profile of a Dutch dune. 220

List of Tables

1 Values of proposed design standards for a seawall in the Southern Coastal Mine. iii

2.1 Tide levels for Port Nolloth (80 km south of Oranjemund) and Luderitz (10 km north of Elizabeth Bay). South African Tide Tables, SA Navy Hydrographic Office, 2011. 12

2.2 Windspeed measurements, Southern Coastal Mine, Namibia. (NAMDEB 2013). 13

8.1 Input of combinations of conditions for offshore waves in SWAN 60

9.1 Upscaling per wave condition after application of input reduction 73

9.2 XBeach optimization results (WTI-settings) found by Deltares (2015). 75

9.3 Offshore H_{ss}- and T_p-values associated with design storms (yearly probability). Values of H_{ss} are approached with a Gumbel extreme values distribution. The analysis done for finding values of T_p is explained below in detail. 77

9.4 Resulting seawall erosion volumes per storm condition. 79

9.5 Parameters to be tested in sensitivity analysis. For each parameter the mean, maximum and minimum value are given. 80

10.1 Resulting seawall erosion volumes for cross-section of Survey Line 9000 per storm condition. 90

10.2 Resulting seawall erosion volumes per storm condition, according to calculation guidelines. 90

10.3 Values of proposed design standards for a seawall in Mining Area No. 1. 101

11.1 Volumes required per year for the shifting of seawalls. 112

11.2 Volumes required for the maintenance of cross-shore profiles per step in changing coastline orientation due to land accretion. 116

12.1 Resulting seawall erosion volumes per storm condition. Repeated from Chapter 10. 120

12.2 Build-up of investment costs for different risk levels. 121

14.1 Values of proposed design standards for a seawall in the Southern Coastal Mine. 133

C.1 Forecast of coastline shift in current business plan. 173

E.1 Upscaling per wave condition after application of input reduction 186

G.1 Wave data Southern Coastal Mine Namibia. Threshold (significant wave height) of 4 m 197

G.2 Comparison of different distribution functions for different thresholds of H_s. The presented results are the significant wave height [m]. 199

G.3 Comparison of γ-values for the three different distribution functions for different thresholds of H_s. 199

G.4 Comparison of H_{ss}-values for the three different distribution functions. (Threshold of H_s is 4m). 200

G.5 Values of wave peak period associated with significant wave height for data above the threshold of Hs = 4.5m and Tp = 11.5s. 202

H.1 Parameters to be tested in sensitivity analysis. For each parameter the mean, maximum and minimum value are given. 204

Appendix A – Map of Southern Coastal Mine

This Appendix presents the outline of the Southern Coastal Mine, also known as MA1, in Namibia. Since the mine is very long in coastline-parallel direction and very narrow in cross-shore direction, the map is cut up in 7 images. The cut-up is done as presented by Figure A.1. Figure A.2 shows the legend that is to be used when reading the maps. A scale is drawn on the first part of the map (see Figure A.3), together with an explanation of lines in front of the coastline. These coloured lines present the high water line at the end of year, as the coastline moves seaward due to land accretion.

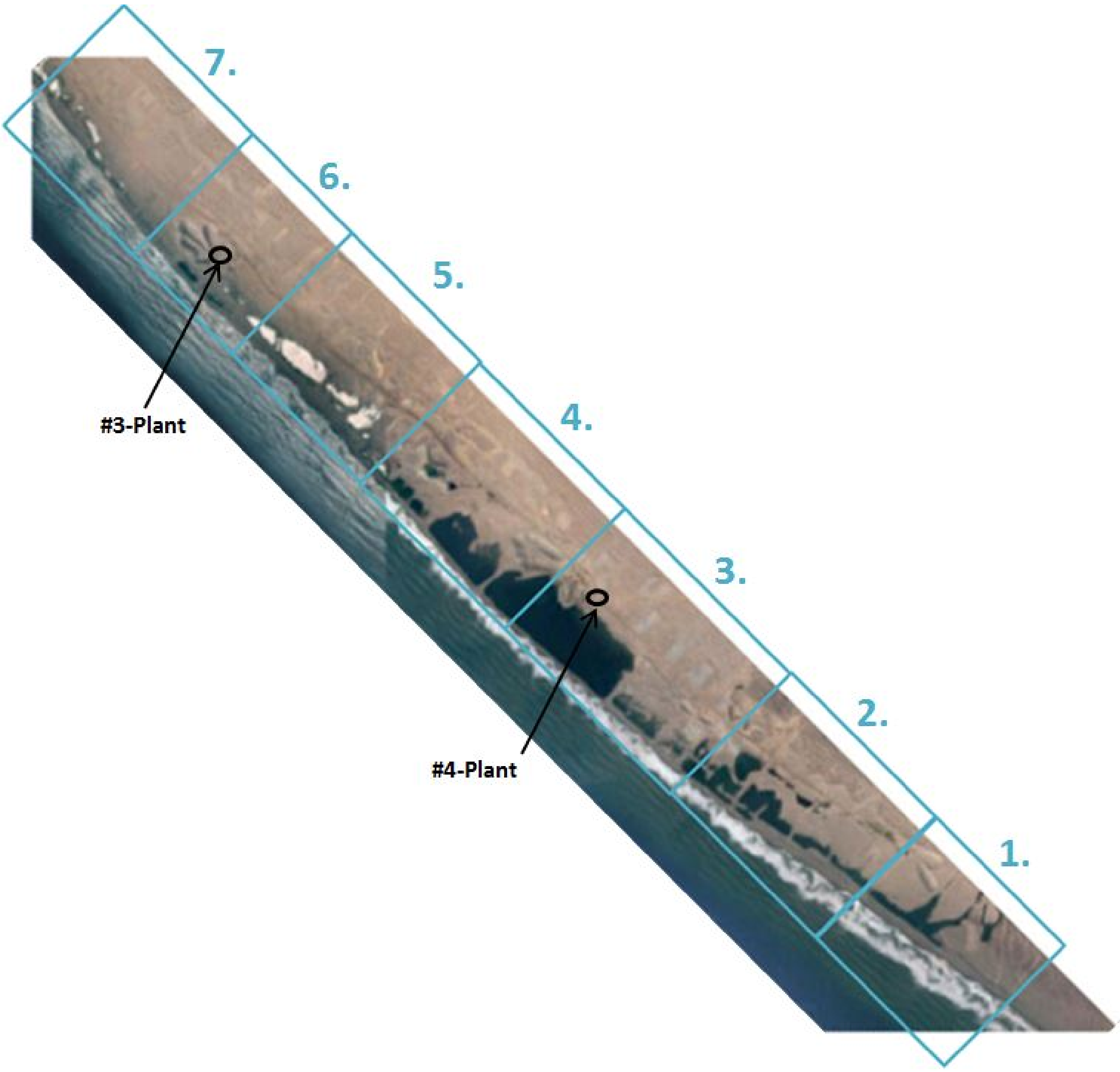

Figure A.1: Satellite image of MA1. The numbered blocks show where the maps of Figure A.3 to Figure A.9 are in the Topography of the coastal stretch.

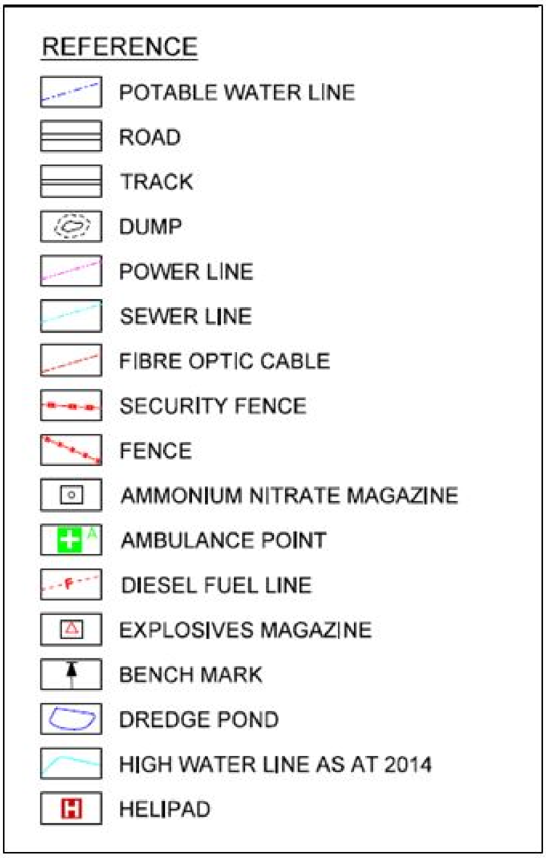

Figure A.2: Topographic legend belonging to the map of MA1, presented in Figure A.3 to Figure A.9

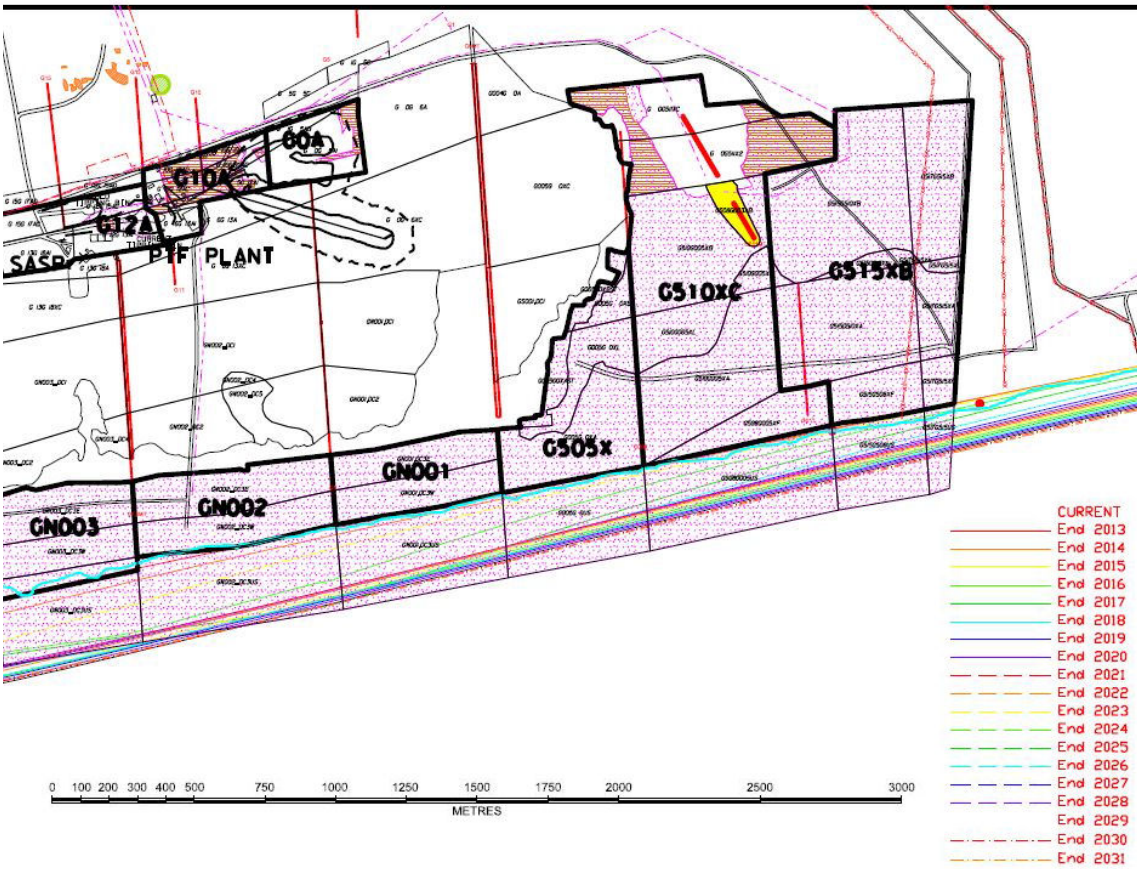

Figure A.3: Part of the map. No.1 (outline is drawn in Figure A.1)

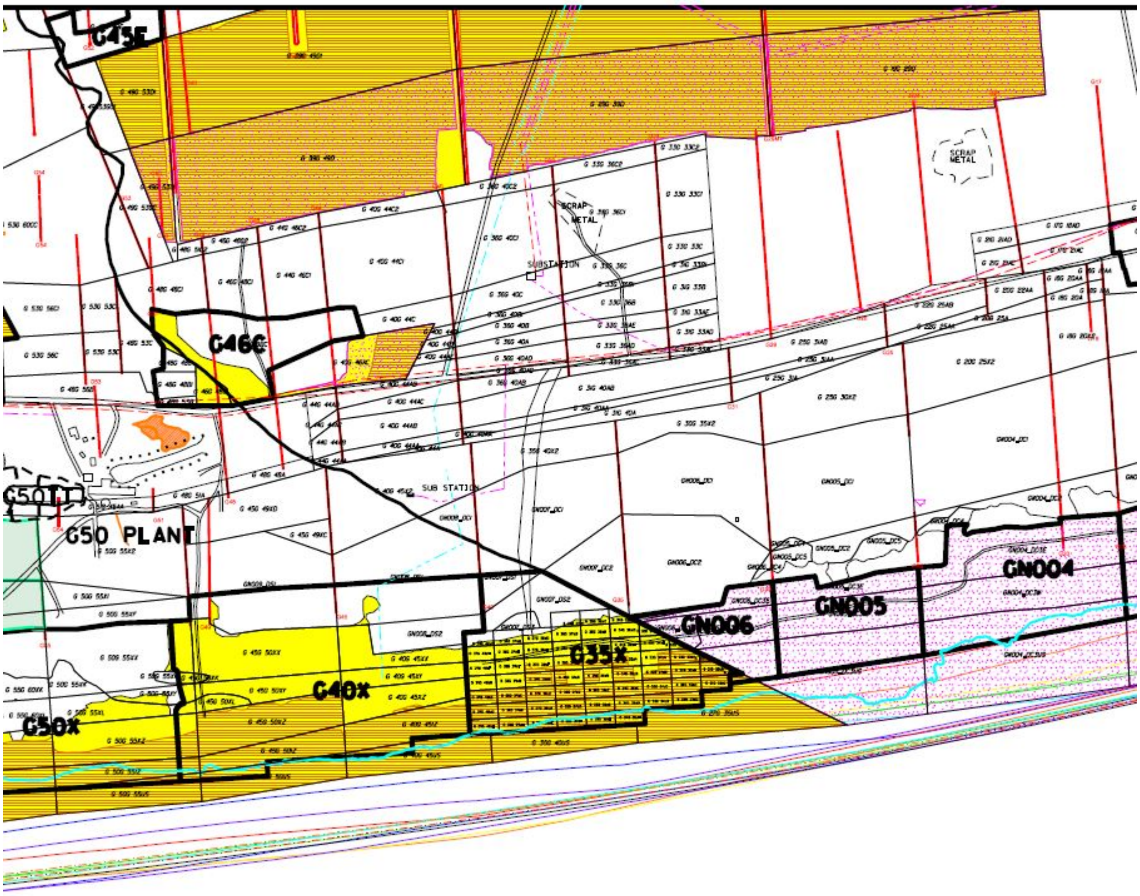

Figure A.4: Part of the map. No.2 (outline is drawn in Figure A.1)

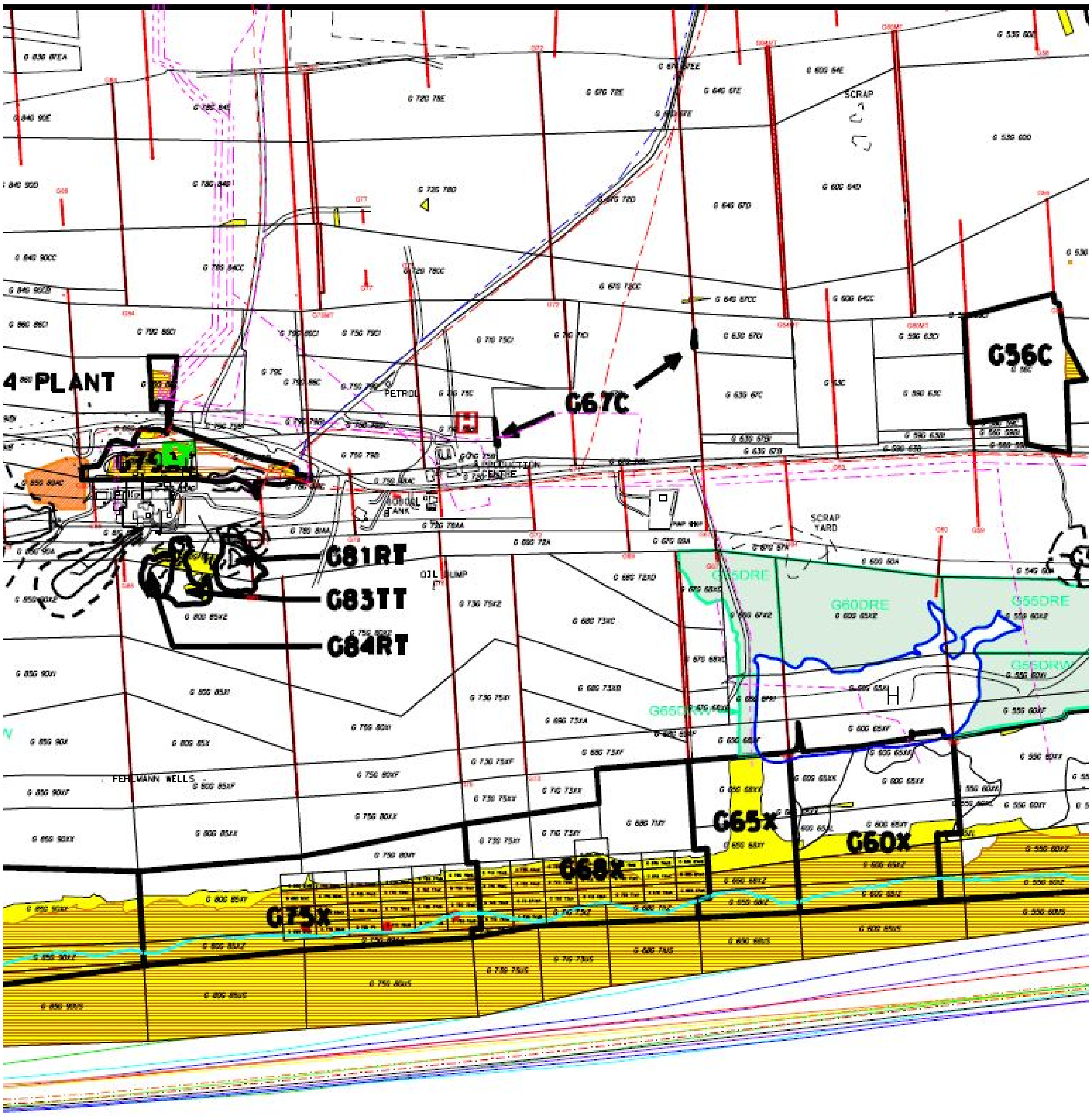

Figure A.5: Part of the map. No.3 (outline is drawn in Figure A.1)

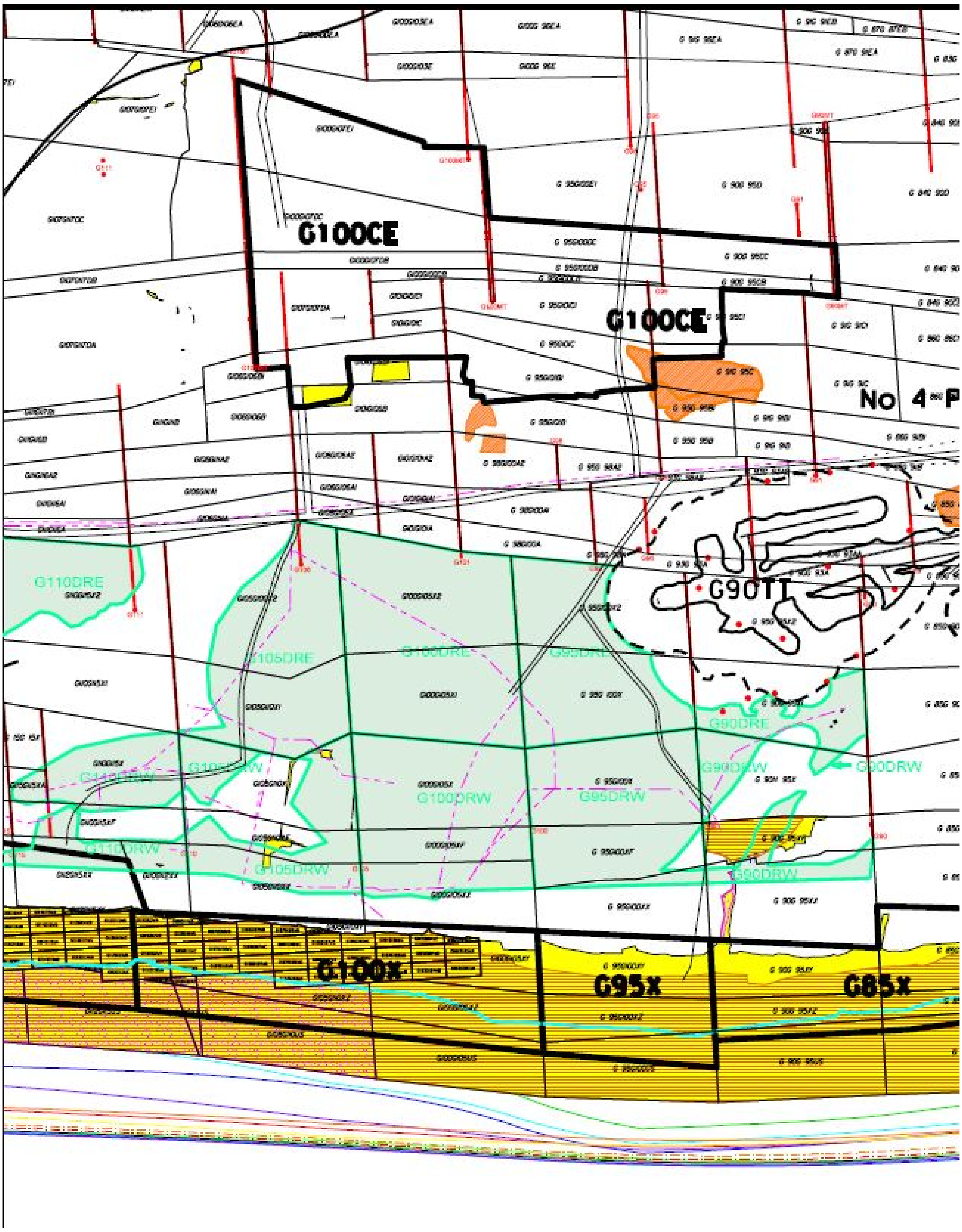

Figure A.6: Part of the map. No.4 (outline is drawn in Figure A.1)

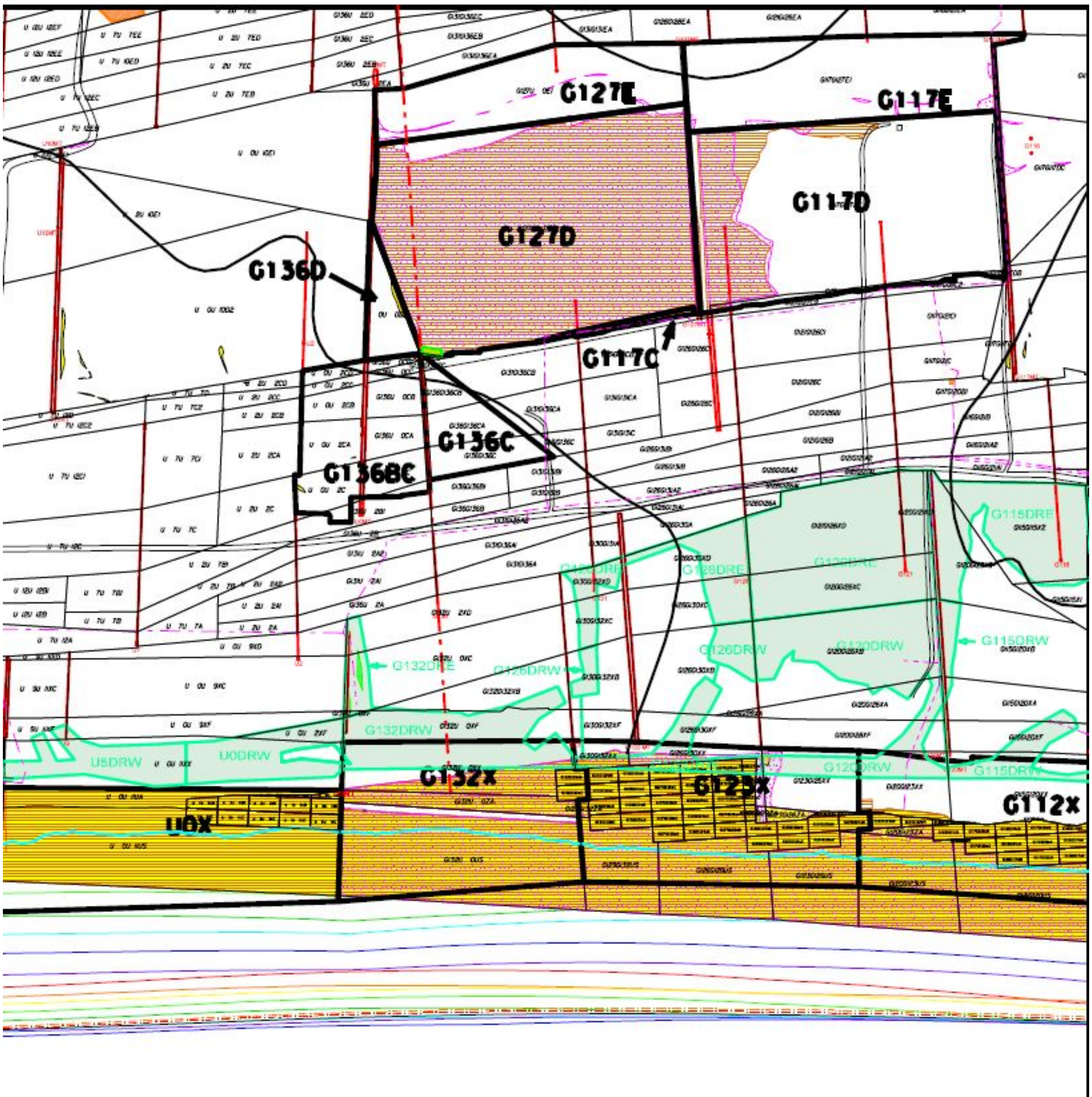

Figure A.7: Part of the map. No.5 (outline is drawn in Figure A.1)

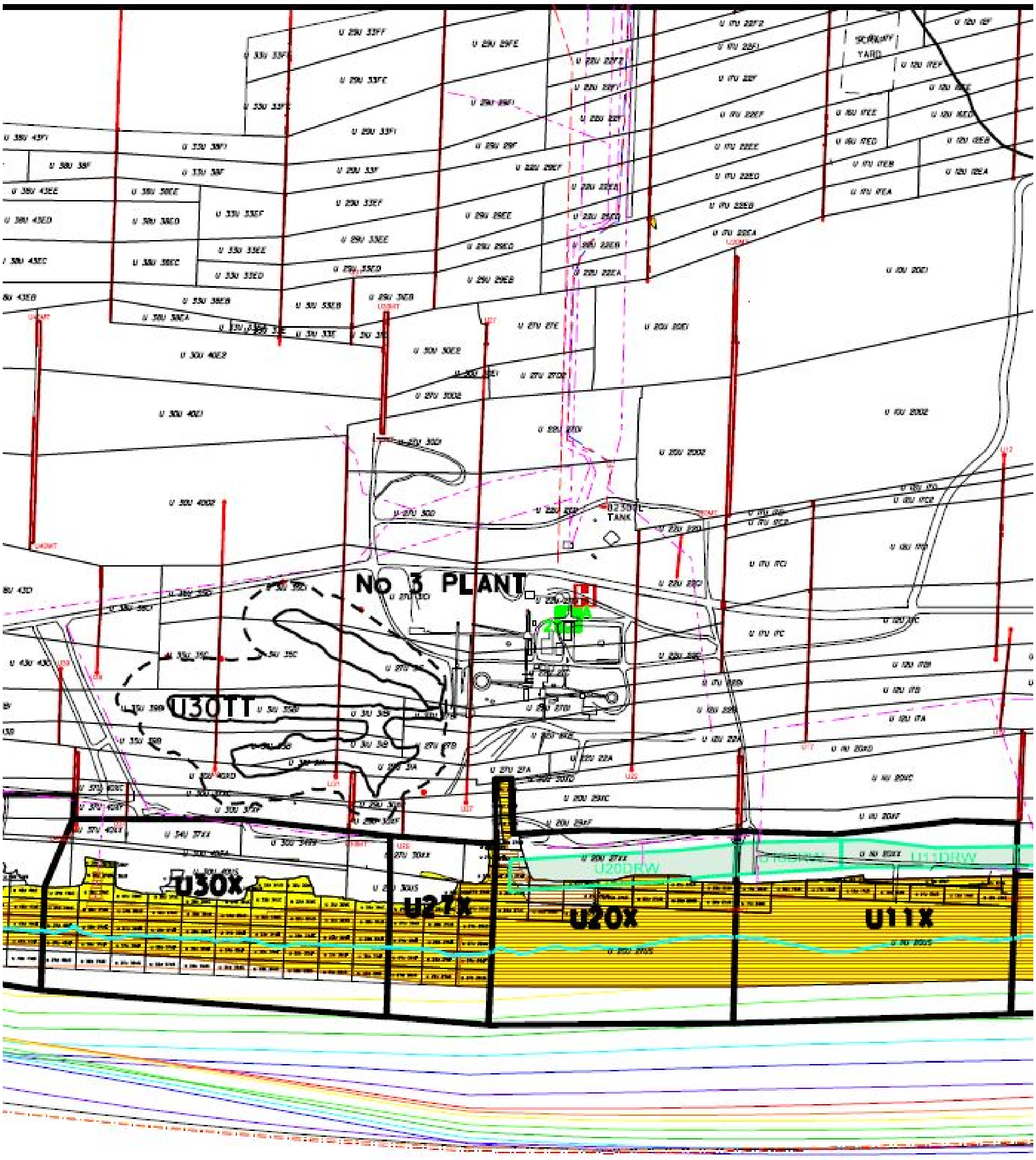

Figure A.8: Part of the map. No.6 (outline is drawn in Figure A.1)

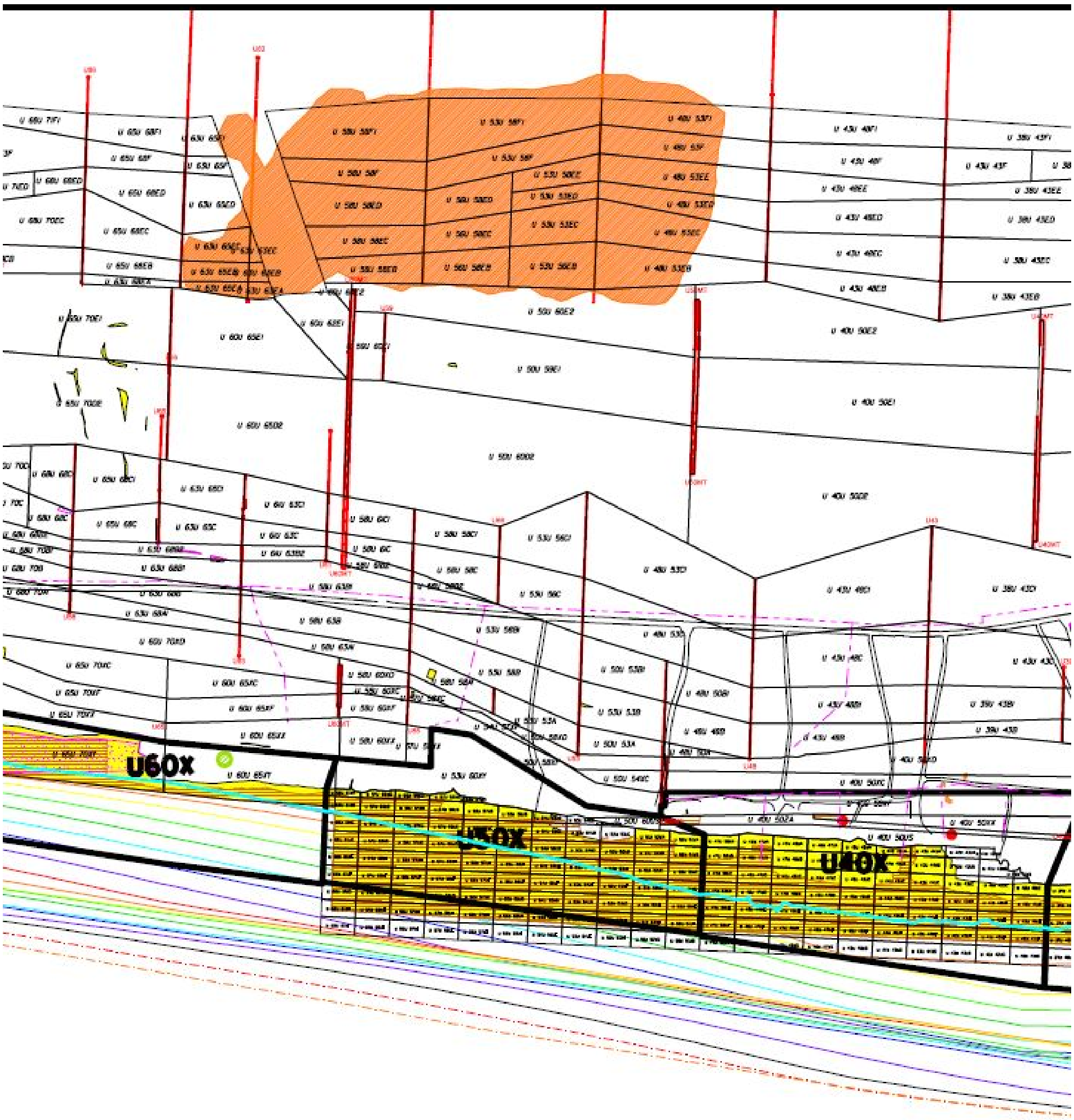

Figure A.9: Part of the map. No.7 (outline is drawn in Figure A.1)

Appendix B – Current mining method explained

This appendix describes the process of the extraction of diamonds from overburden stripping to the hauling of material towards the processing plant.

B.1 Mining blocks

We look again at the figure presented below.

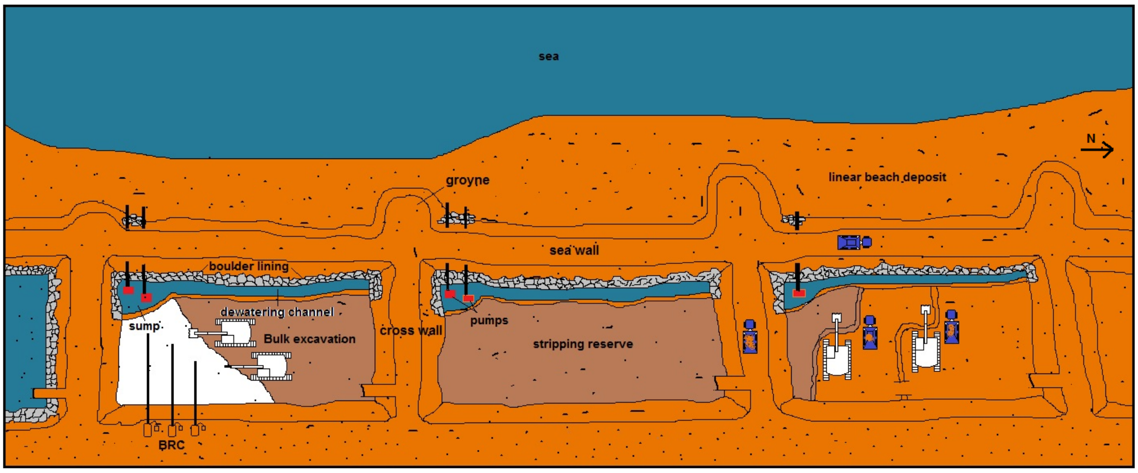

Figure B.1: Schematic drawing of steps in excavation process

In both the G-area and the U-area diamonds are mined in blocks. Mining blocks (or cells) are surrounded by crosswalls and a seawall at the sea side, as shown in Figure B.1. The blocks are "normally" a 150 m wide (in the direction parallel to the coastline) and 80 to 150 m long (in seaward direction). The steps in the extraction of Run of Mine (material to be processed) from a block are as follows:

1. Stripping of overburden until 2 meters above bedrock. This is done partly by dredging in the G-area, and by conventional stripping (Hydraulic Excavator + Articulated Dump Truck) in the U-area and some parts of the G-area.
2. Stripping of top 2 meters of overburden with conventional stripping.
3. Mining the terraces with Hydraulic Excavators + RFT's.
4. Cleaning the bedrock with so-called Transvacs.

B.2 Dredging overburden

The Cutter Suction Dredgers (CSD's) are applied in the blocks/cells in the G-area that are going to be extracted. Figure B.3 shows a typical overburden stripping operation in the G-area of MA1. The area within the G-area where dredging is applied is coloured green in the topographic maps of the Southern Coastal Mine. A snip of a map is shown in Figure B.2, where one can see the green area where dredging is applied.

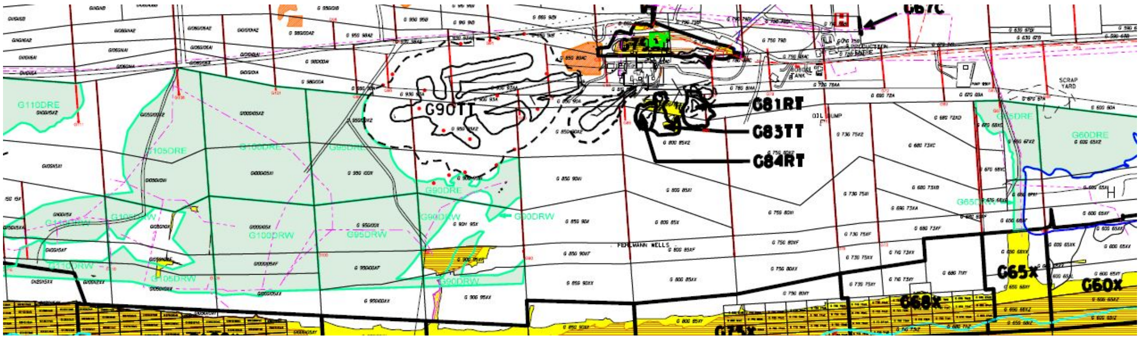

Figure B.2: Snip from a topographic map of MA1. In green the areas that will be stripped with a dredging operation.

The block is surrounded by walls (seawalls and cross-walls) and filled with water. This water is mainly coming from neighbouring blocks that need to be dewatered. The CSD's strip until only 2 meters of overburden remains. A water canon on top of the CSD loosens the material that needs to be dredged. The dredging depth is 14 m.

Figure B.3: Overburden stripping in G-area by Cutter Suction Dredger (Beachcomber)

The dredged material is being pumped to the beach. This material is used for the accretion of land next to the beach. The pumping distance is normally 1 to 1,5 km. After the dredging operation, the mining block/pit is dewatered so hydraulic excavators gain access to the area. Figure B.4 shows the dewatering of the upperleft block/pit after the dredging operation.

Figure B.4: Dewatering mining block after dredging operation

However, since the dredging operation is very large and also rather slow, the current mining activity in the G-area is focused on blocks closer to the beach, where the overburden layer is thinner. Here stripping is done by conventional stripping in the same way as in the U-area. This will be discussed in the next section.

B.3 Conventional stripping of overburden

Conventional stripping is done with Hydraulic Excavators and Articulated Dump Trucks (Figure B.5). Those handle in the order of 10 million m^3 of overburden sand per year (Anker, 2014). Constant dewatering with pumps is necessary since a lot of seepage water is entering the blocks.

Figure B.5: Conventional overburden stripping with excavators and ADT's

B.3.1 G-area

After the dredging operation in a mining block in the G-area, the block is dewatered with water pumps, before conventional stripping can take place. The overburden material is brought to the seawalls and used there as either maintenance material for the seawall in place or as material for the construction of a groyne. A groyne in this case is an extension of the existing crosswalls into the sea.

In the current operation, since the dredging operation is large and rather slow, total conventional stripping of overburden is also applied in the G-area in blocks closer to the beach, where the overburden is thinner.

B.3.2 U-area

In the U-area, all overburden is stripped by means of conventional stripping with excavators and trucks. Also here, the stripped material is used to maintain the seawalls and extend the crosswalls into the sea. The ADT's in the U-area are handling 12.5 Mt of overburden a year. This is all going to the crosswalls/groynes.

B.3.3 Dividing blocks

After the removal of overburden the large mining blocks are divided in smaller blocks. In the dewatered area the smaller blocks are mined out. While one block is being stripped, another block can be cleaned.

B.4 Dewatering

For both the conventional stripping operation and the mining operation the biggest challenge is keeping the site dry. Dewatering pumps are applied extensively in MA1. Figure B.6 presents a typical image of dewatering a block where Terraces are mined. Directly behind the seawall a channel is dug to collect most water. This water is subsequently pumped to the sea by the pumping system in the left of the picture.

Figure B.6: Dewatering mining block during mining operation

B.5 Mining the terraces

Terraces is the name for the sandy layer containing diamonds. The terrace layer is on average 1 meter thick. Below the terrace layer, there is about 1 meter of gravel. Mining these two layers just above the bedrock is done with excavators and trucks, as shown in Figure B.7.

Figure B.7: Mining of terraces in the U-area.

B.5.1 G-area

In the G-area, the Run of Mine from the layer above the bedrock is done by excavators and Articulated Dump Trucks. Those trucks bring the material (Run of Mine) to a Wet Infield Screening Plant (WIFS), next to #4-Plant, where it is screened (around 4 Mt per year). The screened material from the plant is transported to #3-Plant for further processing. This transport is carried out with Rigid Frame Trucks (RFT's).

B.5.2 U-area

In the U-area the Terraces are stripped with Hydraulic Excavators. RFT's bring the material directly to #3-Plant for processing (around 3.6 Mt per year).

B.6 Cleaning the bedrock with Transvacs

The final cleaning of the bedrock is very labor intensive. The gullies in the bedrock are cleaned / mined out by means of large vacuum cleaners, Transvacs. An average of 5 Transvacs is used to clean a mining block. Two workers operate one Transvac. One of the workers is loosening the material from the bedrock with a handshovel and a handsweep, the other workers is following on close foot to suck up the material. The cleaning of bedrock with Transvacs is shown in Figure B.8 and B.9.

Figure B.8: Transvacs used in the cleaning of bed-rock.

Figure B.9: Cleaning the bedrock. Worker operating a Transvac

B.7 After cleaning the bedrock

A mined out block will look like the picture below (Figure B.10). When a block is mined it will be filled up with water in a "natural" way, by seepage through the seawalls and crosswalls. This last stage is since 2013 often postponed because for the shifting of the seawall seawards a dry hinterland is required for safety reasons.

Figure B.10: Mining block after bedrock cleaning

B.8 Difficulties in the current mining process

- The biggest challenge in the current mining operation is dealing with water. Mining blocks need constant dewatering to prevent it from flooding by seepage water. Figure B.11 shows another picture of dewatering. One can easily see that water is flowing through the toe of the seawall at a high rate.

Figure B.11: Dewatering mining block during mining operation. Water is constantly flowing in from the sides at a high rate.

- The overburden layer gets thicker towards the west. The major reason for this is that material is nourished on the seabed to reclaim land. This material now also counts as new overburden.
- The large tailingsdumps next to #3-Plant and #4-Plant still contain some diamonds. NAMDEB is currently carrying out a feasibility study for the reprocessing of tailings. At the same time, NAMDEB is using tailings as part of the Sand-2-Sea program.

Appendix C – Land accretion project

To mine for diamonds in the surfzone, the coastline is moved seawards by means of land accretion/reclamation. Once enough new land is obtained, the new blocks can be mined out. Seawalls are built to protect the mining blocks from flooding. This chapter was part of the report of the Fact-Finding Mission carried out at NAMDEB in 2014.

C.1 History

Land accretion in a "natural" way has been seen since the 80's of the twentieth century. The coastline shifted in seaward direction. NAMDEB built seawalls to protect the area from flooding, so the land behind the seawalls could be mined out. Since 1980 the coastline of in the south of MA1 (this is from the river mouth towards the northern end of the U-area) has moved on average about 300 m. The dumping of slimes into the sea and the constant feeding of the unstable seawall are believed to be the main contributors to land reclamation in the past.

Since April 2013 a new mining strategy has been imposed: The Sand-2-Sea program. With the construction of large groynes in combination with smaller groynes (extensions of the crosswalls) land must be reclaimed. Besides groyne-systems, slimes and dredged material are pumped to the beach directly. Groynes don't have standards yet. The total rate of pushing sand with this Sand-2-Sea program is in the order of 20 million m^3 per year.

C.2 Future plan (according to business plan)

The current business plan is until 2031. The reclamation of land should then have reached the 12 meter water depth line on average. This is a distance of 450 m from the current coastline on average. NAMDEB wants to continue the shifting of the coastline seawards as far as financially and technically feasible. **The focus of the Sand-2-Sea program, and so the land reclamation too, is solely on the south of MA1.** The table below gives a number of distances and depths for different locations in the south of MA1.

Location (from south to north)	Distance from current beach line in meters	Distance from predicted 2014 line in meters	Depth in meters
G50			-12
#4-Plant	314	240	-12.5
Between #4- and #3-Plant	545		-15
#3-Plant	521	487	-16
Uubvlei	384		-6

Table C.1: Forecast of coastline shift in current business plan.

The high-water lines (yearly averaged) according to the current business plan can be found in Appendix A. Here coloured lines are drawn, presenting the modelling results of a currently used coastline model.

C.3 Reason for land reclamation

The reasons for land reclamation are the following:

- The wave climate is very difficult in this region. High swell waves in combination with a shallow sea make a dredging operation “impossible” in the surfzone.
- Land accrued in the past, so it can be expected that this process will continue in the future. By bringing material (waste, tailings and slimes) to the sea this process can even be accelerated.
- “Dry mining” is a must for NAMDEB. With the currently available technology, diamonds in Mining Area 1 (MA1), can only be mined out in a dry way. Since approximately 60% of the diamonds are found within the gullies, the gullies need to be cleaned properly. Wet mining, by means of dredging, is not selective enough to obtain the same high recovery as dry mining. For this reason a new area of land must be reclaimed on the sea first before mining can be done.

C.4 Building groynes

There are currently three types of groyne-systems.

1. A large groyne with spreaders near #3-Plant.
2. Conveyor belt systems to bring old waste and tailings to the sea.
3. The extension of crosswalls, carried out by ADT’s near the mining operations.

This specific area for the groynes is chosen because from historical mining it is known that these areas have a high grade of diamonds. So there areas NAMDEB wants to expose to get maximum benefit for the money spent on accretion.

C.4.1 Groyne with spreaders near #3-Plant

Since April 2013 the tailings from #3-Plant are sent directly to the sea. From the processing plant a conveyor belt system is built to the groyne. At the end of the groyne are 4 spreaders/grashoppers to dump the material on the groyne. The total system has currently reached its maximum length/distance because all grashoppers are in line. NAMDEB is working on a camelback system to extent the groyne with an extendable conveyor belt on a rails. In this way only one of the spreaders/grashoppers is needed at the end of the groyne.

The groyne is about 70 meters wide, enabling the spreaders to make a full turn. The material coming from the spreaders are finally pushed towards the sea by means of dozers. This groyne is the largest groyne in MA1.

Figures C.1, C.2, C.3 and C.4 present the construction of the groyne near #3-Plant.

Figure C.1: Picture taken from the top of the tailingsdump. Conveyor belt feeding groyne system at #3-Plant. Just behind the conveyor belt is a jetty with pipelines, through which slimes are pumped.

Figure C.2: Picture taken from the end of the groyne. Image shows the conveyor belt coming from #3-Plant

Figure C.3: Spreaders dumping tailings from #3-Plant at the end of the groyne

Figure C.4: Spreaders at #3-Plant at maximum distance

All new tailings from #3-Plant are directly transported to the sea with the conveyor belt. Besides this old tailings from the #3-Plant tailingsdump are dumped in a rather slow rate unto the conveyor belt. In total the conveyor belt system has to push 1000 ton per hour to the sea. The current output is between 600 and 1000 t/hour.

C.4.2 Conveyor belt systems for old waste and tailings

There are 3 conveyor belt systems, of which 2 are still under construction, to bring old waste and tailings to the sea.

1. The first one is already operating (see Figures C.5, C.6, C.7 and C.8). Tailings from the tailings dump of #4-Plant are dumped with loaders on a conveyor belt via a tipping bin. The conveyor belt brings the material to the sea and dumps it on a groyne. This process is accompanied with large risks of slumping/avalanching of material down the tailings pile. The conveyor belt does not transport a constant rate of material. Depending on availability of front wheel loaders and on the demand (around 1000 t/h) the conveyor belt is fed.

Figure C.5: Groyne built out of tailings coming from #4-Plant

Figure C.6: Via spreaders material is dumped into the sea to extent the groyne at #4-Plant

Figure C.7: Spreaders at the end of the groyne disposing old tailings from #4-Plant

Figure C.8: Loading old tailings from the dump on to a conveyor belt next to the old #4-Plant

2. The second conveyor belt is constructed just north of #3-Plant. Picture of the construction is shown below. This system is built to bring old waste dumps to the sea.

    (a) The current length is 1.5 km. Close to the sea a camelback system is built. This means that the main conveyor belt dumps on a second conveyor belt system which is on a rails and can move in its axis direction. In this way the system can be extended up to 300 m as it moves towards the sea.

(b) Front wheel loaders will feed a 40t ADT, which will dump the material in a tipping bin, which is the feeding system. Dunes (old waste dumps) will be dug up and dumped on the conveyor belt. This is done starting from 200 m from the end of the conveyor belt until the end.

(c) The design lifetime of this project is 20 years. However, engineers and planners are skeptical whether there will be enough material to feed the conveyor belt without having to bring the material from too far from the conveyor. The bedrock is quite close to the surface here.

(d) The system is designed for 1000t per hour. Maximum capacity is 1250 t/h. The speed of the belt is 3.5 m per minute. The feeding system (tipping bin system) has a higher working capacity and is therefore downscaled.

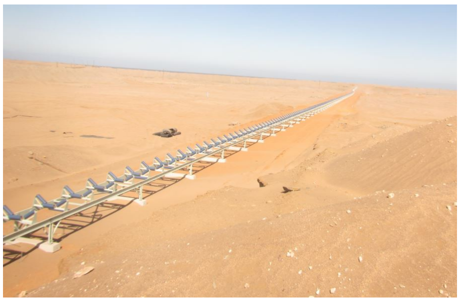

Figure C.9: Under construction: new conveyor belt system for sending old waste dumps to the sea (1)

Figure C.10: Under construction: new conveyor belt system for sending old waste dumps to the sea (2)

Figure C.11: Under construction: camelback for extention of the new conveyor belt system when needed (3)

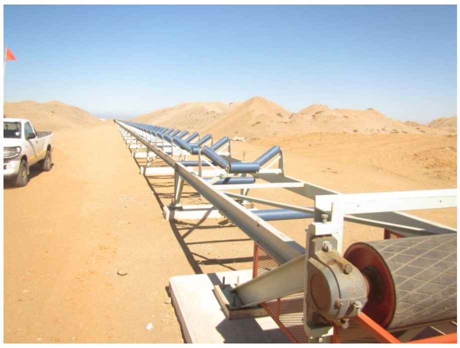

Figure C.12: Under construction: new conveyor belt system (4). End of conveyor belt between dunes / old waste dumps.

3. The third conveyor belt is constructed between #4-Plant and #3-Plant. This system is also built to bring old waste dumps to the sea. The system will be identical to the other conveyor belt system that moves old waste dumps to the sea. The length will also be about 1.5 km. The conveyor belt system is in an earlier stage of construction, but must be operational in 2015.

A problem that can occur in the operation of the new conveyor belts is that wind can blow material on the system and can possibly block the system eventually.

C.4.3 Extension of crosswalls

ADT's bring mining waste from the stripping operations to the end of the crosswalls to extent the crosswall into the sea, creating a kind of groyne system. The width of the seawalls are determined by stability requirements and not by ADT turning radius. To ensure the wall is stable the current standards prescribe to have a minimum width of 20m of the crest of the seawall.

Figure C.13: ADT driving on the seawall to dump material for building a crosswall extension

Figure C.14: Construction of crosswall extension. Dozer pushing dumped material in the sea.

C.5 Pumping material to the beach

Material is pumped unto the beach at three different places.

1. Dredging vessel Beachcomber is pumping overburden from the stripping operation in the G-area directly to the beach.
2. Dredging vessel Gaeb is pumping material from the tailingsdump next to #3-Plant directly to the beach.
3. Slimes (material with a grainsize smaller than 2 mm) coming from #3-plant are pumped directly to the beach.

C.6 Major difficulties

Different parts of the Sand-2-Sea program experience difficulties. The four most important, based on observations, are:

- Risks of slumping/avalanching of the old tailingsdump.
- Process of feeding the conveyor belt doesn't seem constant and seems to have a low rate.

- Output of dredged material from tailingsdump seems to consist of mainly water.
- Wind moving the old waste dumps / dunes.

The question that arises is whether the Sand-2-Sea program will be able to provide enough sand in a sufficient rate for land reclamation. Because mining activity must proceed, thereby utilizing the maximum capacity of the processing plant with a positive cash flow.

Appendix D – Effect of wind to wave-growth

Wind speed and direction are important parameters when modelling waves with a SWAN model. The determination of these parameters for different conditions occurring offshore the Namibian Coast are discussed below.

The correlation between wind and waves is not straight forward. Figure D.1 shows the wave height and wind speed for a time-series at the off shore boundary of the model grid. One can see that for conditions with higher wind speed the wave height becomes higher. The exact relation is somewhat unclear and is probably not one-to-one. When we look at Figure D.2, representing the directions of waves and wind, there seems to be hardly any correlation.

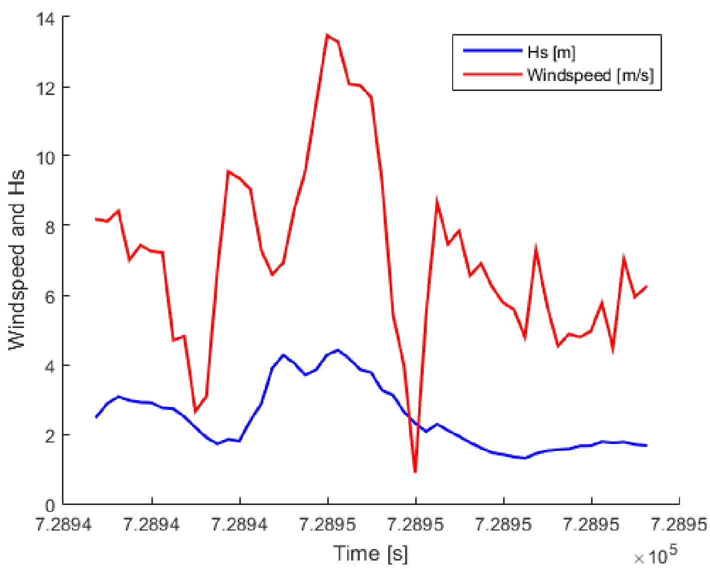

Figure D.1: windspeed (m/s) and waveheight (m) for part of a time record. Latitude: -28.5 , longitude: 13.5

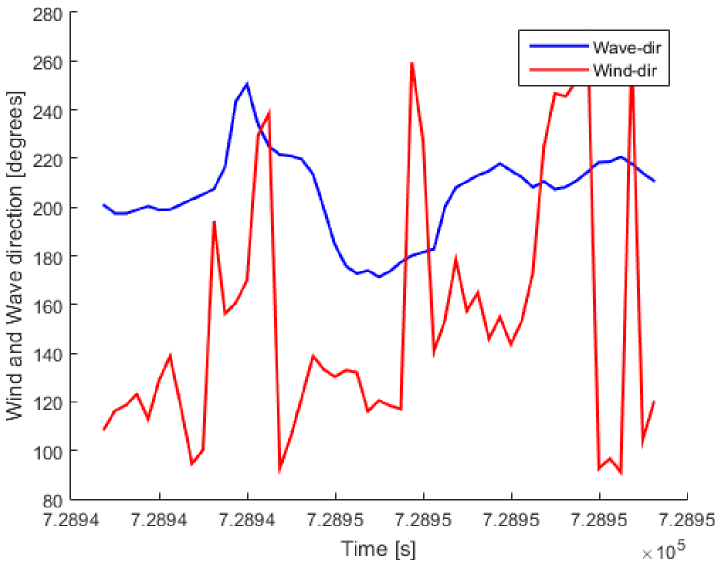

Figure D.2: wind and wave direction for the same time record. Latitude: -28.5 , longitude: 13.5

Figure D.3 is a scatterplot of all conditions recorded in one years' time.

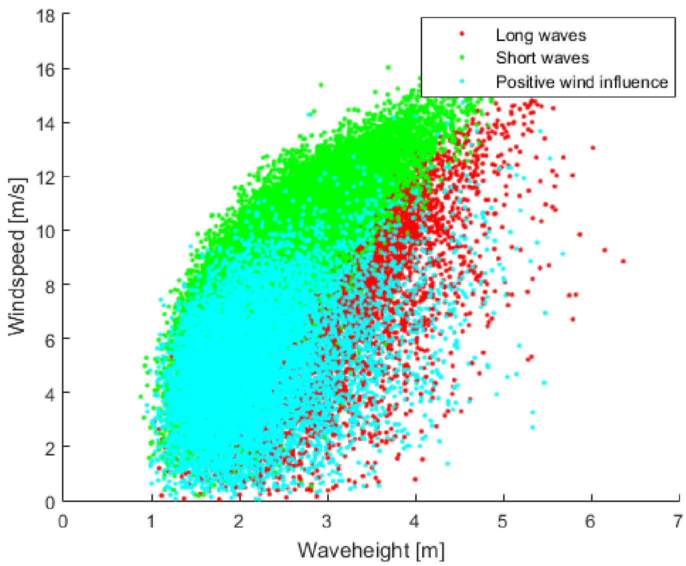

Figure D.3: Scatterplot (wave height and wind speed) for entire time record (one year) . Latitude: -28.5 , longitude: 13.5

A distinction is made between long (Tp $>$ 10sec) and short (Tp $<$ 10sec) waves is made. This is done to distinguish between wind and swell waves. Thereby assuming that swell waves are hardly influenced by local wind conditions, and short waves are. The dots with the colour cyan, represent the conditions where the wind is favourable for wave growth, so a wind direction of 180-320 degrees.

From the plot we can derive that the wind does not play a major role in the generation and propagation of waves in front of the shore of the Southern Coastal Mine. In situations of short waves and a windspeed of less than 10 m/s (and wave heights less than 4 m) the wind has a positive contribution to the wave growth.

SWAN will calculate wave growth for certain wind conditions. The higher the waves, the more severe the dune erosion will be. So the most conservative approach would be to choose a wind direction perpendicular to the coastline and a high wind speed. Analyzing the correlations between waves and wind, visualized in Figure D.3, the following approach is chosen.

- In order not to underestimate the effect of wind the wind direction is chosen to be 225 degrees. Wind blowing perpendicular to the coast.
- Only in case of short waves (Tp $<$ 10sec) wind is accounted for. There is hardly any positive effect of wind to long waves noticeable.
- The maximum wind speed is 10 m/s. And wind for short waves with a wave height of more than 4 m, wind is also not accounted for, judging on the scatterplot in Figure D.3.
- For short waves a linear relation is derived by means of a best-fit curve through the data, as shown in Figure D.4 below. The formula belonging to the best-fit curve is: $Windspeed = 2.602 \cdot H_s + 0.553$.

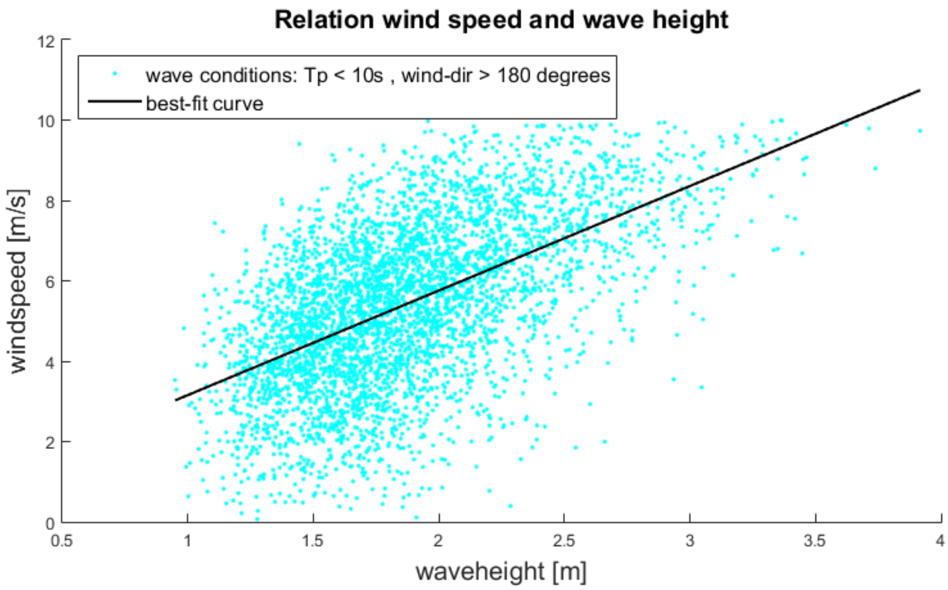

Figure D.4: Best-fit curve to relate between wind speed and wave growth.

Appendix E – Input reduction of wave conditions

To limit the computational effort one must find a set of wave conditions to represent the entire wave climate. To find this set different input reduction techniques have been developed. In the method applied here wave conditions have been grouped manually and the impact of each group on the total annual sediment transport is determined. From this representative wave conditions for each block are chosen and there probability of occurrence is scaled up so they can be applied in the XBeach model. The different steps of the method are explained below.

E.1 Manual grouping of classes

			Wave period T_{p} (s)													
			4.00	5.00	6.00	7.00	8.00	9.00	10.00	11.00	12.00	13.00	14.00	15.00		
	lower	upper	5.00	6.00	7.00	8.00	9.00	10.00	11.00	12.00	13.00	14.00	15.00	16.00	sum	cum sum
Wave height H_{s} (m)	0	0.5	-	-	-	-	-	-	-	-	-	-	-	-	-	-
	0.5	1	-	-	0.00	0.01	0.01	0.00	0.00	-	-	-	-	-	0.03	0.03
	1	1.5	-	-	0.21	0.82	1.49	1.30	0.45	0.09	0.01	-	-	-	4.35	4.39
	1.5	2	-	0.01	0.95	3.51	5.48	6.05	3.66	1.22	0.19	0.02	-	-	21.09	25.48
	2	2.5	-	-	0.80	5.76	7.67	6.91	5.25	2.65	0.86	0.13	0.01	-	30.05	55.52
	2.5	3	-	-	0.10	3.95	6.73	4.87	3.58	2.49	1.04	0.27	0.04	-	23.08	78.61
	3	3.5	-	-	-	0.92	3.85	2.93	2.16	1.49	1.05	0.31	0.04	0.00	12.75	91.35
	3.5	4	-	-	-	0.07	1.44	1.30	1.03	0.98	0.60	0.27	0.06	0.01	5.76	97.12
	4	4.5	-	-	-	-	0.30	0.49	0.36	0.34	0.29	0.21	0.05	0.01	2.06	99.17
	4.5	5	-	-	-	-	0.02	0.11	0.12	0.14	0.09	0.08	0.03	0.00	0.60	99.77
	5	5.5	-	-	-	-	-	0.01	0.04	0.06	0.02	0.03	0.02	0.00	0.17	99.95
	5.5	6	-	-	-	-	-	-	0.01	0.01	0.00	0.01	0.01	0.00	0.05	99.99
	6	6.5	-	-	-	-	-	-	0.00	-	0.00	-	-	0.00	0.01	100.00
	6.5	7	-	-	-	-	-	-	-	-	-	-	-	-	-	100.00
		sum	-	0.01	2.06	15.05	26.97	23.97	16.68	9.46	4.17	1.35	0.25	0.03	100.00	

Figure E.1: Scatterplot of waverecords of Southern Coastal Mine Namibia. Conditions have been sorted for wave height bins and wave period bins

The wave data have been organized in a scatterplot as shown in Figure E.1. The range of the significant wave height (H_s) is divided in bins of 0.5 m (see left column in Figure E.1). The range of the wave peak period (T_p) is divided in bins with a width of 1 second (see upper-row in Figure E.1). The numbers in the different cells of the table show the frequency of occurrence (in %) of a specific wave condition.

The total number of different conditions is 89 according to the scatterplot above. If different wave directions (main angle of a wave condition) are also included, then we would have to deal with 484 different wave conditions. This can be reduced by analyzing the relative contribution of each wave condition to sediment transport.

The approach of CERC, as presented by Bosboom and Stive (2013) is applied in the simplified form. This method states that sediment transport is related to the wave height to the power 2.5. In Figure E.2 all values of the frequency of occurrence have been multiplied by $H_s^{2.5}$.

				4.00	5.00	6.00	7.00	8.00	9.00	10.00	11.00	12.00	13.00	14.00	15.00		
	lower	upper	Average	5.00	6.00	7.00	8.00	9.00	10.00	11.00	12.00	13.00	14.00	15.00	16.00	sum	cum sum
Wave height H_{s} (m)	0	0.5	0.25	-	-	-	-	-	-	-	-	-	-	-	-	-	-
	0.5	1	0.75	-	-	0.00	0.00	0.00	0.00	0.00	-	-	-	-	-	0.00	0.00
	1	1.5	1.25	-	-	0.00	0.01	0.03	0.02	0.01	0.00	0.00	-	-	-	0.08	0.08
	1.5	2	1.75	-	0.00	0.04	0.14	0.22	0.24	0.15	0.05	0.01	0.00	-	-	0.85	0.93
	2	2.5	2.25	-	-	0.06	0.44	0.58	0.52	0.40	0.20	0.07	0.01	0.00	-	2.28	3.21
	2.5	3	2.75	-	-	0.01	0.50	0.84	0.61	0.45	0.31	0.13	0.03	0.00	-	2.89	6.11
	3	3.5	3.25	-	-	-	0.17	0.73	0.56	0.41	0.28	0.20	0.06	0.01	0.00	2.43	8.53
	3.5	4	3.75	-	-	-	0.02	0.39	0.36	0.28	0.27	0.16	0.07	0.02	0.00	1.57	10.10
	4	4.5	4.25	-	-	-	-	0.11	0.18	0.13	0.13	0.11	0.08	0.02	0.00	0.77	10.87
	4.5	5	4.75	-	-	-	-	0.01	0.05	0.06	0.07	0.05	0.04	0.01	0.00	0.30	11.17
	5	5.5	5.25	-	-	-	-	-	0.00	0.02	0.03	0.02	0.02	0.01	0.00	0.11	11.27
	5.5	6	5.75	-	-	-	-	-	-	0.01	0.00	0.00	0.01	0.00	0.00	0.04	11.31
	6	6.5	6.25	-	-	-	-	-	-	0.00	-	0.00	-	-	0.00	0.01	11.32
	6.5	7	6.75	-	-	-	-	-	-	-	-	-	-	-	-	-	11.32
		sum		-	0.00	0.12	1.28	2.92	2.55	1.93	1.35	0.74	0.33	0.08	0.02	11.32	

Figure E.2: Scatterplot presenting sediment transport per wave condition. Calculations done with the simple CERC approach.

By dividing the values of Figure E.2, representing sediment transport, by the total sediment transport, the relative weight to sediment transport of each wave condition can be found. Results are shown in the table of Figure E.3.

				4.00	5.00	6.00	7.00	8.00	9.00	10.00	11.00	12.00	13.00	14.00	15.00		
	lower	upper	Average	5.00	6.00	7.00	8.00	9.00	10.00	11.00	12.00	13.00	14.00	15.00	16.00	sum	cum sum
Wave height H_{s} (m)	0	0.5	0.25	-	-	-	-	-	-	-	-	-	-	-	-	-	-
	0.5	1	0.75	-	-	0.00	0.00	0.00	0.00	0.00	-	-	-	-	-	0.00	0.00
	1	1.5	1.25	-	-	0.00	0.00	0.00	0.00	0.00	0.00	0.00	-	-	-	0.01	0.01
	1.5	2	1.75	-	0.00	0.00	0.01	0.02	0.02	0.01	0.00	0.00	0.00	-	-	0.08	0.08
	2	2.5	2.25	-	-	0.01	0.04	0.05	0.05	0.04	0.02	0.01	0.00	0.00	-	0.20	0.28
	2.5	3	2.75	-	-	0.00	0.04	0.07	0.05	0.04	0.03	0.01	0.00	0.00	-	0.26	0.54
	3	3.5	3.25	-	-	-	0.02	0.06	0.05	0.04	0.03	0.02	0.01	0.00	0.00	0.21	0.75
	3.5	4	3.75	-	-	-	0.00	0.03	0.03	0.02	0.02	0.01	0.01	0.00	0.00	0.14	0.89
	4	4.5	4.25	-	-	-	-	0.01	0.02	0.01	0.01	0.01	0.01	0.00	0.00	0.07	0.96
	4.5	5	4.75	-	-	-	-	0.00	0.00	0.01	0.01	0.00	0.00	0.00	0.00	0.03	0.99
	5	5.5	5.25	-	-	-	-	-	0.00	0.00	0.00	0.00	0.00	0.00	0.00	0.01	1.00
	5.5	6	5.75	-	-	-	-	-	-	0.00	0.00	0.00	0.00	0.00	0.00	0.00	1.00
	6	6.5	6.25	-	-	-	-	-	-	0.00	-	0.00	-	-	0.00	0.00	1.00
	6.5	7	6.75	-	-	-	-	-	-	-	-	-	-	-	-	-	1.00
		sum		-	0.00	0.01	0.11	0.26	0.23	0.17	0.12	0.07	0.03	0.01	0.00	1.00	

Figure E.3: Scatterplot presenting relative sediment transport per wave condition.

Now wave classes are grouped manually. The grouping is based on finding groups with an almost equal weight to sediment transport. Groups of wave conditions can be seen in the table of Figure E.4 outlined in green.

				4.00	5.00	6.00	7.00	8.00	9.00	10.00	11.00	12.00	13.00	14.00	15.00		
	lower	upper	Average	5.00	6.00	7.00	8.00	9.00	10.00	11.00	12.00	13.00	14.00	15.00	16.00	sum	cum sum
Wave height H_{s} (m)	0	0.5	0.25	-	-	-	-	-	-	-	-	-	-	-	-	-	-
	0.5	1	0.75	-	-	0.00	0.00	0.00	0.00	0.00	-	-	-	-	-	0.00	0.00
	1	1.5	1.25	-	-	0.00	0.00	0.00	0.00	0.00	0.00	0.00	-	-	-	0.01	0.01
	1.5	2	1.75	-	0.00	0.00	0.01	0.02	0.02	0.01	0.00	0.00	0.00	-	-	0.08	0.08
	2	2.5	2.25	-	-	0.01	0.04	0.05	0.05	0.04	0.02	0.01	0.00	0.00	-	0.20	0.28
	2.5	3	2.75	-	-	0.00	0.04	0.07	0.05	0.04	0.03	0.01	0.00	0.00	-	0.26	0.54
	3	3.5	3.25	-	-	-	0.02	0.06	0.05	0.04	0.03	0.02	0.01	0.00	0.00	0.21	0.75
	3.5	4	3.75	-	-	-	0.00	0.03	0.03	0.02	0.02	0.01	0.01	0.00	0.00	0.14	0.89
	4	4.5	4.25	-	-	-	-	0.01	0.02	0.01	0.01	0.01	0.01	0.00	0.00	0.07	0.96
	4.5	5	4.75	-	-	-	-	0.00	0.00	0.01	0.01	0.00	0.00	0.00	0.00	0.03	0.99
	5	5.5	5.25	-	-	-	-	-	0.00	0.00	0.00	0.00	0.00	0.00	0.00	0.01	1.00
	5.5	6	5.75	-	-	-	-	-	-	0.00	0.00	0.00	0.00	0.00	0.00	0.00	1.00
	6	6.5	6.25	-	-	-	-	-	-	0.00	-	0.00	-	-	0.00	0.00	1.00
	6.5	7	6.75	-	-	-	-	-	-	-	-	-	-	-	-	-	1.00
		sum		-	0.00	0.01	0.11	0.26	0.23	0.17	0.12	0.07	0.03	0.01	0.00	1.00	

Figure E.4: Wave conditions grouped manually based on equal contribution to sediment transport.

Per group of blocks the integrated weighted contribution to sediment transport can be determined by the summation of the values of sediment transport found in Figure E.2. The next step is to find the representative condition per selected group. The representative significant wave height (H_s) and peak period (T_p) are the "centre of gravity" of each group. Now the upscaled weight (per group j) can be calculated with:

$$F_{up,j} = \frac{S_{p,j}}{P(H_{s,rep,j}, T_{p,rep,j}) \cdot S(H_{s,rep,j}, T_{p,rep,j})} \tag{E.1}$$

In this equation $S_{p,j}$ is the amount of sediment transport induced by the wave group j. P is the probability of occurrence of the representative wave condition of group j. $S(H_{s,rep,j}, T_{p,rep,j})$ is the amount of sediment transport caused by the single wave condition that is later used to represent the entire wave group j.

The resulting conditions (17 in total) are presented in table E.1 below. Freq is the frequency of occurrence of the group of wave conditions of which the representative wave peak period and significant wave height have been chosen. Freq(original) is the original frequency of occurrence of that specific wave condition. F_{up} is the upscaling factor with which the impact of a wave conditions is scaled up.

Table E.1: Upscaling per wave condition after application of input reduction

$H_{s,rep}$	$T_{p,rep}$	Freq	Freq(original)	F_{up}
2.25	7.5	9.18%	5.76%	1.59
2.75	7.5	5.61%	3.95%	1.42
1.75	9.5	18.06%	6.05%	2.99
2.25	8.5	7.67%	7.67%	1.00
2.75	8.5	6.73%	6.73%	1.00
3.25	8.5	3.85%	3.85%	1.00
4.25	9.5	1.59%	0.49%	3.26
2.25	9.5	6.91%	6.91%	1.00
2.75	9.5	4.87%	4.87%	1.00
3.25	9.5	2.93%	2.93%	1.00
3.75	9.5	2.74%	1.30%	2.10
2.25	10.5	7.90%	5.25%	1.50
2.75	10.5	6.07%	3.58%	1.69
3.25	10.5	3.65%	2.16%	1.69
3.75	12.5	2.95%	0.60%	4.88
4.25	12.5	1.67%	0.29%	5.67
2.75	12.5	4.10%	1.04%	3.92

The total scaled duration is now 96.48%, which is not a large reduction. The number of wave conditions however is reduced to 17 conditions to represent the entire wave climate.

Important to notice is that the wave conditions are offshore conditions (not nearshore). With the SWAN model set-up described in section 8.2 these conditions can be translated to nearshore conditions.

E.2 Influence of Tp

Note that the input reduction technique is purely based on the influence of the significant wave height to sediment transport. In section 6.2.1 it was pointed out that the peak period of waves has a significant influence on the erosion rate of the seawall. In section 9.2.5 the relationship between Hs and Tp is investigated for the wave record offshore Southern Coastal Mine Namibia. A higher value of Tp leads to a higher erosion rate.

Appendix F – Assessment of parameters in XBeach simulations

As mentioned in section 9.2.4, long-term simulations were carried out in the 1D XBeach Model to assess the influence and reliability of different parameters.

The cross-shore profile of the bed is presented in Figure F.1. This profile was formed using data from the survey of NAMDEB carried out in October 2014. Mild wave conditions lead to breaker bar, which is clearly visible in Figure F.1. Between the breaker bar and the +2m contour line, there is a data gap. Due to the combination of breaking waves and shallow water, a waterbourne survey cannot be carried out with the techniques available. Also the exact position of the seawall on the beach is not known. Left in the figure one can see a steep straight part, where the bed is dipping from -15m to -30m waterdepth. This is added to the existing data to make sure the hydrodynamic boundary conditions are not affected to much when they enter the computational domain.

The straight line between breaker bar and +2m contour is most probably not a straight line in the real situation. Simulations will result in a more realistic profile of the upper shoreface.

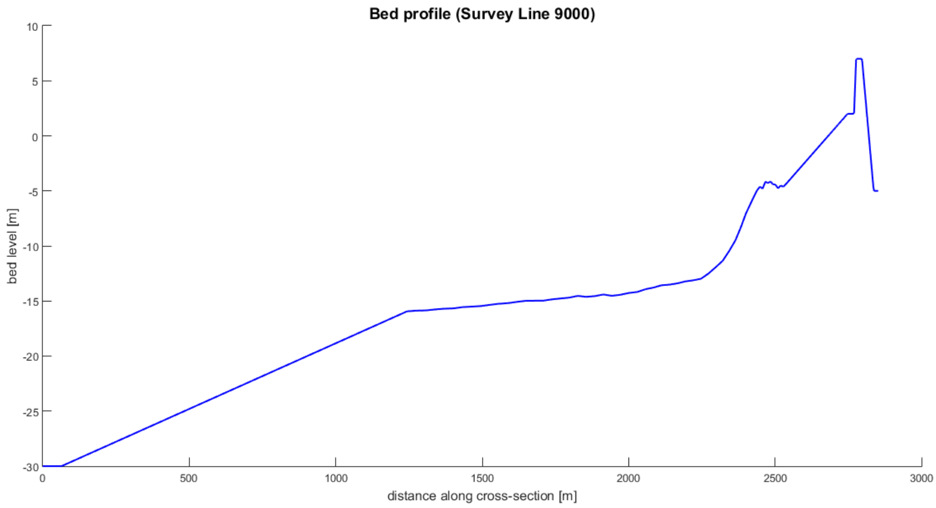

Figure F.1: 1D cross-shore bedprofile of Survey Line 9000 of the Southern Coastal Mine Namibia

F.1 Important parameters in the modelling process

The following cases/parameters are assessed:

- Different wave conditions
- Different grainsize distributions
- Additional onshore sediment transport (Facua-coefficient)

- Different positions of the seawall on the beach
- Influence of different wave peak periods (Tp)
- Influence of different wave directions

To present the results, from now on only the shallow part of the bed profile (so the upper shoreface) is visualized. For all simulations a simulation time of 10 days was used, thereby applying a morphological acceleration factor (Morfac) of 10, so in the end the model accounts for 100 days of morphological evolution.

F.1.1 Different wave conditions

The survey that was done to obtain the bathymetry data, was during very mild wave conditions (verified with wave records). Different sequences of rather mild wave conditions were simulated in XBeach.

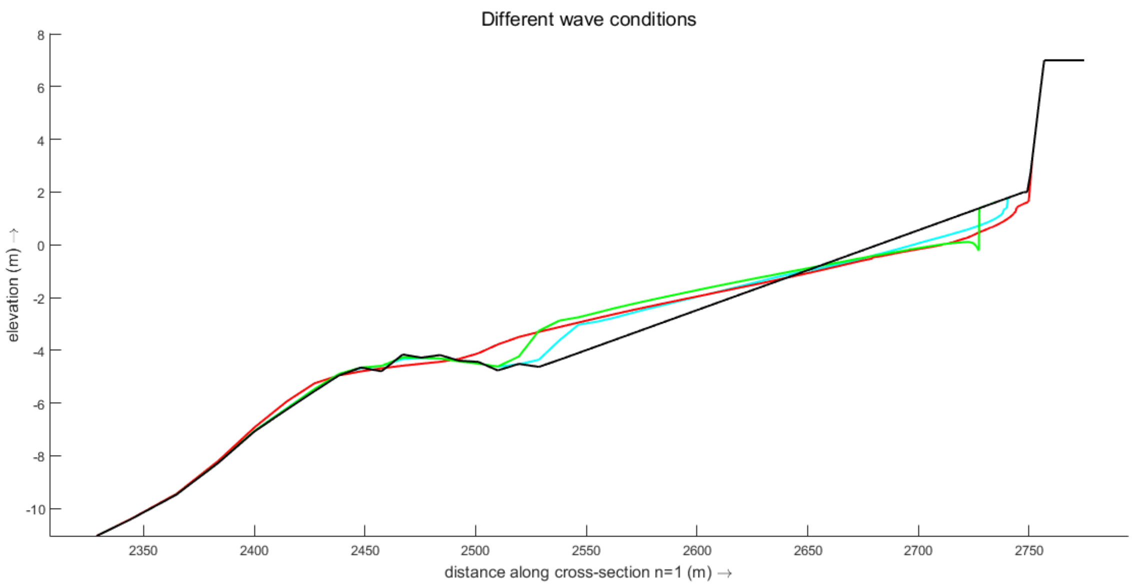

Figure F.2: Coloured lines (representing different mild wave conditions) showing the changes in bed level after 100 days. The red line shows the least mild conditions, the green line the mildest wave conditions.

Under a little less mild conditions (red line in Figure F.2), the breaker bar is already being smoothed out. The climate is highly energetic. The breaker bar will not always be present.

The line in blue (cyan) seems to follow the outline of the breaker bar the closest. For this reason the combination of wave conditions associated with this line are used in assessing other parameters.

F.1.2 Different grainsize distributions

Different grainsize distributions were tested in XBeach, since the grainsize distribution is unknown (see section 2.5). Figure F.3 presents the resulting bed profiles for simulations with different grainsize distributions. Ratio D_{50}/D_{90} is kept constant on 0.667 (discussed in section 9.2.3). The cyan line represents coarse sediment (D_{50} = 800 μm). The green line represents less coarse sediment (D_{50} = 500 μm). The red line represents medium sediment (D_{50} = 300 μm), this is the default setting for sand in XBeach. The orange line represents fine sediment (D_{50} = 200 μm).

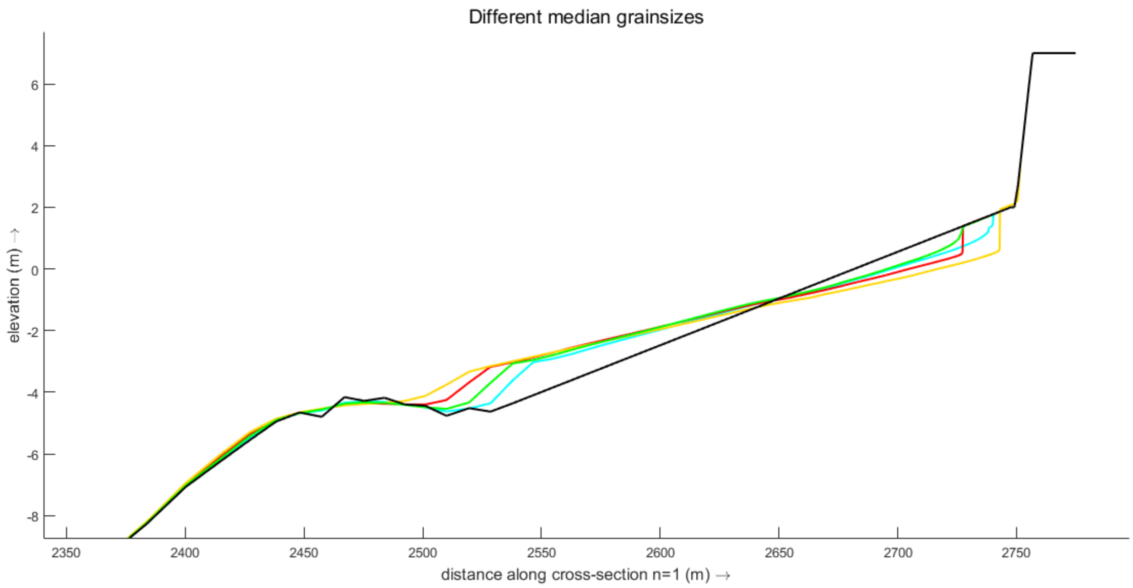

Figure F.3: Coloured lines (representing different grainsize distributions) showing the changes in bed level after 100 days. From coarse to fine sand: Cyan - Red - Green - Orange

The results of grainsize distributions vary a lot. From the figure it can be concluded that the finer the sediment, the more erosion one can expect. For very fine sediment (orange line in figure F.3) erodes away. The beach of the Southern Coastal Mine is said to consist of coarse sediment (also mentioned in section 2.5). Taking the coarsest grainsize distributions from the simulations might lead to an underestimation of beach erosion. Therefore a D_{50} of 500 μm is chosen.

F.1.3 Accounting for onshore sediment transport

The calibration factors f_{Sk} and f_{As} (implemented together in XBeach as the Facua-coefficient) account for extra onshore transport due to wave skewness and wave asymmetry. XBeach doesn't simulate the wave shape. The discretization of Van Thiel de Vries (2009) can be used to account for the affected sediment advection velocity (u_a). The factor Facua is a function of wave skewness and wave asymmetry. A higher factor simulates more onshore sediment transport.

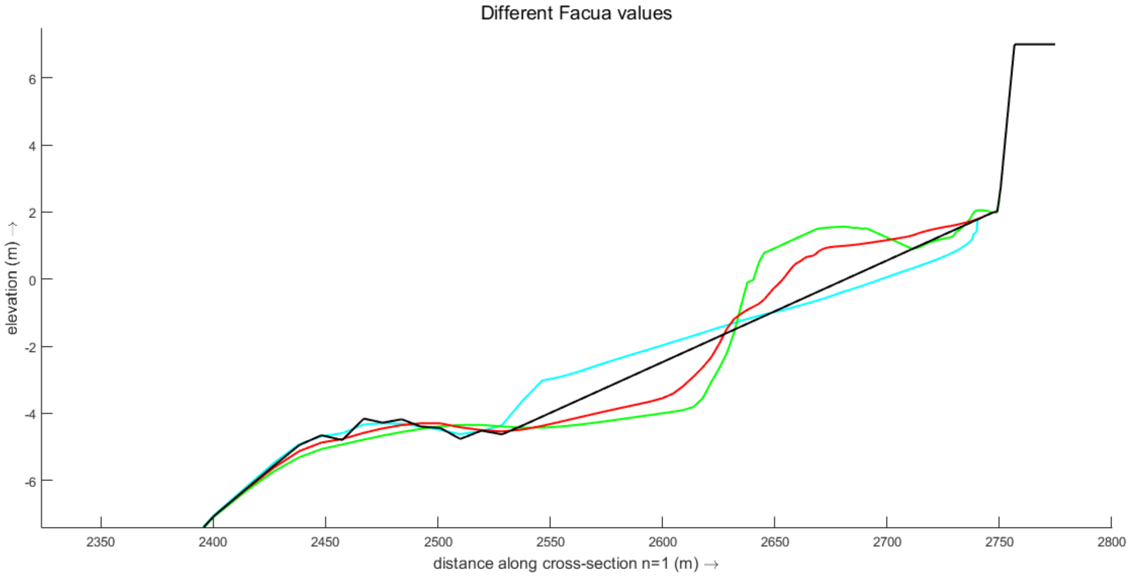

Figure F.4: Colored lines (representing different values of Facua) showing the changes in bed level after 100 days. Cyan line: Facua = 0. Red line: Facua = 0.5. Green line: Facua = 1.0.

The results of simulations with different values for Facua (Figure F.4) differ a lot. Also the shape of the beach changes completely under different values of Facua. The green line seems to be very unrealistic, but a profile as formed by the red line in Figure F.4 (Facua = 0.5) is not ruled out on beforehand.

In case of the Southern Coastal Mine a Facua seems important to apply. As mentioned in section 6.2.2 about hydrodynamics, large swell waves approach the shore and impact the upper shoreface. For short term simulations, where single storm conditions are tested, accounting for extra onshore sediment seems to be less relevant. In that case we are only interested in erosion of the seawall. A too high Facua-coefficient can lead to an underestimation of erosion since it may lead to a shallow surf zone and thus more wave energy dissipation.

F.1.4 Position of the seawall on the beach

The exact position on the beach of the toe of the seawall has been derived from pictures. For Line 9000 (the cross shore profile of interest) the toe coincides probably with the +2m contour of the beach. In Figure F.5 the seawall is shifted landwards to compare the bed level changes with the situation for which the seawall is in its 'normal' position (on the +2m contourline of the beach). To visualize the results better, the water level has been raised in the simulation to make sure some waves would reach the toe of the seawall.

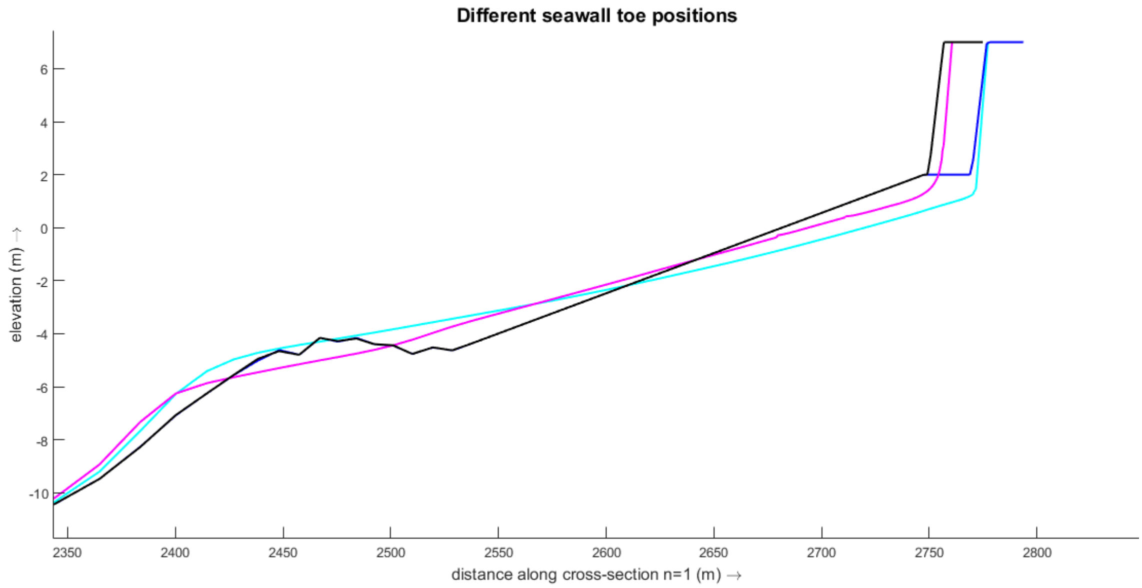

Figure F.5: Colored lines (representing different positions of the seawall on the beach) showing the changes in bed level after 100 days. Blue line: Tp = 12.5 s. Red line: Tp = 7.5 s.

The bed level changes are different. This can be seen the easiest when looking at the location of the breaker bar. If we zoom in (Figure F.6) it becomes clear that the amount of erosion is much larger when the seawall is closer to the water.

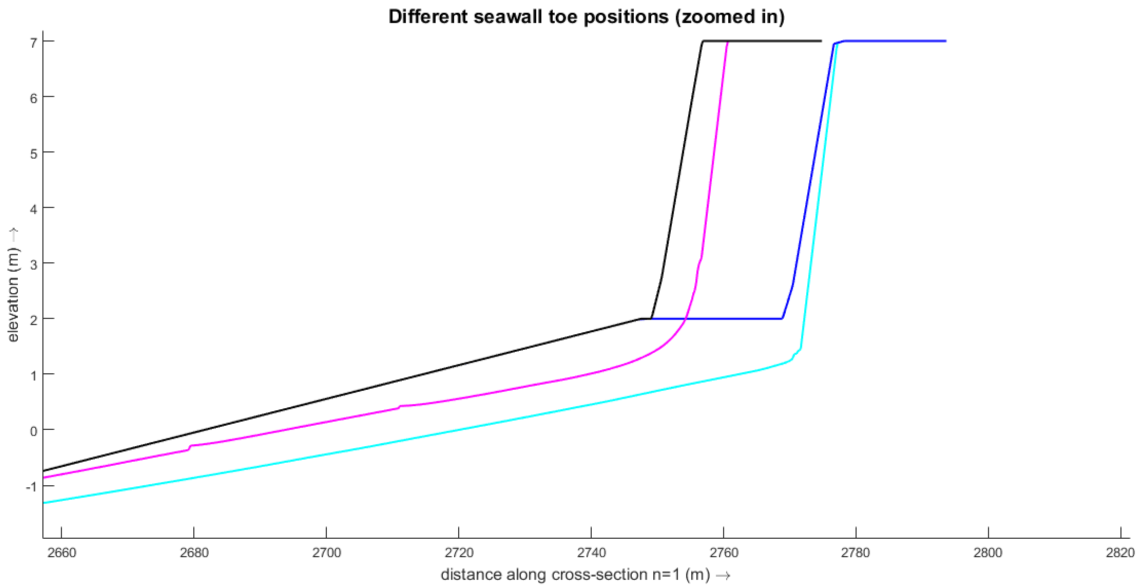

Figure F.6: Colored lines (representing different peak periods for the wave conditions) showing the changes in bed level after 100 days. Blue line: Tp = 12.5 s. Red line: Tp = 7.5 s.

F.1.5 Influence of different wave peak periods (Tp)

Figure F.7 presents two simulations with the same settings, except for the peak period of the waves entering the domain. The blue line represents the resulting bed profile for a simulation with a peak period (Tp) of 12.5 seconds. The red line a peak period of 7.5.

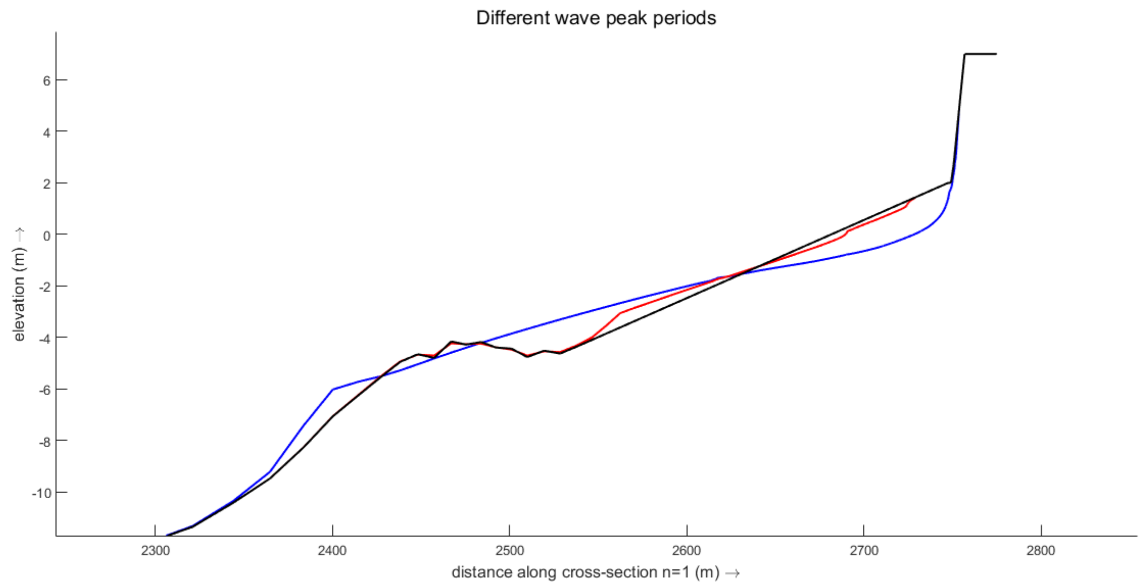

Figure F.7: Colored lines (representing different peak periods for the wave conditions) showing the changes in bed level after 100 days. Blue line: Tp = 12.5 s. Red line: Tp = 7.5 s.

Clearly the effect of Tp on beach erosion is visible. The difference is large. Longer waves (higher value of Tp) carry more energy and lead to more sediment transport. The waves conditions in front of the Southern Coastal Mine are almost equally distributed, in terms of wave peak period between 7.5 and 12.5 seconds (see also the scatterplot in Figure 8.3). Modeling with short waves will lead to an underestimation of the erosion occurring.

F.1.6 Influence of different wave directions

The influence of the main angle of waves approaching the shore is considered to be little. Simulations have been carried out for wave conditions with different main directions in the offshore deep waters. The results are visualized in Figure F.8. Due to the South-West-facing shoreline, waves with an angle of incidence of 220-230 degrees North would approach the shore perpendicularly.

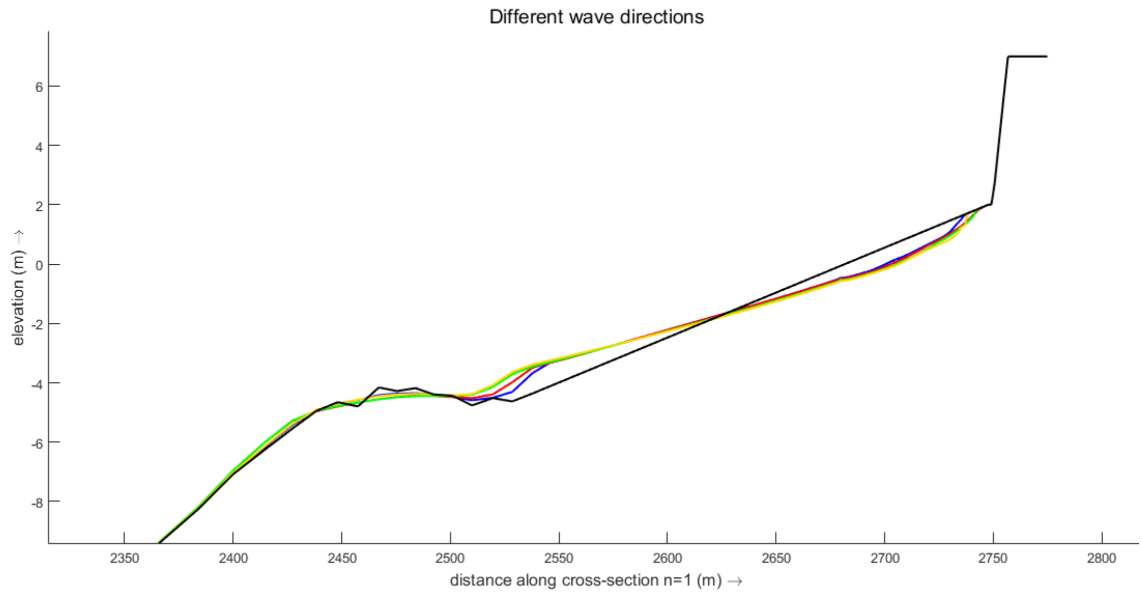

Figure F.8: Colored lines (representing different main directions for the wave conditions) showing the changes in bed level after 100 days. Blue line: Dir = 180 degrees North. Red line: Dir = 210 degrees North. Green line: Dir = 240 degrees North. Orange line: Dir = 270 degrees North.

The differences in terms of cross-shore sediment transport are small. This is due to the fact that waves are refracted to the shoreline when they reach shallower waters. The process of refraction is explained in section 6.2. In front of the Southern Coastal Mine there is a wide area of relatively shallow water, which is favorable for refraction. In the end all waves will approximately reach the shore from the same angle.

Appendix G – Design conditions for the seawall

In this section the storm conditions for which a seawall needs to be designed are given. Also the methodology used to find these conditions is explained.

G.1 Determination of the significant wave height associated with the design storm conditions

G.1.1 Frequency design conditions

The design lifetime of a seawall in the Southern Coastal Mine Namibia varies but is taken as 2 years. After 2 years, the beach in front of the seawall will have accrued far enough so that the wave attack on the seawall is only minor. Or, the seawall has already been moved further seawards. The probability of serious damage during the lifetime of the seawall is given by the following Poison distribution (see Verhagen et al. (2009)):

$$p = 1 - e^{-fT} \tag{G.1}$$

Where p is the probability of occurrence of a design storm during the lifetime of a seawall, f the frequency of the event per year and T the life time of the seawall. If we state that the Serviceability Limit State (SLS) can be exceeded with a probability of 50% during lifetime of the seawall, which is rather low, the storm frequency becomes f=0.347 per year. So the design storm should have a return period of at least 3 years.

For the Ultimate Limit State (ULS) this probability must be lower. The norm can be chosen based on economic considerations. The ULS is exceeded when the seawall can no longer fulfill its function as flood defense for the mine behind the seawall. A more extensive distinction between ULS and SLS was made in 10.1.

G.1.2 Peak over Threshold method

The seawall must be designed to withstand certain storm conditions. A storm condition is defined in this case as the combination of wave height and wave period with a duration of 24 hours. Due to refraction, the wave direction will not play a significant role. The probability of certain storm conditions or extreme events is determined in this section. Important to mention is that the tide, but also the wind set-up, is of minor influence on a storm, as discussed earlier in section 6.2. Measurement data of sequential wave observations of 10 years with a measuring interval of 6 hours were available for the analysis of waves. Those data were averaged over 24 hours. Figure G.1 and G.2 show that the some of the peaks in the data are smoothened, but that this effect is very little and therefore justified. Zooming in on a part of the time-record (see figure G.3) shows that the averaged line follows the trend of the 6-hour-line very well, since the duration of a storm is always longer than 6 hours (mostly longer than 24 hours).

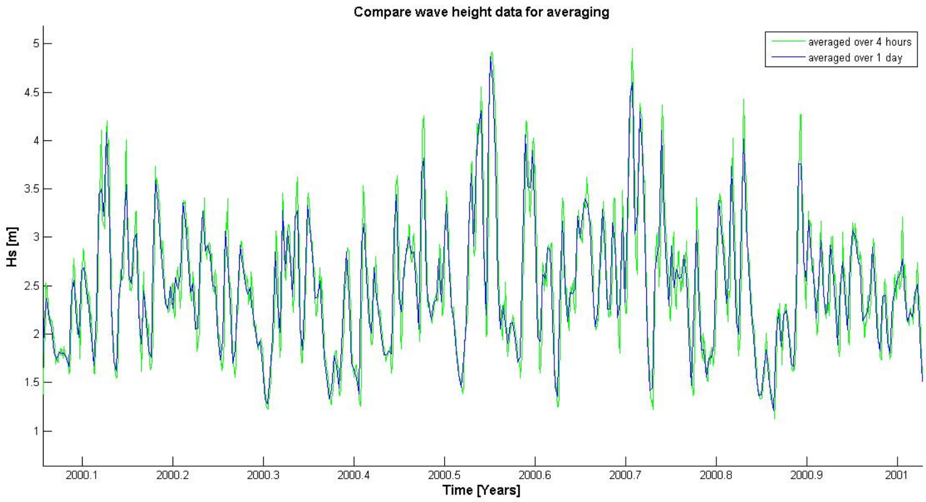

Figure G.1: Comparison of wave height data (Hs) for averaging over 1 day

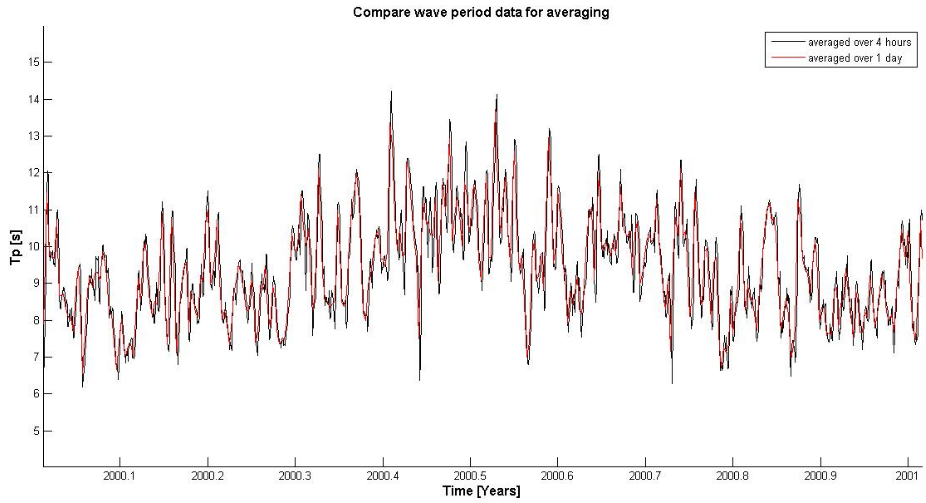

Figure G.2: Comparison of wave period data (Tp) for averaging over 1 day

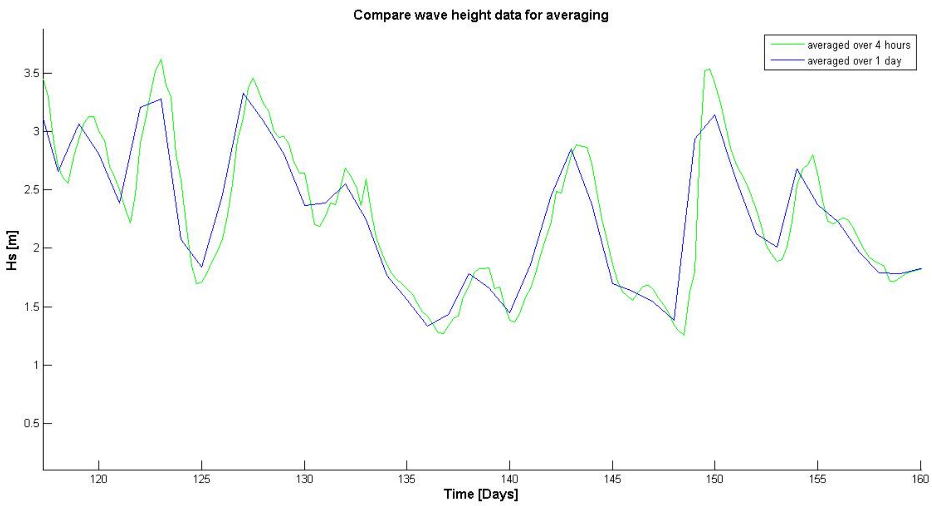

Figure G.3: Wave height data (Hs) averaged over 1 day, zoomed in on a period of 40 days.

The reduced data set contains only storm events. We are however interested in the more extreme events. To analyze those, a threshold is chosen for the significant wave height. Later in this section the effect of a chosen threshold on the results is discussed. Figure G.4 shows all storm events above the threshold of Hs = 4 m. This reduces the data from 3650 events to 119 storm events (12 storms per year).

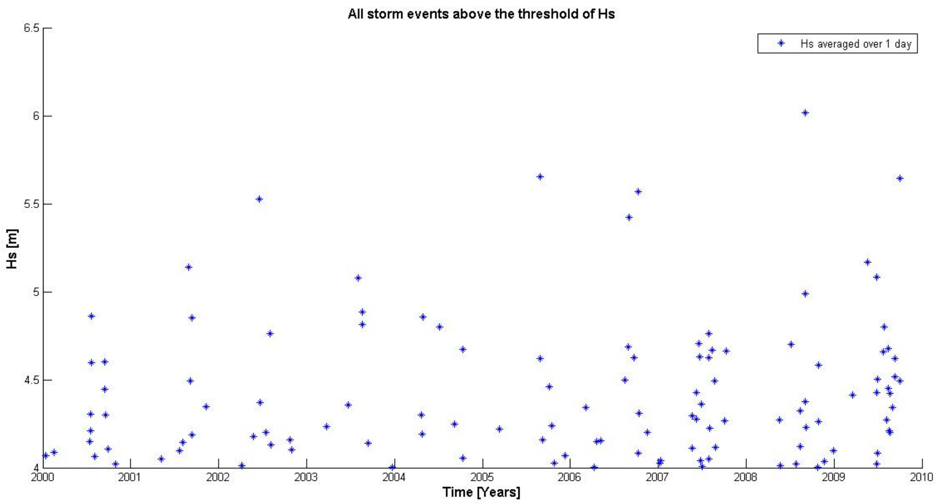

Figure G.4: Wave conditions with a duration of 24 hours exceeding a significant wave height of 4m

The probability of occurrence (P) of each event and the probability of exceedance (Q) can be calculated.

$$P = P(H'_{ss} \leq H_{ss}) \quad \text{(G.2)}$$

$$Q = Q(H'_{ss} > H_{ss}) = 1 - P \quad \text{(G.3)}$$

Table G.1 shows the probabilities for each wave bin above the threshold.

Table G.1: Wave data Southern Coastal Mine Namibia. Threshold (significant wave height) of 4 m

Wave height class		Number of storms			
Lower limit	Upper limit	per bin	cum.	P	Q
0	0.5	0	0	0	1
0.5	1	0	0	0	1
1	1.5	0	0	0	1
1.5	2	0	0	0	1
2	2.5	0	0	0	1
2.5	3	0	0	0	1
3	3.5	0	0	0	1
3.5	4	0	0	0	1
4	4.5	81	81	0.680672269	0.319327731
4.5	5	28	109	0.915966387	0.084033613
5	5.5	5	114	0.957983193	0.042016807
5.5	6	4	118	0.991596639	0.008403361
6	6.5	1	119	1	0
6.5	7	0	119	1	0
7	7.5	0	119	1	0
7.5	8	0	119	1	0
8	8.5	0	119	1	0

The probabilities are extrapolated to find the design condition. Evaluations have been done as if the data were distributed as an exponential distribution, a Gumbel extreme value distribution and a Weibull extreme value distribution.

Exponential distribution

By multiplying the probability of exceedance Q with the number of storms per year N_s, one reads the probability of exceedance of certain conditions per year Q_s. Q_s can be seen as the expected number of storm events per year with a specific storm condition.

Plotting the values of Q_s on a logarithmic scale, as done in Figure G.5, shows that the data events are exponentially distributed.

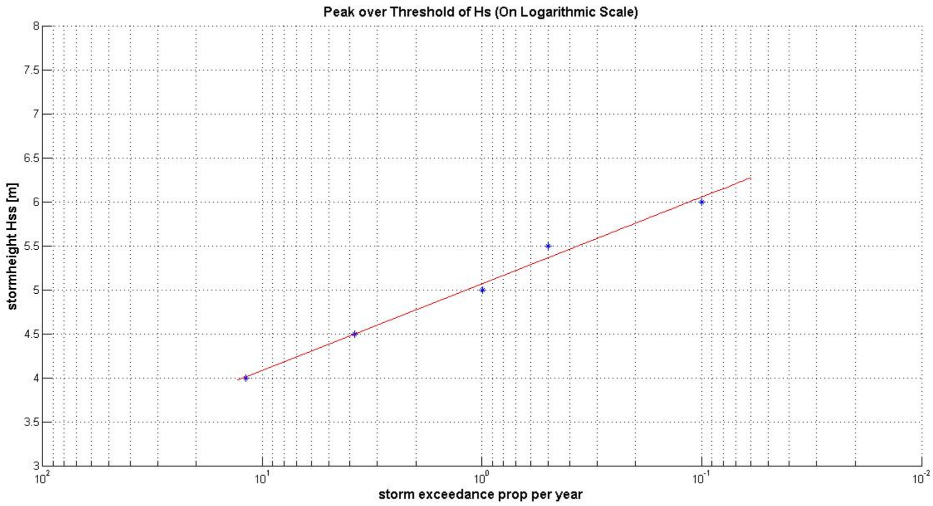

Figure G.5: Exponential distribution of wave conditions

Where the relationship between wave height and exceedance probability is given by:

$$H_{ss} = -\alpha \cdot ln(Q_s) + \gamma \tag{G.4}$$

Extreme value distribution

The analysis done is to extrapolate extreme storm events. For this purpose extreme value distributions, namely the Gumbel distribution and the Weibull distribution, have been evaluated as an alternative to an exponential distribution.

The Gumbel extreme value distribution can be written as:

$$P(H \leq H_{ss}) = Q = \exp\left[-exp\left(-\frac{H_{ss}-\gamma}{\beta}\right)\right] \tag{G.5}$$

This can be translated to a wave height with an exceedance probability per year:

$$H_{ss} = \gamma - \beta \cdot ln(ln(\frac{N_s}{N_s - Q_s})) \tag{G.6}$$

The Weibull extreme value distribution can be written as:

$$P(H_{ss}) = Q = exp\left(-\left[\frac{H_{ss}-\gamma}{\beta}\right]^{\alpha}\right) \tag{G.7}$$

The corresponding significant wave height for a Weibull distribution:

$$H_{ss} = \gamma + \beta \cdot (-ln(Q))^{1/\alpha} \tag{G.8}$$

Both distributions contain a β and a γ. Those two parameters can be found by interpolation of the wave data. The value of α in the Weibull distribution changes the curvature of the best-fit curve through the data points. This value needs to be chosen by expert judgement, meaning that different values have to be tested to see whether the relationship between H_{ss} and $-(ln(Q))^{1/\alpha}$ approaches linearity. A value of $\alpha = 1.25$ seems to give the most linear/straight relationship between H_{ss} and $-(ln(Q))^{1/\alpha}$.

Comparison of distribution functions

The three different distribution functions are evaluated together with the impact of the chosen threshold. Table G.2 shows the wave condition (in terms of significant wave height) for a design storm with a probability of 1/50 per year for different threshold values of Hs. N_s is the number of storms above the threshold value occurring per year. One can see that the value of the chosen threshold is of minor influence to the outcome of the significant wave height, as long as there are multiple storms per year to make extrapolation possible.

Table G.2: Comparison of different distribution functions for different thresholds of H_s. The presented results are the significant wave height [m].

$H_{s,Threshold}$	3	3.5	4	4.5	5	5.5
N_s	85	34	12	4	1	0.5
Exponential	6.8101	6.7649	6.7398	6.7249	6.7017	6.4995
Gumbel	6.7318	6.7146	6.7117	6.7252	6.4381	12.7913
Weibull	6.6126	6.6178	6.6386	6.6761	6.4276	10.4445

Table G.3 presents the gamma value for each distribution function in case of different thresholds. The gamma value theoretically represents the threshold value $H_{s,Threshold}$. So the extreme value distributions give a much better result than the exponential distribution function. This becomes even more important when there is only a low number of storms available in the database.

Table G.3: Comparison of γ-values for the three different distribution functions for different thresholds of H_s.

$H_{s,Threshold}$	3	3.5	4	4.5	5	5.5
Exponential	5.061	5.064	5.069	5.074	5.088	5.284
Gumbel	3.2054	3.6286	4.0886	4.5746	5.4027	0
Weibull	2.81	3.2561	3.7389	4.2458	5.19	0

Table G.4 contains the values of the wave condition (in terms of significant wave height) for different design storms (probability of occurrence per year). The threshold value of Hs is 4 m ($N_s = 12$).

Table G.4: Comparison of H_{ss}-values for the three different distribution functions. (Threshold of H_s is 4m).

Design storm	1/1	1/2	1/5	1/10	1/50	1/100
Exponential	5.069	5.365	5.7564	6.0524	6.7398	7.0359
Gumbel	5.0875	5.3813	5.7629	6.0493	6.7117	6.9966
Weibull	5.0973	5.3939	5.7668	6.0376	6.6386	6.8877

It is easy to notice that the results for the different distribution functions that were tested are close to each other. The results from the Gumbel extreme value distribution are the most extreme. Therefor these values probably lead to the most conservative approach for extreme events. Also, the Weibull distribution has more variables and is therefor less reliable for the little amount of wave data available above the threshold. The Gumbel distribution can be plotted on a logarithmic scale, as done in Figure G.6.

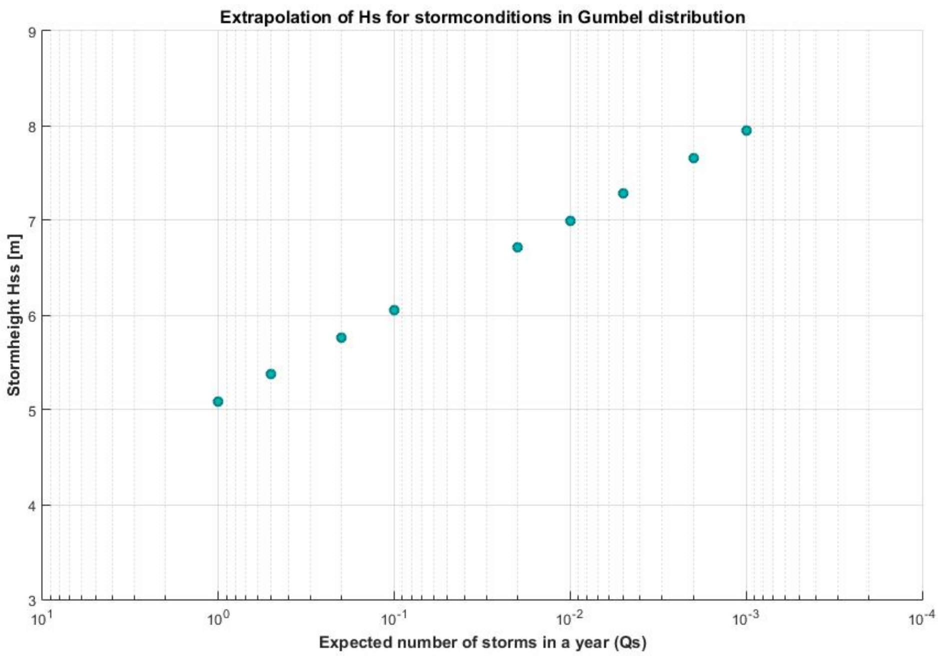

Figure G.6: Wave heights, according to the Gumbel distribution, belonging to certain probabilities of occurrence.

Note that the Hss with a probability of 1/10 per year, is the highest significant wave height that occurred during the wave observation of 10 years. What also should be noticed is that the significant wave heights that have a probability of 1/100 or less per year can be on a different place in the graph.

G.2 Wave peak period (Tp) of design storm conditions

In section 9.2.6 it becomes clear the wave peak period has a significant influence on the cross-shore sediment transport gradient. Below is explained how the wave peak period of the design storm conditions is found, by studying the relationship between wave height and wave period.

The same wave record that was used to find the design wave height is used to find the relationship between significant and wave peak period. This is done to find the peak period (Tp) belonging to the design storm conditions. By plotting the all recordings the following figure is obtained (Figure G.7). A best-fit curve very roughly describes the relationship between significant wave height and wave peak period.

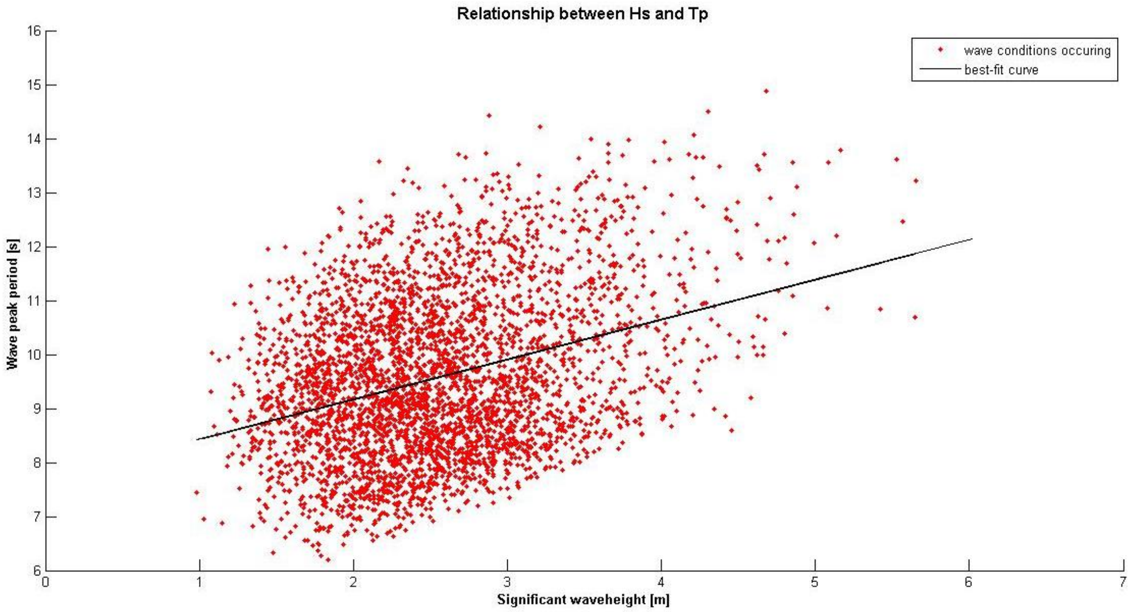

Figure G.7: Graph showing a 10 year wave record, with a trend-line through the data points. (Significant wave height H_s and wave peak period T_p)

Following the best-fit curve of Figure G.7 to find the wave peak period belonging to the significant wave height of the design storm will most definitely lead to an underestimation of the peak period and thus the wave energy and the seawall erosion. Moreover, the scatterplot of Figure G.7 shows that there is no real relationship between Hs and Tp. To narrow down the scatterplot, thresholds can be chosen so one can come to a (very weak) relationship. Since we are interested in extreme events, taking only values above a certain threshold is justified.

The choice of threshold has a lot of influence on the result of Tp. In other words, the relationship between Hs and Tp, obtained by curve-fitting, is very sensitive to the chosen threshold. With data above the threshold of Hs = 4.5m (and Tp = 11.5s) the following results are get (Figure G.8 and table G.5):

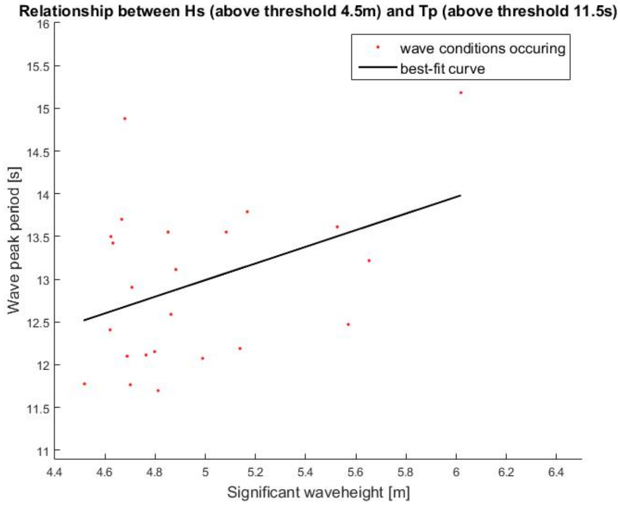

Figure G.8: Relationship between significant wave height H_s and wave peak period T_p for data above the threshold of Hs = 4.5m and Tp = 11.5s.

The relationship between Hs and Tp is now prescribed by:

$$T_p = 0.9727 \cdot H_s + 8.1271 \tag{G.9}$$

Table G.5: Values of wave peak period associated with significant wave height for data above the threshold of Hs = 4.5m and Tp = 11.5s.

Design storm	1/1	1/2	1/5	1/10	1/50	1/100
H_s [m]	5.0875	5.3813	5.7629	6.0493	6.7117	6.9966
T_p [s]	13.0754	13.3612	13.7324	14.0109	14.6552	14.9323

The data of table G.5 will be used in modelling a storm event. One can see, by studying the scatterplots in Figure G.7 and Figure G.8, that the relationship between Hs and Tp is very weak. A rather large standard deviation of 2s for Tp is chosen to cope with the large uncertainties of the relationship.

Offshore wave data

Note that these results present the significant wave height and wave peak period occurring off shore (Longitude: 13.5 degrees, Latitude: -28.5 degrees). They are to be translated to near shore data with the SWAN model (section 8). Also, keep in mind that a storm with a yearly probability of, for example, 1/100 is not a storm that can only occur once per 100 years. With the earlier explained Poisson distribution we can calculate the occurrence of such an event during the lifetime of a seawall. Using equation G.1, we find a probability of 0.0198 for this storm.

Appendix H – Sensitivity analysis of XBeach input parameters

A sensitivity analysis has been carried out to study the influence of certain model parameters. The analysis is solely on the influence of parameters on seawall erosion. A quantitative sensitivity analysis on bed profile changes is out of scope for this research, but an indication can be obtained by looking at figure F.2 to F.8 in Appendix F obtained by long-term simulations.

Each simulation has been done for a period of 10 hours, with an acceleration factor (Morfac) 10. So 100 hours are simulated. Wave conditions are in the range of the design storm conditions (see table 9.3 in section 9.2): Hs = 6m (offshore) and Tp = 13.5 s (offshore). This is very close to the condition with a probability of 1/10 per year, but rounded of for the ease of calculations. No tidal variation is simulated. The effect of tidal variation (different water levels) will have a big impact on the erosion volumes, but is not interesting for this very research. The effect of water level variation will be comparable with the vertical position of the toe of the seawall.

Table H.1 presents the parameters that need to be tested. The maximum variation of each parameter in percentages is based on knowledge obtained from literature and earlier tests. The larger the uncertainty, the larger the chosen maximum variation.

Table H.1: Parameters to be tested in sensitivity analysis. For each parameter the mean, maximum and minimum value are given.

Parameter	**Unit**	**Mean**	**Max variation to be tested (%)**	**Max variation to be tested**	**Left bound**	**Right bound**
Critical angle wet slope	tan(α)	0.26	15%	0.039	0.221	0.299
Critical angle dry slope	tan(α)	1	10%	0.1	0.9	1.1
Median grainsize	μm	400	25%	100	300	500
Facua As	-	0.123	33%	0.04059	0.08241	0.16359
Facua Sk	-	0.375	33%	0.12375	0.25125	0.49875
gamma	-	0.541	33%	0.1785	0.3625	0.7195
Vertical Position Toe Seawall	m (above normal sealevel)	1.5	33%	0.5	1	2
Orientation Coastline	degrees	50.6539335	5%	2.5326967	48.12124	53.18663
Significant wave height	m	6	15%	0.9	5.1	6.9
Wave peak period	s	13.5	15%	2.025	11.475	15.525
Mean wave direction	degrees	210	15%	31.5	178.5	241.5

The sensitivity analysis has been made quantitative by calculating the volume of sand taken away from the seawall at the end of the simulation time. An example is visualized in Figure H.1 and Figure H.2. By extracting the volume underneath the seawall outline of the final state from the volume of the initial state the eroded volume is determined in m^3/m.

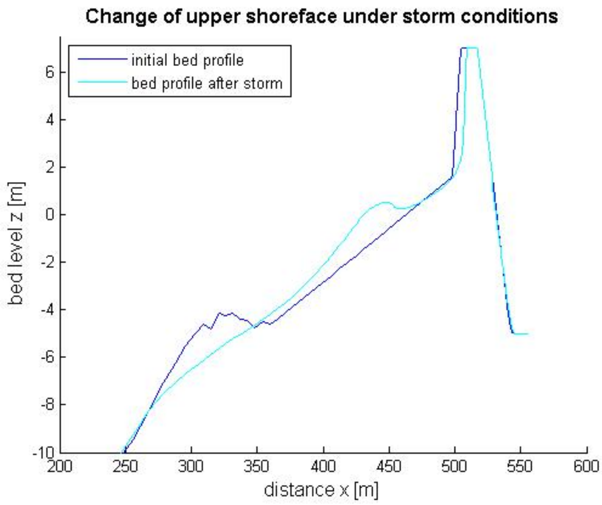

Figure H.1: Example of a simulation to determine the influence of model settings for the 1D XBeach model.

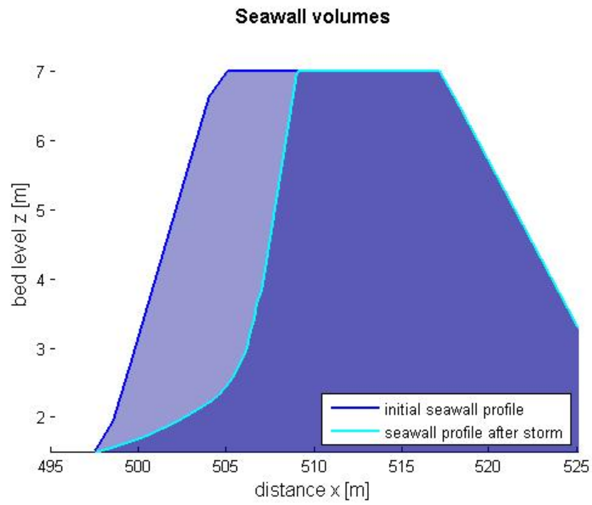

Figure H.2: Same simulation result as in figure H.1. Zoomed in on the seawall to determine the eroded sand volume.

The results of the sensitivity analysis are presented numerically in table H.3 and graphically in the graph of Figure H.4. According to the graph, the relation between erosion volume and any parameter is non-linear (no straight lines appear).

Parameter	-33%	-25%	-20%	-15%	-10%	-5%	0%	5%	10%	15%	20%	25%	33%
Critical angle wet slope				43.801			44.443			44.799			
Critical angle dry slope					43.363		44.443		45.237				
Median grainsize		52.838					44.443					38.439	
Position toe seawall	55.220						44.443						15.669
Orientation Coastline						46.625	44.443	42.099					
Facua	44.545						44.443						28.950
Significant Wave Height (Hs)				23.865			44.443			153.448			
Wave peak period (Tp)				0.443			44.443			150.230			
Mean wave direction				45.250			44.443			13.384			

Figure H.3: Erosion volumes (m^3/m) for varying settings of the 1D XBeach Model.

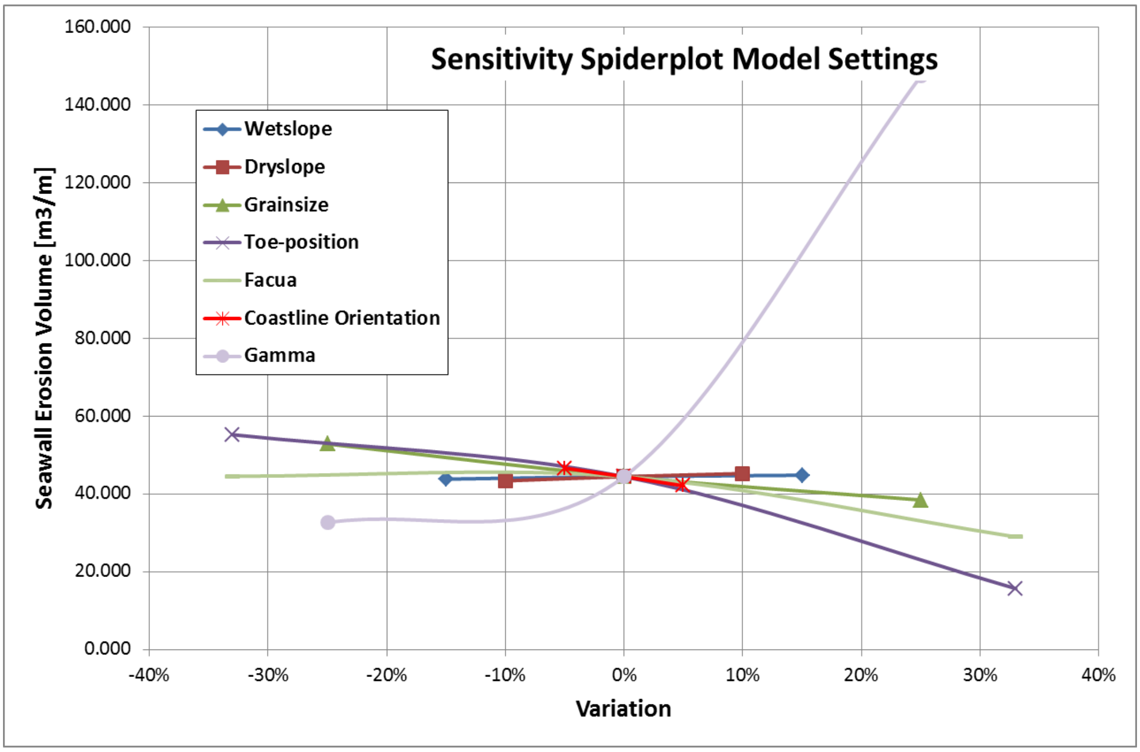

Figure H.4: Spiderplot presenting the result of the sensitivity analysis done for the 1D XBeach Model.

The result (eroded sand volume) is most sensitive to the parameter that with the steepest line in the graph of Figure H.4. This is the gamma, or wave breaking, parameter. A higher value of gamma means that more higher waves are present in shallow water, since they break in a later stage (explained in section 6.1). As a consequence of a higher value for gamma, more waves reach the toe of the seawall and more seawall erosion is present. In section 9.2.4 was explained that a value of 0.541 for gamma would be chosen, according to calibration work done by Deltares (2015) on Dutch beaches. To give a conservative answer, a slightly higher value for gamma is recommended to apply on the Southern Coastal Mine, keeping in mind that the foreshore is rather steep.

The parameter with the second most impact to seawall erosion is the seawall toe position. It is important to mention that the position of the seawall toe will vary a lot along the coastline, but as discussed in section 9.2 the exact location cannot be obtained directly from the bathymetry data provided.

Also the influence of variations in significant wave height, wave peak period and mean wave direction of offshore waves is assessed. These offshore wave data are transformed with the SWAN model to near shore data. Since uncertainties occur in the analysis of available wave data and in the transformation with SWAN, it is important to know how sensitive the XBeach model is to variations in wave input. Simulations have been carried with variations of 15%. The results are shown in the graph of Figure H.5. The effect of variations in significant wave height and wave peak period is very large.

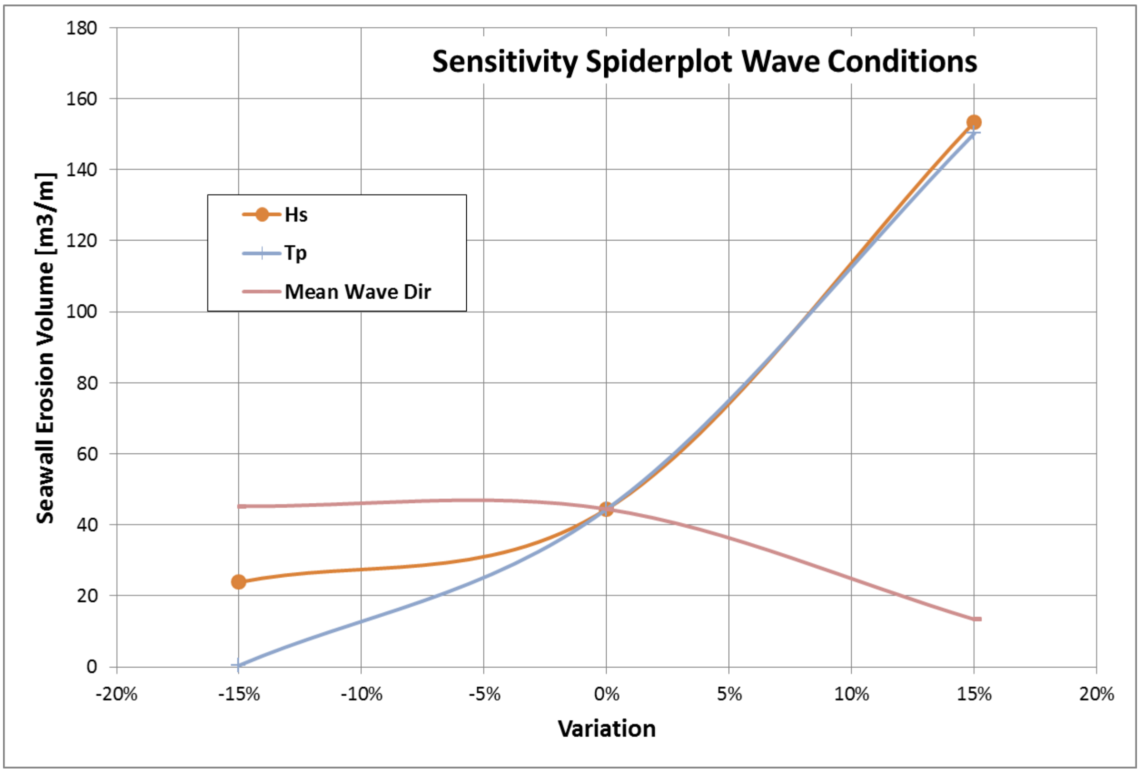

Figure H.5: Spiderplot presenting the impact to the 1D XBeach Model, due to variations in wave conditions.

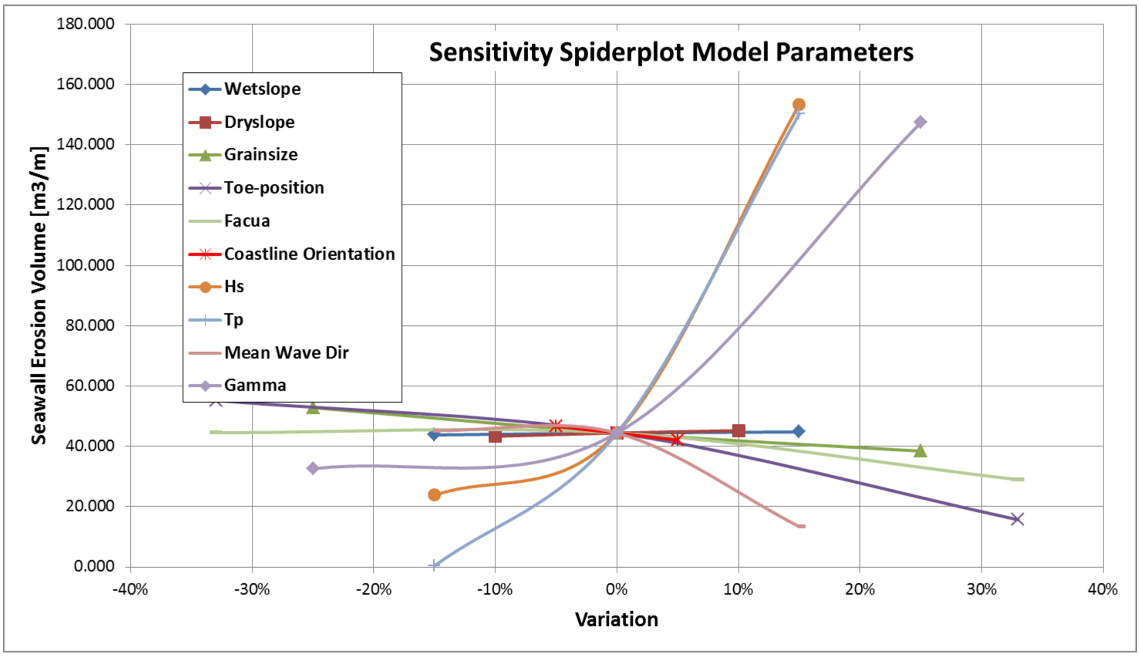

Figure H.6: Spiderplot presenting the influence of all relevant parameters for eroded sand volumes in the 1D XBeach Model.

By plotting the results of the model parameters and the physical parameters in a single plot (Figure H.6), one can see the difference between variations in wave conditions and variations in settings of model parameters. A thorough investigation of wave conditions and an accurate transformation with SWAN are of vital importance for the reliability of the final result, the eroded sand volume.

Appendix I – Storm conditions (May 2015) of Case Study

South Africa - Oranjemund (geoffrey.smith@wspgroup.com) (wave: NWW3 50 km 27.5. 2015 00 UTC) [Options]

Forecast | 2D | Map | Webcams | Wind reports

GFS 27 km 26.05.2015 18 UTC	Tu 26. 20h	We 27. 05h	We 27. 08h	We 27. 11h	We 27. 14h	We 27. 17h	We 27. 20h	Th 28. 05h	Th 28. 08h	Th 28. 11h	Th 28. 14h	Th 28. 17h	Th 28. 20h	Fr 29. 05h	Fr 29. 08h	Fr 29. 11h	Fr 29. 14h	Fr 29. 17h	Fr 29. 20h	Sa 30. 05h	Sa 30. 08h	Sa 30. 11h	Sa 30. 14h	Sa 30. 17h	Sa 30. 20h	Su 31. 05h	Su 31. 08h	Su 31. 11h	Su 31. 14h	Su 31. 17h	Su 31. 20h
Wind speed (knots)	6	7	8	8	8	9	8	9	8	12	14	13	12	5	4	4	5	4	4	3	5	-	8	14	15	20	21	24	26	28	29
Wind gusts (knots)	7	8	10	10	9	11	9	13	10	16	19	16	18	5	5	4	6	5	5	4	6	7	9	20	23	29	31	33	35	38	40
Wind direction	↑	↖	↖	↖	↑	↑	↑	↖	↖	↖	↖	↑	↑	↑	↖	↖	↑	↑	↑	←	↖	-	↑	↑	↖	↖	↖	↖	↖	↖	↖
Wave (m)	-	2	2.1	2.2	2.3	2.3	2.3	2.1	2.1	2	2	2	2.1	2	2	1.9	1.8	1.8	1.7	2.5	3.1	4.1	4.7	5	5.1	5.4	5.3	5.2	5.1	5.1	5.2
Wave period (s)	-	12	11	11	11	11	12	12	12	11	11	12	12	12	12	12	12	12	12	12	15	16	16	16	16	17	16	16	16	16	16
Wave direction	-	↗	↗	↗	↗	↗	↗	↗	↗	↗	↗	↗	↗	↗	↗	↗	↗	↗	↗	↗	↗	↗	↗	↗	↗	↗	↗	↗	↗	↗	↗
Temperature (°C)	15	15	15	15	15	15	15	15	14	15	14	15	15	15	15	15	15	15	15	15	15	-	15	15	15	15	15	15	14	15	15
*0° isotherm (m)	4.2k	4.5k	4.6k	4.6k	4.7k	4.8k	4.8k	4.7k	4.8k	5k	5.1k	5k	5k	5.1k	5.1k	5.1k	5k	5k	4.9k	4.7k	4.7k	-	4.5k	4.4k	4.4k	4k	3.9k	3.9k	3.8k	3.7k	3.6k
Cloud cover (%) high / mid / low	-			9	10			18	9							8	8			48	49	-	30	6							
	-																					-									
*Precip. (mm/3h)	-																					-	-								
Windguru rating										★	★	★	★											★	★★	★★★	★★★	★★★	★★★	★★★	★★★

GFS 27 km 26.05.2015 18 UTC	Mo 01. 05h	Mo 01. 08h	Mo 01. 11h	Mo 01. 14h	Mo 01. 17h	Mo 01. 20h	Tu 02. 05h	Tu 02. 08h	Tu 02. 11h	Tu 02. 14h	Tu 02. 17h	Tu 02. 20h	We 03. 05h	We 03. 08h	We 03. 11h	We 03. 14h	We 03. 17h	We 03. 20h	Th 04. 05h	Th 04. 08h	Th 04. 11h	Th 04. 14h	Th 04. 17h	Th 04. 20h	Fr 05. 05h	Fr 05. 08h	Fr 05. 11h	Fr 05. 14h	Fr 05. 17h	Fr 05. 20h
Wind speed (knots)	26	22	16	12	4	8	16	18	20	15	18	22	27	25	24	22	18	15	8	3	4	4	11	14	21	19	17	18	17	17
Wind gusts (knots)	36	30	22	15	5	9	22	25	29	26	34	38	36	34	32	30	26	22	8	4	5	5	13	19	29	26	22	23	22	24
Wind direction	↖	↖	↖	↖	↑	↘	↓	↓	↘	↘	↓	↓	↘	↘	↘	↘	↘	↘	↘	↘	↙	↖	↑	↖	↖	↖	↖	↖	↖	↖
Wave (m)	4.9	4.6	4.3	4	3.7	3.5	2.9	2.8	2.7	2.7	3	3.6	3.4	3.1	2.9	2.7	-	-	-	-	-	-	-	-	-	-	-	-	-	-
Wave period (s)	15	14	14	14	14	13	13	13	12	12	12	9	9	8	9	9	-	-	-	-	-	-	-	-	-	-	-	-	-	-
Wave direction	↗	↗	↗	↗	↗	↗	↗	↗	↗	↗	↗	↘	↘	↘	↘	→	-	-	-	-	-	-	-	-	-	-	-	-	-	-
Temperature (°C)	15	14	14	14	14	14	14	14	15	15	15	16	15	15	15	15	15	15	15	15	15	15	15	15	15	15	16	16	16	16
*0° isotherm (m)	3.3k	3.3k	3.3k	3.3k	3.3k	3.3k	2.7k	2.5k	2.4k	2.4k	2.5k	2.6k	2.5k	2.5k	2.6k	2.9k	3k	3.3k	4.2k	4.3k	4.2k	4.2k	4.2k	4.1k	3.9k	3.9k	3.9k	3.9k	3.9k	3.9k
Cloud cover (%) high / mid / low																									85	46			63	73
											62	42	24	12																
											72	70	49	31	46	29	12	8												
*Precip. (mm/3h)											0.4				0.4	0.3														

Figure I.1: Weather forecast for May 26th to June 5th 2015 for Oranjemund, Namibia.

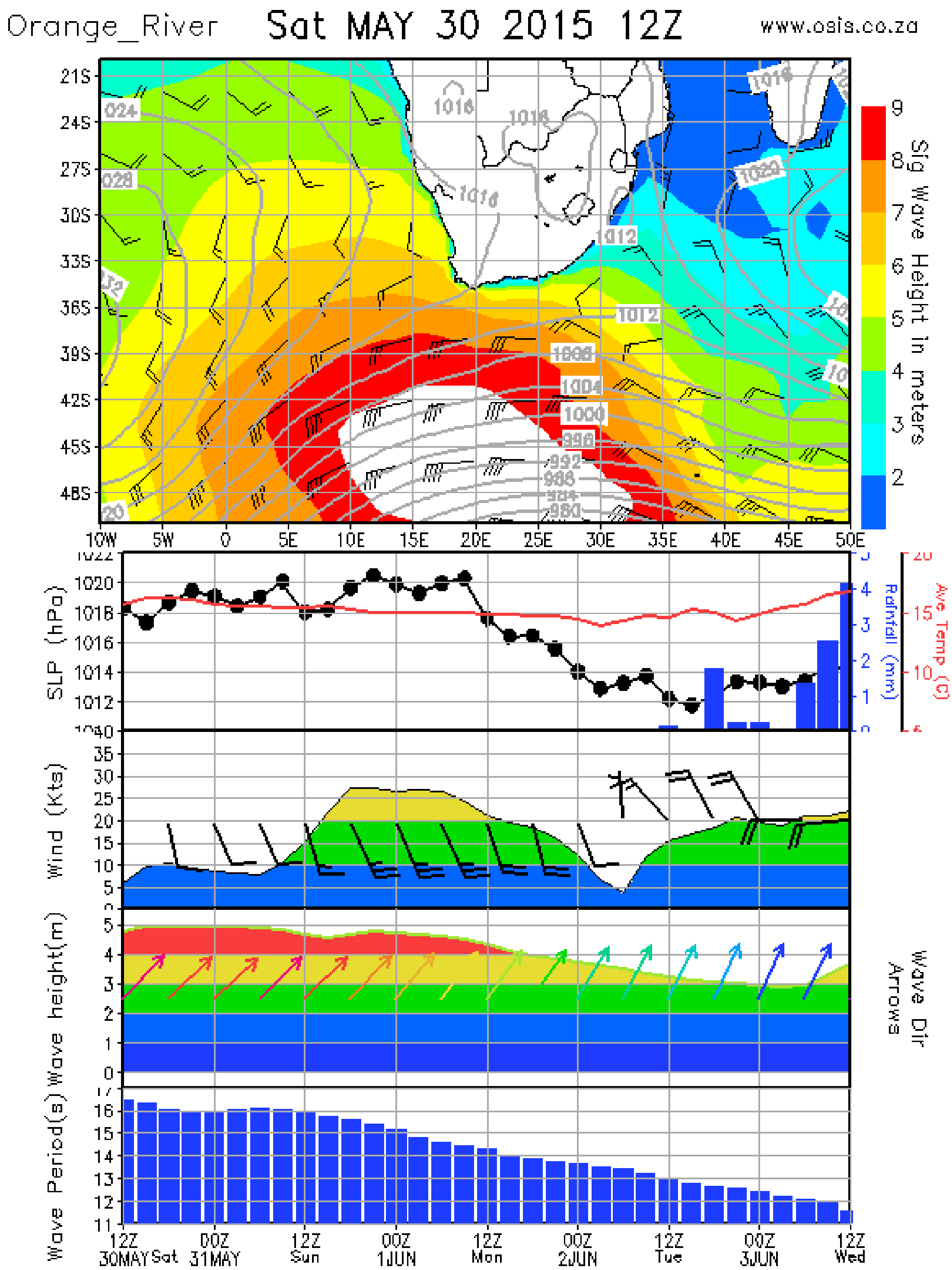

Figure I.2: Wave conditions offshore of the Orange River Mouth, Namibia, on May 29th 2015.

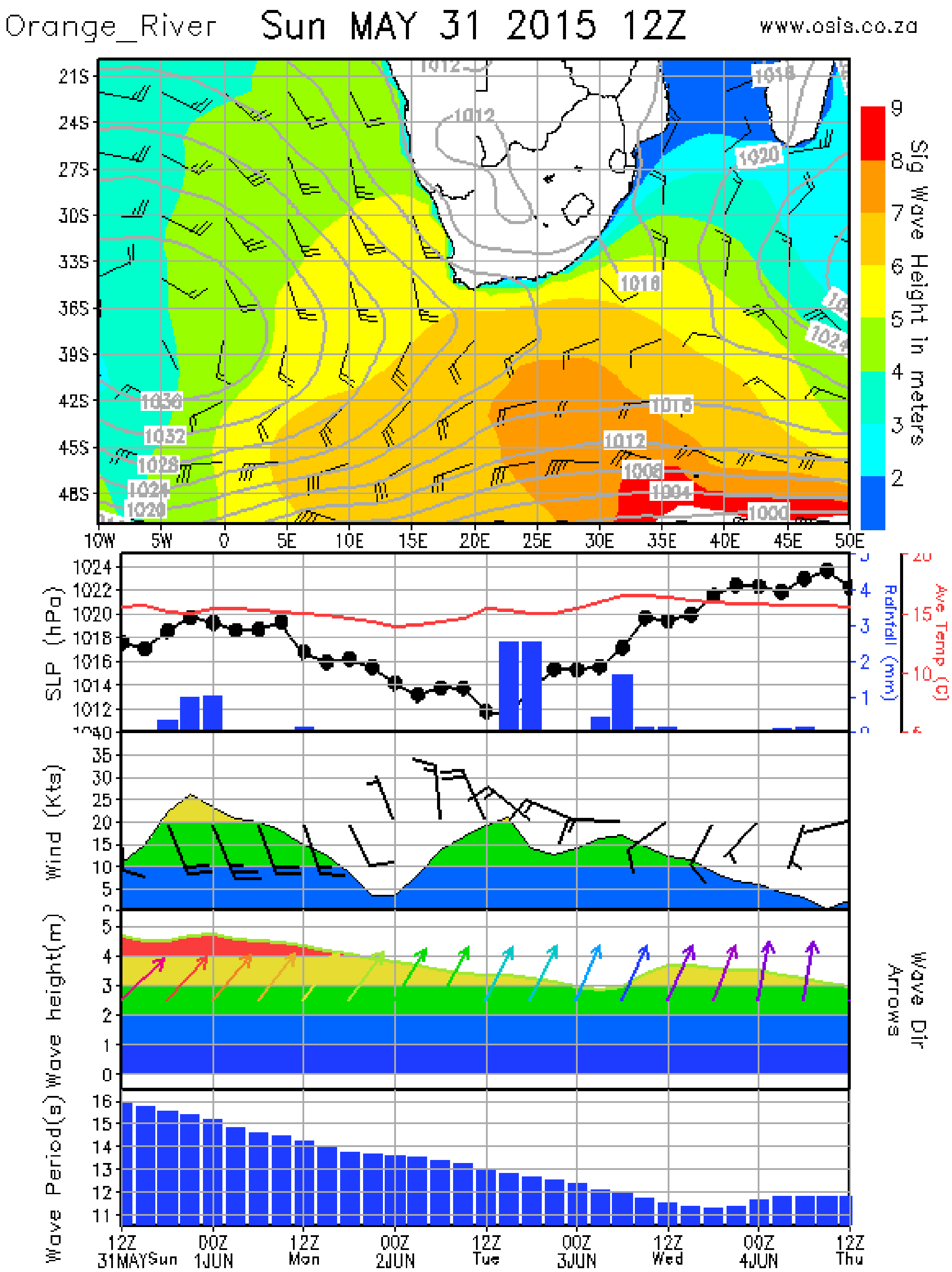

Figure I.3: Wave conditions offshore of the Orange River Mouth, Namibia, on May 30th 2015.

Appendix J – Reliability of a seawall

Whether a seawall design is reliable or not, can be indicated by the probability of failure. This appendix gives a brief overview of the philosophy of different methods, also called calculation levels, to determine the probability of failure. The word level refers to the accuracy of a method. This appendix concludes with stating which method would be most suitable for the design of a seawall in the Southern Coastal Mine Namibia. Appendix K describes how a probabilistic approach can be applied to assess the seawall that is design by an XBeach model.

J.1 Limit state function

The limit state is the state just before failure occurs. Reliability can be defined as the probability that this limit state is not exceeded. The limit state function (or reliability function) is in its most general form:

$$Z = R - S \tag{J.1}$$

Where R is the Resistance to failure, defined by all strength parameters. S is the Sollicitation to failure, defined by all load parameters. The limit state is reached when Z is equal to 0. The probability of failure is:

$$P_f = P(Z \leq 0) = P(S \geq R) \tag{J.2}$$

And consequently the reliability can be described by:

$$P(Z > 0) = 1 - P_f \tag{J.3}$$

J.2 Deterministic approach (Level I calculation method)

The first reliability check of a design, and thus the standard approach used, is the deterministic approach. This approach compares the chosen load with the calculated strength of an element. It is classified as the Level I calculation method. No failure probabilities are calculated.

One can say that the limit state is exceeded with a probability of 50% since the mean values of the strength parameters are used. The problem of such a high probability of exceedance can be overcome by designing according to standards or by using safety margins/factors. A design standard considers an element sufficiently reliable if a certain margin exists between the load values and strength values. Such a margin can be created by multiplying the load values with safety factors, and by dividing strength values with safety factors. When one does not apply safety factors according to standards, conservative values have to be chosen for parameters, to assure the design is over dimensioned and not under dimensioned.

But a more accurate approach would be to calculate the probability of exceedance of the limit state. The next section elaborates on this.

J.3 Probabilistic approach (Level II and Level III calculation methods)

Different probabilistic calculation methods have been developed to determine the reliability of a dune. The same could be used for a the design of a seawall. First the probability distribution function of each parameter (either load or strength parameter) is defined. Next, the limit state function is defined. This is normally in the form of a formula. In the case of a seawall design, which is rather complex, the limit state function is in the form of a model that simulates each case.

First the level III approach is discussed in this section, since the level II approach refers a lot to the level III approach.

J.3.1 Level III full probabilistic approach

Numerical integration

The probability of failure can be determined by integration of the probability function, which reads:

$$P_f = P(Z < 0) = \int \int_{Z(x)<0} ... \int p_x(x) dx_1 ... dx_n \tag{J.4}$$

This method is considered inappropriate for structural design cases. The determination of Pf becomes very complex, since every parameter has its own probability distribution. Computations become very labour-intensive and are both time-consuming and difficult.

Monte Carlo approach

The Monte Carlo approach is based on drawing values for each parameter randomly, taking its probability distribution function into account. With these values Z is calculated. Again, Z<0 leads to failure. The probability of failure approached with a Monte Carlo simulation is:

$$P_f = \frac{N_f}{N} \tag{J.5}$$

Where N is the total number of computations and Nf is the number of computations which resulted in failure. For relative computationally expensive models, like XBeach, the Monte Carlo approach is not feasible since the approach requires a high number of simulations. According to CUR (1997) the minimum number of samples for a 95% confidence level is:

$$N > 400(\frac{1}{P_f} - 1) \tag{J.6}$$

Probabilities, as relevant for Namdeb seawalls, in the order of $O(1 \cdot 10^{-2})$ already require a number of simulations in the order of $O(1 \cdot 10^4)$.

J.3.2 Level II probabilistic approach

A probabilistic calculation on level II uses a method of linearizing the reliability function in the design point that must be selected. The design point is the point on the edge of the failure area (so Z = 0) that indicates the combination of load and strength parameters with the largest probability density that leads to failure. Different level II calculation methods exist. The FORM and the Bayesian Network will be discussed here, since these two methods are used in dune design for the coast of the Netherlands.

FORM

FORM (First Order Reliability Method) linearizes the limit state function in the design point. This point can be found iteratively. For these iterations the variables of the limit state function are approached with standard normal distributions. The procedure is touched upon briefly here. One starts with a limit state function Z, which is nonlinear for dune-erosion problems.

$$P(Failure) = P(Z(\mathbf{X}) < 0) \tag{J.7}$$

With Z being the limit state function and $\mathbf{X}$ a set of random variables.

$$\mathbf{X} = (X_1, X_2, ..., X_{n-1}, X_n) \tag{J.8}$$

A linear Z-function looks as follows:

$$Z = a_1X_1, a_2X_2, ..., a_{n-1}X_{n-1}, a_nX_n + b \tag{J.9}$$

$$\mu_Z = a_1\mu_{X_1}, a_2\mu_{X_2}, ..., a_n\mu_{X_n} + b \tag{J.10}$$

$$\sigma_Z = \sqrt{\sum_{i=1}^{n}\sum_{j=1}^{n} a_i a_j \cdot COV(X_i, X_j)} \tag{J.11}$$

All variables $\mathbf{X}$ have a normal distribution with a mean (μ_{X_i}) and a standard deviation (σ_{X_i}). When a variable has a different distribution, a transformation is made to approach the variable as normally distributed. If the set of variables $\mathbf{X}$ is normally distributed and statistically independent, a set of standard normal distributions U can be found needed for the calculation procedure.

$$U_i = \frac{X_i - \mu_{X_i}}{\sigma_{X_i}} \tag{J.12}$$

By definition these variables have a μ_{U_i} of 0 and a σ_{U_i} of 1. The design point is the point on the line of Z=0, closest to the origin. The distance from the origin to this point on the line is equal to the reliability index β (Hasofer and Lind, 1974):

$$\beta = \frac{\sigma_Z}{\mu_Z} \tag{J.13}$$

When Z is nonlinear, its function must be linearized with Taylor series. The first two terms of the polynomial approximate the limit state function (CUR, 1997). The function can now be read as:

$$Z = g(x_0, y_0) + (x - x_0)\frac{\delta g}{\delta x}(x_0, y_0) + (y - y_0)\frac{\delta g}{\delta y}(x_0, y_0) \tag{J.14}$$

$$\mu_Z = g(x_0, y_0) + (\mu_x - x_0)\frac{\delta g}{\delta x}(x_0, y_0) + (\mu_y - y_0)\frac{\delta g}{\delta y}(x_0, y_0) \tag{J.15}$$

$$\sigma_Z^2 = \left\{\frac{\delta g}{\delta x}(x_0, y_0)\right\}^2 \sigma_x^2 + 2\frac{\delta g}{\delta x}(x_0, y_0)\frac{\delta g}{\delta y}(x_0, y_0) \cdot COV(x, y) + \left\{\frac{\delta g}{\delta y}(x_0, y_0)\right\}^2 \sigma_y^2 \tag{J.16}$$

It is very unlikely that the correct design point is found after a single iteration. The results of the first iteration form the input for the second iteration in the FORM procedure. For this reason also the design points $(X_1^*, X_2^*, ...X_n^*)$ of each variable have to be found. This is done as:

$$X_i = \mu_{X_i} + \alpha_i \beta \cdot \sigma_{X_i} \tag{J.17}$$

Where α is found by

$$\alpha_i = \frac{-a_i \sigma_{X_i}}{\sigma_Z} \tag{J.18}$$

α can also be seen as the influence coefficient for each variable in the limit state function. By calculating the alpha values, one carries out a weighted sensitivity analysis of the solution Z = 0. The solution is most sensitive to the parameter with the largest value of α.

The iterative procedure can also be explained with Figure J.1 and Figure J.2. Numbers in these figures are only illustrative. In Figure J.1 one can see the normal distribution of the load parameters S on the left and the strength parameters R down in the figure. The limit state function Z is to be linearized. The first design point A is chosen arbitrarily. Linearization is possible by finding the tangent line. By following the FORM procedure as explained, on will find after an iteration the design point as presented in Figure J.2. One can see that this point is more likely, considering the probabilities of the strength and load parameters. The procedure must be repeated until a stable value for beta and the design point X^* is found. This is important because if failure occurs it is most probable to occur in the design point.

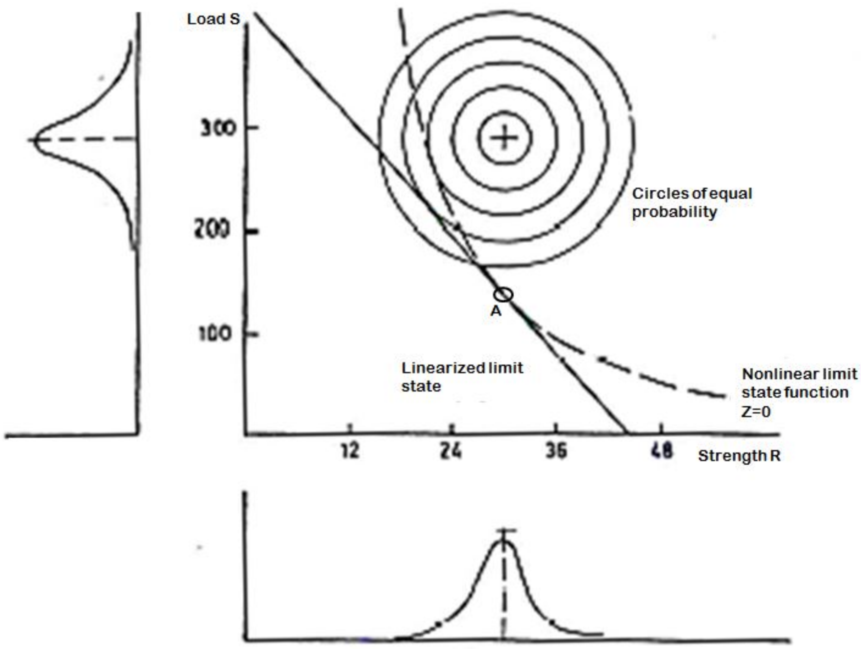

Figure J.1: Schematic representation of FORM procedure. Probability density functions of R and S are combined in the graph. The curved line represents the nonlinear limit state function.

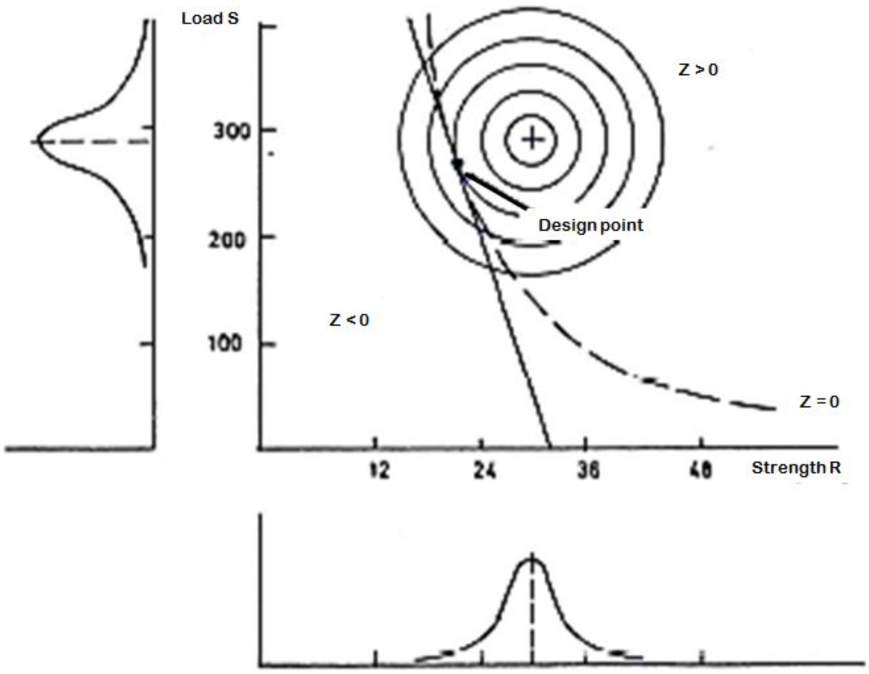

Figure J.2: Follow up of Figure J.1. New design point is found by iterative process of FORM.

Compared to a level III calculation method, the procedure of the FORM analysis saves a lot of computations and thus time/effort.

J.4 Dune erosion problems

For the dunes on the coastline of the Netherlands a level II calculation was used to assess the influence of different parameters that affect the dune erosion when a storm occurs. These tests have led to a formula that can be used as a guideline for coastal managers to know whether a dune section is safe or in need of extra sand. The methodology of drafting this guideline for the Holland Coast is briefly discussed in this section, as it can be relevant for the assessment of seawalls in the Southern Coastal Mine Namibia. For a more extensive explanation of the guideline the reader is referred to Van de Graaff (1984*a*) , and to Van de Graaff (1984*b*) or Van de Graaff (1986) for the background of the probabilistic methods used.

The starting point of the procedure is the required failure probability of a dune, which is the probability that the Ultimate Limit State of a dune is exceeded in terms of erosion. Not to be confused with the exceedance probability of a storm condition. For the central-Holland coast this failure probability is $1 \cdot 10^{-5}$ per year.

DUROS (Vellinga 1983), a 1D dune erosion model, was used to determine the retreat distance of a dune per storm event. The model states that erosion occurs, because the upper shore-face strives towards a post-storm equilibrium profile. This profile is based on three elements, illustrated with figure J.3. The first is an outerslope of 1:1 for the resulting dune. The second element is the resulting seaward slope of 1:12.5 of sand that was relocated offshore at the end of the profile. The third element is the middle part, where a parabolic equilibrium profile is occurs. This profile is the so-called erosion profile according to Vellinga (1983) and can be described by the following equation:

$$(7.6/H_s)y = 0.47[(7.6/H_s)^{1.28} \cdot (w/0.0268)^{0.56}x + 18]^{0.5} - 2.00 \tag{J.19}$$

With:

- H_s significant wave height at deep water [m].
- w the fall velocity of the sediment [m/s].
- x the distance from the new foot of the dune [m].
- y water depth below the maximum storm surge level [m].

The distance x can be described by (starting from the new dune foot):

$$x = 250 \cdot (H_s/7.6) \cdot (0.0268/w)^{0.56} \tag{J.20}$$

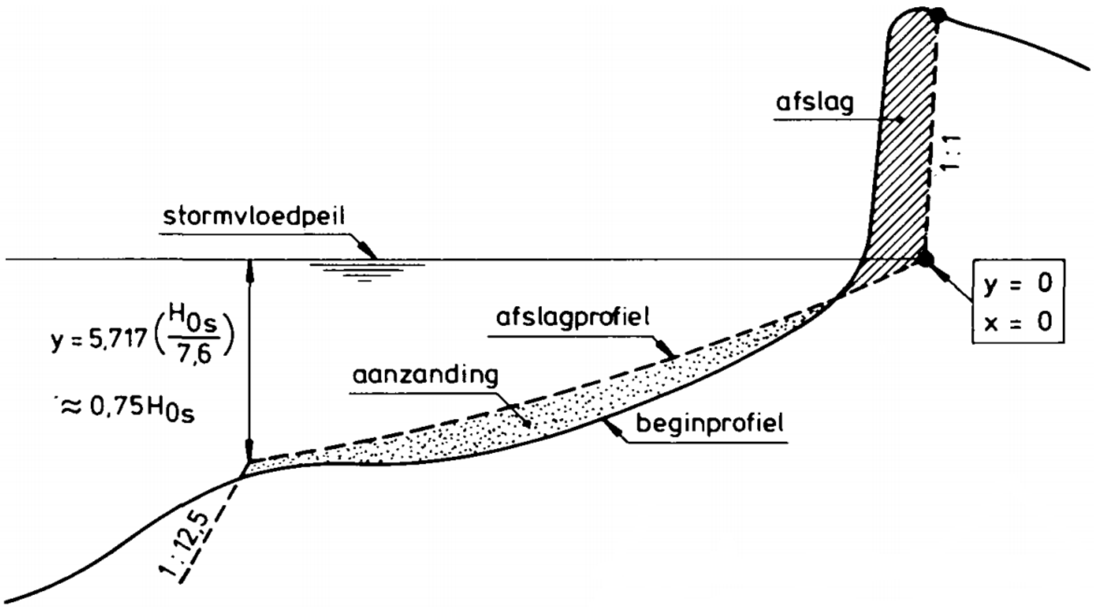

Figure J.3: Schematic drawing of a dune cross-section. Under the influence of a storm surge, the profile strives towards a post-storm equilibrium profile, as prescribed by Vellinga (1983). Labels are in Dutch. afslag = erosion, afslagprofiel = erosionprofile, stormvloedpeil = storm surge level, aanzanding = sedimentation, beginprofiel = beginprofile.

Seven parameters are said to play a role in the erosion of dunes on the Holland Coast. For a level II or level III probabilistic calculation, the probability density functions of these seven variables must be known. They are discussed here below.

1. The maximum waterlevel. Steetzel et al. (2007) found that this variable can be best described with a conditional Weibull distribution. The probability of exceedance determines the mean value for the water level.

2. The significant wave height. For the Dutch situation the wave height and water level are correlated, since both are driven by wind during a storm event. The wave height has a normal distribution, with a standard deviation of 0.6 m, according to Steetzel et al. (2007).

3. The grainsize diameter. The mean value of this is found by tests. The standard deviation of this normally distributed variable is in the order of $0.1 \cdot \mu_{D50}$.

4. The stormsurge duration. This is the duration that the waterlevel is above a certain design waterlevel. It strongly depends on the tidal range of the specific day, in which the storm occurs. The stormsurge duration can be approximated with a normal distribution. It is implemented into the model as a standard deviation of 0.1 times the total erosion volume that is simulated initially. The mean is zero.

5. Rain-oscillations and rain gusts. Van de Graaff (1984*b*) explains how rain gusts can be incorporated in the model. According to Vrijling and Bruinsma (1980) a rain gust height of 0.40 m must be taken as mean value for the Holland Coast. The effect is added to

the initial erosion volume by:

$$\Delta A = 0.05 \cdot A \cdot \Delta h / 0.4 \tag{J.21}$$

6. Initial dune profile. Especially the location of the dune toe on the beach has an important influence on the dune erosion volume. This must be measured and a normal distribution is kept for the probability density function.

7. Model accuracy. This variable is implemented as 0.15 (15%) times the total erosion in the same way as is done for the stormsurge duration.

No level III calculation was done, since DUROS is quite computationally expensive, which is problematic in case of many required simulations. With FORM a level II calculation was carried out. Iteratively the DUROS model calculated the design points for the different parameters. Also the relative influence of parameters to the uncertainty of the final outcome was measured. The relative influence (α-value) of the water level, or the wave height since those two are correlated, was the heighest. If variations in grainsize diameter, dune profile and stormsurge durations, together with model uncertainties, are also taken into account, a value of 0.25 (25%) times the initial erosion must be added to the eroded volume.

The design points that were found could subsequently be used as characteristic values for a level I calculation that can be executed rather easily by coastal managers per case.

With these values the retreat distance of the dune and the eroded volume of sand can be calculated for the $1 \cdot 10^{-5}$ per year case for different locations. This result can be used to determine the limit state of the dune. The limit state is the dune profile which is formed after dune erosion, such that the dune is in critical position but does not fail.

Figure J.4 shows schematically how the erosion pattern of the dune. To the total initially simulated erosion volume A, a volume of T must be added to account for model uncertainties and variations in grainsize diameter, dune profile and stormsurge durations. An outerslope of 1:1 for the resulting dune is used to calculate the retreat distance of the dune. Point P, on design waterlevel, is used to calculate the distance over which the dune foot retreats. Point R is the retreat distance of the dune crest.

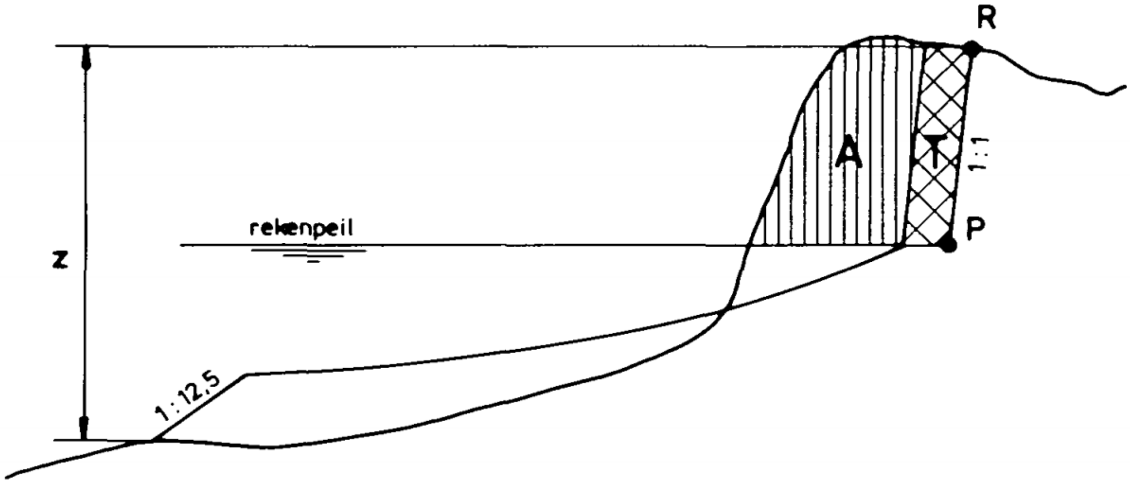

Figure J.4: Cross-section of dune profile showing the post-equilibrium profile. The eroded volume is A. An additional volume T must be taken into account, because of model uncertainties. (rekenpeil = design water level)

A limit state profile was also defined for dunes along the Holland Coast. A schematic drawing is presented in Figure J.5. The crest height and width are defined. Failure means that the retreat distance of the dune during a storm exceeds the outer edge of the limit state profile ("kritieke afslagpunt" in Figure J.5).

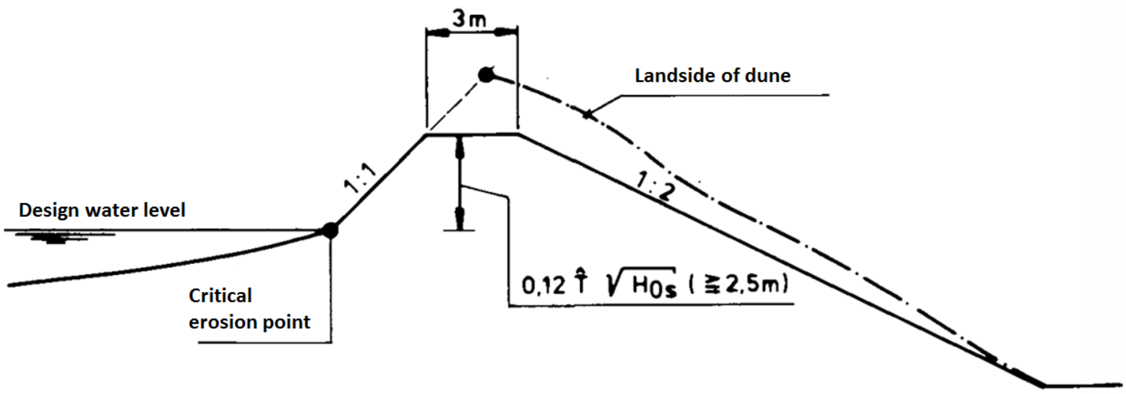

Figure J.5: Limit state profile of a Dutch dune.

Application of guideline

So in the end the guidelines for dune erosion to the Dutch Coast state an erosion volume (or retreat distance) for each dune area, with a certain probability ($1 \cdot 10^{-5}$ per year). This result can relatively easy be updated for a new dune profile. With the limit state profile in mind, the required dune volume for each dune section can easily be determined by a coastal manager.

Appendix K – Probabilistic calculation of required seawall volumes

In Appendix J the procedure of a level II probabilistic calculation for Dutch dunes was explained. For the Namibian seawalls a similar procedure can be developed. This Appendix here gives a set-up, but the simulations needed are not within the scope of this thesis.

K.1 Probabilistic approach

Chapter 10 (Required Seawall Volumes) concluded with a volume of sand that erodes from the seawall per design storm. This approach is deterministic, which basically means that the chance of exceeding the result is 50% (see section J.2 for explanation). In the model set-up of XBeach (see section 9.2) the values for the input parameters have been chosen conservative. This is done to be on the safe side with the seawall design. A probabilistic approach with these values would lead to a rather small failure probability. However, a level II probabilistic approach can lead to a better insight in the influence of parameters and a more accurate statement of the reliability of a seawall.

K.2 Design conditions

The design standard, or allowable failure probability, of the seawall must be chosen by NAMDEB. This is a cost-benefit analysis. The costs of constructing a seawall should in a normal sense be lower than the consequences of seawall failure.

As a first recommendation, but also for the purpose of explaining the design procedure, a standard is chosen of a failure probability of 10% for a storm with an occurrence probability of 1/50 per year. That makes the probability of exceeding the limit state 1/500 per year. This is considered to be a high standard for a seawall with a lifetime of 2 years and the possibility of maintenance.

The limit state function (the Z-function) is the XBeach model, which swash dynamics and avalanching processes as discussed in section 9.

K.3 FORM procedure for the Namibian seawall reliability

The set-up of a FORM (First Order Reliability Method) is discussed here.

Differences Namibian Coast and Holland Coast

Some important differences between the situation of the Holland Coast and the Namibian Coast need to be indicated. First the waterlevel plays a far more important role for the Holland Coast and is correlated with the significant wave height, while for the Namibian situation this is not the case.

Secondly, for the Namibian situation also the wave peak period must be evaluated on itself. According to data analysis summarized in Appendix G a correlation between Tp and Hs is difficult to find and the standard deviation of Tp must be chosen rather large. For the Holland Coast the wave period has a strong correlation with the wave height.

Thirdly, rain gusts do not play a significant role during storm events on the Namibian coast. Storm events that lead to the most severe dune erosion, are those that occur more than 2000 km away and bring large swell waves to the Namibian coast. Appendix I shows an example of that.

The fourth difference is that we can no longer speak of the stormsurge duration but of the storm duration. Dune erosion at the Holland Coast takes place when heavy weather conditions coincide with high tide (normally spring tide). This is why the stormsurge duration has a mean value of 5 hours. For the Namibian Coast seawall erosion does not necessarily coincide with high tide. The duration of a storm that causes dune erosion is mostly dependent on duration of the storm event far offshore. Normally about 3 days.

The seven determining variables for seawall erosion are thus the following:

1. Water level
2. Significant wave height
3. Wave peak period
4. Initial seawall toe location
5. Median grainsize diameter
6. Storm duration
7. Model accuracy

These variables are the starting point for a level II probabilistic calculation (FORM). Instead of DUROS, as used for the Holland Coast, now XBeach is used to simulate dune erosion. The reason for choosing XBeach was explained in Chapter 7. XBeach is relative computationally expensive. For this reason a level III calculation, like the Monte Carlo simulation, is dissuaded. The probability distributions of the 7 parameters for the FORM procedure are discussed here below.

Water level. The tidal range is said to be rather small (maximum of 1.8 for spring tide, according to table 2.1 in section 2.2), but there is also some water level set up due to bound long waves, as explained in section 6.2. The water level during storms had a probability density function with a Conditional Weibull distribution (Steetzel et al., 2007) for the Holland Coast. For the Namibian Coast a normal distribution is chosen, since low tide during storms can still lead to a seawall erosion situation.

Significant wave height. The mean value of the normal distribution comes from table 9.3.

Wave peak period. The mean value of the wave peak period also comes from table 9.3. The standard deviation is expected to be rather large (in the order of 2 seconds).

Initial seawall toe location on the beach. This value differs per seawall section and comes from measurements, executed by the Survey Team of NAMDEB on a six-months basis. In northward direction, starting at the river mouth, every 250 meters the bathymetry is measured with single beam. This parameter has a probability density function that is normally distributed. The standard deviation must be chosen rather large, because a lot of variation along the beach is already visible in pictures.

Median grainsize diameter. The uncertainty about this parameter is large. As explained in section that the chance of exceeding the result is 50% (see section J.2 for explanation). In the model set-up of XBeach (see section 9.2 a mean value for the median grainsize diameter of 400 μm is used, but particle size distribution tests must verify this assumption. Normal distribution is used, with a standard deviation of 10% of the mean.

Storm duration. Like the stormsurge duration, the effect of a longer or shorter storm is taken into account by adding a standard deviation of 10% to the total eroded seawall volume.

Model accuracy + uncertainties due to other parameters (effects of crosswalls and other discontinuities along the coastline, longshore transport gradients, seawall toe protections, wave direction). Some have already been assessed and their influence is considered to be small.

K.3.1 FORM procedure

For the Holland Coast a guideline was developed for Coastal Managers to use. For the Southern Coastal Mine Namibia, such a guideline might not be worth the effort. The cross-shore profile along the coast is not uniform and changing constantly. Besides, the number of different cross-sections of seawalls along the mining area are in the order of 20 sections. An even lower number of cross-sections can be indicated when it comes to seawalls that are standing out in seaward direction. Because of these reason, it is advised to carry out the FORM procedure for each single seawall section. The measured seawall profile can be used as a deterministic input value and subsequently design points of the other parameters can be found. Then the erosion volume (times 1.25 for model uncertainties and storm duration) for the 1/500 case can be found. With the limit state of the seawall in mind, the total seawall volume can be derived.

K.4 Discussion

Carrying out a FORM procedure is not within the scope of this thesis. The computations take too much time. With FORM the design points for the different variables are found and also the influence, by means of an α-value. This is in fact a weighed sensitivity analysis. In order to still know the influence of variables a sensitivity analysis was already done. This can be found in Appendix H.

In his research into dune erosion on the Holland Coast, Den Heijer (2013) found that the FORM procedure with XBeach can experience convergence issues. The method cannot cope with discontinuities (Grooteman, 2011). Since XBeach uses an avalanching module for erosion, the shape of erosion in time is staircase like. And also the waves come from a wave spectrum showing variations. This means that the resulting gradient of the erosion rate is not necessarily regularly. Consequently, the FORM procedure can have convergence issues. Den Heijer (2013) found that the risk of convergence issues can be mitigated by choosing the grainsize deterministic and by choosing similar wave time series for each simulation.

An alternative to the FORM analysis would be creating a Bayesian Network. Den Heijer (2013) pointed out that this is a useful approach for computationally expensive models, and that is does not have convergence problems. Further research into the application of a Bayesian Network to test the reliability of seawalls is recommended, but is not within the scope of this thesis.

Appendix L – Additional activities in support of Master Thesis

This appendix has been added to the thesis to put the research even better into context by explaining the interaction with the client (NAMDEB) and with the MAREC Consortium. The involvement of MAREC (Royal Eijkelkamp Group, Royal IHC and Witteveen+Bos) will be explained as well.

L.1 Background

Before the start of this Master Thesis, I did my internship, in the form of a fact-finding mission, for Witteveen+Bos at the Southern Coastal Mine of NAMDEB in Namibia. The purpose of this fact-finding mission was that the findings would eventually lead to a better understanding of all the processes involved in land reclamation and mining in Mining Area No. 1, Sperrgebiet, Namibia. The results of the fact-finding mission have led to this graduation project, which ideally is part of a proposal with which MAREC offers their services to NAMDEB. Services to support NAMDEB in her strive of expanding diamond mining activity into shallow sea regions in the most optimal way. MAREC (Mining Area Rehabilitation and Environmental Control) is a consortium shaped around three internationally operating companies: Royal Eijkelkamp Group, Royal IHC and Witteveen+Bos. This group of companies, MAREC, has been involved in several mining operations providing both services and consultancy.

Since the start of the my internship in September 2014 I have been involved in negotiations with NAMDEB, on behalf of the MAREC Consortium. This mostly consisted of explaining the mining process of NAMDEB to MAREC, being in contact with Surveyors, Geologists and Project Managers of NAMDEB, and preparing presentations and proposals. The negotiations are still in an early stage. No firm proposals or contracts have been on the table yet.

A number of events where I was involved in are listed here below.

L.2 Fact-Finding Mission (September – November 2014)

As mentioned, I carried out a fact-finding mission on site in Namibia. With interviews, site-visits and gathering documents, I learned how this unique mining process works. I also made a lot of contacts with NAMDEB-personnel which was not only useful during the internship, but also afterwards.

L.3 NAMDEB-delegation in the Netherlands (April 2015)

In April 2015 a delegation of NAMDEB visited the Netherlands to acquire a Sonic Samp Drilling machine and to discuss the possibilities of further co-operation with MAREC.

Each company, Royal Eijkelkamp Group, Royal IHC and Witteveen+Bos, gave a presentation of their company and completed projects, which are relevant to the cases that NAMDEB had.

On behalf of MAREC I presented to NAMDEB the findings of my internship, and also at what areas MAREC can offer their services to NAMDEB.

I was the designated person to do this presentation, since I had come to know the mining operation of NAMDEB inside out. The aspects presented were recognized by the delegation of NAMDEB as issues that need improvements or an entirely new approach.

L.4 Storm of May 2015

In late May 2015 almost 700 meters of seawall length was washed away due to a storm that lasted for multiple days. This storm has been simulated as a case study for my thesis (see section 9.3.1).

This storm also proved the need for a better seawall design and planning. Because of this event, the focus of my thesis work became more on extreme events (storms), rather than on how the coastline evolves and on calculating the final distance seawards for the current mining method.

This storm gave Witteveen+Bos the immediate opportunity to offer their services to NAMDEB, since Witteveen+Bos has great experience in land reclamation project, coastal modelling and the design of sea defenses. I was involved here by writing a memo for Witteveen+Bos, summarizing the results of the simulation of the storm plus recommendations for a better sea defense in the future. This memo became part of a proposal for a second fact-finding mission carried out by MAREC to study specific areas where the consortium can offer services or products.

L.5 Presentations to NAMDEB

In September 2015 I have presented preliminary results of my thesis to the Offshore Portfolio Manager of NAMDEB, in the presence of the other MAREC partners. This was to show the expertise of Witteveen+Bos when it comes to coastal engineering and to make NAMDEB enthusiastic to start a cooperation with MAREC.